Durability of Materials in Pearl-Chain Bridges

Lund, Mia Schou Møller

Publication date:
2016

Document Version
Publisher's PDF, also known as Version of record

Durability of Materials in Pearl-Chain Bridges

Mia Schou Møller Lund

PhD Thesis

Department of Civil Engineering
2016

DTU Civil Engineering Report R-341

DTU Civil Engineering
Department of Civil Engineering

PhD Thesis

Durability of Materials in Pearl-Chain Bridges

Mia Schou Møller Lund

2016

Section for Building Design
Department of Civil Engineering
Technical University of Denmark
Brovej Building 118
DK-2800 Kgs. Lyngby
Denmark

Cover photo: Implementation of pervious concrete as fill material in the Pearl-Chain Bridge crossing Vorgod Stream, Denmark. Photo by Mia S. M. Lund.

Supervisors:
Associate Professor Kurt Kielsgaard Hansen, DTU Byg
Professor Kristian Hertz, DTU Byg

Assessment Committee:
Associate Professor Marianne Tange Hasholt, DTU Byg
Professor Tang Luping, Chalmers University of Technology
Dr. Peter Utgenannt, Swedish Cement and Concrete Research Institute (CBI)

Report R-341
ISBN 9788778774323
ISSN 1601-2917

This thesis is submitted in partial fulfillment of the requirements for the degree of Doctor of Philosophy in Civil Engineering at the Technical University of Denmark.

Durability of Materials in Pearl-Chain Bridges

Preface

This thesis is submitted in partial fulfillment of the requirements for the PhD degree in Civil Engineering at the Technical University of Denmark (DTU). The work was carried out at the Department of Civil Engineering at DTU from February 2013 to February 2016 with Associate Professor Kurt Kielsgaard Hansen as main supervisor and Professor Kristian Hertz as co-supervisor.

The PhD project was part of, and partly supported by, the Innovation Fund Denmark project "Concrete Pearl-Chain Bridges". The Innovation Fund Denmark project was managed by Abeo; in addition to DTU, other contributors to the project's development include Grontmij (now Sweco), Skandinavisk Spændbeton, and "mixing plant A" that prefers to remain anonymous.

Mia Schou Møller Lund
Kgs. Lyngby, Denmark, February 2016

Acknowledgements

I could never have completed this PhD thesis without help from a large group of people to whom I owe my deep thanks. First, I would like to thank my supervisor, Kurt Kielsgaard Hansen, for his endless guidance and indomitable belief in me and in the realization of this project. Thanks for *always* leaving your door and phone open, no matter if it was late evening or early morning just before your morning run. Thanks for teaching me how to fly, yet always allowing me to feel safe, knowing you were there to catch me. Kristian Hertz, thanks for your inspiration and for sharing your profound knowledge. This project would not have been possible without the tireless help of the workers in the workshops at DTU Byg. You surprised me repeatedly with one more impressive test setup after the other. Particularly, I owe deep thanks to Per Leth who long ago probably stopped counting the number of hours he spent on me. Thanks for your great help and your never-ending smiles. They warmed me more than you know. The comprehensive experimental work carried out as part of this project could not have been done without help from the project students I co-supervised. Thank you Michelle, Maria, Søren, Viet, Michael, Lasse, Rasmus, Iben, and Pinar for your enthusiasm and your many hours of hard work.

During my PhD study, I spent four months at Iowa State University (ISU) under the supervision of Professor Vernon R. Schaefer from ISU and Associate Professor John T. Kevern from the University of Missouri-Kansas City. Thank you both, and thanks to Ruth Schaefer for opening your arms and home and making me welcome so far away from Denmark. Also a special thanks to Bob Steffes from ISU.

My PhD project was part of an Innovation Fund Denmark project that involved several partners from industry to whom I owe deep thanks for their inspiration and their new perspective on my research. Especially thanks to my project manager, Nicky E. V. Petersen, from Abeo for believing in the importance of my research and for opening doors that would otherwise have stayed closed.

I owe a big thanks to my colleagues from the DTU building materials research group, and to my PhD colleagues for inspiration, support, and great friendship during the last three years. Thanks for being there to listen and discuss when I faced technical challenges, but also for offering me a world without Pearl-Chain Bridges. Finally, I owe deep thanks to my friends and family for their support and guidance through challenging periods during this project. Thank you for always bearing with me when I was late because I had to finish my measurements. I know it happened way too often. Thanks for listening to my complaints during 60 hours work weeks when I could not see the light at the end of the tunnel. You were right, it was there. This is the light.

Abstract

This PhD thesis contributes to documentation regarding durability of materials used in so-called "Pearl-Chain Bridges". The Pearl-Chain Bridge technology is a new precast bridge solution developed at the Technical University of Denmark. The technology reintroduces the arch structure as an economical beneficial solution primarily for road and railway bridges, and allows for the faster, more environmentally friendly, and cheaper construction of such bridges. A Pearl-Chain Bridge consists of two main parts: the load-carrying Pearl-Chain arch, and the fill material on top of the arch. The construction of the Pearl-Chain arch is simple. The arch is assembled on its side, next to the road that the bridge will span, by placing a number of plane prefabricated Super-Light Decks that consist of lightweight aggregate concrete and conventional concrete, in the desired arch shape. Mortar joints are cast between the decks, and because all decks have a duct cast through them longitudinally, they can be collected on a wire – like pearls on a string. The assembly of the arch is completed by post-tensioning the wire. A crane lifts the arch into place during the night, and subsequently the Pearl-Chain arch is stabilized by casting a fill material between the spandrel walls of the arch. Finally, the road surface is cast on top of the fill material.

New bridges are designed for a service lifetime of at least 100 years. Hence, the specifications of the materials used in Pearl-Chain Bridges are high. This PhD study documents that the materials used in Pearl-Chain Bridges have the necessary strength and durability to ensure their longevity. The scope of the PhD study is limited to assessing the fill material placed on the Pearl-Chain arch, and the mortar joints and lightweight aggregate concrete used in the Pearl-Chain arch itself. This is because these materials, and the application of them, differ from the materials in typical bridge superstructures.

Typically, arch bridges are filled with sub-base gravel; however, in order to examine the possibilities of using alternative fill materials, cement-stabilized gravel and pervious concrete were also investigated. The most suitable fill material for Pearl-Chain Bridges depends on the particular bridge design; the results obtained and presented in the present PhD study provide guidance on how to decide which fill material is most suitable regarding strength, permeability and freeze-thaw durability. In particular, the PhD study explored in depth the use of pervious concrete, because pervious concrete is a relatively unknown material in Denmark. The applicability was demonstrated by using pervious concrete fill in the very first 26 meter-long Pearl-Chain Bridge constructed. Compared with sub-base gravel and cement-stabilized gravel, pervious concrete considerably improves the drainage properties of the superstructure, which has a positive influence on the longevity of

Pearl-Chain Bridges.

The mortar joints in the Pearl-Chain arch were found to be prone to crack formation during hardening, which is undesirable since it provides easy access for water and chloride ions to reach the post-tensioning wires, and initiate corrosion. This crack formation was eliminated by using an expansive mortar product with a constant expansion, and by applying a primer to the concrete surfaces adjacent to the joint, whereby the porosity along the construction joint was decreased. It was documented that the mortar joints did not decrease the durability of the Pearl-Chain arches with regard to chloride ingress, water absorption, or freeze-thaw durability.

The work carried out on lightweight aggregate concrete was, from many perspectives, pioneering. This was mainly because most prior knowledge concerning lightweight aggregate concrete mix design was based on experience and had not been documented in scientific papers, but also because the lightweight aggregate concrete in Pearl-Chain Bridges can be exposed to freeze-thaw, which is not the case with lightweight aggregate concrete in typical fields of application. The freeze-thaw durability of lightweight aggregate concrete was improved by the introduction of air entrainment, which was demonstrated by measuring and correlating the air content of fresh lightweight concrete with the freeze-thaw behavior of hardened lightweight concrete. Recommendations are given to a freeze-thaw resistant lightweight aggregate concrete mix design for Pearl-Chain Bridges, which has greater strength properties than the current lightweight aggregate concrete used in Super-Light Decks for indoor purposes.

Resumé

Denne ph.d.-afhandling bidrager til at dokumentere holdbarheden af de materialer, der anvendes i såkaldte Perlekædebroer. Perlekædebro-teknologien er en ny, præfabrikeret broløsning udviklet på Danmarks Tekniske Universitet. Teknologien reintroducerer buekonstruktionen som en øknonomisk fordelagtig løsning til primært vej- og banebroer og gør opførelsen af sådanne broer mere miljøvenlig og billigere. En Perlekædebro består af to dele: den lastoverførende Perlekædebue og fyldmaterialet oven på buen. Konstruktionen af Perlekædebuen er simpel. Buen samles på siden ved at anbringe et antal Superlette Dæk, der består af letbeton og normal beton, i den ønskede bueform ved siden af den vej, som broen skal krydse. Mørtelsamlinger udstøbes mellem dækkene, og fordi alle dæk har et rør indstøbt i broens længderetning, kan de samles på en wire – som perler på en snor. Ved at efterspænde wiren bliver buen samlet. I løbet af en nat kan Perlekædebuen løftes på plads ved hjælp af en kran og efterfølgende stabiliseres ved at udlægge et fyldmateriale på buen imellem fløjvægge. Til slut bliver vejbanen udstøbt oven på fyldmaterialet.

Nye broer designes til at have en levetid på mindst 100 år. Det betyder, at kravene til materialerne, der anvendes i Perlekædebroer, er høje, og dette ph.d.-projekt dokumenterer, at materialerne i Perlekædebroer har tilstrækkelig styrke og holdbarhed til at sikre en lang levetid. Ph.d.-projektet er afgrænset til at omfatte fyldmaterialet placeret oven på Perlekædebuen og mørtelsamlingerne og letbetonen i selve Perlekædebuen, da disse materialer og anvendelsen af dem adskiller sig fra materialerne, der typisk bliver anvendt i brooverbygninger.

Buebroer bliver som regel fyldt med bundsikringsgrus, men for at undersøge mulighederne ved brug af alternative fyldmaterialer blev cementstabiliseret grus og drænbeton også testet. Det mest velegnede fyldmateriale til Perlekædebroer afhænger af det pågældende brodesign, og de resultater, som dette ph.d.-projekt har fundet frem til og præsenterer, kan anvendes som vejledning i beslutningsprocessen omkring hvilket fyldmateriale, der er mest velegnet med henblik på styrke, permeabilitet og frost/tø-holdbarhed. Ph.d.-projektet gik især i dybden med anvendelsesmuligheden af drænbeton, da drænbeton er et relativt ukendt materiale i Danmark. Anvendeligheden blev demonstreret ved at implementere drænbeton som fyld i den allerførste Perlekædebro, der havde en længde på 26 meter. Sammenlignet med bundsikringsgrus og cementstabiliseret grus, forbedrer drænbeton afdræningen af brooverbygningen betydeligt, hvilket har en positiv indflydelse på levetiden af Perlekædebroer.

Mørtelsamlingerne i Perlekædebuen viste sig at være meget udsatte for revnedannelse under hærdning, hvilket er uønsket, da det giver direkte adgang til at vand

og kloridioner kan trænge ind til den efterspændte wire og forårsage korrosion. Revnedannelsen blev undgået ved at anvende en ekspanderende mørtel med en konstant ekspansion samt ved at påføre en primer på betonoverfladerne, der vendte ind mod samlingen, hvorved porøsiteten langs støbeskellet blev reduceret. Det blev dokumenteret, at støbeskellet ikke reducerer holdbarheden af Perlekædebuen, hvad angår kloridindtrængning, kapillarsugning og frost/tø-holdbarhed.

Det arbejde, der blev udført med letbetonen, var på mange måder banebrydende, først og fremmest fordi eksisterende viden omkring proportionering af letbeton overvejende er erfaringsbaseret og udokumenteret i videnskabelige publikationer, men også fordi letbetonen i Perlekædebroer kan udsættes for en frost/tø-påvirkning, hvilket ikke er tilfældet med typiske anvendelsesområder for letbeton. Frost/tø-holdbarheden af letbetonen blev forbedret ved tilsætning af et luftindblandingsmiddel, hvilket blev dokumenteret ved at måle og korrelere luftindholdet i frisk letbeton med frost/tø-holdbarheden af hærdet letbeton. Ph.d.-projektet giver anbefalinger til proportionering af en frostfast letbeton til Perlekædebroer med forbedrede styrkeegenskaber sammenlignet med den nuværende letbeton, der anvendes i Superlette Dæk til indendørs brug.

Table of contents

List of abbreviations

The abbreviations used in this project are shown below.

AC	Accelerator
AEA	Air Entraining Agent
ASTM	American Society for Testing and Materials
CG	Cement-stabilized Gravel
COV	Coefficient Of Variation
CRREL	Cold Regions Research and Engineering Laboratory
DF	Durability Factor
DRUW	Dry Rodded Unit Weight
DS	Danish Standard
DTU	Technical University of Denmark
EN	European Standard
HRWR	High-Range Water Reducer
HS	Hydration Stabilizer
ISO	International Organization for Standardization
ISU	Iowa State University
Leca	Light expanded clay aggregate
LWA	LightWeight Aggregate
LWAC	LightWeight Aggregate Concrete
PCB	Pearl-Chain Bridge
PCPC	Portland Cement Pervious Concrete

RDM	Relative Dynamic Modulus
SG	Sub-base Gravel
SL-Decks	Super-Light Decks
SP	SuperPlasticizer
UW	Unit Weight
w/c-ratio	water-to-cement ratio

CHAPTER 1

Introduction

This PhD project investigates the strength and durability of the materials used in so-called "Pearl-Chain Bridges" and documents the longevity of the bridges. This chapter describes the relevance of the PhD project, which was part of a larger innovation project, "Concrete Pearl-Chain Bridges", supported by Innovation Fund Denmark. The chapter answers the basic question, "*What is a Pearl-Chain Bridge?*", and provides background information that highlights the importance of this work. To understand the relevance of the innovation project, this chapter includes a helicopter perspective on the traditional construction of road- and railway-carrying concrete bridges in Denmark and the significance of a new bridge technology. In addition, the chapter describes the Pearl-Chain Bridge technology, the materials used in Pearl-Chain Bridges, and the parameters influencing their durability. The scope and the objectives of this PhD project are described in relation to the innovation project, and finally, the chapter outlines the thesis and presents scientific publications to establish a frame of reference for the remainder of the thesis.

1.1 Project background

The winding Danish coastline with many islands in the sea long ago forced the Danish to construct bridges to join the land, marking Denmark as a bridge nation. Approximately 11,300 bridges[1] in Denmark are registered as road- or railway-carrying, in addition to a few super bridges, such as the Great Belt Link and the Öresund Bridge, and a large number of pedestrian bridges. This number comprises all bridges owned by the Danish Road Directorate and the Danish railway traffic, but only 70% of the Danish municipal bridges, since the others are not sufficiently registered. Approximately 94% of these bridges are made of concrete. The road- and railway-carrying bridges in Denmark have a total estimated value of 73 billion Danish kroner, and annual maintenance costs constitute 1% of that value. Moreover, an estimated 1% of the total value is needed per year to replace old bridges, assuming bridges have a lifespan of 100 years (Lauridsen *et al.*, 2000).

[1] Peter Nielsen, The Danish Road Directorate, email to author, October 20, 2015.

The construction of road and railway concrete bridges can be classified into two categories:

1. **In situ bridges**. These bridges are cast at the place of construction, which requires an often comprehensive installation of formwork and scaffolding. On top of being costly and time consuming, this in situ bridge construction interrupts traffic, causing tailbacks and delays. A typical in situ bridge is under construction for three to six months. Because the formwork is installed on site, special bridge shapes, such as curved bridges, can be constructed.

2. **Prefabricated bridges**. These bridges are constructed with prefabricated bridge elements. In Denmark, Spæncom and Perstrup Concrete Industry dominate the prefabricated bridge construction market. The so-called "OT beams" from Spæncom, introduced in the 1970s, can be used for spans of up to 35 m. Perstrup's bridges are arch bridges made of tunnel elements; however, they span only up to 15 m. Internationally, a number of prefabricated arch bridge solutions exist, such as the Macrete FlexiArch system, the Techspan system, and the BEBO Arch system (Bernini, 2000; Bourke, 2010; Hutchinson, 2004). They all have a large rise-to-span ratio and work on the principle of soil-structure interaction, which means the passive soil pressure on the arch structure helps resist the load (Bernini, 2000).

The majority of road and railway bridges bridges in both categories are constructed as either slab or beam bridges. Only 5% of existing Danish road and railway bridges are arch bridges. The Danish Road Directorate owns approximately 135 arch bridges, and according to a search of technical documentation from the Danish bridge database, DANBRO, the vast majority of these bridges were constructed before 1970. Very few new bridges are constructed with arch structures, although, from a bridge engineering perspective, the arch is the most optimal type of construction for many load combinations. A perfectly shaped catenary with only its dead load is exposed to pure compression and zero moments, hence without tension. The same is true for a perfectly shaped parabola with a uniformly distributed load. An arc with a large diameter, hence a small curvature (such as an arc with a span-to-rise ratio of 1/13) can be geometrically placed between the catenary and the parabola, which makes it the most optimal geometry for construction exposed to its dead load and uniformly distributed loads (Halding, Hertz and Schmidt, 2015). In a shallow arch bridge construction that uses the arc geometry, the fill material resting on the arch can be regarded as a uniformly distributed load that, together with the dead load of the arch, causes the arch to be only exposed to compression. This compression is so large that even tensile stresses from live loads such as traffic loads only reduce the pre-compression of the arch, and the resulting force in the arch is still a compression force. This effect explains how masonry arches could be constructed long before reinforcement, as we know it today, was invented. The oldest arches date to before the Egyptians in 3,000 B.C., and around year 0, several examples of Roman arch structures such as viaducts and domes were constructed (Bernini, 2000), as shown in Figure 1.1a. Many of these arch constructions still exist more than 2,000 years after they were constructed, which bears witness to the

superiority of the construction (Hertz, 2010). However, arch structures are rarely used in new constructions because of the expensive scaffolding needed to shape the arch and the high labor costs associated with them (see Figure 1.1b), which was not a consideration 2,000 years ago.

(a) Roman aqueduct Pont del Diable, Tarragona, Spain, constructed around year 0. Photo: `http://flickriver.com/photos/anony_moose/4862040843/`.

(b) This typical scaffolding used to construct an arch structure is expensive and requires many labor hours to complete. Photo: `http://www.idh-design.co.uk/news/rebuilding-of-the-five-arch-bridge`.

Figure 1.1: Roman aqueduct and typical example of scaffolding used for arch constructions.

In October 2012, the three-year development project, "Concrete Pearl-Chain Bridges", supported by Innovation Fund Denmark was launched to develop a prefabricated arch bridge concept for roads and railways. The vision of the project was to *revolutionize the bridge building industry by developing a state-of-the-art bridge construction concept that had superior performance at half the price compared with current bridge structures.* The project was carried out as a cooperation between DTU and several partners from industry: Abeo (the project manager), Grontmij (now Sweco), Skandinavisk Spændbeton and mixing plant A that prefers to remain anonymous. The objective of the project and the main technological idea behind it was to combine Abeo's two patented solutions "Super-Light Structures" and "Pearl-Chain Reinforcement", both developed by DTU Professor Kristian Hertz, and to develop and implement a new technology for close-spandrel arch-shaped bridges created by post-tensioning a number of slab elements and providing them with a stabilizing fill material. This new technology was called "Pearl-Chain Bridge technology".

1.2 Pearl-Chain Bridge technology

1.2.1 Pearl-Chain Bridge superstructure

The load-carrying part of a Pearl-Chain Bridge is the Pearl-Chain arch made of prefabricated Super-Light Decks (SL-Decks) (Hertz, 2015; Hertz *et al.*, 2014). In the first Pearl-Chain Bridge (Section 1.2.4), each SL-Deck was 1.65 m long, 0.27

m thick, and 1.65 m wide; however, the dimensions can vary depending on the bridge design. Each SL-Deck has a slight inclination of 2.1 degrees at the ends; thus, collecting and post-tensioning several SL-Decks on a wire, like pearls on a string, creates the Pearl-Chain arch from plane elements. The geometry of the Pearl-Chain arch is based on an arc with a small curvature.

The SL-Deck was originally developed as an alternative to hollow core slabs, but it also is used as a slab element in the Pearl-Chain arch because of its several advantages compared with traditional deck elements. A SL-Deck consists of lightweight aggregate concrete (LWAC), cast in blocks, and conventional concrete, as shown in Figure 1.2. The LWAC blocks cover the bottom of the SL-Deck and constitute approximately 50% of the total SL-Deck volume, considerably reducing the dead load of the SL-Deck compared with traditional slab elements.

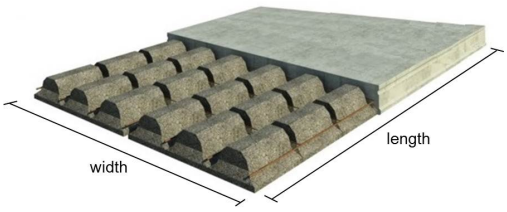

(a) Construction of SL-Deck for indoor use; for use in Pearl-Chain Bridges, the SL-Decks have a duct with a diameter of 80 mm cast into the conventional concrete in the longitudinal bridge direction, centrally between the LWAC blocks. Figure by Abeo.

(b) Demo section of SL-Deck exposing the LWAC blocks and reinforcement to illustrate the principle behind the construction of the SL-Deck.

Figure 1.2: Construction of SL-Deck. The bottom of the SL-Deck is made of LWAC blocks that constitute approximately 50% of the deck's total volume. Pre-stressed reinforcement and slab reinforcement are placed between the LWAC blocks in the longitudinal and transverse direction, respectively, and conventional concrete is cast on top of this.

Definition 1.1
Conventional concrete has a water-to-cement ratio (w/c-ratio) of 0.35–0.50 and a density of 2,200–2,400 kg/m^3.

Definition 1.2
Lightweight aggregate concrete (LWAC) uses lightweight aggregates (LWAs) to obtain a substantially lower mass per unit volume compared to conventional concrete.

The SL-Deck is constructed in such a way that the materials are placed where they are most useful. For most applications, the top of a slab element is typically under compression because the dead load and live loads act in the direction of gravity; therefore, in SL-Decks, conventional concrete is placed at the top of the element to utilize its high compressive strength. The bottom of the slab is typically under tension, and therefore, heavy conventional concrete with a poor tensile strength is replaced by LWAC that has a reduced dead load compared with conventional concrete. At the two SL-Deck ends, at least 200 mm of massive conventional concrete is cast to ensure that the position of the neutral axis is at the center of the cross section, and thus, that the stresses between neighboring elements are transferred evenly. The geometry of the LWAC blocks allows longitudinal pre-stressed reinforcement to be placed at the bottom of the SL-Deck between the LWAC blocks and slab reinforcement to be placed in the transverse direction to transfer the tensile stresses. In addition, a corrugated duct, 80 mm in diameter, is made between the LWAC blocks in the longitudinal direction to enable post-tensioning. In the transverse direction of the SL-Decks, the duct is placed at the center, and in the longitudinal direction of the bridge, the position and curvature of the duct inside the SL-Deck is chosen to follow the arch shape and not to cause any bending moments in the arch; however, the duct meets the end of the SL-Deck at a 90-degree angle to avoid bending the post-tensioning wires at the interface between adjacent SL-Decks.

Collecting several SL-Decks on a number of wires, like pearls on a string, and post-tensioning the wires, creates the Pearl-Chain arch. The number of post-tensioning wires through this duct varies from bridge to bridge. The number of SL-Decks collected on the wires and the number of Pearl-Chain arches placed next to each other determine the span and width of the particular Pearl-Chain Bridge. The concrete elements at the two ends of the Pearl-Chain arches are not SL-Decks, but rather are specially designed abutment concrete elements. These elements are heavily reinforced to transfer the large stress concentration from the anchoring of the post-tensioning wires. The Pearl-Chain arch is two-hinged, with a saddle-bearing hinge between the abutment and the abutment element. The horizontal reaction forces at the bridge ends are either transferred to foundations or through a horizontal tension tie that connects the two bridge ends, as discussed in Section 1.2.3. In the transverse direction, the shear force and moments between the arches are transferred through reinforcement in so-called hammerhead joints (Halding, Hertz and Schmidt, 2015).

The Pearl-Chain arch is stabilized by placing a fill material above the arch between spandrel walls that are first installed along the longitudinal bridge edges. Finally, the road surface is cast on top of the fill material. Especially for long bridge spans, it can be highly advantageous to apply the concept of a “sandwich arch”, where a pre-stressed concrete top plate above the fill exchanges forces with the arch through shear in the fill. If desired, the road surface can be placed on the concrete top plate, or the concrete top plate itself can be used as the road surface. Figure 1.3 shows the principal construction with the main parts of a Pearl-Chain Bridge without a concrete top plate.

The first Pearl-Chain arches constructed were shallow compared with the

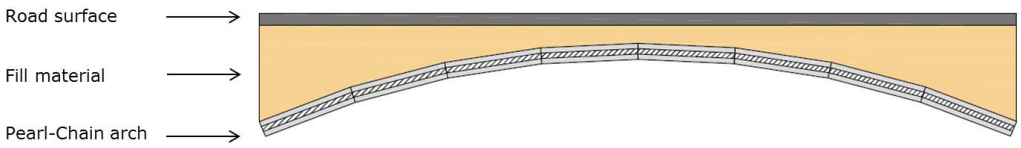

Figure 1.3: Sketch of longitudinal cross section of a Pearl-Chain Bridge.

structures of other prefabricated arch bridge solutions (Long *et al.*, 2014; Bernini, 2000). This means they did not work on the principle of soil-structure interaction in which the passive soil pressure on the arch contributes to the load-carrying capacity of the bridge by resisting the load on the arch (Bernini, 2000). However, for arch bridges with a large rise-to-span ratio, the soil-structure interaction is an important part of the load-carrying capacity.

1.2.2 Construction and emplacement of Pearl-Chain arches

To simplify the assembly, the Pearl-Chain arch is placed on its side. The SL-Decks are emplaced next to each other in the desired arch shape as shown in Figure 1.4. The figure shows the construction of a 13 m-long test Pearl-Chain arch in Denmark in 2014.

(a) One abutment element and three SL-Decks.

(b) One abutment element and four SL-Decks.

(c) Two abutment elements and six SL-Decks.

Figure 1.4: Sequence of emplacement of 13 m-long test Pearl-Chain arch in Denmark in 2014.

After emplacement, self-compacting mortar joints are cast between the SL-Decks (Lund *et al.*, 2015), as shown in Figure 1.5a. Subsequently, the Pearl-Chain arch is post-tensioned (Figure 1.5b).

Upon completion, the Pearl-Chain arch is tilted and lifted into place using a crane (Halding, Hertz, Petersen and Kennedy, 2015). The entire Pearl-Chain arch can be constructed next to the road, and depending on the span and width of the bridge, the Pearl-Chain arch can be put into place overnight.

(a) Installation of formwork for mortar joints.

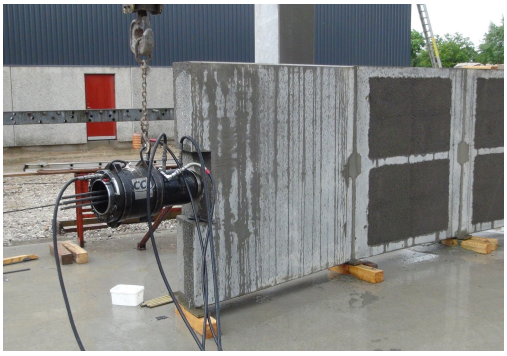

(b) Post-tensioning of the Pearl-Chain arch.

Figure 1.5: Placement of mortar joints between the SL-Decks in the Pearl-Chain arch and post-tensioning of the Pearl-Chain arch.

1.2.3 Advantages and disadvantages of Pearl-Chain Bridges

Compared with traditional technologies for constructing road and railway bridges, Pearl-Chain Bridge technology has the following important advantages:

- The Pearl-Chain Bridge technology reintroduces the arch structure as an economical beneficial solution for road and railway bridges.
- Traffic disruption is minimized because the Pearl-Chain arch can be constructed adjacent to the road and road closure is required only when the Pearl-Chain arch is lifted into place, usually at night. Spandrel walls must be installed before traffic can resume.
- The length and the width of the Pearl-Chain Bridge can easily be varied to fit the relevant project, based on the number of SL-Decks selected and the number and length of the Pearl-Chain arches.
- The combination of LWAC and conventional concrete in the SL-Decks reduces the dead load of the Pearl-Chain arches, which makes it possible to lift longer spans with a single crane.
- Because the SL-Decks in the Pearl-Chain arch are plane, they can easily be stacked on a truck bed for transport to the construction site.
- The material consumption of concrete, especially reinforcement, is minimized because of the static optimal arch shape.
- Because of the arch-shaped structure, water drains naturally from the superstructure, minimizing the moisture exposure of the concrete and optimizing the bridge's lifespan.

The most important limitations and disadvantages of the Pearl-Chain technology compared with other types of construction are:

- The Pearl-Chain Bridge technology has not yet been used for curved bridges.

- For a shallow Pearl-Chain arch, as used in the first Pearl-Chain Bridge (Section 1.2.4), the horizontal forces at the ends of the Pearl-Chain arch are large. Even a small decrease in the rise of the arch causes a considerable increase in the horizontal reaction forces. In such case, the requirements to the rigidity of either the foundations or the horizontal tension tie – whichever solution is chosen to transfer the horizontal forces – are high.

1.2.4 Pearl-Chain Bridge crossing Vorgod Stream

In 2015 the very first Pearl-Chain Bridge was constructed over Vorgod Stream in Jutland, Denmark. The bridge, which carries a road with the load classified for 50 tonnes (DS 1991-2, 2003; DS 1991-2 DK NA, 2003), consists of a 13 m-long arch with a pile height of 0.9 m, and two adjacent 6.5 m-long half arches for a total span of 26 m. Four Pearl-Chain arches were placed next to each other to obtain a width of 6.1 m. Emplacement of the entire Pearl-Chain arch (Figure 1.6a) took only six hours. Figure 1.6b shows the finished bridge.

(a) Emplacement of Pearl-Chain arch.

(b) Finalized Pearl-Chain Bridge crossing Vorgod Stream.

Figure 1.6: Pearl-Chain Bridge crossing Vorgod Stream in Jutland, Denmark. This is the very first Pearl-Chain Bridge that was ever constructed. Photos by Abeo.

The construction and completion of the Pearl-Chain Bridge crossing Vorgod Stream was a revolutionary milestone because the bridge demonstrated that the design and construction of Pearl-Chain Bridges could meet current standards.

1.3 Materials in Pearl-Chain Bridges

Various types of construction materials are used in Pearl-Chain Bridges. In the remainder of this thesis, I distinguish the materials used in the Pearl-Chain arch from the fill material placed above it.

1.3.1 Fill material

After the Pearl-Chain arches are placed and spandrel walls installed, a fill material is laid out, which stabilizes the arch by providing a considerable dead load distributed over the entire arch. Moreover, the fill material supports the road surface, and transfers the loads from the road surface to the arch. Typical fill materials for arch bridges can be divided into two categories:

- Granular (unbound) materials
- Cementitious (bound) materials

Most Danish arch bridges use sub-base gravel as fill material because it is inexpensive and is typically considered a permeable material. However, other types of fill materials should be considered for Pearl-Chain Bridges, too, such as cement-stabilized gravel and pervious concrete, because the choice of fill material enables new construction principles and possibly improves the longevity of the Pearl-Chain Bridges. Cement-stabilized gravel has improved strength properties compared with sub-base gravel. Similarly, pervious concrete has improved strength properties, in addition to a significant void content that provides excellent drainage compared with sub-base gravel and cement-stabilized gravel. Depending on the bridge design and the type of fill, the material can transfer only vertical stresses or also transfer shear stresses between the road surface and the Pearl-Chain arch (sandwich arches, see Section 1.2.1). When the fill material transfers only the vertical traffic loads, the requirements for strength and stiffness are low. However, in constructions in which the fill material also transfers shear stresses, and thereby has a significant structural function, these requirements are raised. For all structural systems, the fill material must drain well to prevent water accumulation and to minimize the exposure of the concrete arch to moisture. In addition, the fill should be easy to place. For arch bridges working on the principle of soil-structure interaction, the placement of the fill is a very critical part of the bridge construction because the filling operation creates one of the most severe loads on the arch structure.

1.3.2 Materials in the Pearl-Chain arch

1.3.2.1 Conventional concrete in SL-Decks

The concrete used for the SL-Decks in Pearl-Chain Bridges is a self-compacting conventional concrete for aggressive environments because the superstructure of the Pearl-Chain Bridges is in an aggressive environment (DS/EN 1992, 2008; DS/EN 1992 DK NA, 2013; Concrete Bridge—GN-P, 2014); however, if the bridge deck is constructed without waterproofing, the environment is classified as extra aggressive (Concrete Bridge—SWP-P, 2012). The concrete used for the SL-Decks in the very first Pearl-Chain Bridge (Section 1.2.4) contained Portland cement, CEM II 52.5 N, with a w/c-ratio of 0.38. Concrete sand with a density of 2,650 kg/m^3, 0.1% absorption and a gradation of 0–2 mm was used with a single granite fraction of 4–16 mm, having a density of 2,770 kg/m^3 and 0.2% absorption. The gradation curves for the materials are shown in Figure 1.7.

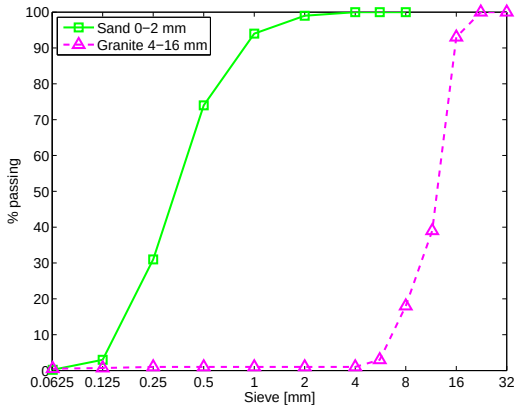

Figure 1.7: Gradation of 0–2 mm concrete sand, and 4–16 mm granite in conventional concrete in SL-Decks for the very first Pearl-Chain Bridge.

Moreover, combined and synthetic air entrainment (AEA), superplasticizer (SP) with polyether-ester as the active component, and accelerator (AC) with nitrate as the active component were used. The AEA, SP, and AC dosages were 0.35%, 0.68% and 1.0% of the powder mass, respectively. The concrete mix design is shown in Table 1.1.

Table 1.1: Mix design for conventional concrete for aggressive environments used in SL-Decks for the very first Pearl-Chain Bridge.

Material	Mass [kg/m^3]
Cement, CEM II 52.5 N	455.0
Water	144.2
Air entrainment	1.57
Superplasticizer	3.07
Accelerator	4.55
Sand 0–2 mm	698.6
Granite 4–16 mm	1,047.9
Density	2,354.9

1.3.2.2 Lightweight aggregate concrete in SL-Decks

Lightweight aggregate concrete is an overall term for a wide range of concrete mix designs that use lightweight aggregates to obtain a substantially lower mass per unit volume than conventional concrete (Definition 1.2). In Denmark, LWAC is typically classified into two categories: (1) structural LWAC with 28-day compressive strengths of 10–70 MPa (Chandra and Berntsson, 2002), and (2) non-load-carrying LWAC for blocks with a low density of approximately 500–900 kg/m^3 (Busch, 2003a). The LWAC used for Pearl-Chain Bridges, and SL-Decks in general, belongs mainly to the second category; hence, in this study, the term "LWAC" refers to category (2). Various types of LWA can be used to produce LWAC, including light expanded clay

aggregate (Leca), one of the most common types. Leca is fabricated from plastic clay that is heated and expanded in a rotary kiln at 1,100°C by which spherical particles form with a very porous core and a less porous shell (Busch, 2003a). Other common materials used as LWA are shale and slate. The LWA used for the LWAC in SL-Decks is Leca® from Weber Denmark, which dominates the Danish market, although many suppliers exist. LWAC blocks have been used in Denmark since 1939. Today, the most typical fields of application are various wall constructions, such as outer walls, partition walls and basement walls, and foundations in which the excellent thermal properties of LWAC are used to minimize thermal bridges. The two most common LWAC block densities are 600 kg/m^3 and 800 kg/m^3 with characteristic compressive strengths of 2.3 MPa and 3.8 MPa, respectively. The thermal conductivity of such LWAC blocks is considerably reduced compared with conventional concrete; Busch (2003b) provides guiding values. Moreover, the sound insulation and fire resistance of LWAC are much better than those of conventional concrete.

Because the SL-Decks carry the load in Pearl-Chain Bridges, the LWAC in the SL-Decks must have certain strength properties; however, the density of LWAC still needs to remain low to reduce the weight of the SL-Decks and to optimize their acoustical and fire-resistant properties. Table 1.2 summarizes the strength and density requirements[2,3] for the LWAC in SL-Decks for Pearl-Chain Bridges.

Table 1.2: Requirements for the 28-day compressive strength, f_c, and dry density, ρ_d, of LWAC in SL-Decks in Pearl-Chain Bridges.

f_c [MPa]	ρ_d [kg/m^3]
> 3.0	700

The LWAC blocks in the SL-Decks are produced on a LWAC block machine. Figure 1.8 shows the patented LWAC block machine that can place a maximum of six LWAC blocks across the width of the SL-Deck. Figure 1.8b shows the entire production of the SL-Decks.

Figure 1.9 shows the geometry of a single LWAC block. Each block has a total volume of 26 liters. The distinctive block geometry allows reinforcement to be placed in the longitudinal and transverse direction between the LWAC blocks in the SL-Deck.

Today, the LWAC has been developed for SL-Decks used indoors; however, the requirements of LWAC in SL-Decks used in buildings and that in Pearl-Chain Bridges differ, and the LWAC mix design for the bridges must be improved, for example, to be freeze-thaw resistant.

[2]This strength requirement relates to a *characteristic* value; however, the data set obtained in this PhD study is not considered large enough to support the calculation of characteristic values. Therefore, all strength properties determined in the following chapters are calculated as *average* values. This is the case for all materials tested as part of this PhD study.

[3]The density requirement relates to an *average* value rather than a characteristic value because it is not unambiguous whether a larger density is an advantage or not.

(a) Patented LWAC block machine. The LWAC block machine can place a maximum of six LWAC blocks next to each other across the width of a SL-Deck. Two horizontal vibrators (yellow) are installed in one end of each mold.

(b) Ongoing casting of SL-Decks. The LWAC blocks have been cast, reinforcement has been laid out, and conventional concrete is being poured on top. The photo shows the casting of SL-Decks for indoor usage; hence, there is no duct for post-tensioning cables.

Figure 1.8: LWAC block machine and production of SL-Decks.

1.3.2.3 Mortar joints between SL-Decks

The mortar joints between the SL-Decks in the Pearl-Chain arch transfer the forces among the SL-Decks; however, such cement-based joints are rarely used as load-carrying elements in other types of bridge constructions, and therefore, their strength and durability should be documented carefully. Because each Pearl-Chain arch consists of several SL-Decks, a Pearl-Chain Bridge contains several mortar joints. These mortar joints are 20 mm wide, but are wider around the ducts for post-tensioning wires to allow the ducts of neighboring SL-Decks to be connected by hand. Because the Pearl-Chain arch is assembled on its side, the mortar joints are placed with a height of up to 2.40 m, depending on the width of the SL-Decks in the arch. However, 2.40 m is the standard width of the SL-Decks. To ease the casting procedure, a commercialized expansive, self-compacting mortar product is used for the mortar joints to eliminate shrinkage cracks and provide sufficient strength.

The mortar joints in Pearl-Chain Bridges are considered a weak link in the durability of the Pearl-Chain arch because the post-tensioning wires in the Pearl-Chain arch pass through the joints. Hence, if the joints are not sufficiently resistant to water and chloride ingress, the post-tensioning wires are exposed to possible corrosion, a fatal for the overall stability of the bridge when the post-tensioning wires are needed after bridge erection.

In the longitudinal bridge direction between the Pearl-Chain arches, the longitudinal joints and the hammerhead joint recesses (Section 1.2.1) are also cast with mortar. These joints are first cast when the Pearl-Chain arches are placed, and thus have a low placing depth corresponding to the deck thickness or less. Because they are not horizontal, but curved as the arch, they are cast with a dry low slump

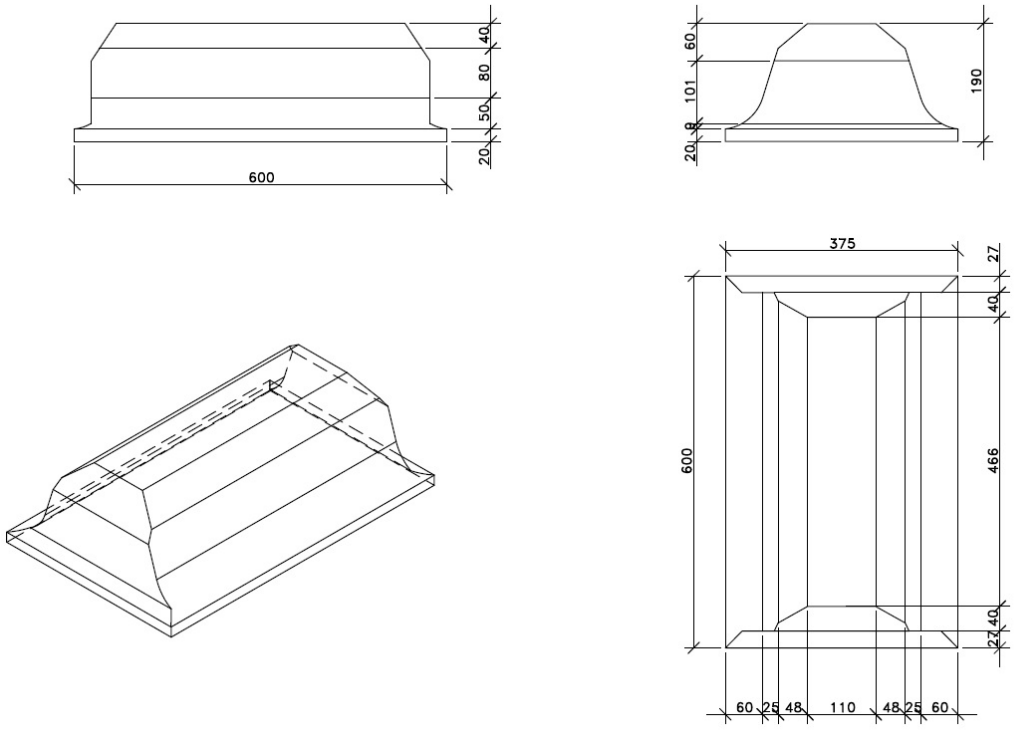

Figure 1.9: Geometry of LWAC block for SL-Decks. Dimensions are in mm.

mortar rather than a self-compacting mortar.

1.4 Durability and lifespan of Pearl-Chain Bridges

In general, the durability and lifespan of concrete structures are closely related, yet differently defined. Durability is often considered a single property, even though it is not a property, but rather a general term that covers a wide range of parameters. Portland Cement Association defines concrete durability as "*the ability of concrete to resist weathering action, chemical attack, and abrasion while maintaining its desired engineering properties*" (Portland Cement Association, 2016). Hence, durability of concrete structures concerns the concrete's resistance to various damaging mechanisms. The durability is considerably connected to the presence of cracks, which often reduce concrete strength, and work as an easy passage for water and chlorides to penetrate the concrete. The most common issues in concrete durability are described below; however, many other durability related topics, such as leaching, creep, separation, acid attacks, and physical damages, also exist (Poulsen *et al.*, 1985).

- **Alkali-silica reactions**. Aggregates (such as porous flint) containing reactive silica minerals react with alkalies from the cement and/or from external sources, such as deicing salt, under the presence of water and high pH-value.

Thus, a swelling gel around or inside the aggregates is produced that causes severe crack formation in the cement paste.

- **Carbonation**. Carbon dioxide from the surrounding air reacts with calcium hydroxide in the cement paste, which decreases the pH-value of the concrete pore solution. The alkaline protective reinforcement environment breaks down, which can initiate reinforcement corrosion.

- **Chloride ingress**. Chloride ions from sea water or deicing salt can penetrate the concrete through the pore solution. A concentration of chloride ions in excess of the critical chloride threshold can initiate depassivation of the reinforcement, and eventually, corrosion.

- **Freeze-thaw attacks**. Frost damage occurs if the pore structure of the cement paste is not designed with a sufficiently fine entrained air system and the concrete is exposed to repeated freezing and thawing under the influence of water or salt water. Concrete frost damage is typically considered as either 'internal damage' or 'surface scaling'. Different theories such as the hydraulic pressure theory and the microscopic ice body growth theory attempt to explain the mechanisms behind freeze-thaw damaging of concrete; however, researchers still seek for a greater understanding because not all mechanisms are yet fully understood.

- **Shrinkage:**

  - *Autogenous shrinkage.* The deformation of cement paste taking place under autogenous conditions (that is, completely sealed and isothermal) because of several physical and chemical phenomena such as self-desiccation (Jensen and Hansen, 1994).
  - *Drying shrinkage.* The deformation of hardened cement paste taking place because of the loss of capillary water during drying. The cement paste contracts, and the resulting tensile stresses can cause shrinkage cracking. All concretes are exposed to drying shrinkage during hydration.
  - *Plastic shrinkage.* The deformation of fresh cement paste taking place because of a reduction in the volume of fresh concrete caused by severe drying before setting.

- **Sulfate attack**. Sulfate ions, typically from water, react with the hydration products of the cement paste, which causes an increase in the volume of the cement paste due to formation of ettringite. This leads to crack formation.

- **Thermal damages**. A large temperature increase during concrete hardening causes damages of the cement paste structure that becomes more porous. Moreover, large temperature variations cause temperature dependent deformations that build up tensile stresses and can cause thermal cracking.

In practice, these degradation mechanisms can be overcome through careful design of the concrete according to the environment where it will be used.

Lifespan, or service life, of concrete structures often relates to the state at which the reinforcement corrodes; however, the degree of corrosion crucial to the termination of this so-called lifespan is not well defined. The lifespan of concrete structures is conditioned by their durability, and thus, the two terms are linked. Bridges are designed for a service life of a minimum of 100 years, whereas all other constructions are designed for only 50 years (Bourke, 2010). A lifespan of 100 years should first of all be considered as an indication of the importance of constructing new bridges with a high standard of the materials used. For Pearl-Chain Bridges, the lifespan is even longer, 120 years, which emphasizes using materials with particularly good durability properties. However, despite the increased requirements to durability of bridges, they are often much more exposed to the surroundings than other types of constructions. A bridge is a sensitive point in a road construction because it freezes from both below and above. Road signs are often placed to warn drivers that bridges freeze and become slippery before the road (see Figure 1.10).

(a) Bispebuen bridge, Copenhagen. (b) Nova Scotia, Canada.

Figure 1.10: Road signs warning drivers that bridges freeze before roads and that extra caution should be taken at freezing temperatures. Photos by Mia S. M. Lund.

In mild climate countries like Denmark, the many annual freeze-thaw cycles have a harsh impact on bridges, particularly in areas where deicing salt is used to decrease the freezing point of roads during winter. The freeze-thaw durability of the materials in the Pearl-Chain Bridges is closely related to their permeability or water absorption properties since water must be present for materials to deteriorate from freezing and thawing. In fact, water is a condition of most other damaging mechanisms discussed. All structural elements of Pearl-Chain Bridges should be designed to be resistant to the listed durability topics by using materials that are made to endure an aggressive environment (DS/EN 1992, 2008; DS/EN 1992 DK NA, 2013). However, not all of the degradation mechanisms, such as alkali-silica reactions and sulfate attacks, are relevant for Pearl-Chain Bridges.

According to the Danish regulations, all upper horizontal concrete surfaces used in bridge decks must be protected by waterproofing (thick coating) to minimize moisture exposure (Danish Road Directorate, 2010). Various types of thick coating exist, but the most commonly used is bitumen-based. However, for arch bridges, the regulations allow a so-called thin coating, such as geotextile, except for the joints, which should still be protected with a bitumen coating. Because the SL-Decks are prefabricated, they are cast under more controlled conditions than the concrete used for in situ bridges, and therefore, the quality of the concrete is improved and the risk of defects minimized. Stoltzner, Wegan, and Henriksen (2005) suggested that a concrete deck cast without any defect has the economic advantage of not requiring waterproofing. Moreover, the concrete used for Pearl-Chain Bridges has a low w/c-ratio, which makes it more resistant to water and chloride ingress than concretes with a higher w/c-ratio. Finally, the water that penetrates the fill material and reaches the upper surface of the arch structure drains naturally toward the bridge ends because of the arch curvature. All these factors are expected to minimize the moisture exposure of the Pearl-Chain arch, and positively influence the durability of Pearl-Chain Bridges. Waterproofing for Pearl-Chain Bridges may not be needed at all.

1.5 Scope and objectives

The scope of this project is to ensure that the materials used in Pearl-Chain Bridges have the necessary strength and durability to yield a 120-year lifespan for the bridges. Hence, this thesis focuses on *various* materials used in Pearl-Chain Bridges. For the Pearl-Chain arch, these materials include the mortar joints and the lightweight aggregate concrete that have not yet been applied for such purpose. Possible fill materials to be placed on the Pearl-Chain arch include sub-base gravel, cement-stabilized gravel, and pervious concrete. Other materials used in Pearl-Chain Bridges are generally used for all types of bridge constructions, and therefore, are not included. These include, for example, the conventional concrete in the SL-Decks that is a "standard" concrete for aggressive environments, which has been developed and tested at concrete mixing plants such as mixing plant A for this study, and the mortar cast between the Pearl-Chain arches in the longitudinal bridge direction.

The overall objectives of the PhD project are to:

- Identify and understand the challenges concerning the durability of all materials in Pearl-Chain Bridges
- Develop and implement suitable materials for Pearl-Chain Bridges
- Test the materials in Pearl-Chain Bridges to various conditions, such as freeze-thaw and water and chloride ingress
- Document the durability of the materials in Pearl-Chain Bridges, since any new technology has to be thoroughly tested and well-described

- Demonstrate the applicability of the Pearl-Chain Bridge technology by participating in a full-scale construction of a Pearl-Chain Bridge

1.6 Thesis outline

The structure of this thesis follows the "paper based model", which means that scientific papers constitute the following chapters. I selected this model because the project relates to various materials that have been developed and tested for their applicability in Pearl-Chain Bridges; therefore, this thesis is a collection of individual projects under the same "Pearl-Chain Bridge umbrella":

Hence, the project had three main focus points:

1. The **fill material** above the Pearl-Chain arch (chapter 2)
2. The **mortar joints** in the Pearl-Chain arch (chapter 3)
3. The **lightweight aggregate concrete** in the SL-Decks (chapter 4)

Chapter 2, which discusses the durability of the fill material in Pearl-Chain Bridges, includes a collection of four journal papers and one conference paper related to three different types of fill: sub-base gravel, cement-stabilized gravel, and pervious concrete. The first journal paper (Paper I) describes the determination of strength, permeability, and freeze-thaw durability of the three materials, and compares their properties to find the most optimal fill material for Pearl-Chain Bridges. The second journal paper (Paper II) describes the implementation of pervious concrete in the Pearl-Chain Bridge over Vorgod Stream, and the tests performed beforehand to develop the mix design and casting procedures applied during the full-scale implementation. The third journal paper (Paper III) describes different approaches to improve the strength and durability of the pervious concrete mix designed for fill in Pearl-Chain Bridges, such as the addition of AEA, SP, fibers, and pre-wetted lightweight sand (expanded shale). The conference paper (Paper IV) describes the freeze-thaw durability of pervious concrete, and compares freeze-thaw results from tests on hardened pervious concrete with air void analysis for six different pervious concrete mix designs. The fourth journal paper (Paper V) describes permeability tests and freeze-thaw tests made on two Danish sub-base gravel materials to determine their frost susceptibility, which should be negligible, according to Danish road regulations based on empirical knowledge.

Chapter 3, which discusses durability of the mortar joints in the Pearl-Chain arch, consists of one journal paper (Paper VI) describing the approaches to develop mortar joints that will not show shrinkage cracking. The paper describes tests performed to investigate the strength and durability properties of the joints.

Chapter 4 concerns the durability of the LWAC in the SL-Decks. The approach to this topic started on a very fragile foundation because most knowledge about LWAC is based on experience and undocumented scientifically. Moreover, I faced challenges in enlisting cooperation from industry. Consequently, the final results and conclusions about LWAC are certainly interesting, but more experimental work is required to have sufficient data for publication in a scientific journal. Therefore, chapter 4 provides a summary of the experimental work on LWAC and recommendations for future studies.

Finally, chapter 5 summarizes the main findings of this PhD study.

1.7 Publications arising from thesis

Five ISI journal papers were written and submitted based on work carried out during this PhD project. Moreover, five conference papers, of which one is part of this thesis, were accepted for proceedings and presentation at international conferences.

Journal papers arising from thesis

Paper I **Lund MSM**, Hansen KK, Hertz KD. Experimental investigation of different fill materials in arch bridges with particular focus on Pearl-Chain Bridges. Constr Build Mater. 2016;124:922–36.

Paper II **Lund MSM**, Hansen KK, Truelsen R, Johansen L. Pervious concrete fill in Pearl-Chain Bridges: Using small-scale results in full-scale implementation. Constr Build Mater. 2016;106:404–14.

Paper III **Lund MSM**, Kevern JT, Schaefer VR, Hansen KK. Mix design for improved strength and freeze-thaw durability of pervious concrete used as fill in Pearl-Chain Bridges. Mater Struct. 2017;50:42-56.

Paper V **Lund MSM**, Hansen KK, Andersen IB. Frost susceptibility of sub-base gravel used in Pearl-Chain Bridges: an experimental investigation. Int J Pavement Eng. 2016, doi: 10.1080/10298436.2016.1230429.

Paper VI **Lund MSM**, Hansen KK, Arvidsson M. Durability of vertically cast mortar joints in Pearl-Chain Bridges. Submitted to Construction and Building Materials in 2016.

Conference papers arising from thesis (included)

Paper IV **Lund MSM**, Kevern JT, Hansen KK, Schaefer VR. Evaluation and comparison of freeze-thaw tests and air void analysis of pervious concrete. In: Maekawa K, Kasuga A, Yamazaki J, editors. Proceedings of the 11th fib International PhD Symposium in Civil Engineering; 2016 Aug 29–31; Tokyo, Japan. Tokyo: The University of Tokyo; 2016. p. 245–52.

Conference papers arising from thesis (not included)

- **Lund MSM**, Hansen KK, Hertz KD. Frost resistance and permeability of cement stabilized gravel used as filling material for Pearl-Chain Bridges. In: Bastien J, Rouleau N, Fiset M, Thomassin M, editors. Proceedings of the 10th fib International PhD Symposium in Civil Engineering; 2014 Jul 21–23; Québec, Canada. Québec: Research Center on Concrete Infrastructure (CRIB), Université Laval; 2014. p. 155–60.
- **Lund MSM**, Hansen KK. Shrinkage properties of cement stabilized gravel. In: The Nordic Concrete Federation, editors. Proceedings of XXII Nordic Concrete Research Symposium; 2014 Aug 13–15; Reykjavik. Oslo: Norsk Betongforening; 2014. p. 303–06.
- **Lund MSM**, Hansen KK, Hertz KD. Experimental study of properties of pervious concrete used for bridge superstructure. In: Proceedings of 12th International Symposium on Concrete Roads; 2014 Sep 23–26; Prague.
- **Lund MSM**, Arvidsson M, Hansen KK. Homogeneity and strength of mortar joints in Pearl-Chain Bridges. In: Proceedings of fib Symposium; 2015 May 18–20; Copenhagen. p. 187–88.

CHAPTER 2

Durability of fill materials in Pearl-Chain Bridges

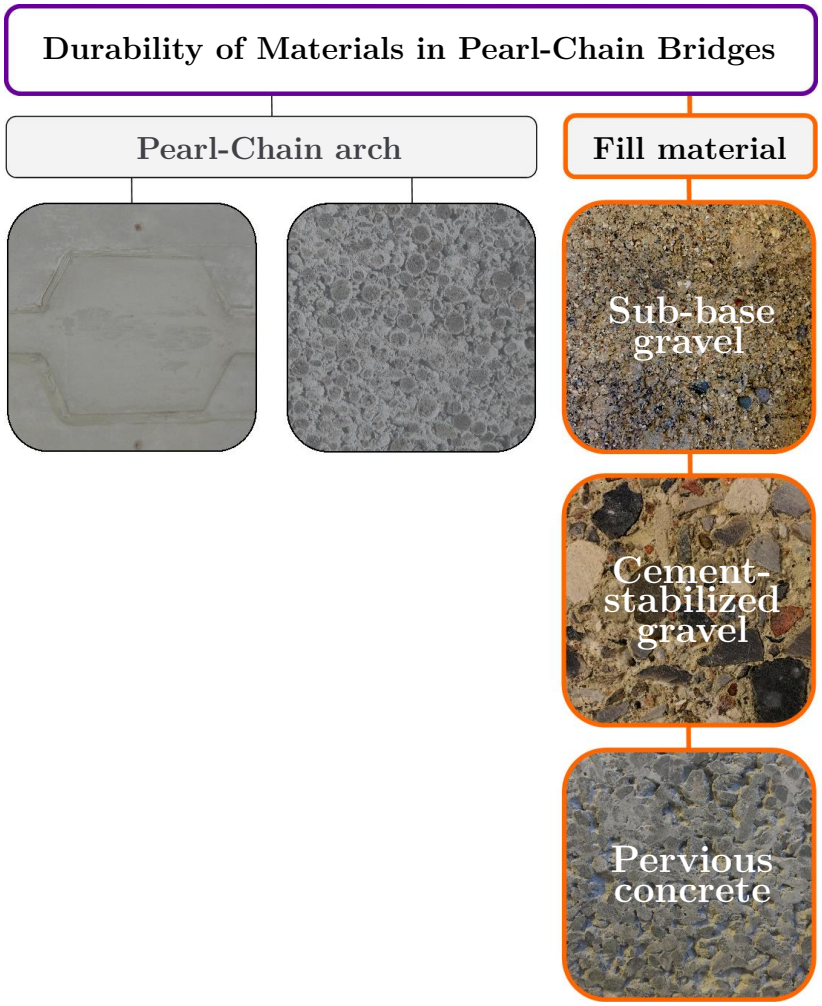

Paper I

"Experimental investigation of different fill materials in arch bridges with particular focus on Pearl-Chain Bridges"

M.S.M. Lund, K.K. Hansen, and K.D. Hertz

Published in: *Construction and Building Materials, 2016;124:922–36*

Construction and Building Materials 124 (2016) 922–936

Contents lists available at ScienceDirect

Construction and Building Materials

journal homepage: www.elsevier.com/locate/conbuildmat

Experimental investigation of different fill materials in arch bridges with particular focus on Pearl-Chain Bridges

M.S.M. Lund *, K.K. Hansen, K.D. Hertz

Technical University of Denmark, Department of Civil Engineering, Brovej 118, DK-2800 Kgs, Lyngby, Denmark

HIGHLIGHTS

- The strength and durability of three fills for arch bridges were tested and compared.
- Sub-base gravel, cement-stabilized gravel and pervious concrete were investigated.
- Advantages and disadvantages for the three fill materials are listed.
- Recommendations for fill in Pearl-Chain Bridges are given.

ARTICLE INFO

Article history:
Received 28 February 2016
Received in revised form 29 June 2016
Accepted 15 July 2016

Keywords:
Arch bridge
Cement-stabilized gravel
Fill material
Pearl-Chain Bridge
Pervious concrete
Sub-base gravel

ABSTRACT

Pearl-Chain Bridge technology is a recently developed prefabricated arch solution for road and railway bridges allowing faster, more environmentally friendly, and cheaper bridge construction. This study compared the strength and durability properties of three different types of fill material to find the most optimal fill for Pearl-Chain Bridges. Sub-base gravel, cement-stabilized gravel, and pervious concrete were tested with respect to compressive strength, stiffness, splitting tensile strength, permeability, freeze–thaw durability, and shrinkage. This paper summarizes the advantages and disadvantages of implementing the different types of fill material in arch bridges, particularly in Pearl-Chain Bridges.

1. Introduction

The fill material resting on the arch in closed-spandrel arch bridges is an important part of the construction with respect to the bridge's structural system and the durability. Bridges are designed for a service lifetime of a minimum of 100 years, whereas all other constructions are designed for only 50 years [1]. This length of time places certain requirements on the materials used in bridges, including the fill material. A typical closed-spandrel arch bridge consists of the arch structure itself (made of concrete or masonry), spandrel walls, and a fill material, as shown in Fig. 1.

The static system of an arch bridge is based on the arch being in constant compression, first of all because of the considerable dead load from the fill material. Even when the arch is exposed to tensile stresses, such as from traffic loads, the compression force in the arch arising from the dead load of the fill is so large that the resulting force is most often also a compression force. Thus, reinforcement is rarely found in old masonry arches, such as the ancient Roman viaducts, and many of these arch constructions still exist 2000 years after they were constructed, which bears witness of the superiority of this type of construction. However, the fill material in arch bridges is more than dead load ensuring stabilization of the arch; it also supports the road surface and in arch constructions with a large rise/span ratio, the fill contributes to the load carrying capacity of the arch structure through soil-structure interaction in which the passive soil pressure on the arch structure helps resist the horizontal forces from the load [2]. Until now, fill has only transferred vertical traffic loads from the road surface to the arch, and does so for the present Pearl-Chain Bridge research project described in Section 1.2.4; however, during the project the inventor of Pearl-Chain structures, Kristian Hertz, discovered a possibility of increasing the load-bearing capacity of the arch bridge by incorporating the fill as a structural part of a new design, which he calls a "sandwich arch bridge" (see Section 1.2.4).

* Corresponding author.
E-mail addresses: msml@byg.dtu.dk (M.S.M. Lund), kkh@byg.dtu.dk (K.K. Hansen), khz@byg.dtu.dk (K.D. Hertz).

http://dx.doi.org/10.1016/j.conbuildmat.2016.07.089
0950-0618/

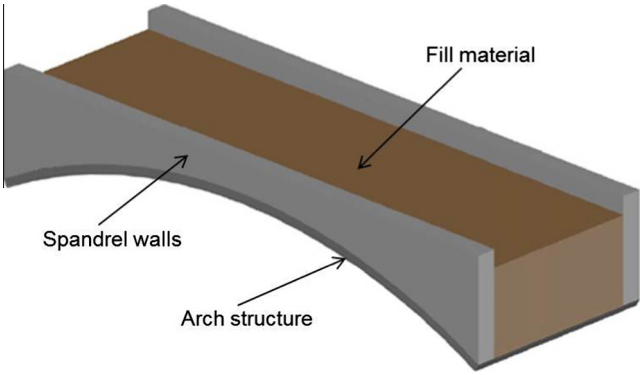

Fig. 1. Typical closed-spandrel arch bridge construction with arch structure, fill material, and spandrel walls to retain the fill.

Throughout history, various types of fill have been used worldwide, depending on several factors, such as economic considerations and the static system of the arch bridge. Typical types of fill can be divided into two categories:

- Granular (unbound) materials including soil [3–5].
- Cementitious (bound) materials [6,7].

The fill material itself is a vulnerable part of the construction. Fill made from poor quality material or with a lack of compaction is sensitive to deterioration and defects [3]. Water trapped in the fill because of bad drainage or poor permeability can cause problems during winter when the bridge is exposed to freezing from below, above, and from the sides. Negative temperatures of the surrounding air create a freezing front that moves through the fill, and if the fill material is granular and water is trapped in it, ice crystals form and coalesce into ice lenses that can cause frost heaving. The expansion of the fill due to frost heaving will damage the construction by either exerting a high pressure on the spandrel walls or by cracking and deteriorating the road surface. Moreover, water trapped in granular fill reduces the strength of the fill material, which also results in the bridge's overall deterioration. Several examples show how old arch bridges have been strengthened by replacing old granular fill with concrete fill [3]. However, cementitious fill materials are also sensitive to frost exposure. Freezing and thawing can cause internal damages as well as scaling if the pore structure of cementitious materials is not properly designed; therefore, concrete used as fill material must be designed carefully to avoid this result.

1.1. Fill used in Danish in situ arch bridges

To create an overview of the fill material used in previous bridges, we reviewed the accessible drawings of Danish closed spandrel arch bridges. Among the approximately 11300 Danish bridges registered as road- or railway-carrying, less than 5% are closed-spandrel arch bridges. The number comprises all bridges owned by the Danish Road Directorate and the Danish railway traffic, but only 70% of the Danish municipal bridges, since these latter are not sufficiently registered. However, since most arch bridges are older, the amount of technical drawings is limited. For all bridges with accessible technical documentation, a well-grained, often coarse grained, gravel material was prescribed to be filled around the arch. In some cases this well-draining gravel material was only prescribed for the fill in the vicinity of 30 cm of the arch, and the remaining fill was either a well-compacted sand fill or a cement-stabilized gravel fill. We did not see any examples of concrete fill.

1.2. Fill used in prefabricated arch bridge systems

The arch is rarely chosen for in situ bridges nowadays because of the extensive scaffolding usually required to construct arch bridges. This requirement involves comprehensive preparatory work, intensive labor, and road closure for weeks because the scaffold and formwork take up a lot of space. Because it is no longer economically beneficial to cast in situ arch bridges, a number of different prefabricated arch bridge systems have been developed. However, currently none of these prefabricated arch systems have gained ground in Denmark. We will now review three examples of well-established prefabricated arch bridge systems that are all so-called closed-spandrel arch bridges that work on the principle of soil-structure interaction. Finally, we will present the newly developed Danish Pearl-Chain Bridge technology that can be constructed without application of expensive curved molds and erected quickly without unnecessarily disturbing traffic.

1.2.1. The FlexiArch bridge system

The Macrete FlexiArch bridge system was developed in Ireland, and currently more than 40 FlexiArch bridges have been constructed. The arch structure is made of unreinforced precast concrete voussoirs connected by a flexible polymeric geotextile bonded to the top of all elements. The arch is flat on the ground, but shapes when it is lifted [1]. Two different types of fill have been tested on the FlexiArch bridges: a low-strength concrete backfill and a granular backfill. When using granular backfill, the gradation of the gravel was found to have a large influence on the load capacity. A well-graded fill resulted in lower deflections and higher load capacity than fill that was not well-graded. Developers of the FlexiArch system have not specifically defined a "well-graded fill"; however, they have found that the strength of FlexiArch bridges was much higher when using concrete backfill rather than granular backfill. Moreover, economical reasons urge the use of concrete backfill rather than granular because concrete needs no compaction, inhibits the ingress of flood water, and also allows the bridge to be used for traffic just a few days after installation [7].

1.2.2. The TechSpan bridge system

The TechSpan bridge system was developed in the United States, and currently more than 500 TechSpan bridges have been constructed. The superstructure is made of two-piece, funicular curve-shaped, precast arches that are lifted into place using a crane. The total width of the bridge depends on the number of arches placed next to each other. The arch is filled with a granular material. The fill material around the arch is divided into three zones. Zone 1 is select granular material placed 1.0 m around the perimeter of the arch structure. Compaction of the material in zone 1 may be achieved through a light walk. Zone 2 fill material is placed vertically and horizontally around zone 1. Compaction of the material in zone 2 may be achieved with heavy compaction equipment without any vibration. Zone 3 is all remaining fill around the arch, with compaction achieved with heavy compaction equipment with vibration [4]. The type of fill used in zone 2 and 3 is not prescribed.

1.2.3. The BEBO arch system

The BEBO arch system was developed in Switzerland, and currently more than 800 BEBO arch bridges have been constructed. The arch construction is similar to that of the TechSpan arch. For smaller spans a single concrete element is used, but larger spans require two elements per arch. The description of the fill requirements for the BEBO arch system are more detailed compared with the FlexiArch and TechSpan systems. The fill is an integrated load-carrying part of the bridge structure, and therefore, must permanently fulfill that purpose. The filling operation creates one of the

most severe loads experienced by the structure; hence, the operation must be carefully planned and realized. The fill material should be granular with angular grains, and should be well-graded. The material around the arch is divided into three zones. Zone A describes all material not included in zone B and C. The material used in zone A should have properties and compaction procedures equal to that of normal road embankments. Zone B describes the fill material located 2.0 m around the perimeter of the arch from the footings of the arch and up to 3/4 of the height of the arch. The material used in zone B should be granular and should not exceed 75 mm in diameter. The gradation should fall within the limits in Fig. 3 [5]. Granular materials with a high content of silt and clay are unacceptable for backfill in zone B, unless they are stabilized with cement to improve their strength. The water content should allow maximum compaction; hence it should be compacted a minimum of 98% of the maximum dry density as determined by the standard proctor test. The fill placed 0.3 m around the perimeter of the arch in zone A and B should be compacted only with hand-operated equipment. Zone C describes the road section and consists of gravel, asphalt, or concrete [5].

1.2.4. The Pearl-Chain Bridge system

The Pearl-Chain Bridge system was developed in Denmark after 2013, and currently only one of these bridges has been constructed. The Pearl-Chain arch is constructed of Super-Light Decks (SL-Decks) that are collected on a post-tensioning wire, like pearls on a string [8]. Each SL-Deck is given a slight inclination at the ends, and has a duct cast through it longitudinally. Thus, the Pearl-Chain arch is formed from plane elements. To simplify the assembly, the Pearl-Chain arch is placed on its side; when the SL-Decks are emplaced, self-compacting mortar joints are cast between the decks, after which the arch is post-tensioned [9]. Next, a crane tilts and lifts the arch and places it at the correct location [10]. The entire arch is constructed next to the road, and depending on the span and width of the bridge, the Pearl-Chain arch can be placed during a night. After installation of spandrel walls, the fill material is laid out, and the road surface is placed on the fill.

Especially for long bridge spans, it can be highly advantageous to apply the new concept of a "sandwich arch", where a pre-stressed concrete top plate above the fill exchanges forces with the arch through shear in the fill. It is therefore important that the fill material is able to transfer shear stresses for these future applications.

Compared with the FlexiArch, TechSpan, and BEBO arch systems, the rise/span ratio of the very first Pearl-Chain Bridge was considerably shallower, and the bridge did not work on the soil-structure interaction principle. Fig. 2 shows a longitudinal cross-section of the bridge.

1.3. Fill materials tested in the current study

In this study, three different fill materials were tested to determine the most appropriate fill material for Pearl-Chain Bridges. The materials tested were sub-base gravel (SG), cement-stabilized gravel (CG), and Portland cement pervious concrete (PCPC). Sub-base gravel was tested because it is the most common fill material in Danish arch bridges, is inexpensive, and is typically considered a permeable material used for purposes in which the permeability of other types of gravel is too low. Moreover, the fines content of sub-base gravel is so low that the material is expected to be frost safe, avoiding frost heave [12]. Cement-stabilized gravel was tested because it is also relatively inexpensive due to its low cement content and also because it, opposed to sub-base gravel, is able to transfer shear stresses. Pervious concrete has a significant void content—typically 11–35% [13]—providing excellent drainage. We tested pervious concrete because we expected its permeability properties to be improved compared to sub-base gravel and cement-stabilized gravel and because it is able to transfer shear stresses.

The strength and durability properties of the three different types of fill material were tested and compared for their compressive strength, Young's modulus, splitting tensile strength, permeability, freeze–thaw durability and shrinkage behavior. Different testing standards and procedures apply for different materials, which naturally caused some challenges for comparison of the materials.

2. Experimental method

2.1. Material properties

2.1.1. Material properties for sub-base gravel

Two types of Danish sub-base gravel were tested. Type SG8 had a gradation of 0–8 mm and type SG32 had a gradation of 0–32 mm. The two materials represent a geographical variation in the gradation of sub-base gravels in Denmark. Depending on where a Pearl-Chain Bridge is to be constructed, the gradation of a possible sub-base fill will vary. Fig. 3 shows the gradation curves for the two sub-base gravels. SG8 had 1.1% particles with a diameter of less than 0.063 mm and for SG32 the fines content was 2.4%.

2.1.2. Material properties for cement-stabilized gravel

One type of gravel, CG16, with a gradation of 0–16 mm, as shown in Fig. 3, was used to prepare the cement-stabilized gravel specimens. The gradation was thereby within envelope B in the Danish Standard (DS) 14277-1 [14], with an oversize of 7% on the 16 mm sieve. Envelope B describes well-graded coarse aggregates with a limited fines content that can be successfully compacted to meet the requirements for hydraulically bound materials [14]. Moreover, the cement-stabilized gravel specimens

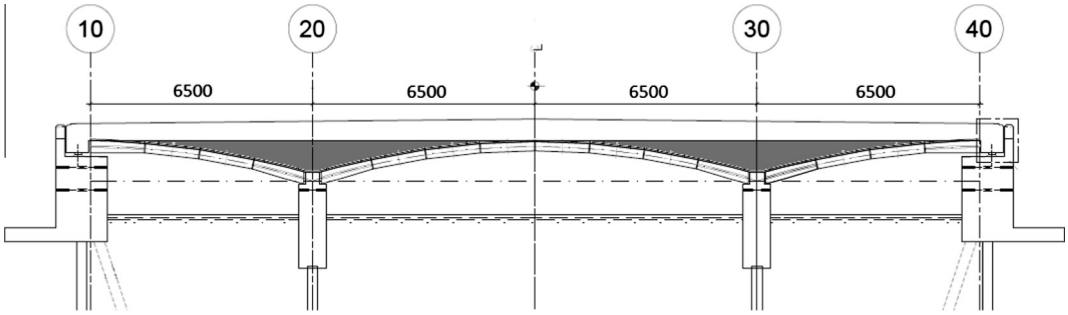

Fig. 2. Longitudinal cross section of the very first Pearl-Chain Bridge constructed in Denmark in 2015. Dimensions are in mm. From: Lund et al. [11].

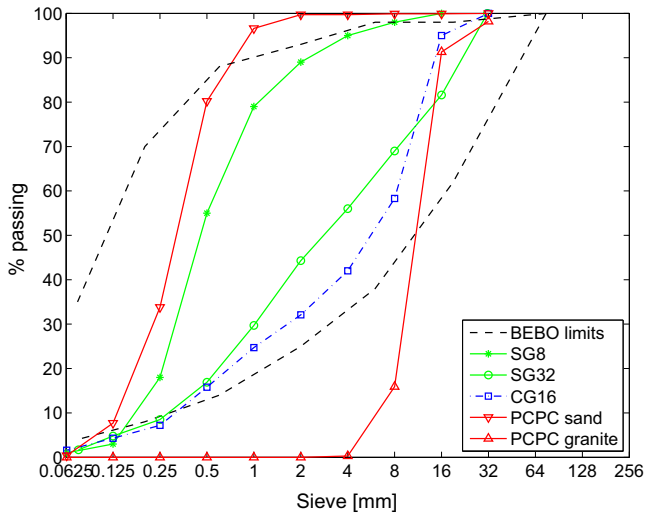

Fig. 3. Gradation curves for sub-base gravel (SG), gravel used for cement-stabilization (CG), and sand and granite used for pervious concrete (PCPC). The BEBO limits show the gradation of the fill material used in the BEBO arch system, zone B.

were prepared with low alkali Portland cement, CEM I 42.5 N, with a particle density of 3210 kg/m^3.

2.1.3. Material properties for pervious concrete

Pervious concrete consists of cement, water, sand and a single-sized coarse aggregate that is used to maximize the void content. Crushed granite was used as coarse aggregate. The granite had a particle density of 2670 kg/m^3, absorption of 0.5%, and a gradation of 8–16 mm as shown in Fig. 3. Concrete sand with a gradation of 0–2 mm as shown in Fig. 3, a particle density of 2630 kg/m^3 and absorption of 0.5%, was used as fine aggregate. Portland cement, CEM II/A-LL 52.5 N, with a particle density of 3100 kg/m^3, and Danish fly ash type B4 with a particle density of 2300 kg/m^3 also were used. Moreover a combined natural and synthetic air entrainment (AEA) was used.

2.2. Mix designs

2.2.1. Mix design of sub-base gravel

The optimal water content and maximum dry density was determined for gravels SG8 and SG32 using the vibrating table method, as described in the DS 13286-5 standard [15]. Thereby, the necessary amount of water for the two sub-base mixes and the maximum dry density were found as shown in Table 1.

In the mix design of sub-base gravel specimens the water content was one percentage point less than the optimal water content corresponding to water saturation determined from the vibrating table method as recommended in the Danish design guide for sub-base of sand and gravel [12]. Table 2 shows the mix designs for SG8 and SG32.

Table 1
Optimal water content, w_{opt}, and maximum dry density, $\rho_{d,max}$, for sub-base gravel (SG) and gravel used for cement-stabilization (CG). SG8 and SG32 have a gradation of 0–8 mm and 0–32 mm, respectively, as explained in Section 2.1.1. CG4% and CG5% contain 4% cement and 5% cement, respectively, as explained in Section 2.2.2.

	SG8	SG32	CG4%	CG5%
w_{opt} [%]	12.8	7.9	7.1	8.0
$\rho_{d,max}$ [kg/m^3]	1911	2171	2249	2235

Table 2
Mix designs for sub-base gravel (SG), cement-stabilized gravel (CG) and pervious concrete (PCPC). SG8 and SG32 have a gradation of 0–8 mm and 0–32 mm, respectively, as explained in Section 2.1.1. CG4% and CG5% contain 4% cement and 5% cement, respectively, as explained in Section 2.2.2.

	Cement [kg/m^3]	Fly ash [kg/m^3]	Water [kg/m^3]	AEA [kg/m^3]	Gravel [kg/m^3]	Sand [kg/m^3]
SG8	–	–	220	–	1851†	–
SG32	–	–	154	–	2143†	–
CG4%	90	–	179	–	2146†	–
CG5%	113	–	160	–	2134†	–
PCPC	340	68	105	5.3	1300	121

† Dry mass.

2.2.2. Mix design of cement-stabilized gravel

The cement contents for the cement-stabilized gravel specimens were chosen as 4% and 5% of the dry material in an attempt to design specimens corresponding to strength classes $C_{5/6}$ and $C_{12/15}$ with 28-day compressive cylinder strengths of 5 MPa and 12 MPa, respectively [14]. For economic reasons, the lowest possible cement content for Pearl-Chain Bridges is desired. The optimal water content was determined from proctor tests in accordance with the DS 13286-2 standard [16] by including the influence of both cement contents on the compaction of the gravel [17]. The cement content was substituted with the equivalent amount of fly ash, since the particle size distribution of the two materials is similar and fly ash does not react with water. Thereby, we determined the necessary amount of water for the mixes. Table 1 shows the optimal water content and the maximum dry density of cement-stabilized gravel with 4% cement (CG4%) and 5% cement (CG5%) determined from the proctor tests. Table 2 shows the mix designs for the cement-stabilized gravel specimens.

2.2.3. Mix design of pervious concrete

The pervious concrete mix was designed to have a water-to-cement (w/c) ratio of 0.29, a fly ash-to-cement ratio of 20%, and 9.5% of the mass of coarse aggregate replaced by sand [18]. Moreover, we designed it to have a void content of 17.5% and 6% entrained air. For Pearl-Chain Bridges the pervious concrete mix design should be kept as simple as possible for economic reasons. Therefore, for example, the mix design tested in this study did not include other additives than air entrainment. Table 2 shows the mix design.

2.3. Preparation of specimens

2.3.1. Preparation of sub-base gravel specimens

The sub-base gravel specimens were prepared by mixing sub-base gravel and water for 10 min in a pre-wetted compulsory mixer. Afterwards, we prepared the specimens as described in the American Society for Testing and Materials (ASTM) D5918-13 standard [19] with only a few deviations. The specimens were compacted in 150 mm high acrylic molds assembled from six cylindrical acrylic pieces, each with an inside diameter of 140 mm and a height of 25 mm. A 1 mm thick butyl membrane with an outer diameter of 140 mm sealed the specimens inside the mold. A circular plate with a diameter of 140 mm placed was below the mold, and the membrane was stretched around the circular plate and the top of the mold, allowing room for the specimen to be compacted. To compact the specimens, we placed the mass of gravel corresponding to the inside volume of the acrylic mold in the mold in five loads of equal heights, applying 56 blows from a rammer to each load. For SG32, we also used vibration. After compaction, we saturated the specimens using capillary absorption by placing them in water reaching 50 mm up the sides of

the specimen for three days. The compaction degree, defined as the ratio between the actual dry density of the specimen and the optimal dry density determined from laboratory tests, was above 97% for all specimens. A more detailed description of the preparation of the specimens is found in Lund et al. [20].

2.3.2. Preparation of cement-stabilized gravel specimens

The cement-stabilized gravel specimens were prepared by mixing gravel, low alkali cement, and water for three minutes in a pre-wetted compulsory mixer. The specimens were cast in split molds with a diameter of 150 mm and a height of 300 mm, using the vibrating table compaction method, according to the European Standard (EN) 13286-50 [21]. The mass of the mixture corresponding to the inside volume of the mold was placed in the mold during compaction with a rammer. The minimum degree of compaction was 97%, and therefore, in agreement with the specifications in the Danish general work specification for hydraulic bound layers [22]. After curing for one day at 20 °C, the molds were split and the specimens were cured in water at 20 °C until they achieved an age of 28 days.

2.3.3. Preparation of pervious concrete specimens

The pervious concrete specimens were prepared by first mixing the aggregates and 5% of the cement for one minute in a pre-wetted compulsory mixer. This process was done to coat all aggregates with cement to improve the mixture's strength [13]. Afterwards, air entrainment mixed with water in the ratio 1:9 was added to the mix. Finally, fly ash, the remaining cement and water was added and mixed for three minutes. The mixture was allowed to rest for three minutes and then mixed for an additional two minutes. The workability of the mixture was considered good because it was possible to form a ball without the paste draining off [23]. The air content in the fresh pervious concrete was measured to 6% with a press-ur-meter, using boiled and then cooled, demineralized water to eliminate air bubbles in the water from affecting the reading. The specimens were prepared in molds 150 mm in diameter and 300 mm high, with a collar attached to enable overfilling before compaction. We determined the mass of pervious concrete that corresponded to the inside volume of the mold from the mix design density, and then placed the material in the mold in a single lift. By using a mass of 40 kg—corresponding to a pressure of 22.2 kPa—the specimen was compacted from above to a height of 300 mm. Hereby the cylinder achieved the mix design void content of 17.5%; however, because the compaction was applied from above, there was a variation in void content within the cylinder. Thus, the void content of the bottom half and the top half of the cylinder varied between 9.3–9.8% and 15.6–20.2%, respectively, which meant that specimens cut from the different halves for permeability and freeze–thaw tests had different void contents. No vibration was used when placing the pervious concrete mix in the molds to avoid problems with cement paste draining off the aggregates and to better control the void content. After curing in the molds for one day at 20 °C, the molds were split and the specimens were cured in water at 20 °C until they achieved an age of 28 days.

2.4. Testing procedures

2.4.1. Determination of void content for pervious concrete

We measured the void content of the hardened pervious concrete specimens using the water displacement method based on Archimedes' principle. We measured the mass of the cylinder under water and above water, after removing excess surface water with a wrung cloth and allowing the specimens to drain for 15 min. The void content, P [%], was calculated using the formula:

$$P = \left(1 - \frac{m - m_{sw}}{\rho_w V_{tot}}\right) \times 100\% \quad (1)$$

where m [kg] is the mass of the specimen above water, m_{sw} [kg] is the mass of the specimen submerged in water, ρ_w [kg/m^3] is the water density, and V_{tot} [m^3] is the total volume of the specimen.

2.4.2. Strength and stiffness test setup

The 28-day compressive strength, the 28-day Young's modulus, and the 28-day splitting tensile strength were measured for cement-stabilized gravel specimens and pervious concrete specimens. For both materials, six specimens were measured in each test.

2.4.2.1. 28-Day compressive strength and Young's modulus. For the cement-stabilized gravel specimens the compressive strength and Young's modulus were determined in agreement with the EN 13286-41 standard [24] and the EN 13286-43 standard [25], respectively. For pervious concrete, no standards exist regarding strength determination; therefore, we carried out the compression test as a combination of the procedure described for conventional concrete in the DS 12390-3 standard [26], and in the International Organization for Standardization (ISO) 6784 standard [27]. The compressive tests were performed on a TONI 3000 kN loading machine with a load rate of 3 and 5 kN/s for cement-stabilized gravel specimens with 4% cement and 5% cement contents, respectively, and 7 kN/s for pervious concrete specimens. The strain was measured by installing a system with two rigid rings tightly mounted around the specimens, and two extensometers placed between the rings as shown in Fig. 4a.

2.4.2.2. 28-Day splitting tensile strength. For the cement-stabilized gravel specimens, the splitting tensile strength test was performed in agreement with the EN 13286-42 standard [28], and for pervious concrete it was performed in agreement with the standard for conventional concrete, ISO 4108 [29]. The splitting tensile strength tests were performed on a TONI 3000 kN loading machine with a load rate of 1.8 kN/s for cement-stabilized gravel specimens and 4 kN/s for pervious concrete specimens.

2.4.3. Permeability test setup

Permeability of soils and other permeable materials typically is determined using one of two standard laboratory tests: the falling-head test and the constant-head test. The falling-head test is most suitable for materials with a low permeability, and therefore, we used this method to determine the permeability coefficient for sub-base gravel with a gradation of 0–8 mm and

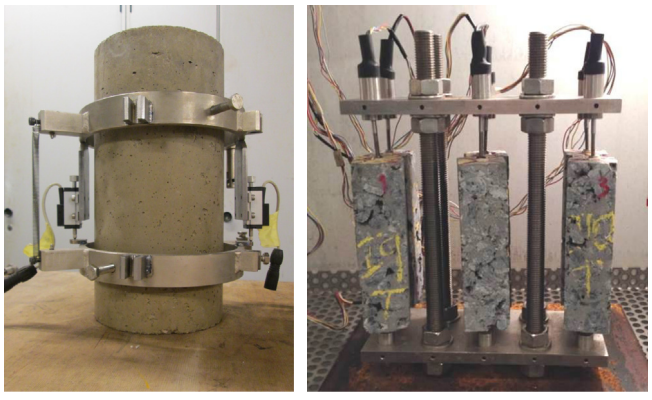

(a) (b)

Fig. 4. Test setups for measurement of strain and shrinkage.

for cement-stabilized gravel. On the other hand, the constant-head test, which is described in the ASTM D2434-68 standard [30], is most suitable for materials with a medium to high permeability. Therefore, we used the constant-head test to determine the permeability coefficient for sub-base gravel with a gradation of 0–32 mm and for pervious concrete.

2.4.3.1. Falling-head test. In the falling-head test, the time difference, t [s], between the initial and final water head difference, $h_1 - h_2$ [m], is used to determine the permeability coefficient at 20 °C, k_{20} [m/s], using the formula:

$$k_{20} = 2.303 \frac{aL}{At} \log_{10} \frac{h_1}{h_2} \frac{\eta_T}{\eta_{20}} \quad (2)$$

where a [m^2] is the cross-sectional area of the standpipe, L [m] is the length of the specimen, A [m^2] is the cross-sectional area of the specimen, η_T [Pa·s] is the water viscosity at the temperature, T [°C], at which the test is conducted, and η_{20} [Pa·s] is the water viscosity at 20 °C.

Fig. 5 shows a principle sketch of the falling-head test setup used to determine the permeability coefficient for cement-stabilized gravel.

The entire setup was sealed in a 3 mm thick rubber membrane with an inner diameter of 150 mm. To assembly the setup, we first pulled the membrane over an aluminum bottom plate, 150 mm in diameter, and closed it tightly using a hose clamp. For the water outlet, a 20 mm hole was drilled at the center of the bottom plate and a plastic tube was connected. Next, a 50 mm layer of 2–4 mm aggregate was placed on the bottom plate inside the rubber membrane and compacted with a rammer to provide a firm and even surface. The aggregate was filled with water, and we adjusted the height of the plastic tube for water outlet to ensure the water level reached exactly the top side of the aggregate layer. Subsequently, a 50 mm high vacuum water saturated cement-stabilized gravel specimen, cut from the center of the 300 mm high cylinder specimens, was placed on the aggregate inside the rubber membrane. Using hose clamps, the rubber membrane and the specimen were tightened together to prevent water from escaping along the specimen sides. Hence, during the experiment, the aggregate below the specimen was filled with water and the underside of the specimen was not in contact with air. Thus, we prevented

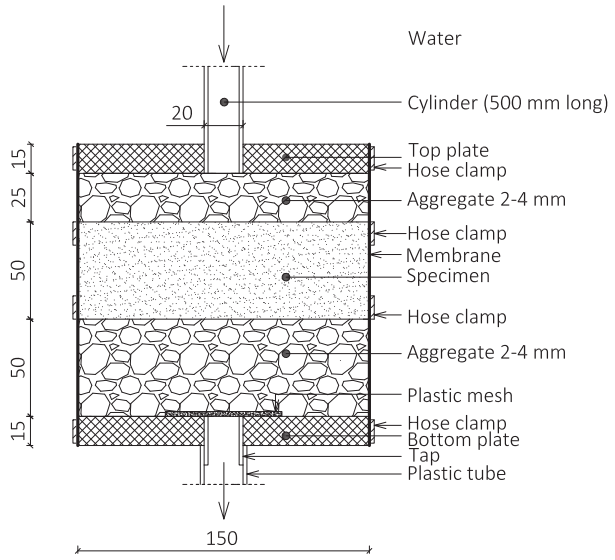

Fig. 5. Test setup for falling-head test of cement-stabilized gravel specimens. Dimensions are in mm.

any menisci from forming in the cement-stabilized gravel specimens. A 25 mm layer of 2–4 mm aggregate was placed on the specimen and compacted lightly so that the surface was firm and even, after which it was filled with water. The permeability of the 2–4 mm aggregate layer was considerably greater than that of the specimen and did not influence the measurements. An aluminum top plate was placed on the aggregate and the rubber membrane was pulled around it, and closed tightly with a hose clamp. A 500 mm high plastic cylinder with a 16 mm inner diameter and a measurement scale along its height was fastened to a 20 mm hole drilled at the center of the top plate to control and measure the water inlet. For the 0–8 mm sub-base gravel, the setup was the same; however, the specimen tested was 125 mm high and was contained in the acrylic cylinder mold inside the rubber membrane.

For the cement-stabilized gravel specimens, the initial water head was 500 mm above the bottom of the specimen, and we monitored the decrease in water head during a period of at least seven days. Three different specimens were tested for cement-stabilized gravel with both 4% cement and 5% cement, and the test was repeated four times for each specimen. For 0–8 mm sub-base gravel, the initial water head was 600 mm above the bottom of the specimen, and we monitored the decrease in steps of 50 mm down to 200 mm above the bottom of the specimen for three specimens.

2.4.3.2. Constant-head test. In the constant-head test a constant water head, h [m], is established on top of a specimen with length L [m] and cross-sectional area A [m^2], and the water volume, Q [m^3], penetrating the specimen during time t [s] is used to calculate the permeability coefficient at 20 °C, k_{20} [m/s], using the formula:

$$k_{20} = \frac{QL}{Aht} \frac{\eta_T}{\eta_{20}} \quad (3)$$

where η_T [Pa·s] is the water viscosity at the temperature, T [°C], at which the test is conducted, and η_{20} [Pa·s] is the water viscosity at 20 °C.

For 0–32 mm sub-base gravel, we used the same setup described for 0–8 mm sub-base gravel (Fig. 5), except that the water level remained constant during the test period. Two constant water heads of 200 mm and 450 mm above the bottom of the specimen were tested for three specimens. For pervious concrete, we used the test setup shown in Fig. 6.

Each 300 mm high pervious concrete specimen was cut in two halves of 150 mm in height, and both were tested. A 3 mm rubber membrane, with an inner diameter of 150 mm, was pulled over a 150 mm high pervious concrete specimen and closed tightly with hose clamps to prevent water from escaping along the specimen sides. An acrylic cylinder with inner and outer diameters of 143 mm and 150 mm respectively, was placed on top of the specimen, inside the rubber membrane. The rubber membrane was tightly closed to the acrylic cylinder to provide a sealed connection. Two constant water heads of 270 mm and 500 mm above the bottom of the specimen were tested for six specimens.

2.4.4. Freeze–thaw test setup

2.4.4.1. Freeze–thaw test of sub-base gravel. The freeze–thaw test of sub-base gravel was performed in accordance with the ASTM D5918-13 standard [19]. The sub-base gravel specimen was installed in the freeze–thaw setup shown in Fig. 7 and two specimens were tested for each type of sub-base gravel.

In the freeze–thaw setup the specimen was placed on an aluminum base plate that fed the specimen with water through the specimen's bottom. The base plate was connected to a tube for

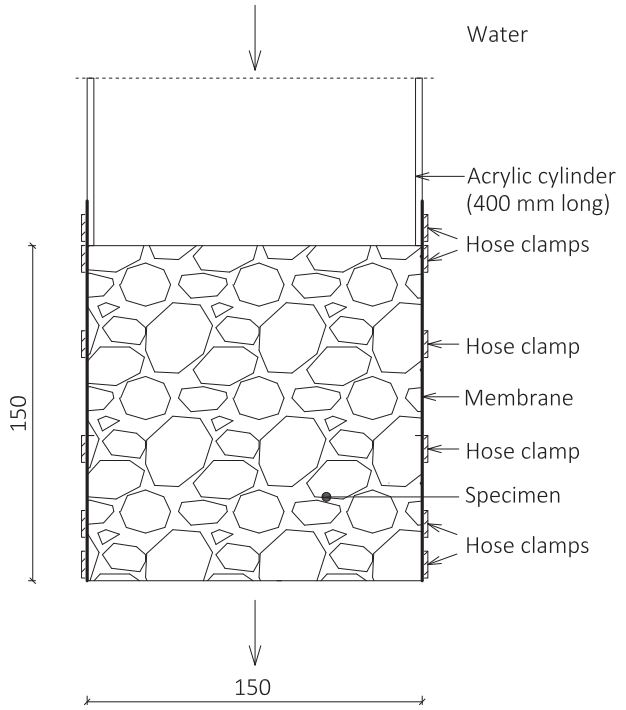

Fig. 6. Test setup for constant-head test of pervious concrete. Dimensions are in mm.

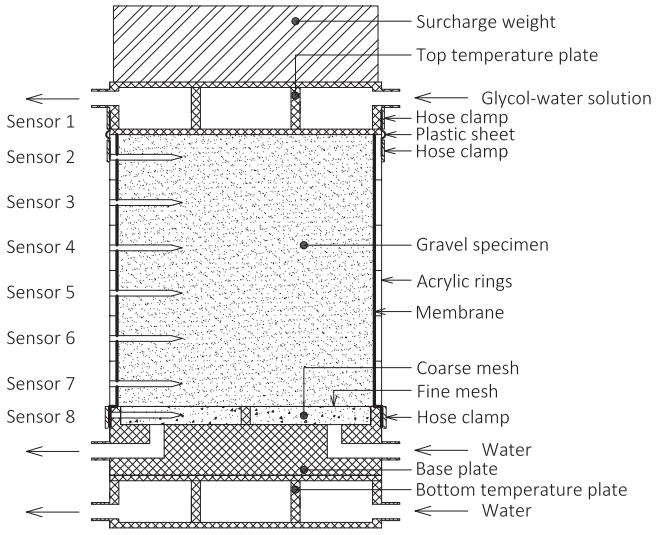

Fig. 7. Setup for freeze–thaw test of sub-base gravel according to the ASTM D5918-13 standard [19]. Thermal insulation around the specimen is not shown.

water outlet and to a Mariotte water supply with a bubble tube that made it possible to adjust the water head to be 5 cm above the bottom of the specimen. The base plate was placed on an aluminum bottom temperature plate that controlled the temperature variation in the specimen from below. By connecting the bottom plate to a temperature bath with a thermostat and a pump unit, water was run through the bottom plate to obtain and maintain the desired temperature variation. The temperature variation of the bottom plate remained positive during the freeze–thaw test, as shown in Table 3.

The temperatures in Table 3 correspond to the values in the ASTM D5918-13 standard [19], corrected with respect to the freezing point depression measured for the sub-base gravels. Moreover,

Table 3
Temperature variation of the two plates with time during the freeze–thaw test of sub-base gravel.

Day	t [h]	$T_{top\ plate}$ [°C]	$T_{bot.\ plate}$ [°C]	Comment
1	24	2.55	2.55	Conditioning
2	8	−3.45	2.55	Freezing period #1
	16	−12.45	0.50	
3	16	11.55	2.55	Thawing period #1
	8	2.55	2.55	Stabilization
4	8	−3.45	2.55	Freezing period #2
	16	−12.45	0.50	
5	16	11.55	2.55	Thawing period #2
	8	2.55	3.00	Stabilization

t = time [h], $T_{top\ plate}$ = temperature of top plate [°C], $T_{bot.\ plate}$ = temperature of bottom plate [°C].

the minimum temperature of the bottom plate was increased from 0 °C to 0.5 °C because the thermostat's temperature band around the set point otherwise caused the temperature of the bottom plate to drop below 0 °C by which the water below the specimen would freeze; however, this was assumed not to influence the results. An aluminum top temperature plate was placed on top of the specimen to control the temperature variation of the specimen from above. As with the bottom plate, the top plate was connected to a temperature bath that controlled the temperature by leading a glycol–water solution through the plate. As Table 3 indicates, freezing of the specimen was initiated from above. A surcharge weight of mass 5.5 kg was laid on the top plate. The entire setup was installed in a refrigerator at a temperature of 2 °C. However, during the test the temperature in the refrigerator varied between −4 °C and 8 °C. The entire setup and the tubes connecting the temperature plates to the temperature baths were covered in 25 mm thick insulation to prevent condensation. Finally, a small hole was made in the insulation on top of the surcharge weight to install an extensometer to measure vertical displacement with an accuracy of 4 μm.

During the freeze–thaw test, we measured the temperature variation in the specimen at six points by inserting temperature sensors in dip pipes into the specimen, as shown in Fig. 7. We also measured the temperature in the water feed below the specimen, directly below the top plate, in the temperature baths, and inside the refrigerator.

It took five days to complete one freeze–thaw test, as shown in Table 3. After an initial 24-h conditioning period, the specimens were exposed to two identical freeze–thaw periods. Each freeze–thaw period consisted of a 24-h freezing period in which the temperature decreased in two steps, and a 16-h thawing period followed by an 8-h stabilization period in which the temperature was brought back to the original.

2.4.4.2. Freeze–thaw test of cement-stabilized gravel. Two cubes measuring $100 \times 100 \times 100$ mm^3 were cut from each of the cement-stabilized gravel cylinder specimens. One of the cubes was exposed to freezing and thawing; to serve as a reference, the other was stored in water at 20 °C for later strength comparison. The freeze–thaw tests were carried out on specimens that were either saturated with water or with a 3% NaCl solution. Fick's second law of diffusion was used to make a conservative estimate of the time needed for the chlorides to penetrate to the core of the specimen. Hence, the specimens to be saturated with salt water were soaked in a 3% NaCl solution for 40 days before they were exposed to freezing and thawing. In total, six specimens were exposed to salt water and six specimens were exposed to demineralized water before freeze–thaw testing for both cement contents.

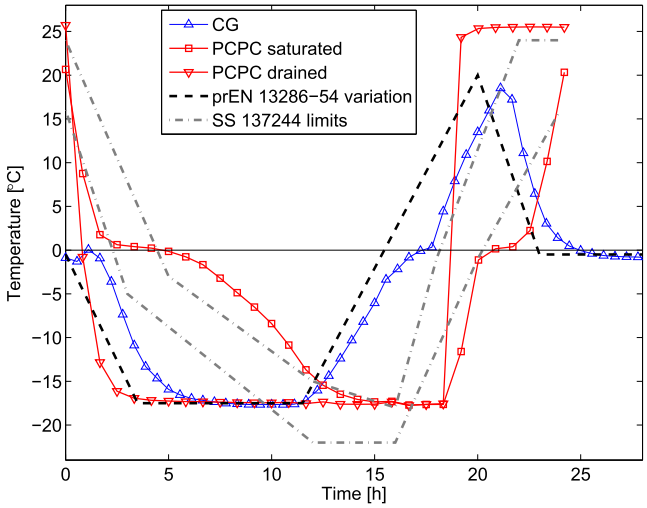

Fig. 8. Core temperatures of cement-stabilized gravel specimens (CG) and pervious concrete specimens (PCPC) during a single freeze–thaw cycle. PCPC saturated = pervious concrete specimens that are frozen in water and thawed in air. PCPC drained = pervious concrete specimens that are frozen and thawed in air. An acceptable temperature variation based on the prEN 13286–54 standard [31] is also shown together with the temperature limits for freeze–thaw test of conventional concrete, as described in the SS 137244 standard [32].

After water saturation and salt water saturation, each specimen was wrapped in two layers of plastic and placed in a freezing cabinet. The temperature variation was chosen in correspondence with the prEN 13286-54 standard [31], and the core temperature of two cubes was measured during the test to ensure that the temperature variation of the specimens was as expected. Fig. 8 shows the temperature variation of a cement-stabilized gravel specimen during a single freeze–thaw cycle that took 28 h to complete. The test was terminated after 56 frost cycles.

After every sixth frost cycle, we recorded the mass loss of each specimen and made a visual assessment of the specimen. Moreover, we measured the ultrasonic wave speed through the specimen. Finally, after 20 cycles and after 56 cycles, we determined the compressive strength for half of the specimens as well as for their references stored in water at 20 °C during the frost tests.

2.4.4.3. Freeze–thaw test of pervious concrete. The freeze–thaw durability of pervious concrete is typically tested according to the same standards as conventional concrete; however, this exposure is typically considered to be too harsh and not representative of on-site behavior, since the drainage nature is not taken into account. In this study, we tested the freeze–thaw durability of the pervious concrete specimens according to these four methods:

1. Saturated method with demineralized water (SMW): specimens freezing and thawing in demineralized water.
2. Saturated method with salt water (SMS): specimens freezing and thawing in a 3% NaCl solution.
3. Drained method with demineralized water (DMW): specimens freezing in air and thawing in demineralized water.
4. Drained method with salt water (DMS): specimens freezing in air and thawing in a 3% NaCl solution.

We included the saturated method as a worst-case scenario, whereas, we considered the drained method to be a more realistic estimate of the actual behavior of pervious concrete due to its excellent drainage properties. However, in real life pervious concrete is not at any time expected to be submerged in water or salt water over a longer period of time and therefore the applied test procedures only represent an adapted reality.

Two cubes measuring $100 \times 100 \times 100\,mm^3$ were cut from each of the pervious concrete cylinder specimens and exposed to freezing and thawing. 12 cubes were used for each of the four different methods, six of them representing the bottom part of the cylinders and six representing the top. Freezing of the specimens took place in a frost room at a temperature of −20 °C for 18 h, and thawing took place in either demineralized water or in a 3% NaCl solution with a constant temperature of 25 °C for six hours. The salt water was changed every sixth cycle. Fig. 8 shows the variation of the core temperature of a pervious concrete specimen exposed to the saturated method and of a pervious concrete specimen exposed to the drained method during a single frost cycle that took 24 h to complete. Moreover, the figure shows the temperature limits prescribed in the Borås method for testing scaling of conventional concrete during freeze–thaw according to the Swedish Standard (SS) 137244 standard [32]. Because the boundary conditions in this study differed significantly from the Borås method, the temperature variation in the study also differed from the Borås method.

After every sixth frost cycle, the ultrasonic wave speed and the mass loss were recorded for each specimen. After 24 cycles and after 56 cycles the compressive strength was determined for half of the specimens. The compressive strength was also determined for reference specimens that were not exposed to freezing and thawing but were cast at the same time as the specimens that were. The test was terminated after 56 frost cycles.

2.4.5. Shrinkage test setup

We measured shrinkage only for cement-stabilized gravel. The specimens in the shrinkage tests were cut from the cylinder specimens and measured $40 \times 40 \times 150\,mm^3$. The specimens were mounted in vertical position in a steel frame in a climate chamber with a temperature range from −10 °C to 60 °C and a relative humidity range of 10–95%. Extensometers with an accuracy of 2 μm and a measuring range of ±5 mm were used to measure displacements. Three specimens were tested for each cement content. The setup in the climate chamber is shown in Fig. 4b. We conducted a total of four different tests to investigate the temperature dependent shrinkage and the moisture dependent shrinkage. In all tests the boundary conditions were reasonable estimates of the expected influence from the surrounding climate on the fill material in a bridge. In the first test, the relative humidity was fixed at 65% and the temperature varied between 5 °C and 20 °C; in the second, the relative humidity was fixed at 65% and the temperature varied between 5 °C and 40 °C; and in the third test, the temperature was fixed at 20 °C and the relative humidity varied between 65% and 85%. Finally, the temperature was fixed at 20 °C and the relative humidity varied between 45% and 85% in the fourth test. In all four tests, the boundary conditions were first changed when a steady deformation was obtained. For tests with a variation in temperature, a steady deformation was obtained after three days; whereas it was obtained after seven days in tests with a variation in relative humidity. The steady deformation was determined when the variation in deformation was less than 0.005 per mile during a 12 h period. Furthermore, we made two repetitions to support the observations [33].

We calculated the shrinkage induced by the variation in either temperature or relative humidity as the difference in strain between the measured steady strain at, for example, 5 °C and 20 °C for a fixed relative humidity. The strain calculations for a temperature variation were corrected with respect to the deformation of the steel frame that holds the specimen in position. This was done by estimating the coefficient of linear temperature expansion of the steel frame itself by inserting an Invar steel bar in the frame. Because Invar steel has a negligible coefficient of linear temperature expansion, we assumed the deformation

measured over the Invar steel bar would correspond to the deformation of the steel frame. For the variation in temperature, the coefficient of linear temperature expansion was calculated using the formula:

$$\varepsilon = \alpha \Delta T \quad (4)$$

where ε [–] is the strain, α [°C^{-1}] is the coefficient of linear temperature expansion and ΔT [°C] is the temperature difference.

3. Results

3.1. Strength property results

Table 4 shows the 28-day compressive strength, the 28-day Young's modulus, and the 28-day splitting tensile strength for cement-stabilized gravel and pervious concrete tested in this study and Young's modulus for sub-base gravel.

Danish road standards prescribe the value of Young's modulus for sub-base gravel as 0.150 GPa [34]. For the cement-stabilized gravel specimens, the 28-day compressive strength and the 28-day Young's modulus increased by 97% and 55%, respectively, when increasing the cement content by 25%. The 28-day splitting tensile strength increased by 100%. The strength properties of the pervious concrete specimens relate to specimens having an average void content of 18.1%.

3.2. Permeability results

Table 5 shows the results from the permeability tests.

The permeability coefficient of sub-base gravel was approximately five times larger when using gravel with a gradation of 0–32 mm compared with 0–8 mm. For cement-stabilized gravel, the permeability coefficient of specimens containing 5% cement was approximately five times smaller than for specimens containing 4% cement. For pervious concrete, the permeability coefficient varied with the void content, as expected, and the permeability coefficient for specimens with 20.2% voids was approximately nine times larger than for specimens with 9.3% voids.

Table 4
28-day compressive strength (f_c), Young's modulus (E), and splitting tensile strength (f_s), for sub-base gravel (SG), cement-stabilized gravel (CG) and pervious concrete (PCPC). SG8 and SG32 have a gradation of 0–8 mm and 0–32 mm, respectively, as explained in Section 2.1.1. CG4% and CG5% contain 4% cement and 5% cement, respectively, as explained in Section 2.2.2. P is void content. Table values are based on Danish road regulations [34].

	Test results			Table values
Material	f_c [MPa]	E [GPa]	f_s [MPa]	E [GPa]
SG8	–	–	–	0.150
SG32	–	–	–	0.150
CG4%	6.2	14.7	2.6	11.5
CG5%	12.3	22.8	5.2	18.0
PCPC, $P = 18.1\%$	9.9	16.2	1.5	–

Table 5
Permeability coefficients, k_{20}, for sub-base gravel (SG), cement-stabilized gravel (CG) and pervious concrete (PCPC). SG8 and SG32 have a gradation of 0–8 mm and 0–32 mm, respectively, as explained in Section 2.1.1. CG4% and CG5% contain 4% cement and 5% cement, respectively, as explained in Section 2.2.2. P is void content.

Material	Average [cm/s]	Std. dev. [cm/s]
SG8	7.3×10^{-4}	1.4×10^{-4}
SG32	35.1×10^{-4}	12.2×10^{-4}
CG4%	7.2×10^{-8}	15.8×10^{-9}
CG5%	1.4×10^{-8}	5.3×10^{-9}
PCPC, $P = 9.3\%$	7.4×10^{-2}	3.7×10^{-2}
PCPC, $P = 20.2\%$	69.3×10^{-2}	30.2×10^{-2}

3.3. Freeze–thaw durability results

3.3.1. Freeze–thaw results for sub-base gravel

The frost susceptibility of gravels tested according to the ASTM D5918-13 standard [19] are assessed from the 8-h heave rates, based on the deformation that occurred during the first and second freezing period. Table 6 shows the heave rates for both specimens for each of the sub-base gravels.

In climates where many annual frost cycles take place, such as Denmark's, the second heave rate should be used to evaluate the frost susceptibility according to the ASTM D5918-13 standard [19]. On a frost susceptibility scale with classifications of negligible, very low, low, medium, high and very high, the frost susceptibility of sub-base gravel with a gradation of 0–8 mm was negligible; however, it was medium for sub-base gravel with a gradation of 0–32 mm.

3.3.2. Freeze–thaw results for cement-stabilized gravel

During the freeze–thaw exposure of the cement-stabilized gravel specimens, the maximum mass loss was 0.5%, considered insignificant. Also, there were no visual signs of degradation or scaling. However, we observed a decrease in the compressive strength as indicated in Fig. 9. This figure compares the compressive strength of the specimens exposed to freezing and thawing

Table 6
8-h heave rates during frost cycles #1 and #2, and frost susceptibility classifications for sub-base gravels. SG8 and SG32 have a gradation of 0–8 mm and 0–32 mm, respectively, as explained in Section 2.1.1.

Specimen no.	Heave rate #1 [mm/day]	Heave rate #2 [mm/day]	Frost susceptibility classification
SG8-1	1.4	0.3	Negligible
SG8-2	0.8	0.4	Negligible
SG32-1	7.1	5.4	Medium
SG32-2	6.9	4.1	Medium

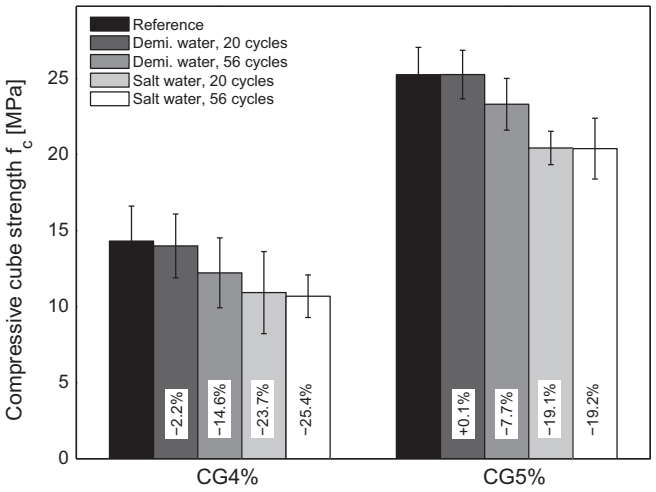

Fig. 9. Compressive cube strength for cement-stabilized gravel specimens after 20 frost cycles and 56 frost cycles compared to reference specimens unexposed to freezing and thawing. The results are divided between specimens with 4% cement (CG4%) and 5% cement (CG5%) exposed to either demineralized water or a 3% NaCl solution.

Table 7
Relative decrease in wave speed, v_{rel}, for cement-stabilized gravel specimens with 4% cement (CG4%) and 5% cement (CG5%) saturated with demineralized water or a 3% NaCl solution and exposed to 56 frost cycles.

	Demi. water		Salt water	
	CG4%	CG5%	CG4%	CG5%
v_{rel} [%]	41.8	22.9	64.5	46.2

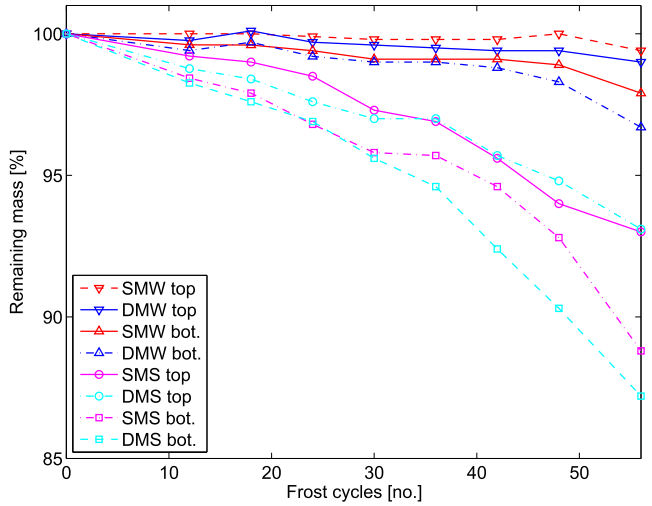

Fig. 10. Remaining mass during freezing and thawing of pervious concrete specimens. SMW = Saturated method with demineralized water, DMW = Drained method with demineralized water, SMS = Saturated method with salt water, and DMS = Drained method with salt water, top = top specimens with a void content of 9.8%, bot. = bottom specimens with a void content of 15.6%.

for 20 days and 56 days with the reference compressive strength determined for specimens unexposed to freezing and thawing. The reference values represent an average of the reference compressive strengths determined after 20 cycles and 56 cycles since no difference between these strengths was observed. The results are divided between specimens with 4% and 5% cement.

Table 7 shows the relative change in wave speed between 0 and 56 frost cycles for the cement-stabilized gravel specimens with 4% cement and 5% cement either saturated with demineralized water or with a 3% NaCl solution. For all specimens, the wave speed was approximately 4,100 m/s before frost exposure, and therefore independent of the percentage of cement content.

3.3.3. Freeze–thaw results for pervious concrete

The evaluation of freeze–thaw damages of pervious concrete is complicated by the already large influence of the void content on pervious concrete properties. A direct evaluation can be made only between specimens with the same void content.

We observed no change in the ultrasonic wave speed for the pervious concrete specimens exposed to freezing and thawing; however, a change in mass loss was detected. Fig. 10 shows the mass loss for the pervious concrete specimens during the freeze–thaw test. The figure distinguishes specimens cut from the top of the cylinder from those cut from the bottom because they had a different void content. The average void content of the top and bottom specimens was 9.8% and 15.6%, respectively. The figure also distinguishes specimens exposed to the saturated method from those exposed to the drained method, and specimens exposed to demineralized water from those exposed to salt water.

Fig. 11 shows the appearance of two specimens after 0 frost cycles and 56 frost cycles with and without the presence of salt ions.

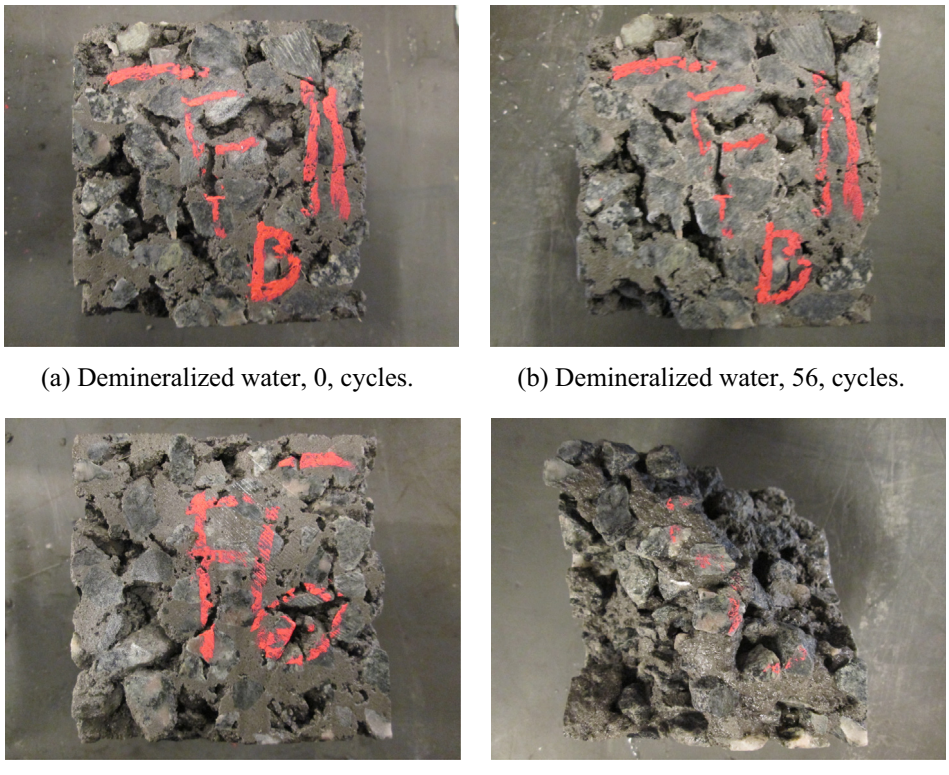

(a) Demineralized water, 0, cycles. (b) Demineralized water, 56, cycles.

(c) 3%NaCl solution, 0, cycles. (d) 3%NaCl solution, 56, cycles.

Fig. 11. Visual appearance of pervious concrete cubes measuring 100 × 100 × 100 mm^3 after 0 and 56 frost cycles. The specimens were freezing in air and thawing in either demineralized water or salt water.

Table 8
Strains, ε, and coefficients of linear temperature expansion, α, for cement-stabilized gravel exposed to various boundary conditions. CG4% and CG5% contain 4% cement and 5% cement, respectively, as explained in Section 2.2.2.

		CG4%		CG5%	
RH [%]	T [°C]	ε [–]	α [°C^{-1}]	ε [–]	α [°C^{-1}]
65	5–20	1.5×10^{-4}	9.9×10^{-6}	1.7×10^{-4}	11.2×10^{-6}
65	5–40	3.5×10^{-4}	9.9×10^{-6}	4.0×10^{-4}	11.4×10^{-6}
65–85	20	3.6×10^{-5}	–	3.5×10^{-5}	–
45–85	20	8.5×10^{-5}	–	8.4×10^{-5}	–

RH = relative humidity [%], T = temperature [°C].

3.4. Shrinkage results

Table 8 shows the strains and coefficients of linear temperature expansion for cement-stabilized gravel exposed to a variation in temperature and relative humidity.

Based on the tests in which the relative humidity was constant and the temperature varied, the coefficient of linear temperature expansion, as expected, was independent of the interval of temperature variation, as Table 8 indicates. We made this observation for both cement content of 4% and 5%. In tests in which the temperature was constant and the relative humidity varied, the size of the strains approximately doubled when the range of the relative humidity variation was doubled. Again, we found this result for both cement contents. However, we observed no difference between the strains for a cement content of 4% and 5%.

4. Discussion

4.1. Discussion of strength properties

4.1.1. Strength properties of sub-base gravel

The compressive strength and splitting tensile strength are not typical parameters used to characterize sub-base gravel. Instead, the design of sub-base gravel pavements, and such, are typically based on Young's modulus. The determination of Young's modulus of gravel materials is very sensitive to the stiffness of the surroundings, and therefore, would be determined from large-scale falling weight deflectometer tests, which are often expensive and cumbersome to carry out. Therefore, in the design of constructions with sub-base gravel it is a common standard to use table values to characterize the material rather than actual measurements; thus, we find it reasonable to also use table values for this study. Danish road standards assume that Young's modulus is the same for both types of sub-base gravel tested in this study, although they have a different gradation [34].

4.1.2. Strength properties of cement-stabilized gravel

As Table 4 shows, the 28-day compressive strength of cement-stabilized gravel with 4% cement and 5% was 6.2 MPa and 12.3 MPa, respectively. This finding classifies CG4% and CG5% as belonging to strength classes $C_{5/6}$ and $C_{12/15}$, respectively, according to the DS 14227-1 standard [14]. Because the specimens were designed with gravel within envelopes B in the DS 14227-1 standard [14], Danish road standards prescribe that the initial Young's moduli for the particular strength classes are 11.5 GPa and 18.0 GPa for CG4% and CG5%, respectively, [34]. Young's moduli determined for the cement-stabilized gravel in this study were slightly larger, but still consistent with the values in Danish road standards.

4.1.3. Strength properties of pervious concrete

For pervious concrete, the strength properties are highly dependent on the void content. Often a linear correlation between void content and strength properties is assumed with the strength decreasing as the void content increases [13]. In this study, a 28-day compressive strength of 9.9 MPa was obtained for a void content of 18.1%, as shown in Table 4. It is important to note that the void content of the specimens in this study expressed an average value of the voids inside the specimens. In fact, the void content varied throughout the specimen. Because compaction was applied from the top, the void content of the specimens was lowest at the top and increased down through the specimen. This finding also explains why the specimens for permeability and freeze–thaw testing cut from the upper and lower part of the cylinder specimens had different void contents and why it was not possible to test specimens with similar void contents in all types of tests. In fact, the strength properties were connected with the part of the specimen having the highest void content, that is, the bottom of the specimens, which had a void content higher than 18.1%. However, correlating the strength properties of pervious concrete with the average void content is a common practice.

4.1.4. Comparison of strength properties

Young's modulus of sub-base gravel is less by a factor of 10^2 than Young's modulus of cement-stabilized gravel and pervious concrete because the material does not contain any cement. Hence, of all the tested materials, the sub-base gravel fill had the poorest bearing capacity. However, in constructions in which the fill material serves only to stabilize the arch structure and transfer the vertical loads from the road surface to the arch structure, the stiffness requirements are very low, and Young's modulus for sub-gravel fill is typically sufficient. On the other hand, in arch bridge constructions in which the fill has a structural purpose and should be designed to carry, for example, shear stresses, a sub-base gravel fill is inappropriate. Instead, either cement-stabilized gravel or pervious concrete provides improved strength properties and bearing capacity.

The 28-day compressive strength and the 28-day Young's modulus of pervious concrete fell between the corresponding values for cement-stabilized gravel with 4% and 5% cement. The 28-day splitting tensile strength for pervious concrete was 42% less than for cement-stabilized gravel containing 4% cement. For pervious concrete, we considered only a single mix design void content of 17.5% in this study; hence, only cylinders with a single void content were tested in compression. If the void content were decreased, the strength properties would be expected to increase accordingly. However, these results indicated that the strength properties of pervious concrete and cement-stabilized gravel are comparable.

4.2. Discussion of permeability

4.2.1. Permeability of sub-base gravel

When considering the permeability of sub-base gravel as shown in Table 5, note that the determination of the permeability was performed on specimens with a compaction degree of approximately 100%. Typical values for the permeability of gravel materials are given for loosely compacted specimens; however, according to Lambe and Whitman [35] the permeability is minimum at maximum compaction, which means that the values in Table 5 are less than most table values. We believe, the permeability of 0–32 mm sub-base gravel was larger than the permeability of 0–8 mm sub-base gravel because the tortuosity of the pore system is less for 0–32 mm sub-base gravel, as discussed in Lund et al. [20].

4.2.2. Permeability of cement-stabilized gravel

As far as we could ascertain, very little literature exists on permeability of cement-stabilized gravel, and we could not find

comparable results. Our results indicate that permeability decreases when increasing cement content because the fines content is increased.

4.2.3. Permeability of pervious concrete

The permeability coefficient of pervious concrete is highly dependent on the void content; however, the void contents of 9.3% and 20.2% considered in the permeability tests in this study represent the expected void content limits for pervious concrete fill in Pearl-Chain Bridges. Typically, the permeability coefficient of pervious concrete with a void content between 15 and 20% is between 0.20 and 0.54 cm/s [23], and our results agreed with this expectation.

4.2.4. Comparison of permeability

The permeability coefficients of sub-base gravel, cement-stabilized gravel, and pervious concrete vary substantially. Pervious concrete, the most permeable material we tested, has a permeability coefficient that is a factor of 10^2 times larger than the permeability coefficient of sub-base gravel, and a factor of 10^6 times larger than the permeability coefficient of cement-stabilized gravel, the least permeable material tested.

In Denmark the maximum intensity of a rain event with a 1-year return period is 2.5×10^{-3} cm/s [36]. The tested 0–32 mm sub-base gravel specimens could exactly drain the water from a rain event with a 1-year return period; however, the 0–8 mm sub-base gravel specimens could not. The permeability of the cement-stabilized gravel specimens that we tested was also too low to drain that amount of rainwater. However, the permeability of the pervious concrete specimens was large enough to drain this maximum intensity instantaneously. In fact the pervious concrete specimens tested were permeable enough to instantaneously remove water from a rain event with a 100-year return period in Denmark [36].

4.3. Discussion of freeze–thaw durability

4.3.1. Freeze–thaw durability of sub-base gravel

According to Danish tender specifications, the sub-base gravel materials tested in this study are not expected to be frost-susceptible [12] because their fines content is low. However, we found that 0–32 mm sub-base gravel had a medium frost susceptibility, and therefore, could be expected to experience a certain degree of frost heaving. On the other hand, results indicated that the frost susceptibility of 0–8 mm sub-base gravel is negligible. The difference in frost susceptibility seemed to be correlated to the difference in permeability; thus, our results indicated that the freeze–thaw damages of sub-base gravel can be minimized by carefully selecting a material with low fines content and a small permeability.

The applied test method for determination of the frost susceptibility was chosen because it is the only well-known method to determine the frost susceptibility of gravel; however, the test method assumes a constant water table below the gravel specimen. Considering the permeability of sub-base gravel (Section 4.2.4) such water table is only expected below a sub-base gravel fill in arch bridges under extreme conditions. This is because, in most cases, the permeability of sub-base gravel is large enough to drain penetrating rainwater and furthermore, the arch shape naturally directs water that penetrates the fill towards the bridge ends. Therefore, in general, a sub-base gravel fill is not expected to experience problems with frost heave.

4.3.2. Freeze–thaw durability of cement-stabilized gravel

As shown in Fig. 9, the presence of salt ions had a significant influence on the freeze–thaw durability of cement-stabilized gravel, and the impact was greatest for specimens containing 4% cement compared with 5% cement. The compressive strength decreased 25.4% and 19.2%, respectively, after 56 frost cycles, compared with the reference specimens. When demineralized water was used, the compressive strength decreased 14.6% and 7.7% for specimens with 4% and 5% cement, respectively, after 56 frost cycles. For all specimens exposed to salt ions, the decrease in compressive strength after 20 frost cycles was similar to the decrease in compressive strength after 56 frost cycles. Hence, the major part of the deterioration took place in the early frost period. We did not observe the same tendency for the specimens exposed to demineralized water in which a larger reduction in compressive strength was observed after 56 frost cycles compared with 20 frost cycles. After 20 frost cycles, the specimens with 5% cement exposed to demineralized water had not experienced any change in compressive strength compared with the reference specimens. For a cement content of 4% this change also was minor. Overall, the results indicated that addition of 5% cement compared with 4% increased the frost resistance of cement-stabilized gravel with respect to compressive strength. This result also was supported by the measurements of the ultrasonic wave speed shown in Table 7. Specimens exposed to demineralized water experienced a smaller decrease in wave speed than specimens exposed to a 3% NaCl solution, and specimens with 5% cement experience a smaller decrease in wave speed than specimens with 4% cement.

We believe that the applied test method for determination of the freeze–thaw behavior of cement-stabilized gravel is representative of the behavior of a cement-stabilized gravel fill material. The permeability results (Section 4.2.4) indicated that cement-stabilized gravel fill can be expected to become water saturated and due to freeze–thaw, this can cause a severe reduction in the compressive strength of the fill.

4.3.3. Freeze–thaw durability of pervious concrete

The mass loss of the pervious concrete specimens exposed to freezing and thawing was the easiest indication of the extent of freeze–thaw damages of the specimens. First, specimens exposed to a 3% NaCl solution experienced a greater mass loss than specimens exposed to demineralized water, as Fig. 10 indicates. Second, the mass loss of the specimens exposed to the drained method was as large as the mass loss of the specimens exposed to the saturated method. Finally, the mass loss of the bottom specimens was larger than the mass loss of the top specimens; that is, the specimens having the largest void content were most exposed to deterioration during freeze–thaw. Also, those tendencies could be clearly visually observed, as Fig. 11 indicates. Whereas only minor damages were observed for the specimen exposed to demineralized water, larger damages were observed for the specimen exposed to a 3% NaCl solution. Schaefer et al. [13] used a mass loss of 15% to represent the terminal serviceability acceptable level. None of the mass loses in Fig. 10 exceeded this limit.

The mass loss made it difficult to determine the compressive strength for specimens exposed to 24 frost cycles and 56 frost cycles because the end surfaces were deteriorated, especially for the specimens exposed to salt ions. Hence, the decrease in compressive strength was not an appropriate method to assess the freeze–thaw durability of pervious concrete.

Although we used air entrainment to improve the freeze–thaw durability of the pervious concrete specimens, the specimens nevertheless experienced frost damage. The reason might be that the amount of air entrainment added to the mix was insufficient for the applied test method. We determined the necessary amount of air entrainment from press-ur-meter readings as for conven-

tional concrete. However, the amount added might have been too low. Studies have indicated that press-ur-meter readings of entrained air in pervious concrete can be incorrect because air caught in the large voids is also included [37].

The applied testing procedure is not very representative for the freeze–thaw behavior of a pervious concrete fill. This is because such fill is not expected to be water saturated at any time after placement because of the large permeability of pervious concrete (Section 4.2.4); hence, the applied test procedure is too harsh. For pervious concrete, several studies have shown that air-entrained pervious concrete performs well in the field in areas that undergo several frost cycles per year because the water drains away [38]. In practice, we believe that the recorded levels of freeze–thaw durability are sufficient for a pervious concrete fill.

4.3.4. Comparison of freeze–thaw durability

All tested materials showed damages due to freezing and thawing under the applied test procedures; however, not all test procedures were good representations of the freeze–thaw behavior of fill in arch bridges. We believe that cement-stabilized gravel is very much exposed to freeze–thaw damages if implemented as fill in arch bridges, whereas pervious concrete fill has sufficient freeze–thaw durability because water is entirely prevented from accumulating in the fill. Sub-base gravel fill is in general not expected to experience problems with frost heave; however, because the permeability of sub-base gravel is much lower than of pervious concrete, there is a risk for water accumulation in the fill and thereby a constant water table can build up below the fill. In such case frost heave of the fill might occur.

4.4. Discussion of shrinkage

In this study, we determined shrinkage behavior for cement-stabilized gravel only. Although literature has described that the shrinkage behavior of cement-stabilized gravel as a major concern that can cause shrinkage cracking, so-called reflection cracking, the underlying phenomena are not well-understood or well-described. Today, the most common method to prevent reflection cracking of cement-stabilized pavements is crack control in which cracks are cut halfway through the cement-stabilized gravel layer every 2 m. However, this solution is not economical attractive. Several factors influence the shrinkage properties of cement-stabilized gravel, such as the mix design and the degree of compaction. However, for specimens of a given mix design, two main parameters are believed to influence the shrinkage behavior: variation in temperature and variation in relative humidity. The results shown in Table 8 indicate that the size of the strains induced by a variation in relative humidity was an order of magnitude less than that of the strains induced by a variation in temperature. Therefore, shrinkage cracking observed for cement-stabilized pavements is mainly explained by temperature-dependent rather than moisture-dependent shrinkage. Table 8 also indicates that for both cement contents we tested, the coefficient of linear temperature expansion was similar to that of conventional concrete that has a coefficient of linear temperature expansion of 10×10^{-6} °C^{-1} for a cement-to-aggregate ratio of 1:6 [39]. As the cement content of cement-stabilized gravel increases the coefficient of linear temperature expansion increases, which aligns with findings of Neville [39]. The values listed in Table 8 relate to a cement-stabilized gravel fill placed on a concrete arch that is rigid and does not move due to creep, relaxation, and temperature expansion. This is a simplification, and in reality it is expected that movements of the concrete arch cause a build-up of stresses in the fill which should also be considered; however, this is outside of the scope of the present study.

For pervious concrete, the literature has shown that cracking caused by shrinkage is not a concern and that many pervious concretes are made without control joints [23]. Again, considerations on the shrinkage behavior of pervious concrete fill should not be isolated but correlated to the movements of the concrete arch.

4.5. Pros and cons of different fill materials

Based on the findings in this study, we can summarize the advantages and disadvantages of using either sub-base gravel, cement-stabilized gravel or pervious concrete as fill material in arch bridges as shown in Table 9. Table 9 also includes parameters not previously discussed in this paper, such as considerations of cost and placing technique.

Economy is an essential consideration in all construction projects and therefore should be included when discussing pros and cons of different fill materials. Sub-base gravel is the least expensive fill material, and therefore the most attractive choice if price is the only consideration. On the other hand, pervious concrete is the most expensive fill. However, economic aspects should not be based on the prices alone, but must be seen in a broader perspective and over the entire lifespan of the bridge because materials with better durability require less maintenance.

When placing sub-base gravel and cement-stabilized gravel, the material must be placed in layers no thicker than 30 cm in order to provide necessary compaction. Studies have shown that it is possible to design self-compacting pervious concrete [40]; therefore, we can assume that it would be possible to design a self-compacting

Table 9
Pros and cons of using sub-base gravel fill, cement-stabilized gravel fill, and pervious concrete fill in arch bridges.

Fill material	Pros	Cons
Sub-base gravel	– Low material price – Reasonable permeability – Reasonable freeze–thaw durability	– Poor shear strength – Maximum layer thickness of 30 cm
Cement-stabilized gravel	– Relatively low material price – Good strength properties – Shear transferring	– Poor permeability – Poor freeze–thaw durability – Maximum layer thickness of 30 cm – Reflection cracking (need for control joints)
Pervious concrete	– Good strength properties – Shear transferring – Excellent permeability – Sufficient freeze–thaw durability – Self-compacting and easy to place (not tested in the present study) – No need for control joints (not tested in the present study)	– High material price compared to sub-base gravel and cement-stabilized gravel

pervious concrete mix that could be cast simply by pouring it onto the arch in a single lift and compacting it only from the top. Such an approach would be highly attractive because it would minimize the work involved in placing the fill.

4.6. Applicable fill materials for Pearl-Chain Bridges

Based on the advantages and disadvantages of the three different fill materials listed in Table 9, the following fill materials are found to be applicable for Pearl-Chain Bridges:

1. Pearl-Chain Bridges *without* sandwich effect:
   - Sub-base gravel or pervious concrete.
     In Pearl-Chain Bridges without the sandwich effect (no concrete top plate), the shear transferring properties of pervious concrete are not needed and the strength properties of sub-base gravel are sufficient. However, this study has shown that the permeability of pervious concrete is much improved in comparison to sub-base gravel. We believe this is an important factor concerning the durability of the bridges because penetrating water is entirely prevented from accumulating in a pervious concrete fill. Despite the higher material price, pervious concrete is a strong and reasonable alternative to sub-base gravel considering the entire life span of the bridges.
2. Pearl-Chain Bridges *with* sandwich effect (concrete top plate):
   - Pervious concrete.
     For this type of arch bridge construction, the fill material needs to transfer shear stresses and therefore pervious concrete is recommended. Compared to cement-stabilized gravel it has much improved freeze–thaw durability and permeability which positively influence the lifespan of the bridge.

5. Conclusions

In this study, we tested and compared the strength and durability properties of three different fill materials. These materials included two types of sub-base gravel with gradations of 0–8 mm and 0–32 mm, two types of cement-stabilized gravel with 0–16 mm gravel mixed with 4% and 5% cement, and one type of pervious concrete with a mix design void content of 17.5%. The final choice of the most appropriate filling material for an arch bridge depends on several factors, such as the static system of the bridge, the total maximum thickness of the fill, and the surrounding climate. For Pearl-Chain Bridges without sandwich effect we found that either sub-base gravel or pervious concrete are applicable as fill, whereas for Pearl-Chain Bridges constructed as sandwich arches, only pervious concrete is applicable as fill. Cement-stabilized gravel is not recommended. These recommendations originate from the strength and durability properties we determined from the tested mixes:

1. The compressive strength and splitting tensile strength of cement-stabilized gravel was comparable to pervious concrete, according to measurements of 28-day compressive strengths and 28-day splitting tensile strengths of 6.2–12.3 MPa and 1.5–5.2 MPa, respectively.
2. Young's modulus of sub-base gravel is 0.150 GPa according to Danish road regulations [34], which was less by a factor of 10^2 than Young's modulus of cement-stabilized gravel and pervious concrete.
3. The permeability of pervious concrete was 10^2 times larger than the permeability of sub-base gravel, and larger by a factor of 10^6 than the permeability of cement-stabilized gravel. The permeability of 0–32 mm sub-base gravel was large enough to drain the maximum intensity of a rain event with a 1-year return period in Denmark but neither 0–8 mm sub-base gravel nor cement-stabilized gravel could do so. However, the permeability of pervious concrete was large enough to drain the maximum intensity of a rain event with a 100-year return period in Denmark.
4. All tested materials showed damages due to freezing and thawing under the applied test procedures; however, the results should be seen in the light of how well these procedures represent the actual freeze–thaw situations for fill materials in arch bridges. It is expected that cement-stabilized gravel is very much exposed to freeze–thaw damages if implemented as fill material, whereas the freeze–thaw durability of pervious concrete fill is expected to be sufficient. Sub-base gravel fill is not expected to experience problems with frost heave unless a constant water table builds up below the fill.
5. The shrinkage behavior is expected to be a durability concern only for cement-stabilized gravel. The shrinkage behavior for cement-stabilized gravel can mainly be explained by temperature-dependent rather than moisture-dependent shrinkage, which is an order of magnitude less.

Acknowledgments

The authors wish to thank Innovation Fund Denmark for supporting this project.

Appendix A. Supplementary data

Supplementary data associated with this article can be found, in the online version, at http://dx.doi.org/10.1016/j.conbuildmat.2016.07.089.

References

[1] J. Bourke, S. Taylor, D. Robinson, A. Long, Analysis of a flexible concrete arch, in: B. Chen, J. Wei (Eds.), ARCH'10: Proceedings of 6th International Conference on Arch Bridges; 2012 Oct 11–13; Fuzhou, China, 2012, pp. 133–139.
[2] J. Bernini, Overfilled Precast Concrete Arch Bridge Structures, BEBO of America, Inc, Zürich, 2000.
[3] L. Sihwa, Computer Data Base Assessment of Masonry Bridges, University of Edinburgh, Edinburgh, UK, 1987 [dissertation].
[4] D. Hutchinson, Application and design of segmental precast arches, in: M.K. Yegian, E. Kavazanjian (Eds.), Proceedings of Geo-Trans; 2004 Jul 27–31; Los Angeles, 2004, pp. 452–459.
[5] BEBO Arch Systems, BEBO System Technical Documentation: Installation Guide, BEBO Arch Systems, Zürich, 2009.
[6] C. Melbourne, The testing of a mass concrete arch bridge, in: F.K. Garas, G.S.T. Armer, J.I. Clarke (Eds.), Building the Future: Innovation in Design, Materials and Construction, E & FN Spon, London, 1993, pp. 226–233.
[7] A. Long, P. McPolin, J. Kirkpatrick, A. Gupta, D. Courtenay, FlexiArch: From concept to practical applications, Struct. Eng. 92 (7) (2014) 10–15.
[8] P.S. Halding, K.D. Hertz, J.W. Schmidt, Precast Pearl-Chain concrete arch bridges, J. Eng. Struct. 103 (2015) 214–227.
[9] M.S.M. Lund, M. Arvidsson, K.K. Hansen, Homogeneity and strength of mortar joints in Pearl-Chain Bridges, Proceedings of fib Symposium; 2015 May 18–20; Copenhagen, 2015, pp. 187–188.
[10] P.S. Halding, K.D. Hertz, N.E.V. Petersen, B. Kennedy, Assembly and lifting of Pearl-Chain arches, Proceedings of fib Symposium; 2015 May 18–20; Copenhagen, Denmark, 2015, pp. 185–186.
[11] M.S.M. Lund, K.K. Hansen, R. Truelsen, L. Johansen, Pervious concrete fill in Pearl-Chain Bridges: using small-scale results in full-scale implementation, Constr. Build. Mater. 106 (2016) 404–414.
[12] Danish Road Directorate. Sub-base of sand and gravel—Design guide. Tender specification. Copenhagen: The Directorate; 2003, ISBN: 87-7923-502-6. Danish.
[13] V.R. Schaefer, K. Wang, M.T. Suleiman, J.T. Kevern, Mix Design Development for Pervious Concrete in Cold Weather Climates, National Concrete Pavement Technology Center and Iowa State University, Ames, IA, 2006.
[14] DS Standard 14227-1. Hydraulically bound mixtures – Specifications – Part 1: Cement bound granular mixtures. Copenhagen: Danish Standards, 2004.
[15] DS Standard 13286-5. Unbound and hydraulically bound mixtures – Part 5: Test methods for laboratory reference density and water content – Vibrating table. Copenhagen: Danish Standards, 2003.

[16] DS Standard 13286-2. Unbound and hydraulically bound mixtures – Part 2: Test methods for laboratory reference density and water content – Proctor compaction. Copenhagen: Danish Standards, 2011.
[17] M.S.M. Lund, K.K. Hansen, K.D. Hertz, Frost resistance and permeability of cement stabilized gravel used as filling material for Pearl-Chain Bridges, in: J. Bastien, N. Rouleau, M. Fiset, M. Thomassin (Eds.), Proceedings of 10th fib International PhD Symposium in Civil Engineering; 2014 Jul 21–23; Québec, Canada, Research Center on Concrete Infrastructure (CRIB), Université Laval, Québec, 2014, pp. 155–160.
[18] M.S.M. Lund, K.K. Hansen, K.D. Hertz, Experimental study of properties of pervious concrete used for bridge superstructure, Proceedings of 12th International Symposium on Concrete Roads; 2014 Sep 23–26; Prague, 2014.
[19] ASTM Standard D5918-13. Standard Test Methods for Frost Heave and Thaw Weakening Susceptibility of Soils. West Conshohocken, PA: ASTM International, doi:http://dx.doi.org/10.1520/D5918-13, 2013.
[20] M.S.M. Lund, K.K. Hansen, I.B. Andersen, Frost susceptibility of sub-base gravel used in Pearl-Chain Bridges: an experimental investigation, Int. J. Pavement Eng. (2016) (submitted for publication).
[21] EN Standard 13286-50, Unbound and Hydraulically Bound Mixtures – Part 50: Method for the Manufacture of test Specimens of Hydraulically Bound Mixtures using Proctor Equipment or Vibrating Table Compaction, European Standards, Brussels, 2011.
[22] Danish Road Directorate. Hydraulic bound layers—General work specification (GWS). Tender specification. Copenhagen: The Directorate, ISBN: 978-87-7060-129-0. Danish, 2009.
[23] P.D. Tennis, M.L. Leming, D.J. Akers, Pervious concrete pavements. EB302.02, Portland Cement Association/National Ready Mixed Concrete Association, Skokie, IL/Silver Spring, MD, 2004.
[24] EN Standard 13286-41, Unbound and Hydraulically Bound Mixtures – Part 41: Test Method for the Determination of the Compressive Strength of Hydraulically Bound Mixtures, European Standards, Brussels, 2003.
[25] EN Standard 13286-43, Unbound and Hydraulically Bound Mixtures – Part 43: Test Method of the Modulus of Elasticity of Hydraulically Bound Mixtures, European Standards, Brussels, 2003.
[26] DS Standard 12390-3, Testing Hardened Concrete – Part 3: Compressive Strength of Test Specimens, Danish Standards, Copenhagen, 2009.
[27] ISO Standard 6784, Concrete – Determination of Static Modulus of Elasticity in Compression, International Standard, London, 1984.
[28] EN Standard 13286-42, Unbound and Hydraulically Bound Mixtures – Part 42: Test Method for the Determination of the Indirect Tensile Strength of Hydraulically Bound Mixtures, European Standards, Brussels, 2003.
[29] ISO Standard 4108, Concrete – Determination of Tensile Splitting Strength of Test Specimens, International Standard, London, 1980.
[30] ASTM Standard D2434-68. Standard Test Method for Permeability of Granular Soils (Constant Head). West Conshohocken, PA: ASTM International; 2006. doi: http://dx.doi.org/10.1520/D2434-68R06.
[31] prEN Standard 13286-54, Unbound and Hydraulically Bound Mixtures – Part 54: Test Method for Determination of Frost Susceptibility – Resistance to Freezing and Thawing of Hydraulically Bound Mixtures, European Standard, Brussels, 2011.
[32] SS Standard 137244, Concrete testing – Hardened Concrete – Scaling at Freezing, Swedish Standards, Stockholm, 2005.
[33] M.S.M. Lund, K.K. Hansen, Shrinkage properties of cement stabilized gravel, in: The Nordic Concrete Federation (Ed.), Proceedings of XXII Nordic Concrete Research Symposium; 2014 Aug 13–15; Reykjavik. Oslo: Norsk Betongforening, 2014, pp. 303–306.
[34] Danish Road Directorate. Design of pavements and reinforcement layers. Handbook. Construction and planning. Copenhagen: The Directorate; 2013. URL: http://english-vejregler.lovportaler.dk/ShowDoc.aspx?q=Design+of+pavements+and+reinforcement+layers&docId=vde-2015-0060-full.
[35] T.W. Lambe, R.V. Whitman, Soil Mechanics, John Wiley & Sons, New York, 1969.
[36] IDA Wastewater Commission. Regional variation of extreme rain in Denmark – a new analysis, 1979–2005. Pamphlet No. 28. Copenhagen: The Commission; 2006. ISBN: 87-7923-502-6. Danish.
[37] J.T. Kevern, K. Wang, V.R. Schaefer, Test methods for characterizing air void systems in Portland cement pervious concrete, J. ASTM Int. 6 (9) (2009) 119–134, http://dx.doi.org/10.1520/JAI102451.
[38] National Ready Mixed Concrete Association (NRMCA). Freeze-thaw resistance of pervious concrete. Silver Spring, MD: NRMCA, 2004.
[39] A.M. Neville, Properties of Concrete, fourth ed., Pearson Education Limited, Essex, 1995.
[40] J.T. Kevern, Self-consolidating pervious concrete: A discussion of material properties and behaviors, Proceedings of the Fifth North American Conference on the Design and Use of Self-Consolidating Concrete; 2012 May 12–15; Chicago, 2012.

Paper II

"Pervious concrete fill in Pearl-Chain Bridges: Using small-scale results in full-scale implementation"

M.S.M. Lund, K.K. Hansen, R. Truelsen, and L. Johansen

Published in: *Construction and Building Materials, 2016;106:404–14*

Construction and Building Materials 106 (2016) 404–414

Contents lists available at ScienceDirect

Construction and Building Materials

journal homepage: www.elsevier.com/locate/conbuildmat

Pervious concrete fill in Pearl-Chain Bridges: Using small-scale results in full-scale implementation

M.S.M. Lund *, K.K. Hansen, R. Truelsen, L. Johansen

Technical University of Denmark, Department of Civil Engineering, Brovej 118, DK-2800 Kgs. Lyngby, Denmark

HIGHLIGHTS

- The void content follows a logarithmic tendency through layers compacted from above.
- Layer thicknesses of 27 cm before compaction give homogenous void contents in layers.
- The compressive strength of homogeneous specimens is linear with void content.
- Pervious concrete is implemented as fill in a 26 m long Pearl-Chain Bridge.
- European quality control regulations are needed for pervious concrete in the field.

ARTICLE INFO

Article history:
Received 11 August 2015
Received in revised form 14 November 2015
Accepted 15 December 2015

Keywords:
Filling material
Pearl-Chain Bridge
Pervious concrete
Strength property
Vertical void distribution

ABSTRACT

Pearl-Chain Bridge technology is a new prefabricated arch solution for highway bridges. This study investigates the feasibility of pervious concrete as a filling material in Pearl-Chain Bridges. The study is divided into two steps: (1) small-scale tests where the variation in vertical void distribution and strength properties is determined for 800 mm high blocks cast in different numbers of layers, and (2) full-scale implementation in a 26 m long Pearl-Chain Bridge. With a layer thickness of 27 cm, the small-scale tests indicated homogenous results; however, for the full-scale implementation, the same degree of homogeneity was not shown.

1. Introduction

Pearl-Chain Bridge technology is an innovative arch solution for highway bridges [1]. Despite its optimal shape, the arch is rarely used for highway bridges because of the extensive need for scaffolding that closes down the highway for weeks. With the Pearl-Chain Bridge technology, the highway is closed for a minimum period of time, which reduces traffic disturbances and carbon dioxide emissions. Furthermore, the material consumption is minimized due to the optimal arch shape. The Pearl-Chain arch is created by collecting and post-tensioning several Super-Light Decks on a wire, like pearls on a string. Subsequently a crane is used to lift the arch into place [2]. When the arch is placed, spandrel walls are installed, a filling material is laid out and possibly a post-tensioned concrete top plate is cast. The first Pearl-Chain Bridge ever built was constructed in 2015. Crossing Vorgod Stream in Jutland, Denmark, and connecting two gravel roads on each side, the bridge load is classified for 50 tonnes [3,4]. The bridge consists of a 13 m long arch and two 6.5 m long adjacent half arches as shown in Fig. 1. This gives the bridge a total span length of 26 m. The width of the bridge is 6.1 m and the pile height is 0.9 m.

The filling material in the bridge is shown as shaded areas in Fig. 1. The maximum placing depth of the filling material is 0.9 m and the filling material has a total volume of 45 m^3.

Portland cement pervious concrete (PCPC) is a concrete with a significant void content—typically 11–35% [5]—which gives it excellent drainage properties. Typically, the fill in arch bridges is cast with a granular material; however, for the Pearl-Chain Bridge shown in Fig. 1, PCPC was chosen as the filling material because of several considerations:

1. PCPC fill is expected to contribute positively to the lifetime of the bridge. A bridge is a sensitive point in a road construction because it is exposed to freezing from below as well as from

* Corresponding author.
E-mail addresses: msml@byg.dtu.dk (M.S.M. Lund), kkh@byg.dtu.dk (K.K. Hansen).

http://dx.doi.org/10.1016/j.conbuildmat.2015.12.104
0950-0618/

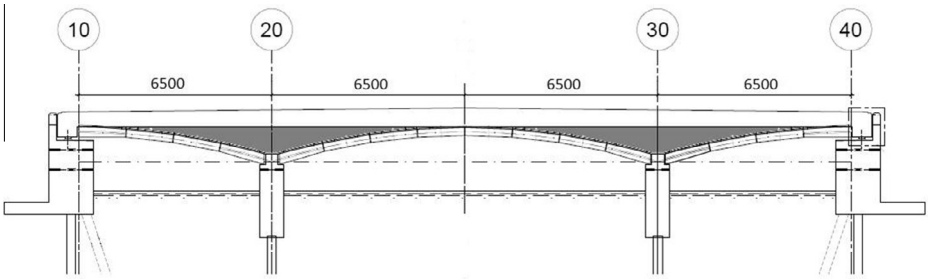

Fig. 1. Longitudinal section of Pearl-Chain Bridge over Vorgod Stream. The shaded areas mark the location of pervious concrete filling material. Dimensions are in mm.

above. The lower permeability of typical unbound filling materials such as gravel and soil may cause water accumulation, leading to potential frost damages when the bridge freezes. Using PCPC as a filling material improves arch bridge durability because such water accumulation is entirely prevented due to the large permeability of PCPC.
2. PCPC fill can be incorporated structurally because the strength properties are significantly improved compared to unbound filling materials. This means, for example, that the fill material is able to transfer shear stresses.
3. PCPC fill is easier to cast than typical unbound filling materials that need to be compacted in layers of 30 cm in thickness. It is expected that it is possible to design a self-compacting PCPC mix that can simply be cast by pouring it onto the arch in a single lift and only compact it from the top. However, this is outside the scope of the present study.

For the use of PCPC as fill in Pearl-Chain Bridges it is required that the 28-days compressive strength and the 28-days splitting tensile strength are minimum 10 MPa and 1 MPa, respectively. Furthermore, the freeze–thaw durability should be good. If PCPC fill has a permeability of at least 4×10^{-3} cm/s it is able to drain the rain from a 10-year rain event in Denmark [6]. Without compromising the quality of PCPC fill, it is desired that the mentioned strength and durability requirements are fulfilled with the highest possible void content to keep the PCPC cost at a minimum.

While the literature proves it is possible to design a PCPC mixture that meets filling material strength and durability requirements, such research is lacking on PCPC placed at high depths. The present paper investigates the use of PCPC as a fill in Pearl-Chain Bridges. Small-scale tests where PCPC is placed in layers of up to 800 mm serves three main purposes:

1. To investigate the feasibility of casting homogeneous pervious concrete in layers of up to 0.8 m.
2. To identify a suitable compaction method.
3. To determine the strength properties—compressive strength, Young's modulus, splitting tensile strength, and shear strength—and the variation of these strength properties through a 0.8 m deep pervious concrete layer.

Based on the findings and conclusions from the laboratory tests, PCPC is implemented as fill in the Pearl-Chain Bridge over Vorgod Stream in Denmark. The experiences, results and conclusions from this are also described herein.

2. Background

PCPC consists of cement, water, and a single-sized coarse aggregate that is used to maximize the void content. PCPC has less cement paste than conventional Portland cement concrete, which leaves space for the interconnected void structure. The cement paste typically has a low water-to-cement (w/c) ratio of 0.27–0.34, which causes stiff PCPC workability. The strength of PCPC increases significantly when substituting up to 7% of the coarse aggregate with sand [7]. Using chemical admixtures such as air entrainment (AEA), superplasticizers, and hydration stabilizers also improves strength properties and freeze–thaw durability [7,8]. Tests have shown that in order to obtain the best PCPC durability the AEA dosage should correspond to the use in regular concrete, whereas the retarder dosage should be much higher [9].

There is a linear correlation between the void content and the density of PCPC [7]. PCPC strength properties are strongly related to the void content and therefore to the density, and 28-days compressive strength values of 5.5–32 MPa are reported [5]. As far as can be ascertained, very little information about Young's modulus of PCPC is published, although studies have reported a static modulus of elasticity of 13–32 GPa for void contents of 15–35% [10]. Permeability coefficients of 0.20–0.54 cm/s are most common [11]. The freeze–thaw durability of PCPC is typically tested according to the American Society for Testing and Materials (ASTM) C666 standard [12]. However, several examples have shown that air-entrained PCPC performs much better in the field than in the laboratory, where the test method is often considered to be a worst-case scenario and not representative of on-site behavior, since drainage is not taken into account [13,14]. In the field, PCPC pavements perform well over several years in areas that undergo a large number of annual freeze–thaw cycles, provided it remains unsaturated [8].

PCPC is typically used for pavements as it helps reduce stormwater runoff [11]. This implies that its placing depth is rarely particularly large. In the field, PCPC is typically placed in a single lift followed by compaction from the top. This produces a vertical void distribution variation with the lowest content at the top of the layer and the highest at the bottom. The distribution of the void content and hence the properties of PCPC are highly dependent on the compaction method [15].

3. Experimental method

In the small-scale tests, pervious concrete was mixed and cast in 0.8 m high molds with a volume of 1 m^3 at two different Danish mixing plants, mixing plant A and mixing plant B. Different layer thicknesses were investigated to determine which was most appropriate for full-scale implementation. Table 1 summarizes the outline of the experimental plan for the small-scale tests.

Table 1
Outline of experimental plan for small-scale tests.

	Mix No. 1	Mix No. 2
Place	Mixing plant A	Mixing plant B
Date	Sep. 29, 2014	Nov. 10, 2014
No. 1 m^3 blocks	2	2
No. of layers	1 and 2	2 and 3
Layer thickness	80 cm and 40 cm	40 cm and 27 cm

3.1. Material properties

Crushed granite was used as coarse aggregate for both of the mixes seen in Table 1. The granite was delivered from Yeoman Glensenda, Scotland, and Aarhus, Denmark, for mix No. 1 and mix No. 2, respectively. Quarry sand from Zealand, Denmark, was used for mix No. 1, and concrete sand from Jutland, Denmark, was used for mix No. 2. All aggregates belonged to environmental class E [16]. The density and absorption of the aggregates are shown in Table 2.

Fig. 2 shows the gradation curves for the aggregates.

Low-alkali Portland cement CEM I 42.5 N was used with fly ash type B4 from Denmark. Two different types of AEA were used at the two mixing plants; however, both types of AEA were combined natural and synthetic.

The materials used for the full-scale implementation were the same as those listed for mix No. 2; in addition a phosphate-based retarder was used.

3.2. Mixture proportions

3.2.1. Mix design for small-scale tests

The mix design used for mix Nos. 1 and 2 was mainly the same; only minor corrections in the amount of AEA were made to achieve an air content of 6% in the fresh pervious concrete. Both mixtures were designed to have a w/c ratio of 0.29, a fly ash to cement ratio of 20%, and 9.5% of the mass of coarse aggregate replaced by sand. Furthermore, both mixes were designed to have a void content of 17.5% in addition to entrained air. Table 3 shows the two mixture proportions.

The air content in the fresh concrete was measured with a press-ur-meter, though studies have indicated that this will cause incorrect readings because air caught in the large voids is also included in the measurement [14]. No standards exist for measuring the amount of entrained air in fresh PCPC, so the technique was nonetheless applied and found to provide reasonable results. Boiled, cooled, demineralised water was used to eliminate air bubbles. Mix No. 1 showed a direct correlation between the added amount of AEA and the amount of entrained air read off the press-ur-meter. The added amount of AEA was higher than for regular concrete.

The stiff consistency of pervious concrete prevents evaluating the workability of a given mixture from a slump test. Therefore, the workability of the PCPC mixtures for the small-scale tests was assessed by forming a ball of the PCPC [11]. Both mix No. 1 and mix No. 2 showed good cohesion and no excess of water when forming a ball, indicating a good workability.

3.2.2. Mix design for full-scale implementation

The mix design used in the full-scale implementation was basically the same as mix No. 2. However, because transportation from the mixing plant to the construction site took one hour, it was necessary to add a retarder. Table 4 shows the mix design used for the full-scale implementation.

3.3. Preparation of specimens for small-scale tests

A total of 4 m^3 PCPC was mixed and poured into a concrete truck for each of the two mixes. From here it was placed in the molds applying the smallest possible lift. The molds used to cast the PCPC blocks measured 1600 × 800 × 800 mm^3. The height of the molds corresponded fairly well with the maximum thickness of the filling material in the Pearl-Chain Bridge over Vorgod Stream. Table 1 summarizes the layer thickness for the different blocks before a plate compactor with an area of 53 × 35 cm^2 and 5500 vibrations per minute was used on them. The compaction was carried out by moving the plate compactor over the top surface of the PCPC layer in lanes just overlapping each other. The block cast in one layer was compacted two times, while the blocks cast in two and three layers were compacted one time per layer. To improve the bond between the layers, the topside of each layer was raked before casting the overlying layer. Fig. 3 shows the appearance of the two blocks with mix No. 1 after the molds were split.

The core temperature of the blocks was measured during hardening and a maximum temperature of 51 °C was achieved after 12 h.

The concrete blocks were covered with two layers of plastic immediately after casting to prevent moisture evaporation. The

Table 2
Fine and coarse aggregate properties for mix Nos. 1 and 2.

Material	Density [kg/m^3]	Absorption [%]
Quarry sand 0/4 mm, mix No. 1	2630	0.4
Concrete sand 0/4 mm, mix No. 2	2640	0.1
Granite 4/8 mm, mix No. 1	2630	0.4
Granite 4/8 mm, mix No. 2	3030	0.4

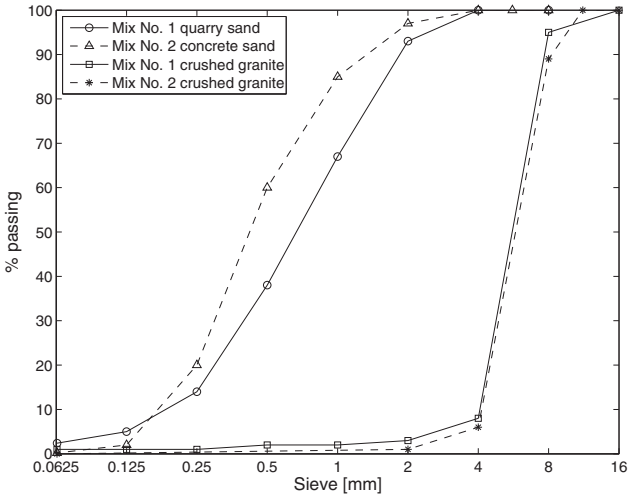

Fig. 2. Gradation curves for fine aggregate (quarry or concrete sand) and coarse aggregate (crushed granite).

Table 3
Mix design of 1 m^3 PCPC for mix Nos. 1 and 2.

Place	Mix No. 1 Mixing plant A	Mix No. 2 Mixing plant B
Cement [kg/m^3]	317.6	317.6
Fly ash [kg/m^3]	63.5	63.5
Water [kg/m^3]	95.2	94.1
Air entrainment [kg/m^3]	5.0	6.1
Sand [kg/m^3]	122.4	122.8
Granite [kg/m^3]	1291.7	1488.1
Density [kg/m^3]	1895.3	2092.2

Table 4
Mix design of 1 m^3 PCPC for Pearl-Chain Bridge over Vorgod Stream.

Place	Mixing plant B
Cement [kg/m^3]	317.6
Fly ash [kg/m^3]	63.5
Water [kg/m^3]	88.8
Air entrainment [kg/m^3]	6.1
Retarder [kg/m^3]	7.2
Sand [kg/m^3]	122.6
Granite [kg/m^3]	1486.1
Density [kg/m^3]	2092.0

plastic was kept on for one week after hardening; subsequently, concrete cores were drilled from the blocks with a specially constructed 800 mm long diamond drill having an external diameter of 150 mm and an internal diameter of 143 mm which enabled drilling all the way through the blocks for a core representing the entire thickness of the block. Nine cores were drilled from each block. Fig. 4 shows the appearance of a full core with a length of approximately 650 mm.

For each block, three full-length cores were used to determine compressive strength and Young's modulus, three to determine splitting tensile strength, and three to determine the variation in void distribution. Each full-length core used for strength tests was cut into two cylinders with a height-to-diameter ratio (h/d) of 2; one cylinder represented the top of the block and one represented the bottom. Each core used to determine the variation in void content was cut into 6–7 100 mm high specimens throughout the layer depending on the total height of the block. Each specimen was cured in a 50 °C water basin until reaching an equivalent 28-days age at 20 °C.

Only mix No. 2 was tested for shear strength. A total of 16 prisms were cut from each of the blocks to determine the shear strength. When cutting these prisms, the outer approximately 100 mm surface was first removed. Fig. 5 shows the position from where the prisms were taken. Each prism measured $320 \times 160 \times 100\ mm^3$.

The upper prisms (U) do not contain any layer interface for any of the two blocks whereas all lower prisms (L) contain one layer interface. The prisms were stored in a 20 °C water basin until reaching an equivalent 28-days age at 20 °C.

3.4. Preparation of PCPC for full-scale test

The preliminary results from the small-scale test suggested that the filling material in the Pearl-Chain Bridge should be cast in layers with a thickness of approximately 30 cm before compaction. Since the maximum placing depth after compaction was 0.9 m, the filling material had to be cast in a total of four layers with each being compacted by the same plate compactor as used in the small-scale tests. A wood formwork was placed in the transverse bridge direction to ensure the correct layer thicknesses. The three lower layers all had a thickness of approximately 25 cm after compaction, whereas the thickness of the upper layer was only approximately 15 cm. As a result, the upper layer was only compacted once whereas the underlying layers were each compacted twice. Due to the distance between the bridge ends and the center of the bridge, it was necessary to pour PCPC by use of a belt. The fill over the two middle abutments was laid out simultaneously. A protruding reinforcement was installed in the top of the side elements for the concrete top plate being cast at a later stage. Due to this reinforcement, it was not possible to compact the outer

Fig. 4. 650 mm long pervious concrete core drilled from block cast in two layers at mixing plant A. The core is rotated 90° compared to the drilling direction.

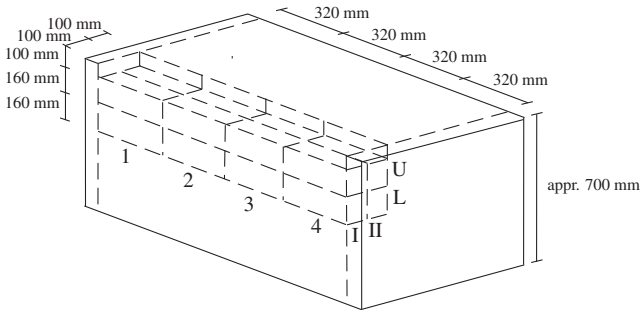

Fig. 5. Position and naming of prisms cut for shear strength tests. For clarity, the outer 100 mm thick surface in front of the specimens is not shown in the figure. This surface was removed before cutting the prisms.

0.5 m of the two upper layers along the long bridge edge using the plate compactor. Instead, this area was compacted with a hand compactor created from a $200 \times 200\ mm^2$ plate connected to a handle. Fig. 6 illustrates how the PCPC filling material was stepwise laid out.

Because of fresh PCPC's stiff consistency, it is not possible to assess its workability from the standard slump cone test. Instead, fresh PCPC mixture workability was determined by assessing the fresh unit weight. When a new PCPC batch arrived, the fresh unit weight was determined in accordance with Procedure A in the ASTM C1688 standard [17], by compacting a specified PCPC volume with a standard Proctor hammer. By weighing the mass of the compacted PCPC, the density of the fresh PCPC was calculated. In total, 10 PCPC batches were delivered to the construction site; five to the east end of the bridge and five to the west end. Table 5 shows the fresh unit weight determined for the different batches.

Problems were experienced when placing the third layer of the filling material due to batch No. 4 being too wet. The mixing plant later explained this shift in consistency with a mistake in the correction of aggregate moisture content. This change is also clear from Table 5 where the unit weight of batch No. 4 is seen to be higher than the remaining material. However, the batch was still

Fig. 3. Appearance of PCPC blocks cast with mix No. 1. Left: block cast in one layer. Right: block cast in two layers.

Fig. 6. Filling of pervious concrete on Pearl-Chain Bridge over Vorgod Stream. a: compaction of first layer; b: casting of second layer; c: casting of third layer; d: finishing of fourth layer.

placed and this caused a visibly lower void content of the third layer as seen in Fig. 7. The PCPC close to the bridge edge is seen to be drier than that close to the bridge center.

Three temperature sensors were placed in the same vertical section over each middle abutment. One sensor was placed below the filling material and two sensors were placed in the two lower layer interfaces. Furthermore, the air temperature was measured. Fig. 8 shows the variation in temperature over one of the abutments; as shown, the maximum temperature is only 41 °C.

After emplacement, the filling material was tightly covered with plastic and allowed to cure for 15 days before the plastic was removed. Immediately afterwards, 12 cores with a diameter of 100 mm and a length of 300 mm were drilled before casting the concrete top plate. Fig. 9 shows the location of the cores taken from the filling material. The location of the cores had to be close to the middle abutments where the thickness of the filling material was largest.

Each core was wrapped in two layers of plastic to prevent moisture evaporation. Subsequently, each core was cut to a length of 200 mm and placed in a 20 °C water basin until reaching an equivalent 28-days age at 20 °C. At that time, the void content of the cores was determined, six cores were tested in compression, and six cores were tested in splitting tension.

3.5. Testing procedure

3.5.1. Determination of void content

The void content of the specimens was determined from a water displacement setup based on Archimedes' principle. The specimens were submerged and weighed under water, then oven-dried at 40 °C for 24 h, and finally weighed above water, whereby it was possible to calculate the void content, P [%], as

$$P = \left(1 - \frac{m_{40^\circ C} - m_{sw}}{\rho_w \, V_{tot}}\right) \times 100\% \quad (1)$$

where $m_{40^\circ C}$ [kg] is the mass of the oven-dried specimen after 24 h, m_{sw} [kg] is the mass of the specimen submerged in water, ρ_w [kg/m^3] is the water density, and V_{tot} [m^3] is the total volume of the specimen.

Table 5
Fresh unit weight (UW) of PCPC batches delivered to east and west end of construction site of Pearl-Chain Bridge over Vorgod Stream. UW was not measured for batch No. 3.

Batch No.	UW [kg/m^3]	
	East	West
1	2142	2107
2	2171	2089
4	2264	2236
5	2084	2040

Fig. 7. Difference in consistency in PCPC placed in third layer of filling material on Pearl-Chain Bridge over Vorgod Stream. PCPC close to the bridge center (right hand side of photo) is considerably wetter than PCPC close to the bridge edge (left hand side of photo).

3.5.2. Determination of strength and stiffness

The compressive strength and Young's modulus were determined from the same test setup. No standards exist regarding strength-testing procedures for pervious concrete; hence modified versions of the Danish Standard (DS) 12390-3 [18], and the International Organization for Standardization (ISO) 6784 standard [19], were used. The compressive test was performed on a TONI

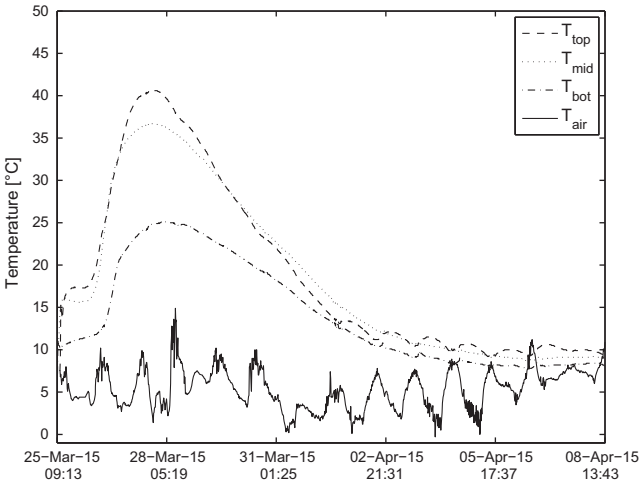

Fig. 8. Temperature variation over one abutment in PCPC filling material on Pearl-Chain Bridge over Vorgod Stream. The temperature profile measured over the other abutment looks similar.

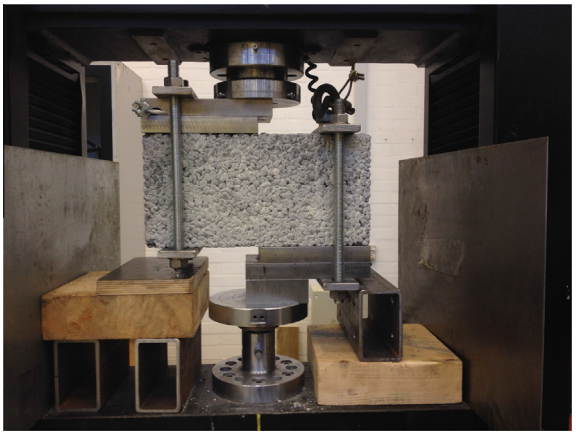

Fig. 10. Shear strength test setup. Specimen measures 160 × 100 × 320 mm^3.

3000 kN machine with a load rate of 7 kN/s for specimens with a diameter of 143 mm, and a load rate of 3 kN/s for specimens with a diameter of 100 mm. When measuring the strain of the specimen, rigid rings were tightly mounted around the top and bottom and two extensometers were placed between the rings. Following this, the correlation between load and deformation was logged during compression. When determining Young's modulus, the main difference from the ISO 6784 standard [19], was that no reloading took place and the modulus of elasticity was determined from the first loading. The Young's modulus was only determined for mix No. 2 specimens.

The splitting tensile strength was determined from the DS 12390-6 standard [20], on a TONI 3000 kN machine with a load rate of 4 kN/s for the specimens with a diameter of 143 mm, and a load rate of 2 kN/s for those with a diameter of 100 mm. Hard fiberboard plates measuring 4 × 10 × 300 mm^3 were placed below and above the specimen.

The shear strength was determined from the test setup shown in Fig. 10 inspired by [21] with the load applied over a 160 × 100 mm^2 shear plane. The test was carried out on an Instron 100 kN machine with a load rate of 0.4 mm/minute.

4. Results and discussion

4.1. Results and discussion of small-scale tests

4.1.1. Density and void content for small-scale tests

Fig. 11 shows the variation in dry density with void content for a total of 12 specimens cut from each block.

A strong linear correlation with R^2-values greater than 0.85 between the void content and the density of the specimens is seen.

4.1.2. Vertical variation in void content for small-scale tests

The total height of the hardened block varied between 650 mm and 750 mm dependent on the number of layers. The vertical variation in void content through a block was determined for blocks cast in one, two, and three layers. Figs. 12–14 show the variation in void content with depth for these three scenarios.

Considering Fig. 12, the variation in vertical void content for the block cast in one layer is seen to vary between approximately 5% close to the top of the block and 33% close to the bottom of the block. Furthermore, it is evident that the plate compactor influence has a limited range after which the void constant aligns with depth. The estimated range is marked with a vertical black line that corresponds to a depth of approximately 40 cm. The points below this depth are not believed to be representative for the variation in the layer void content; hence, they are omitted from the further analysis. Previous studies such as [15] have suggested a linear variation in the vertical void content with depth. The compaction method is expected to influence the results; however, the present study indicates a strong logarithmic tendency in the vertical void variation with depth, with R^2-values of 0.99 and 1.00.

Considering Fig. 13, only three void content measurements are obtained for each of the layers for the blocks cast in two layers; hence, it is not possible to comment on whether the vertical variation in void content is also logarithmic. Nevertheless, it is seen that the variation has decreased compared to the block cast in one layer. The vertical void content is now varying between 15–20% at the top of a layer and 30–35% at the bottom of a layer.

Considering Fig. 14, the variation in void content has decreased even further when the block is cast in three layers. The variation in

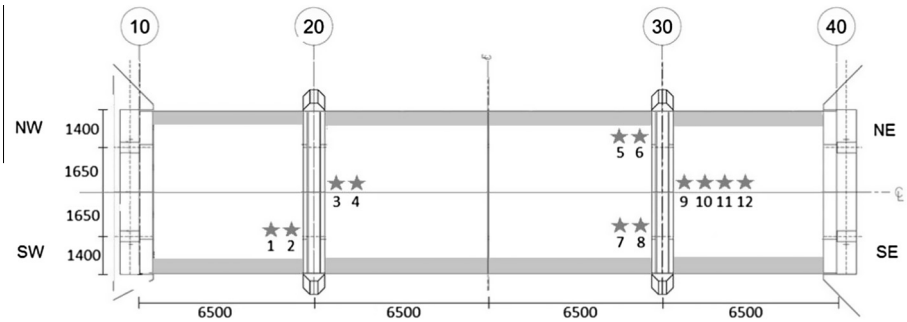

Fig. 9. Top view of Pearl-Chain Bridge over Vorgod Stream with location (stars) of cores drilled from filling material. Dimensions are in mm.

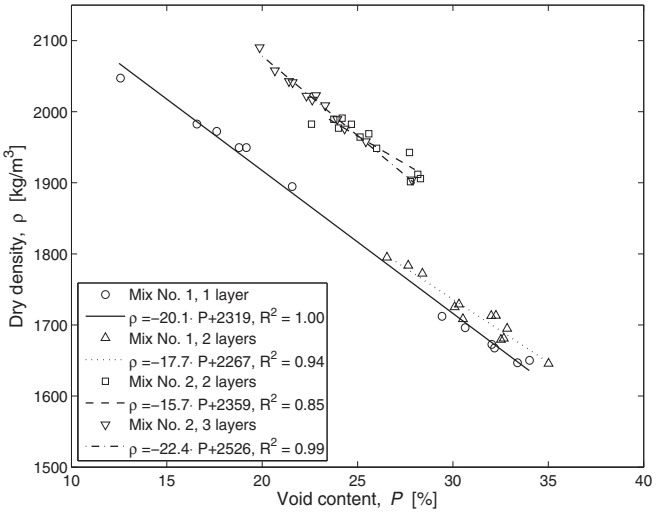

Fig. 11. Variation in dry density with void content for cores drilled from blocks. Note the scale on the axes.

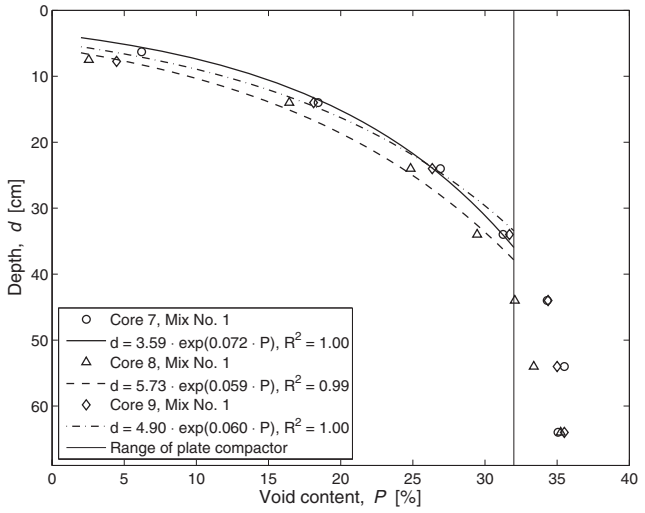

Fig. 12. Variation in void content of block cast in one layer with mix No. 1. A depth of 0 cm corresponds to the surface of the block where the compaction took place. The total height of the block after compaction was 69 cm.

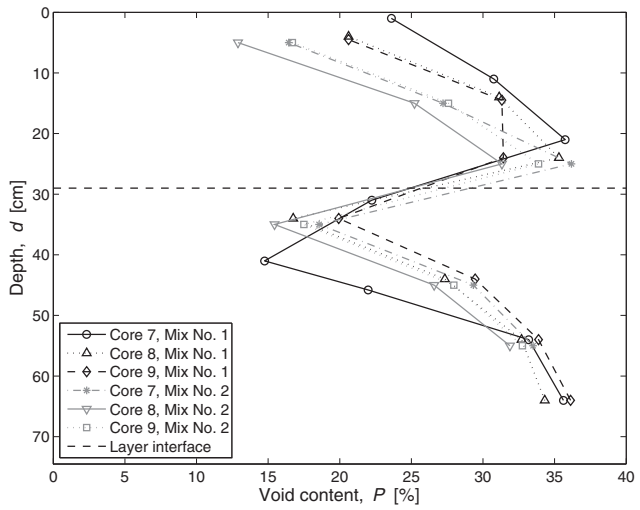

Fig. 13. Variation in void content of block cast in two layers with mix Nos. 1 and 2. A depth of 0 cm corresponds to the surface of the block where the compaction took place. The total height of the blocks after compaction was 70 cm and 65 cm.

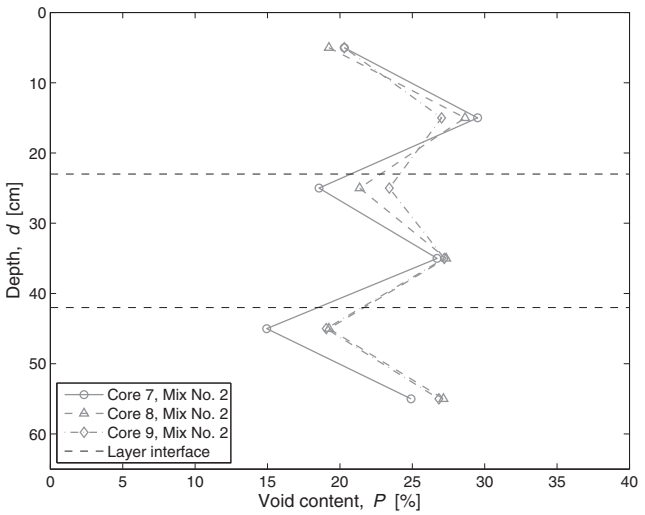

Fig. 14. Variation in void content of block cast in three layers with mix No. 2. A depth of 0 cm corresponds to the surface of the block where the compaction took place. The total height of the block after compaction was 65 cm.

each layer is now reduced to ~20% at the top of the layer and ~30% at the bottom of the layer. Moreover, it is seen from Figs. 13 and 14 that the void variation in underlying layers is not influenced by casting and compacting overlying layers.

The same specimens that were used to determine the vertical variation in void content were subsequently tested in compression at an equivalent 28-days age at 20 °C. The rationale behind this was that these specimens, which had $h/d = 100/143 \sim 0.7$, had a more homogeneous void content than the usual test specimens with $h/d = 2$. For this reason, a better understanding of the actual correlation between void content and compressive strength was expected. Fig. 15 shows the variation in the compressive strength of the $h/d = 0.7$ specimens from the one layer block from mix No. 1 and the two layer block from mix No. 2. For clarity, the data from the other two blocks is not included, but provide similar results.

Fig. 15 suggests there is a strong linear correlation between the void content and the compressive strength of the specimen. All results have R^2-values greater than 0.95.

All strength tests used to characterize strength properties of the PCPC mixes were performed on cylinders with $h/d = 2$. The void content of all cylinders was determined as described in Section 3.5.1 prior to the strength testing. Table 6 shows the void contents of the cores drilled for strength tests from the block cast in one layer from mix No. 1. The table illustrates the void content of top cylinders and the corresponding bottom cylinders.

According to Table 6, the void content of the top cylinders from the block cast in one layer with mix No. 1 is 13–22%. However, analyzing the depth between d = 0–300 mm in Fig. 12 reveals that the void content within each cylinder actually varies between 5–33%. Hence, the void content used to characterize and connect with a certain strength property is an average value that does not cover the variation in void content within the cylinder itself. The same is true when comparing the void content of bottom specimens, and also when comparing cores drilled from the remaining three blocks even though the error is minimized when increasing the number of layers. Because the strength properties determined for cylinder specimens with $h/d = 2$ are typically connected with the

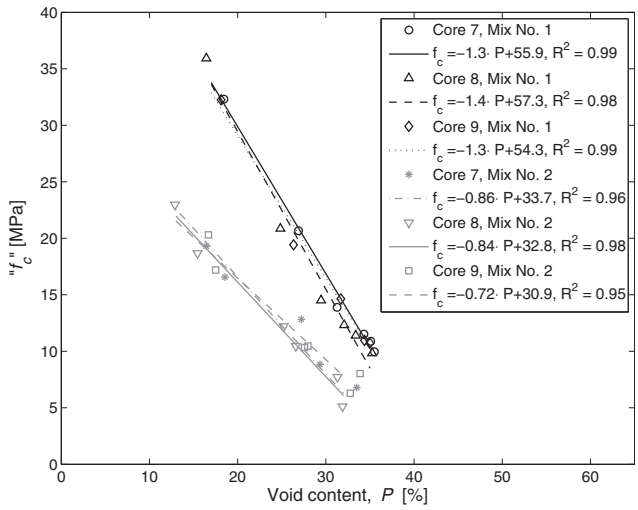

Fig. 15. Variation in compressive strength with void content for block cast in one layer with mix No. 1 and two layers with mix No. 2. "f_c" is measured on specimens with $h/d = 0.7$.

Table 6
Average void content of specimens with $h/d = 2$ from block used for strength determination cast in one layer with mix No. 1.

	Core No.					
Void content [%]	1	2	3	4	5	6
Top of layer	19.2	17.6	21.6	16.6	12.6	18.8
Bottom of layer	34.0	32.0	33.4	30.6	29.4	32.2

average void content of the specimen, there is a miscorrelation between the strength variation with void content. In fact, the strength properties presented express those of the part of the specimen with the highest void content.

4.1.3. 28-Days compressive strength for small-scale tests

Fig. 16 shows the 28-days compressive strength of the specimens drilled from the four blocks, comparing that of those taken from the top of the block with that of those taken from the bottom of the block. The compressive strength values of pervious concrete should always be seen in the light of the void content since these two parameters are strongly correlated. Therefore the figure also shows the average void content of the specimens.

Considering "Mix No. 1, 2 layers", "Mix No. 2, 2 layers", and "Mix No. 2, 3 layers", the top and bottom specimens within each block have void contents that are statistically equivalent. As shown in Fig. 16, this also explains why the compressive strengths for bottom and top specimens for each block are statistically equivalent. The average 28-days compressive strength for "Mix No. 2, 3 layers" is 9.1 MPa, whereas it is 7.7 MPa for "Mix No. 2, 2 layers", and 6.9 MPa for "Mix No. 1, 2 layers". The decrease in compressive strength between the blocks is believed to be directly correlated to the corresponding increase in void content; see Fig. 16.

Considering "Mix No. 1, 1 layer", the void content of top and bottom specimens varies. The average 28-days compressive strength of the bottom specimens is 7.3 MPa, which is comparable with the specimens from "Mix No. 1, 2 layers" that also have void contents in the same order of magnitude. The average 28-days compressive strength of the top specimens is 14.6 MPa which is twice as high as that of the bottom specimens. This is explained by the correspondingly lower void content, which is in the same order of magnitude as the top specimens from "Mix No. 2, 3 layers"; nevertheless, the average 28-days compressive strength is significantly higher. The explanation might be that even though the average void content is the same, a relatively large variation within the specimens themselves is found as discussed in connection with Table 6.

4.1.4. 28-Days Young's modulus for small-scale tests

The 28-days Young's modulus was determined from the stress–strain curves obtained from the compression tests of the specimens from mix No. 2. An example of such a stress–strain curve can be found in Fig. 17.

Due to the high void content of the pervious concrete specimens, it was rather difficult to fasten and fix the rings for strain measurements to make sure they would not move during the compressive tests. In some cases the stress–strain curves revealed that the rings had moved. Fig. 18 shows the variation in Young's modulus with void content for the blocks cast with mix No. 2.

For Fig. 18, the results are omitted from tests where the ring system is believed to have moved. Nevertheless, a big scattering of the results is still observed and no clear dependency on the void

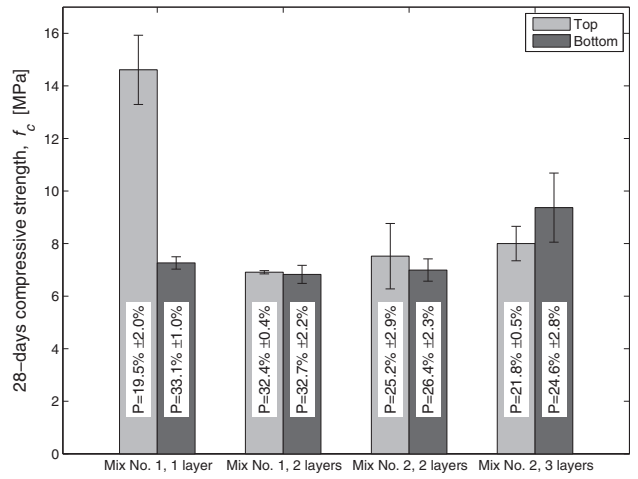

Fig. 16. 28-days compressive strength, f_c, of top and bottom specimens from mix Nos. 1 and 2. The figure also shows the corresponding average void contents of the specimens and the standard deviation of the void content and the compressive strength.

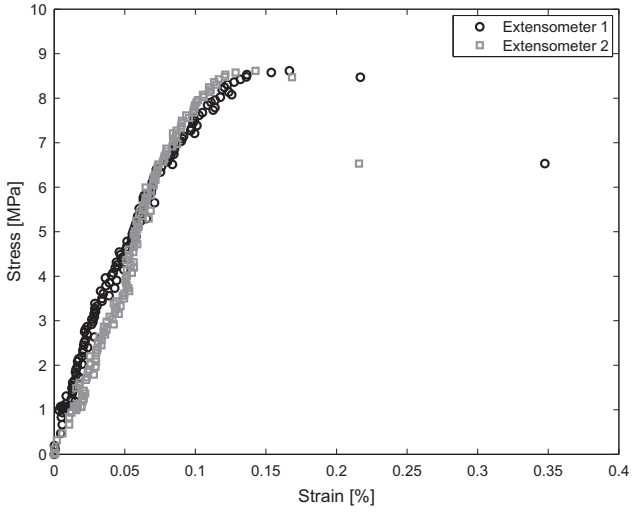

Fig. 17. Stress–strain curve for compression test of a top specimen from the block cast in three layers with mix No. 2. Two extensometers, Nos. 1 and 2, were fastened to log the strains.

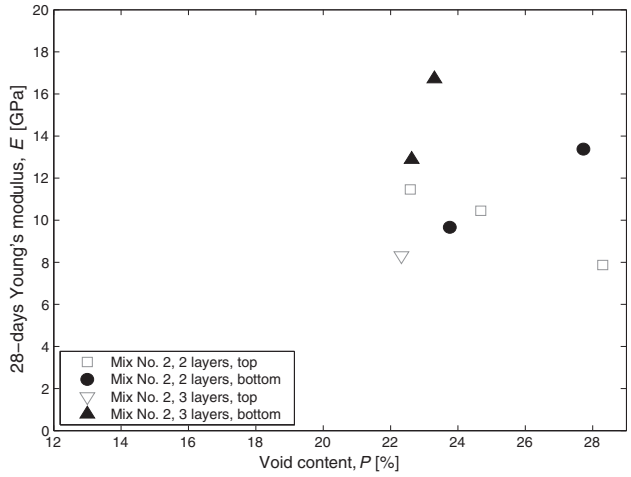

Fig. 18. Variation in 28-days Young's modulus with void content for specimens cast in two layers and three layers with mix No. 2.

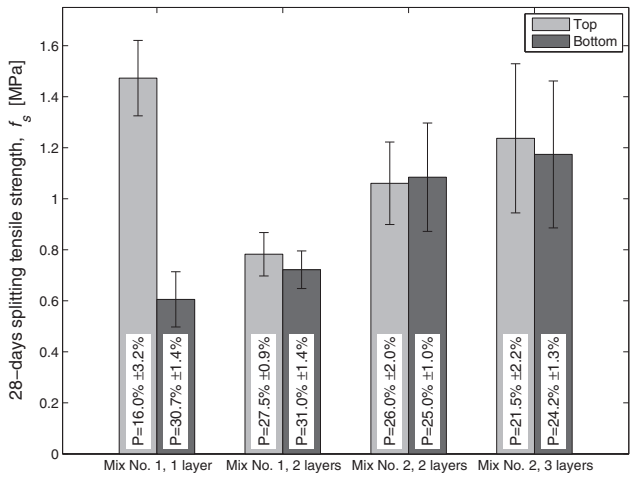

Fig. 19. 28-days splitting tensile strength, f_s, of top and bottom specimens from mix No. 1 and 2. The figure also shows the corresponding average void contents of the specimens and the standard deviation of the void content and the splitting tensile strength.

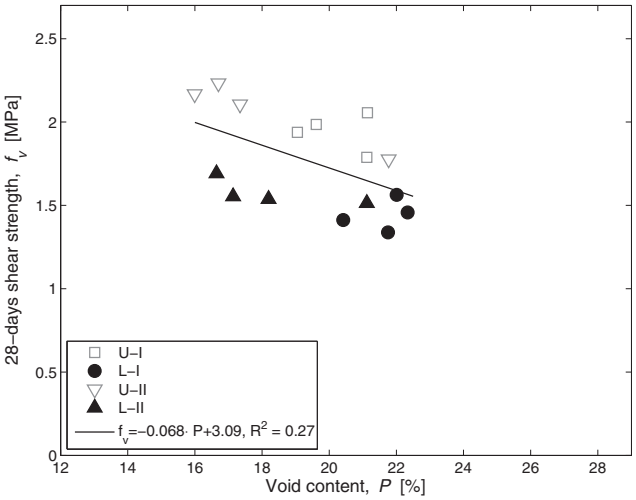

Fig. 20. Variation in 28-days shear strength with void content for blocks cast in two layers with mix No. 2.

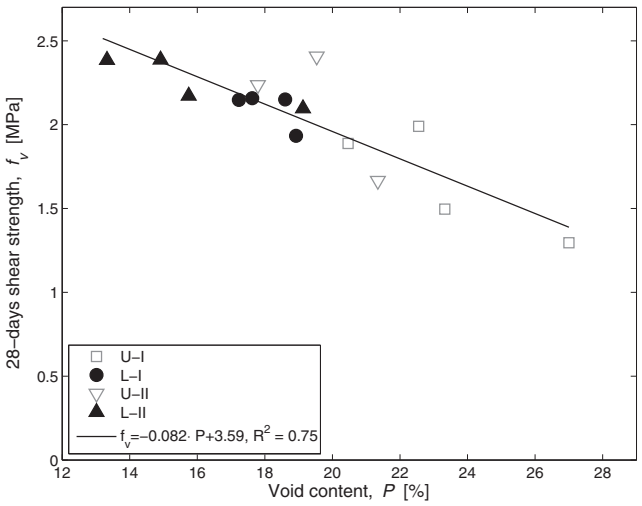

Fig. 21. Variation in 28-days shear strength with void content for blocks cast in three layers with mix No. 2.

Table 7
28-days compressive strength, f_c, and 28-days splitting tensile strength test, f_s, for cores from PCPC filling material on Pearl-Chain Bridge over Vorgod Stream.

Core No.	Void content [%]	f_c [MPa]	f_s [MPa]
1	3.8	25.0	–
3	2.6	28.8	–
5	14.2	17.4	–
7	8.4	22.6	–
9	5.8	26.1	–
11	4.0	22.5	–
2	3.7	–	2.7
4	3.0	–	2.4
6	14.5	–	1.4
8	4.3	–	3.4
10	4.7	–	3.4
12	3.3	–	3.6

variation is observed, possibly because the range of void contents considered is relatively narrow. However, an indication of the size of Young's modulus can be found from the results.

4.1.5. 28-Days splitting tensile strength for small-scale tests

Fig. 19 shows the 28-days splitting tensile strength of the specimens drilled from the four blocks. The figure compares those taken from the top of the block with those taken from the bottom. The figure also shows the average void content of the specimens.

Considering "Mix No. 2, 2 layers" and "Mix No. 2, 3 layers", the top and bottom specimens are seen to have void contents that are statistically equivalent. This also explains why the splitting tensile strengths for bottom and top specimens from each block are statistically equivalent. The average 28-days splitting tensile strength for "Mix No. 2, 2 layers" is 1.1 MPa, whereas it is 1.2 MPa for "Mix No. 2, 3 layers". The increase in splitting tensile strength is believed to be directly correlated to the corresponding decrease in void content. However, the standard deviation of the results, especially with mix No. 2, reveals that they are subject to a certain scattering.

Considering "Mix No. 1, 1 layer" and "Mix No. 1, 2 layers", the void variation between the top specimens and bottom specimens is seen to be larger than for the blocks cast with mix No. 2, especially for the block cast in one layer where the void content of the bottom specimens is twice as high as for the top specimens. The corresponding average 28-days splitting tensile strength for the top specimens is 1.5 MPa, whereas it is 0.6 MPa for the bottom specimens.

Overall, the observed difference between specimens from the different blocks is believed to be caused by the variation in void content. The higher the void content, the lower the splitting tensile strength.

4.1.6. 28-Days shear strength for small-scale tests

The 28-days shear strength of the prisms cut from the blocks in two and three layers from mix No. 2 is shown in Figs. 20 and 21.

The results are divided into upper (U) and lower (L) specimens, and front (I) and back (II) specimens. Reference is made to Fig. 5 for the positions of these specimens.

From Fig. 21, a linear variation in shear strength with void content is observed; the same tendency is not found from the results in Fig. 20. From the shear strength determined for the block cast in two layers, there is a clear difference between those determined from the upper specimens and from the lower specimens. The upper specimens have an average shear strength that is 0.5 MPa higher than that of the lower specimens even though the difference in void content is only one percentage point. The reason for this difference can be that the lower specimens contain a layer interface, which is not the case for the upper specimens. However, the same tendency is not observed for the specimens from the block cast in three layers.

4.2. Results and discussion of full-scale test

Table 7 shows the void content and the corresponding compressive strength and splitting tensile strength of cores taken from the PCPC filling material on the Pearl-Chain Bridge over Vorgod Stream.

As seen in Table 7, the void content of most of the cores is considerably lower than the design void content. This also means that the strength values are considerably higher than those determined from the small-scale tests. It is believed that the reason for this is that PCPC batch No. 4 was too wet. The cores tested were drilled 300 mm vertically down in the filling material from the top, and subsequently, the upper 50–70 mm were removed; hence, a big part of each core represents the third layer which is known to be too wet causing the PCPC skeleton to collapse. If it had been possible to take out samples from the first two PCPC layers, it is expected that the void content would have been considerably larger.

The influence of hand compaction of the two upper layers closest to the bridge edges is clear from the void content of core Nos. 5 and 6 that were taken close to the northern bridge edge, below the protruding reinforcement, as seen in Fig. 9. The void content of core Nos. 5 and 6 is higher than that of the remaining cores and it approaches the design void content. This also affects the strength properties, which, according to Table 7, are lower than for the remaining cores.

The strength properties of all cores meet the requirements to PCPC fill in Pearl-Chain Bridges. It should be noted that the increase in strength properties of the PCPC filling material compared to the design values has no negative influence on the static function of the bridge.

The experiences drawn from the present study emphasize the need for general regulations on quality control of pervious concrete. No such European regulations exist. An assessment of whether a given batch is too dry or too wet is subjective and therefore impossible to use as a quality control. Even though the authors assessed that PCPC batch No. 4 was too wet, any less-experienced personnel will not be able to do so. Therefore, a measurable quality routine should be adapted. Since 2013, the American Concrete Institute (ACI) has recommended that the difference in fresh unit weight between mixture proportion and a given batch be used as quality control. According to the ACI 522.1M-13 standard [22], a batch is only accepted if the fresh unit weight is within ±80 kg/m^3 from the submitted mixture proportion. An equivalent quality control would in all probability have prevented batch No. 4 from being cast on the Pearl-Chain Bridge over Vorgod Stream since a clear increase in fresh unit weight was measured, as commented previously.

5. Conclusions

In this study, pervious concrete was used as filling material with a total depth of up to 0.9 m in a 26 m long Pearl-Chain Bridge. The planning of the full-scale implementation was based on small-scale tests where the variations in void content and strength properties were investigated to find the most appropriate layer thickness. The main conclusions from the study can be summarized as follows:

1. The variation in void content throughout a layer compacted from above follows a logarithmic tendency with the lowest void content at the top of the layer and the highest void content at the bottom of the layer.
2. It is possible to cast several pervious concrete layers on top of each other without influencing the void content and strength properties of underlying layers.
3. Layer thicknesses exceeding 27 cm before compaction cause inhomogeneous specimens with respect to void content when the layer is compacted from above. With a layer thickness of 27 cm, a void content of 20–30% was obtained throughout each layer.
4. A 28-days compressive strength of 9.1 MPa and a 28-days splitting tensile strength of 1.2 MPa were obtained with a pervious concrete mix containing no admixtures except from air entrainment and with a layer thickness of 27 cm and a void content of 20–30% through the layer. Moreover, a linear variation in the 28-days shear strength with void content was found for the same pervious concrete mix and layer thickness. The shear strength values varied between 1.3 MPa and 2.4 MPa for void contents between 27% and 13%.
5. Determination of Young's modulus of pervious concrete is connected with a significant scattering because of difficulties in installing the testing equipment due to the voids.
6. The strength properties determined for a cylinder specimen with $h/d = 2$ are often related to the average void content of the specimen. This causes a miscorrelation of the strength variation with void content when the specimen is compacted from above because the strength properties actually relate to the part of the specimen with the highest void content; typically, the lower part of the specimen.
7. There is a linear correlation with R^2-values of 1.0 between void content and 28-days compressive strength when the compressive strength is measured on cylindrical specimens with $h/d = 0.7$, which have a more homogeneous void distribution than cylinders with $h/d = 2$.
8. It is possible to implement pervious concrete as filling material in arch bridges, including Pearl-Chain Bridges. However, quality control regulations are needed to ensure proper consistency and workability of PCPC in the field so the results after placing are satisfying. Restrictions on the variation in fresh unit weight seem to be an appropriate quality control.

Acknowledgments

The authors wish to thank Innovation Fund Denmark for supporting this project and the Danish concrete mixing plants Wewers and IBF for their contributions.

Appendix A. Supplementary data

Supplementary data associated with this article can be found, in the online version, at http://dx.doi.org/10.1016/j.conbuildmat.2015.12.104.

References

[1] P.S. Halding, K.D. Hertz, J.W. Schmidt, Precast Pearl-Chain concrete arch bridges, J. Eng. Struct. 103 (2015) 214–227.
[2] P.S. Halding, K.D. Hertz, N.E.V. Petersen, B. Kennedy, Assembly and lifting of Pearl-Chain arches, in: Proceedings of fib Symposium, 18–20 May 2015, Copenhagen, 2015, pp. 185–186.
[3] DS Standard 1991-2, Eurocode 1: Actions on structures – Part 2: Traffic loads on bridges, Danish Standards, Denmark, 2003.
[4] DS Standard 1991-2 DK NA, Annex A (Normative) Load models for classification and evaluation of load carrying capacity, Danish Standards, Denmark (In Danish), 2003.
[5] V.R. Schaefer, K. Wang, M.T. Suleiman, J.T. Kevern, Mix design development for pervious concrete in cold weather climates, Report from the National Concrete Pavement Technology Center, Iowa State University, Ames, IA, USA, 2006.
[6] Regional variation of extreme rain in Denmark – a new analysis 1979–2005, Pamphlet No. 28, IDA Wastewater Commission, Copenhagen, 2006, ISBN: 87-7923-502-6 (In Danish).
[7] J.T. Kevern, V.R. Schaefer, K. Wang, S.T. Suleiman, Pervious concrete mixture proportions for improved freeze-thaw durability, J. ASTM Int. 5 (2) (2008). JAI101320.
[8] National Ready Mixed Concrete Association (NRMCA), Freeze-Thaw Resistance of Pervious Concrete, NRMCA, Silver Spring, MD, USA, 2004.
[9] V.R. Schaefer, J.T. Kevern, An integrated study of pervious concrete mixture design for wearing course applications, Report from the National Concrete Pavement Technology Center, Iowa State University, Ames, IA, USA, 2011.
[10] L.K. Crouch, J. Pitt, R. Hewitt, Aggregate effects on pervious portland cement concrete static modulus of elasticity, J. Mater. Civ. Eng. ASCE 19 (7) (2007) 561–568, http://dx.doi.org/10.1061/(ASCE)0899-1561(2007) 19:7(561).
[11] P.D. Tennis, M.L. Leming, D.J. Akers, Pervious Concrete Pavements. EB302.02, Portland Cement Association, Skokie, IL, and National Ready Mixed Concrete Association, Silver Spring, MD, USA, 2004.
[12] ASTM Standard C666/C666M-03, Standard Test Method for Resistance of Concrete to Rapid Freezing and Thawing, ASTM International, West Conshohocken, PA, 2008, DOI: http://dx.doi.org/10.1520/C0666_C0666M-03R08.
[13] V. Henderson, S. Tighe, Evaluation of pervious concrete pavement performance in cold weather climates, Int. J. Pavement Eng. 13 (3) (2012) 197–208, http://dx.doi.org/10.1080/10298436.2011.572970.
[14] J.T. Kevern, K. Wang, V.R. Schaefer, Test methods for characterizing air void systems in portland cement pervious concrete, J. ASTM Int., 9, 2009, http://dx.doi.org/10.1520/JAI102451.
[15] L.M. Haselbach, R.M. Freeman, Vertical porosity distributions in pervious concrete pavement, ACI Mater. J. 103 (6) (2006) 452–458.
[16] DS Standard 2426, Concrete – Materials – Rules for application of EN 206-1 in Denmark, Danish Standards, Denmark, 2011.
[17] ASTM Standard C1688/C1688M-14a, Standard Test Method for Density and Void Content of Freshly Mixed Pervious Concrete, ASTM International, West Conshohocken, PA, 2014, DOI: http://dx.doi.org/10.1520/C1688_C1688M-14A.
[18] DS Standard 12390-3, Testing hardened concrete – Part 3: Compressive strength of test specimens, Danish Standards, Denmark, 2009.
[19] ISO Standard 6784, Concrete – Determination of static modulus of elasticity in compression, International Standard, 1982.
[20] DS Standard 12390-6, Testing hardened concrete – Part 6: Tensile splitting strength of test specimens, Danish Standards, Denmark, 2002.
[21] H.K.M. Schmit, E.R.E. Reid, A.A. Beatty, T.J. Stratford, L.A. Bisby, Shear strength of concrete at elevated temperature, in: Proceedings of Application of Structural Fire Engineering 2011, Prague, Czech Republic, 2011.
[22] ACI 522.1M-13 Standard, Specification for Pervious Concrete Pavement, ACI Standard, Reported by ACI Committee 522, 2013, ISBN-13: 978-0-87031-848-1.

Paper III

"Mix design for improved strength and freeze-thaw durability of pervious concrete fill in Pearl-Chain Bridges"

M.S.M. Lund, J.T. Kevern, V.R. Schaefer, and K.K. Hansen

Published in: *Materials and Structures, 2017;50:42-56*

Materials and Structures (2017)50:42
DOI 10.1617/s11527-016-0907-4

ORIGINAL ARTICLE

Mix design for improved strength and freeze-thaw durability of pervious concrete fill in Pearl-Chain Bridges

Mia S. M. Lund · John T. Kevern · Vernon R. Schaefer · Kurt K. Hansen

Received: 27 February 2016 / Accepted: 6 June 2016

Abstract Pearl-Chain Bridges are an innovative precast arch bridge technology which can utilize pervious concrete as fill material. The present study investigates how the mix design of the pervious concrete fill can be influenced by use of an air-entraining admixture, a high-range water reducing admixture, fibers, and by internal curing using lightweight aggregate to best possibly meet the requirements for a fill material in Pearl-Chain Bridges. The 28-day compressive strength, splitting tensile strength, shear strength, permeability, and freeze-thaw durability were determined and compared for eight different mixture proportions using two different sizes of granite coarse aggregate and at two different water-to-cement ratios. The specimens had an average void content of 24–28 %. Specimens containing air entraining and high-range water reducing admixtures were most workable, as determined by fresh density, and thus the easiest to place. The addition of a high-range water reducing admixture and lightweight sand (expanded shale) for internal curing improved the 28-day compressive strength and splitting tensile strength. The coarse aggregate gradation had a large influence on permeability; however, all tested permeabilities were high enough to drain the rain from a 100-year rain event in Denmark. The air entraining agent dosage used was not sufficiently high to create the necessary protective air content in the cement paste, and the freeze-thaw durability of the specimens were generally poor for the utilized test procedure; however, the mix design containing lightweight sand showed improved freeze-thaw durability compared to the other mix designs.

Keywords Fill material · Freeze-thaw durability · Pearl-Chain Bridge · Permeability · Pervious concrete · Strength properties

M. S. M. Lund (✉) · K. K. Hansen
Technical University of Denmark, Brovej 118, 2800 Kongens Lyngby, Denmark
e-mail: msml@byg.dtu.dk

K. K. Hansen
e-mail: kkh@byg.dtu.dk

J. T. Kevern
University of Missouri-Kansas City, 352 Flarsheim Hall, 5100 Rockhill Rd, Kansas City, MO 64110, USA
e-mail: kevernj@umkc.edu

V. R. Schaefer
Department of Civil, Construction, and Environmental Engineering, Iowa State University, Ames, IA 50011, USA
e-mail: vern@iastate.edu

Published online: 10 August 2016

1 Introduction

Pearl-Chain Bridge (PCB) technology is a new prefabricated arch bridge concept developed primarily for road and railway bridges. Arches are no longer a widely utilized shape for new bridges because construction typically requires a comprehensive

scaffolding that is both expensive, cumbersome, and closes down the underpassing road for weeks. PCB reintroduces the arch structure as an economic rapid bridge construction solution because the construction of the arch is moved to the roadside, by which the underpassing road only needs to close down when the arch is lifted into place by a crane and spandrel walls are installed. Placing the entire arch structure is only expected to take a night. The construction of PCB arch is fairly simply: a number of plane concrete elements with inclined end surfaces (so-called SL-Decks [1, 2]) is collected on a wire, like pearls on a string, and by post-tensioning the wire the arch is assembled [3]. During the post-tensioning process the SL-Decks arch due to bearing on the inclined ends. The number of elements controls the span length and the width of the bridge is determined by the number of Pearl-Chain arches placed next to each other. In 2015, the first PCB was constructed in Denmark. The bridge consisted of a main arch with a span length of 13 m and two adjacent half-arches with a span length of 6.5 m each. The pile height was 0.9 m and the total width was 6.1 m. The bridge was filled with Portland Cement Pervious Concrete (PCPC) as seen in Fig. 1 and described in [4].

The decision to use PCPC as the fill material rather than a more commonly used material, such as coarse aggregate, was based on several considerations taking both the strength and durability properties of the fill material and the entire PCB into account. From a durability perspective, a bridge is a sensitive point in a road construction because it is more vulnerable to the environment than the rest of the road construction. A bridge is, for example, cooled from the underside as well as from the topside during winter months which makes it more exposed to frost damages. Water is unwanted in any bridge superstructure because it is involved in most deterioration mechanisms of concrete such as freeze-thaw. PCPC fill has excellent drainage properties that prevent water accumulation in the fill, thus minimizing the risk of frost damage of the fill material itself. Moreover, water that penetrates the fill material and reaches the upper surface of the arch structure drains naturally toward the bridge ends because of the arch curvature, which minimizes the moisture exposure of the PCB arch. With a permeability of at least 4×10^{-3} cm/s, the PCPC fill can drain the rain from a 10-year rain event in Denmark [5]. Another advantage of implementing PCPC fill in PCB is that it can be incorporated as a structural part

Fig. 1 PCPC cast as fill material in the very first Pearl-Chain Bridge constructed in Denmark in 2015. *Upper* The longitudinal bridge section shows that the bridge consisted of a main arch between two adjacent half arches. *Lower* Placement of PCPC fill. The formwork wood beams were removed as the different layers were cast

and contribute to the load-carrying capacity of the superstructure. Hence, the implementation of PCPC as fill in PCB is expected to improve the longevity and strength of the bridges. For most applications, the requirements of the strength properties of a PCPC fill are a 28-day compressive strength and 28-day splitting tensile strength of a minimum of 10 MPa and 1 MPa, respectively. However, for certain applications, these requirements are raised, and the potential range of PCPC strength properties should therefore be known. The PCPC shear strength is not a parameter that is typically reported in the literature because PCPC is seldom applied in constructions in which its shear capacity is critical. However, in PCB the PCPC fill material can be designed to transfer shear stresses between the road surface and the PCB arch if the shear capacity of the PCPC fill is known and sufficient, and therefore it is very relevant for the application of PCPC fill in PCB to measure shear strength.

The present study investigates how the mixture proportions of PCPC can be improved to provide the most suitable fill for PCB; however, the findings also apply to other PCPC applications. This was investigated by considering the influence of air entraining admixture (AEA), high-range water reducing admixture (HRWR), polypropylene fibers, and internal curing using expanded shale lightweight aggregate on strength (compressive strength, splitting tensile strength and shear strength), permeability, and freeze-thaw durability of the same PCPC mix design as was used for the fill in the very first Pearl-Chain Bridge.

2 Background

PCPC is a highly permeable concrete that is typically used for permeable pavements to rapidly drain and remove rainwater from the pavement surface. Common uses include low-density roads and parking areas [6]. Permeability typically ranges from 0.20–0.54 cm/s and is achieved through a large interconnected void structure with a significant void content of typically 11–35 % [7]. PCPC consists of cement, water, and a single-sized coarse aggregate that is used to maximize the void content. However, often a small portion of the coarse aggregate volume is replaced by fine aggregate (sand) because it improves the strength and durability significantly [8]. The maximum void content is achieved by designing PCPC to have just enough cement paste to coat the aggregates and bind them together in the contact points between the aggregates. Hence, PCPC may have less cement paste than conventional Portland cement concrete. The water-to-cement ratio (w/c-ratio) of PCPC is typically 0.27–0.34, which produces a stiff material and in many cases makes the slump test ill-suited for PCPC workability measurements [6].

The void content of PCPC is a function of the compaction energy, aggregate gradation, and cementitious paste content. Because of the high amount of voids, the strength of PCPC is usually lower than that of conventional Portland cement concrete. Strength and unit weight decrease linearly with increasing void content [4, 7]. However, addition of chemical admixtures such as AEA, HRWR, and hydration stabilizers (HS) affect the strength properties positively, and 28-day compressive strengths of up to 28 MPa can be achieved [8, 6]. Moreover, it has previously been found that by replacing the small portion of conventional concrete sand with pre-wetted lightweight sand for internal curing, both the the compressive strength and the splitting tensile strength increase [9].

The void structure of PCPC is more complex than that of conventional Portland cement concrete because it is combined by larger water carrying voids and smaller natural and entrained air bubbles in the cement paste. The freeze-thaw durability of PCPC is often a major durability concern because of the larger voids; however, the open void structure is only critical if the voids become water saturated and freeze. The freeze-that durability of PCPC is improved by creating a sufficiently fine entrained air system in the cement paste. Addition of first of all AEA but also fibers and lightweight sand have been found to improve the freeze-thaw durability [9–11]. American Society for Testing and Materials (ASTM) C666 [12] is typically used to test and determine the freeze-thaw durability of PCPC; however, many examples show that air-entrained PCPC performs much better in the field than in the laboratory. According to ASTM C666 [12], the PCPC specimens are fully submerged in water during laboratory testing which can be considered a worst-case scenario that is not representative of field conditions where the PCPC drainage effect naturally occurs [13]. In the field, PCPC pavements perform well over several years in areas that undergo a large number of annual freeze-thaw cycles, provided it remains unsaturated [11]. Even though a more realistic frost test method is needed for PCPC, ASTM C666 [12] provides a consistent test method to compare different PCPC mix designs.

3 Methods

3.1 Material properties

All mixes were prepared with ASTM C150 cement meeting both Type I and Type II classification and ASTM C618 Class F fly ash with a specific gravity of 3.15 and 2.28, respectively [14, 15]. The fly ash had 0.1 % carbon content measured using the Eltra carbon analyzer and 0.0 % loss on ignition as determined in accordance with ASTM C311 [16]. Two different types of coarse aggregate were used: granite A and B with a maximum aggregate size of 12.7 mm (1/2 in.) and 9.5 mm (3/8 in.), respectively, both from

Minnesota, USA. The specific gravity and absorption were 2.70 and 0.6 % for granite A, and 2.70 and 0.7 % for granite B, respectively. A sieving analysis was performed in accordance with ASTM C136 [17], and Fig. 2 shows the gradation curves.

The dry rodded unit weight (DRUW) and the void ratio were measured in accordance with ASTM C29 [18], and the results are summarized in Table 1. The gradation of granite B was finer than that of granite A and had a larger void ratio.

As fine aggregate, concrete sand with a fineness modulus of 3.1, a specific gravity of 2.64 and 1.8 % absorption was used. Moreover, expanded shale with a dry bulk specific gravity of 1.75 and a 72 h absorption of 16 % was used. Figure 2 shows the gradation of the concrete sand and of the lightweight sand. Finally, vinsol resin-based air entraining agent and polycarboxylate based high-range water reducer with specific gravities of 1.02 and 1.10, respectively, and polypropylene fibrillated fibers with a specific gravity of 0.91, a graded length between 12.7 mm and 19.1 mm and a specific surface area of 20.65 cm^2/g were used.

3.2 Mixture proportions

A total of eight mixes were placed for this study. Three used granite A (Mix A) and five used granite B (Mix B). A baseline mixture consisting of cement, fly ash, water, AEA, granite and concrete sand was prepared with both granites. Different variations of the baseline mix were investigated to improve the strength and freeze-thaw durability. A mix without AEA was also prepared to consider the influence of AEA. The key for the different mix designs was as follows:

- Mix 1: No admixtures
- Mix 2: **Baseline mixture** with air entrainment
- Mix 3: Air entrainment and high-range water reducer
- Mix 4: Air entrainment and fibers
- Mix 5: Air entrainment and lightweight sand (expanded shale)

Mixtures 1–3 were prepared with both granite A and granite B, whereas mixtures 4–5 were only prepared with granite B.

All mixtures were prepared with a constant amount of cement paste, and 20 % cement replaced with fly ash, by weight, to improve workability, later age strength and sustainability. Mix A and B had a w/c-ratio of 0.29 and 0.31, respectively. The fine aggregate to coarse aggregate ratio was 0.09, also by weight. Furthermore, all mixes were designed to have a void content of 18 % in addition to 3 % entrained air (21 % total air), except from Mix 1-A and Mix 1-B that did not include AEA. The AEA dosage was slightly higher than the standard dosage used for conventional concrete, that is, 0.125 % of the cementitious material mass. The HRWR dosage was 0.375 %. The amount of fibers corresponded to 0.9 kg/m^3. In mixes where concrete sand was replaced by lightweight sand, the mass of lightweight sand was based on a volume consideration to keep the volume of fine aggregate constant. Table 2 shows the mixture proportions for Mix A and Mix B.

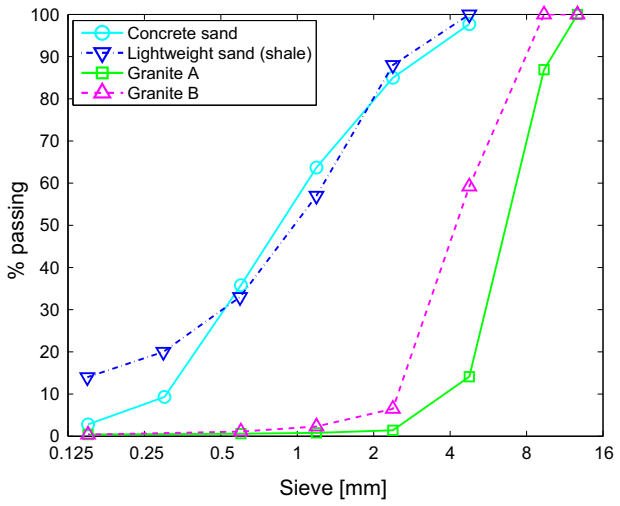

Fig. 2 Gradation curves for concrete sand, lightweight sand (expanded shale) and granite A and granite B

3.3 Mixing and sample preparation

Mixtures were prepared by first mixing the aggregates and 5 % of the cement in a 0.04 m^3 rotating-drum mixer for 1 min in order to coat all aggregates with cement to improve the PCPC strength [7]. The AEA was diluted in the water and added to the mix. When foam was observed, fly ash and the rest of the cement was added and mixed for 3 min. The mixture was allowed to rest for 3 min and mixed for additionally 2 min before preparing the samples. In mixes with HRWR, one third of the water was held back, mixed with HRWR and added when the mix appeared uniform after addition of cement and fly ash. In

Table 1 Dry rodded unit weight (DRUW) and specific gravity of coarse aggregates

	DRUW (kg/m^3)	Void ratio (%)	Spec. gravity (−)	Absorption (%)
Granite A	1524	43	2.70	0.6
Granite B	1405	48	2.70	0.7

Table 2 Mixture proportions for Mix A and Mix B with w/c = 0.29 and w/c = 0.31, respectively

Mix	1-A	2-A	3-A	1-B	2-B	3-B	4-B	5-B
Cement (kg/m^3)	315	315	315	315	315	315	315	315
Fly ash (kg/m^3)	64	64	64	64	64	64	64	64
Water (kg/m^3)	100	100	100	114	114	114	114	114
Granite (kg/m^3)	1435	1385	1382	1401	1350	1347	1350	1350
Concrete sand (kg/m^3)	133	128	128	130	125	125	125	–
LW sand (ssd*) (kg/m^3)	–	–	–	–	–	–	–	96.2
AEA (kg/m^3)	–	0.47	0.47	–	0.47	0.47	0.47	0.47
HWRW (kg/m^3)	–	–	1.42	–	–	1.42	–	–
Fibers (kg/m^3)	–	–	–	–	–	–	0.89	–

* The 'saturated surface dry' (ssd) state is defined as the state at which the lightweight sand is water saturated to its 72 h absorption value

mixtures containing fibers, the fibers were added together with the aggregates and 5 % of the cement in the very beginning, and mixed until the fibers were visually uniformly dispersed. In the mixture containing lightweight sand, the lightweight sand was pre-wetted for 72 h before use [19]. The lightweight sand was allowed to drain for 60 min before mixing, and the mix design was adjusted according to the moisture content of the lightweight sand measured immediately prior mixing.

Cylinder samples were prepared in d100/h200 mm (4/8 in.) cylinder molds for strength and permeability tests and in 75 × 100 × 400 mm (3 × 4 × 16 in.) beam molds for freeze-thaw tests. The mass of PCPC corresponding to the volume of the mold was determined from the mix design density and placed in the mold in three equal lifts. For the cylinder specimens, each layer was rodded a maximum of 25 times, depending on the particular mix design. The more workable the mixture was, the fewer times was each layer rodded. For the beams, each layer was rodded a maximum of 75 times. The layers were meshed together by vibrating each new layer for three seconds. For some of the specimens, extra mass had to be added because they compacted better than expected from the mix design; however, for other specimens it was not possible to fill all mass into the mold. The samples were demolded after 24 h and cured in a fog room with a relative humidity >98 % until 28 days in accordance with ASTM C192 [20].

3.4 Testing procedures

3.4.1 Fresh unit weight

Because of the stiff consistency it was not possible to assess the workability of PCPC from a standard slump cone test. Instead, the workability of fresh PCPC mixtures was determined by assessing the fresh unit weight (UW) immediately after mixing in accordance with ASTM C1688 [21]. The method prescribes that a defined compaction energy is applied to a specified PCPC volume, and by weighing this compacted volume of PCPC, the fresh UW is obtained. The fresh UW was measured immediately after mixing (5 min after water addition), and again 2 h after water addition to consider the stiffening with time. During the time between water addition and the second fresh UW measurement the PCPC mixture was left in the mixer and rotated every 15 min.

3.4.2 Hardened unit weight and void content

The hardened UW and the void content of the specimens were determined in accordance with ASTM C1754 [22]. Three cylinder specimens of all mixes

were oven dried at 38 °C and weighed every 24 h until the difference between any two subsequent mass determinations was less than 0.5 %. Subsequently, the specimens were submerged in water for 30 min and trapped air was released by tapping the sides of the specimens 10 times with a rubber mallet. Based on the weight of the specimen under water, the void content, P (%), of the specimen was determined from Archimedes' principle using the formula:

$$P = \left(1 - \frac{m_{38\,^\circ\mathrm{C}} - m_{sw}}{\rho_w \, V_{\mathrm{tot}}}\right) \times 100\% \quad (1)$$

where $m_{38\,^\circ\mathrm{C}}$ (kg) is the constant mass of the oven-dried specimen, m_{sw} (kg) is the mass of the specimen submerged in water, ρ_w (kg/m^3) is the water density, and V_{tot} (m^3) is the total volume of the specimen.

The hardened UW of the same specimens as used for the void content determination was found as the ratio between $m_{38\,^\circ\mathrm{C}}$ and V_{tot}. Afterwards, a linear relationship between the hardened UW and the void content was obtained. Before oven drying, the specimens were placed on a wrung towel and allowed to drain for 30 min before weighing. Hence, another UW relating to this moisture content was obtained and also correlated to the void content of the specimens.

3.4.3 Strength test setups

When removed from the fog room at 28 days, the specimens were allowed to drain on a wrung towel for 30 min. Subsequently, they were weighed by which their UW was determined, and the linear relationship between the hardened UW and the void content could be used to determine the void content of the specimens.

The compressive strength was determined in accordance with ASTM C39 [23] using sulfur capping. In addition to sulfur capping, the compressive strength was also performed with 4.7 mm (3/16 in.) thick plywood placed between the testing machine and the specimen ends. Three specimens were tested for each type of compressive strength test and for each mix design. The splitting tensile strength was determined in accordance with ASTM C496 [24] and six specimens were tested for each mix design. The shear strength was tested according to Iowa DOT test method 406-C [25] by placing the cylinder horizontally in the space between the two circular halves of the testing jig, see Fig. 3 (left). A constant load at a rate of 2.8–3.4 MPa/min. was subsequently applied over the cross section of the specimen at the specimen mid-height until the specimen failed. Three specimens were tested for each mix design.

3.4.4 Permeability test setup

Permeability was determined using a falling head test setup. The cylinder end surfaces were cut off to obtain a uniform sample with a length of 15 cm. The cylinders were sealed in PVC shrink wrap, and rubber sleeves were tightened around the cylinder top and bottom with hose clamps, see Fig. 3 (right). The initial water head was approximately 22.9 cm (9 in.) and the final water head was approximately 2.5 cm (1 in.). The permeability coefficient, k (cm/s), was determined using the formula:

$$k = \frac{a\,L}{A\,t} \ln\left(\frac{h_1}{h_2}\right) \quad (2)$$

where a (cm^2) is the cross-sectional area of the standpipe, L (cm) is the height of the specimen, A (cm^2) is the cross-sectional area of the specimen, and t (s) is the time between the initial head h_1 (cm) and the final head h_2 (cm).

3.4.5 Freeze-thaw test setup

The freeze thaw durability was evaluated from ASTM C666 Procedure A [12], where beam specimens are frozen and thawed in water and the core temperature varies between -18 ± 2 and 4 ± 2 °C during a freeze-thaw cycle. Prior to the beginning of the freeze-thaw exposure, the specimens were water saturated for 24 h at 4 °C. The mass loss and the durability factor (DF) calculated from relative dynamic modulus were used to evaluate the freeze-thaw durability of the specimens, and the tests were terminated when the specimens reached 15 % mass loss, 300 frost cycles, or a reduction in the relative dynamic modulus to 60 %. The mass loss and the transverse frequency were measured every 30 cycles. DF (%) was calculated using the formula:

$$DF = \frac{P\,N}{M} \quad (3)$$

where P (%) is the relative dynamic modulus at N cycles, N is the number of cycles at which P reaches

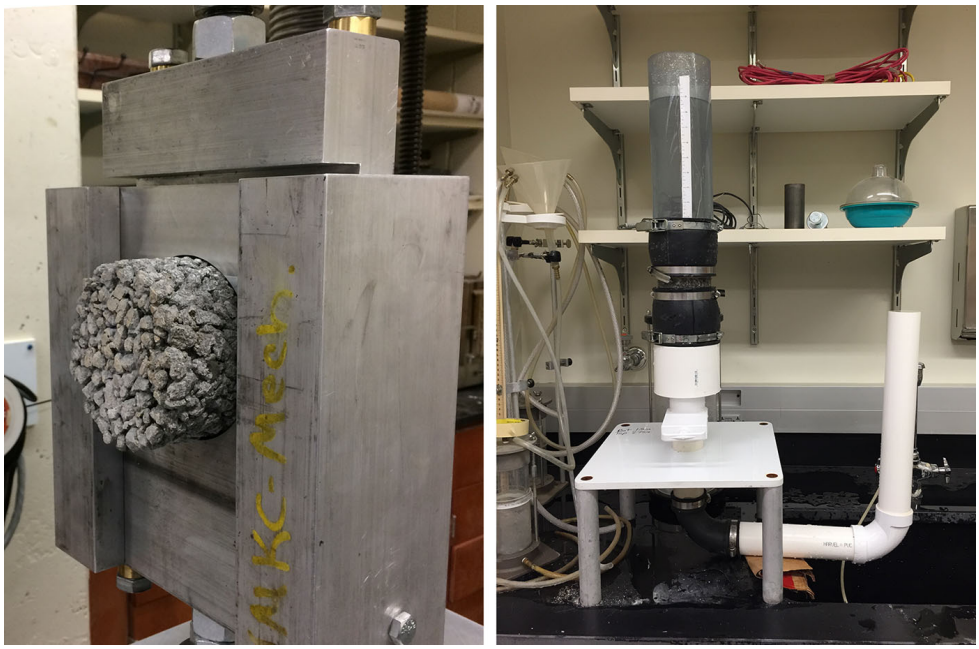

Fig. 3 *Left* shear test setup according to Iowa DOT test method 406-C. *Right* Falling head permeability test setup

the specified minimum value for discontinuing the test—chosen as 60 % of the relative dynamic modulus—or the specified number of cycles at which the exposure is to be terminated, whichever is less, and $M = 300$ cycles is the number of cycles at which the exposure is to be terminated. The relative dynamic modulus at c cycles, RDM_c (%), was calculated using the formula:

$$\mathrm{RDM}_c = \frac{n_c^2}{n^2} \times 100\% \quad (4)$$

where n_c is the fundamental transverse frequency after c frost cycles and n is the fundamental transverse frequency after 0 frost cycles.

In total, three beam specimens were tested for each of the mix designs except from Mix 1-A that was not tested.

4 Results and discussion

4.1 Fresh and hardened unit weight and void content

Results for workability, hardened unit weight, and void content are shown in Table 3. The void content also includes entrained air voids that became water filled during the testing procedure. Void content was measured individually for both cylinder specimens used for strength and permeability tests and for beam specimens used for freeze-thaw tests.

The fresh UW in Table 3 relates to the values measured immediately after mixing (5 min after water addition) and 2 h after water addition (Sect. 3.4.1). Typically, concrete is not constantly mixed for a long period in the lab. However, the high degree of friction, exposed surface area, and low w/c-ratio of PCPC results in rapid stiffening of the material during transport. Since the strength is linearly related to unit weight, any increases in void content due to stiffening directly result in lower strength. Ideally recommended PCPC mixtures should have consistent unit weight values between the initial test and the later test. The difference between these unit weights is considered the stiffening with time. Mix 3-B containing HRWR had the highest fresh UW which indicates that this mix had the best initial workability. On the other hand, Mix 1-B that did not contain AEA had the lowest fresh UW which indicates that this mix was the stiffest mix with the poorest workability. Thus, AEA and HRWR positively effect the workability of PCPC. There was not observed any influence from fibers or lightweight sand on the fresh UW. Considering the stiffening with time, Mix 2-B experienced a larger difference in fresh UW than any of the other mixes. This means that the workability of Mix 2-B became stiffer compared to the

Table 3 Fresh unit weight (UW) measured 5 min and 2 h after water addition, hardened UW, and void content of all mixes for both cylinder and beam specimens

Mix	Fresh UW (kg/m^3)			Hardened UW		Voids, cyl.		Voids, beam	
	(A) 5 min	(B) 2 h	(A)-(B)	Avg. (kg/m^3)	COV (%)	Avg. (%)	COV (%)	Avg. (%)	COV (%)
1-A*	–	–	–	1840	1.8	28.0	5.5	–	–
2-A*	–	–	–	1865	1.0	27.4	2.9	19.4	0.6
3-A*	–	–	–	1847	0.6	27.7	2.7	18.5	1.0
1-B	1840	1794	46	1858	0.6	25.0	2.5	18.8	2.5
2-B	1903	1806	97	1832	1.6	25.8	5.9	19.0	1.3
3-B	1914	1840	74	1827	1.0	25.8	5.7	13.8	5.0
4-B	1874	1803	71	1811	0.6	26.6	3.2	19.4	3.1
5-B	1857	1806	51	1805	0.6	24.4	3.6	13.3	3.8

Average (avg.) values as well as coefficients of variation (COV) are shown

* The fresh UW was not measured for Mix A, and no beam specimens were cast with Mix 1-A

other mixes and therefore was harder to place. Mix 5-B contained the expanded shale lightweight aggregate for internal curing and experienced much less stiffening over the mixing period than the other mixtures containing AEA.

The variability on the hardened UW and the void content was low and within reported variability of the test method in ASTM C1754 [22] for all mixes except from Mix 2-B that exceeded reported single-operator COV of 5.82%. This might be related to Mix 2-B stiffening with time by which a larger variation in the void content is expected, as considered above. The void content of all mixes was higher than the void content estimated in the mix design because some water that was not bound by cement and fly ash evaporated during the oven drying along with the extra water added to satisfy aggregate absorption. Moreover, the void content of mixes with granite B was slightly lower than that of mixes with granite A because of the difference in gradation and w/c-ratio making it easier to compact specimens with granite B.

No particular differences in hardened UW or void content were observed within the different variants of Mix A and Mix B.

4.2 28-Day compressive strength

The 28-day compressive strength test results are shown in Fig. 4. As mentioned, the compressive strength was determined from tests where either sulfur capping or wood end plates were used to distribute the compression force over the entire specimen cross section. There were no statistically significant differences between the average values of these two groups for any of the mix designs as determined by one-way ANOVA; hence, the results in Fig. 4 include the results from both methods. Also shown are the average void contents of the specimens tested for the particular mix designs. Figure 4 depicts the results in a box plot where the data is shown through their quartiles. The top and bottom of each box are the first and third quartile, and the middle line is the median. The whiskers indicate the furthest data points outside the quartiles, and outliers are plotted as individual points.

The average compressive strengths are summarized in Table 4, neglecting the outliers indicated in the box plot in Fig. 4; however, it should be noted that all of the

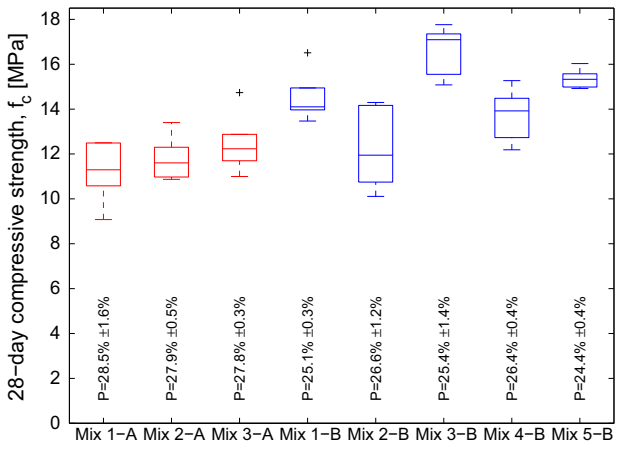

Fig. 4 Box plot of 28-day compressive strength, f_c, for all mixes. The average void content for the specimens tested is also shown. Six specimens were tested for each mix design

Table 4 28-day compressive strength f_c, splitting tensile strength f_s, and shear strength f_v, for all mixes

Mix	f_c		f_s		f_v	
	Avg. (MPa)	COV (%)	Avg. (MPa)	COV (%)	Avg. (MPa)	COV (%)
1-A	11.6	7.0	1.7	1.3	4.5	41
2-A	11.8	8.0	1.5	9.7	2.1	36
3-A	12.0	6.0	1.9	4.9	3.8	34
1-B	14.1	3.8	1.8	11.8	3.0	10
2-B	12.3	15.2	1.7	13.8	4.8	25
3-B	16.7	6.5	1.9	11.5	3.9	29
4-B	13.8	8.3	1.6	2.2	4.3	38
5-B	15.4	2.8	2.0	6.2	4.1	17

Average (avg.) values as well as coefficients of variation (COV) are shown

outliers had much greater strength than the corresponding samples. The variability of Mix 2-B is larger than the variability of the remaining mix designs which is believed to be connected with the correspondingly larger variability of the void content of Mix 2-B.

Figure 4 shows that, in general, the 28-day compressive strengths of Mix B were higher than those of Mix A. As determined by one-way ANOVA there were statistically significant differences between the average compressive strength of Mix 1-A and 1-B ($p = 2.6 \times 10^{-5}$), and Mix 3-A and 3-B ($p = 3.8 \times 10^{-7}$) with the B mixes having the greatest compressive strength; however, there were no statistically significant differences between the average compressive strength of Mix 2-A and 2-B ($p = 0.89$). The void content of Mix A specimens was slightly higher than that of Mix B specimens, because Mix B compacted better than Mix A, and therefore the compressive strengths of the Mix A specimens were also expected to be lower than those of Mix B. Mix B had a higher w/c-ratio than Mix A which would typically decrease the compressive strength; however, because granite B contained smaller aggregates than granite A (Fig. 2), the number of contact points between the aggregates were increased which influenced the compressive strength positively.

As determined by one-way ANOVA there were no statistically significant differences between the average compressive strength of Mix 1-A, 2-A and 3-A ($p = 0.21$); however, for Mix B there were statistically significant differences between the average compressive strengths of Mix 1-B, 2-B, 3-B, 4-B and 5-B ($p = 8.2 \times 10^{-6}$). A paired-samples t-test showed that the average compressive strengths of Mix 1-B, 3-B, 4-B and 5-B were all statistically significant different than that of Mix 2-B (the baseline mix). Table 4 shows that the greatest increase in the average 28-day compressive strength was obtained by addition of HRWR (Mix 3-B) by which the strength increased 35.5 % compared to the baseline mix (Mix 2-B). Also fibers and lightweight sand influenced the compressive strength positively. By adding 0.9 kg/m^3 fibers (Mix 4-B) and by replacing concrete sand with lightweight sand (Mix 5-B), the average 28-day compressive strength was increased by 11.9 and 25.0 %, respectively.

4.3 28-Day splitting tensile strength

Figure 5 shows the results from the 28-day splitting tensile strength tests and the average void contents of the specimens tested for the particular mix designs. The average splitting tensile strengths are summarized in Table 4, neglecting the outlier indicated in the box plot in Fig. 5. The variability on the splitting tensile strengths was all within the limits for d100/h200mm cylinders in ASTM C496 [24].

When comparing the 28-day splitting tensile strength of Mix 1-A with Mix 1-B, Mix 2-A with Mix 2-B, and Mix 3-A with Mix 3-B, one-way ANOVA showed that there were no statistically significant differences between the average splitting tensile strengths when using granite B rather than granite A while increasing the w/c-ratio from 0.29 to 0.31. The increased number of contact points due to the reduction in coarse aggregate gradation did therefore not have the same positive influence on the splitting tensile strength as on the compressive strength. As with the specimens tested for compressive strength, the void content of specimens of Mix A was higher than that of specimens of Mix B, because Mix B compacted better than Mix A.

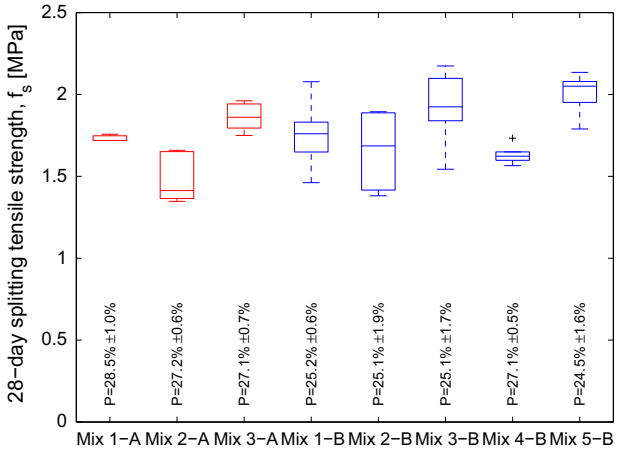

Fig. 5 Box plot of 28-day splitting tensile strength, f_s, for all mixes. The average void content for the specimens tested is also shown. Six specimens were tested for each mix design

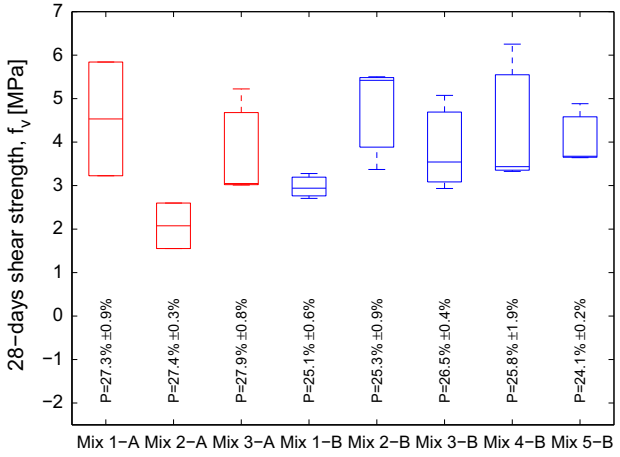

Fig. 6 Box plot of 28-day shear strength, f_v, for all mixes. The average void content for the specimens tested is also shown. Three specimens were tested for each mix design

As determined by one-way ANOVA and paired-samples t-test there were statistically significant differences between the average splitting tensile strength of Mix 1-A and 2-A ($p = 5.8 \times 10^{-3}$), and Mix 2-A and 3-A ($p = 5.3 \times 10^{-5}$). The 28-day splitting tensile strength increased 26.5 % when adding HRWR (Mix 3-A) to the baseline mix (Mix 2-A).

For Mix B, one-way ANOVA and paired-samples t-test showed that the average splitting tensile strength of Mix 3-B and 5-B was statistically significant different than that of the baseline mix (Mix 2-B) ($p = 0.021$ and $p = 2.5 \times 10^{-3}$, respectively), whereas the average splitting tensile strength of Mix 1-B and 4-B was not statistically significant different from that of the baseline mix ($p = 0.36$ and $p = 0.24$, respectively). The increase in splitting tensile strength when adding HRWR (Mix 3-B) to the baseline mix was 15.7 %. However for Mix B, the largest influence on the splitting tensile strength was caused by internal curing. By replacing concrete sand with lightweight sand (Mix 5-B), the splitting tensile strength increased 21.1 %. Figure 5 shows, as also determined from one-way ANOVA, that the addition of fibers did not have a statistically significant influence on the splitting tensile strength.

4.4 28-Day shear strength

Figure 6 shows the results from the 28-day shear strength tests and the average void contents of the specimens tested for the particular mix designs. Shear strength has never before been previously presented on cylinder specimens so no comment can be made regarding the variability as compared to other results.

The average shear strengths are summarized in Table 4. The variability on the 28-day shear strengths was considerably higher than for the 28-day compressive strengths and splitting tensile strengths, and it makes it more difficult to base any conclusions on Fig. 6. For Mix A, Fig. 6 shows that the 28-day shear strength of Mix 2-A was significantly less than that of Mix 1-A and 3-A. The average shear strength of Mix 3-A was 81.1 % larger than that of Mix 2-A. For Mix B, one-way ANOVA showed that there were no statistically significant differences between the average 28-day shear strength of any of the mix designs.

4.5 Permeability

Figure 7 shows the results from the permeability tests and the average void contents of the specimens tested for the particular mix designs. The average permeability coefficients are summarized in Table 5.

The permeability of Mix B was less than that of Mix A because the coarse aggregate for Mix B (granite B) was finer than that for Mix A (granite A) causing Mix B to have smaller diameter pores. As determined by one-way ANOVA and paired-samples t-test there were no statistically significant differences between the average permeability of mixes A ($p = 0.54$) or

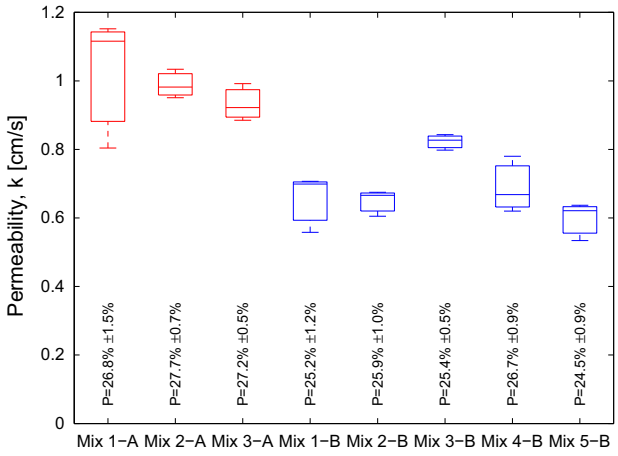

Fig. 7 Box plot of permeability, *k*, for all mixes. The average void content for the specimens tested is also shown. Three specimens were tested for each mix design

mixes B ($p = 0.86$); however, there was a statistically significant difference between the average permeability of Mix 3-B (with HRWR) and the remaining B mixes. The average permeability of Mix 3-B was 26.2 % larger than that of the baseline mixture (Mix 2-B); however, the same tendency was not observed for Mix A.

Overall, the mix designs tested in the present study had average permeability coefficients of 0.60–1.02 cm/s which is more than sufficient to drain the rain from a 10-year rain event in Denmark that has a maximum intensity of 0.004 cm/s [5]. In fact, the PCPC mixes in the present study can drain the rain from a 100-year rain event in Denmark because the maximum intensity of such rain event is 0.007 cm/s. Thus, for application in PCBs, the permeability of PCPC is considered sufficient. On top of that, for most PCBs, a road surface of either concrete or asphalt concrete is expected to be placed on the PCPC fill, by which the requirements to the permeability of the PCPC fill is even less. Thus, as for most PCPC applications, the permeability and flow rate through the subgrade, in this case at the bridge ends, are restrictive.

4.6 Freeze-thaw durability

The freeze-thaw durability was evaluated for all mixes except Mix 1-A. Three beam specimens were tested for each mix and a large variation in the freeze-thaw behavior was observed within each mix. Figure 8 shows the remaining mass as function of the number of frost cycles, and for the sake of simplicity, only the behavior of a single beam specimen for all mix designs is shown. The specimens representing each mix design in Fig. 8 are chosen as the specimens that experienced the second least mass loss. The failure mechanism for the specimens was either complete deterioration into cement paste-coated aggregate pieces or fracture of the intact beam into two or three large pieces.

Although specimens were first soaked in water before initial testing, Fig. 8 also shows that some specimens gained weight during the freeze-thaw tests. This is because the cement paste absorbed water when the specimens were immersed and cycled. The weight gain was largest for Mix 5-B that contained lightweight sand, which is because lightweight sand has a high water absorption due to its large porosity. Moreover, Fig. 8 shows that the mass loss of most PCPC specimens was insignificant until the point of failure at which an abrupt decrease in the mass occurred. At the point of failure the mass loss was set to 100 % and linear interpolation was used to determine the number of frost cycles it took each specimen to exceed the maximum acceptable mass loss which is defined as 15 %. Table 6 shows the number of frost cycles at which this mass loss limit was reached for all specimens. Table 6 also provides a description of the observed condition of the samples at failure. The A mixes failed by breaking into two or three large pieces without any significant freeze-thaw type deterioration. In PCPC specimens with high void content or large pores, such as Mix A, the hydraulic stresses from the expanding water can be sufficient enough to cause this loading type failure. All category B mixes with the smaller coarse aggregate experienced a traditional

Table 5 Permeability coefficients, *k*, for all mixes

Mix	1-A	2-A	3-A	1-B	2-B	3-B	4-B	5-B
Avg. (cm/s)	1.02	0.99	0.93	0.65	0.65	0.82	0.69	0.60
COV (%)	18.7	4.3	5.8	12.8	5.9	2.8	11.9	9.3

Average (avg.) values as well as coefficients of variation (COV) are shown

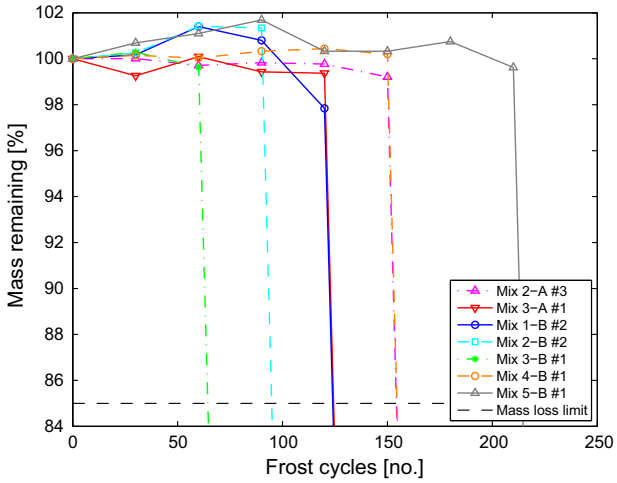

Fig. 8 Remaining mass as function of number of frost cycles for a single specimen from Mix 2-A, 3-A, 1-B, 2-B, 3-B, 4-B and 5-B. Because a certain variation was observed within each mix design, the results should not be seen isolated but in the light of Table 6

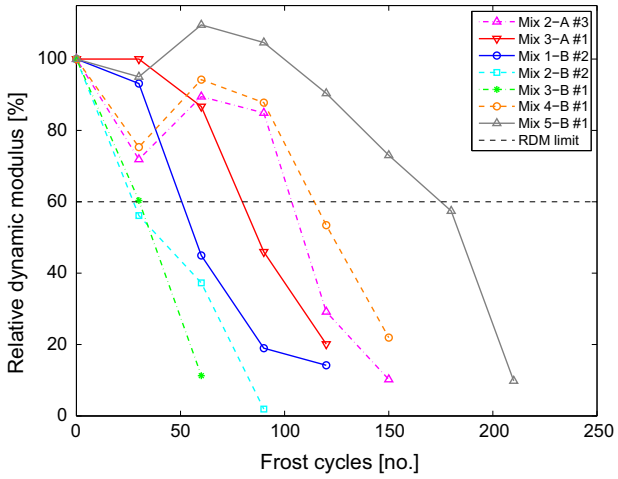

Fig. 9 RDM as function of number of frost cycles for a single specimen from Mix 2-A, 3-A, 1-B, 2-B, 3-B, 4-B and 5-B. Because a certain variation was observed within each mix design, the results should not be seen isolated but in the light of Table 6

paste failure, except for Mix 5-B which failed through cracking from structural loading caused by ice expansion.

Figure 9 shows the decrease in RDM calculated from Eq. (4) as a function of the number of freeze-thaw cycles, and the 60 % cut-off limit. The same specimens as depicted in Fig. 8 are shown. Mix 2-A, 4-B and 5-B experienced a small drop in RDM after 30 frost cycles which is due to the uncertainties related to this test method rather than an actual decrease and subsequent increase in RDM. It should be noted that RDM testing uses a small accelerometer placed on the sample surface which evaluates excitation of the sample from an impact hammer. The low density of PCPC specimens and presence of loose particles on the surface results in more variability than for plain concrete.

Compared to the decrease in mass loss, the decrease in RDM occurred faster and more gradually, and most specimens failed due to RDM exceeding its cut-off value rather than the mass. Table 6 also shows the average *DF*s calculated from Eq. (3). The equation shows that *DF* is very dependent on the choice of *M* and *P* which means that it is only reasonable to compare *DF*s calculated under the same assumptions. It would be more reasonable to directly compare the decrease in RDM; however, since it is normal standard to evaluate the freeze-thaw behavior of PCPC from *DF*, this is also done in the present study, and the

Table 6 Void content of beam specimens exposed to freezing and thawing, durability factors, *DF*, and the number of frost cycles, *n*, for all specimens, and the average number, at which the mass loss is 15 %

Mix	*DF* (%)		*n* (−)				Observed failure
	Avg.	COV	#1	#2	#3	Avg.	
2-A	18.6	9.6	154	184	124	154	Fracture into large pieces
3-A	20.0	22.0	124	124	184	144	Fracture into large pieces
1-B	16.3	55.1	86	124	184	132	Complete deterioration
2-B	12.0	91.0	183	95	34	104	Fracture and deterioration
3-B	10.5	88.3	64	64	125	84	Complete deterioration
4-B	17.4	30.9	155	94	154	134	Fracture and deterioration
5-B	26.3	47.3	214	214	64	164	Corner broke off

Average (avg.) values and coefficient of variations (COV) are shown for the void content and the *DF*s

values used for M and P are chosen as typically values used for PCPC [10, 26, 27]. The results in [26, 27] suggest that acceptable freeze-thaw behavior occurs for DFs larger than 40 %; hence, the DFs found in this study are slightly low which indicate that the freeze-thaw durability of the specimens were not good as compared with values normally applied to conventional concrete. The same conclusion was reached from the mass loss consideration, where all mix designs had at least one specimen failing before it reached 100 frost cycles. The freeze-thaw durability results were much more variable than what is typically observed and allowable for conventional concrete.

Table 6 and Figs. 8 and 9 indicate that the freeze-thaw durability of Mix 2-A and 3-A was similar. For Mix B, the results indicate that there was no significant improvement in the freeze-thaw behavior when adding AEA. The freeze-thaw durability of Mix 1-B (no AEA) was better than that of Mix 2-B and 3-B (with AEA). Hence, the results indicate that the AEA dosage used was not sufficiently high to create the necessary protective entrained air system in the cement paste. A possible explanation of the lacking entrained air content could be the high fly ash content used in this study compared to other studies where good freeze-thaw results have been obtained with a similar AEA dosage but without fly ash [26]. It is expected that improved durability results would be obtained with an increased AEA dosage. For Mix B, Mix 3-B (with HRWR) had the worst durability, and Mix 5-B (with lightweight sand) had the best durability. The beam specimens from Mix 3-B and 5-B had similar void contents and those were the lowest of all specimens tested in this study (Table 3). A low void content is known to improve the freeze-thaw durability of PCPC; however, it has not improved the durability of Mix 3-B. It has been hypothesized that after the water saturated voids in lightweight aggregate empty during hydration the resulting void space is available to improve freeze-thaw durability. These results therefore suggest that lightweight sand can be used to improve the freeze-thaw durability of PCPC. While the freeze-thaw response of these mixtures was lower than considered acceptable for conventional concrete, it is functionally impossible for complete saturation of the PCPC fill layer in PCBs so even the durability level recorded for these mixtures should be sufficient in practice.

5 Conclusions

In the present study it was investigated how the mix design of the pervious concrete fill in Pearl-Chain Bridges can be improved by use of air entrainment, high-range water reducer, fibers and through internal curing; however, the research results also apply to pervious concrete used for other purposes. The investigation involved consideration of the compressive strength, splitting tensile strength, shear strength, permeability, and the freeze-thaw durability of eight different mix designs using two different coarse aggregate gradations and two w/c-ratios. The main conclusions from the study were as follows:

(1) The void content of pervious concrete decreased when decreasing the maximum aggregate size and increasing the w/c-ratio from 0.29 to 0.31.
(2) The addition of air entrainment and high-range water reducer increased the workability of pervious concrete. Thus, addition of air entrainment and high-range water reducer eases the placement of pervious concrete fill in Pearl-Chain Bridges.
(3) The addition, of particularly, high-range water reducer and lightweight sand (expanded shale) for internal curing improved the strength properties significantly. The addition of high-range water reducer increased the 28-day compressive strength and the 28-day splitting tensile strength with up to 36 and 27 %, respectively, and the addition of lightweight sand increased the 28-day compressive strength with 25 % and the 28-day splitting tensile strength with 21 % compared to the baseline mixture. The addition of fibers increased the 28-day compressive strength with 12 % but did not influence the 28-day splitting tensile strength.
(4) The aggregate gradation was the predominant factor with respect to the permeability. The larger the aggregates, the higher the permeability. The permeability coefficient for all mixes was 0.60–1.02 cm/s which is more than sufficient to drain the rain from a 100-year rain event in Denmark with a maximum intensity of 0.007 cm/s. Thus, for Pearl-Chain Bridges with pervious concrete fill, the permeability coefficient of the sub-grade at the bridge ends is restrictive.

(5) The air entrainment dosage of 0.125 % of the cementitious material mass was too low to create a sufficiently fine entrained air content that could improve the freeze-thaw durability of the specimens. Therefore, the freeze-thaw durability of all specimens was less and much more variable than what is typically observed and allowable for conventional concrete. The decrease in the relative dynamic modulus was faster and more gradual than the decrease in the mass during the freeze-thaw tests. Most specimens were considered failed due to reduction in the relative dynamic modulus rather than due to reduction in mass. The freeze-thaw durability of the specimens containing lightweight sand (expanded shale) was improved compared to the other mix designs.

(6) Fully-saturated, rapid, freeze thaw testing as used in this study is not representative of field conditions for pervious concrete used as a permeable pavement and even less representative when pervious concrete is used in Pearl-Chain Bridges. The industry is in need of a more representative standard for testing pervious concrete which would allow a true comparison as relatable to field results.

References

1. Hertz KD (2015) Super-light SL-Deck elements with fixed end connections. In: Proceedings of fib symposium May 18–20, Copenhagen, pp 465–466
2. Hertz KD, Castberg A, Christensen J (2014) Super-light concrete decks for building floor slabs. Struct Concr J 15:522–529
3. Halding PS, Hertz KD, Schmidt JW (2015b) Precast Pearl-Chain concrete arch bridges. J Eng Struct 103:214–227
4. Lund MSM, Hansen KK, Truelsen R, Johansen L (2016) Pervious concrete fill in Pearl-Chain Bridges: using small-scale results in full-scale implementation. Constr Build Mater 106:404–414
5. IDA Wastewater Commission. Regional variation of extreme rain in Denmark—a new analysis, 1979–2005. Pamphlet No. 28. The Commission, Copenhagen (2006). ISBN: 87-7923-502-6. Danish
6. Tennis PD, Leming ML, Akers DJ (2004) Pervious concrete pavements. EB302.02, Portland Cement Association, Skokie. National Ready Mixed Concrete Association, Silver Spring
7. Schaefer VR, Wang K, Suleiman MT, Kevern JT (2006) Mix design development for pervious concrete in cold weather climates. National Concrete Pavement Technology Center and Iowa State University, Ames
8. Kevern JT, Schaefer VR, Wang K, Suleiman ST (2008) Pervious concrete mixture proportions for improved freeze-thaw durability. J ASTM Int 5(2):1–12
9. Kevern JT (2013) Reducing the curing requirements of pervious concrete using prewetted lightweight aggregate for internal curing [Internet]. University of Missouri-Kansas City, Kansas City. http://www.escsi.org/uploadedFiles/Technical_Docs/Internal_Curing/Pervious20Report20-20Kevern
10. Kevern JT, Biddle D, Cao Q (2015) Effect of macro-synthetic fibers on pervious concrete properties. J Mater Civil Eng 27(9):119–134. doi:10.1061/(ASCE)MT.1943-5533.0001213
11. National Ready Mixed Concrete Association (NRMCA). Freeze-thaw resistance of pervious concrete. NRMCA, Silver Spring (2004)
12. ASTM Standard C666/C666M-03. Standard test method for resistance of concrete to rapid freezing and thawing. ASTM International, West Conshohocken (2008). doi:10.1520/C0666_C0666M-03R08
13. Henderson V, Tighe S (2012) Evaluation of pervious concrete pavement performance in cold weather climates. Int J Pavement Eng. 13(3):197–208. doi:10.1080/10298436.2011.572970
14. ASTM Standard C150/C150M-12. Standard specification for portland cement. ASTM International, West Conshohocken (2012). doi:10.1520/C0150_C0150M-12
15. ASTM Standard C618-12a. Standard specification for coal fly ash and raw or calcined natural pozzolan for use in concrete. ASTM International, West Conshohocken (2012). doi:10.1520/C061812a
16. ASTM Standard C311/C311-13. Standard test methods for sampling and testing fly ash or natural pozzolans for use in portland-cement concrete. ASTM International, West Conshohocken (2014). doi:10.1520/C0311-13
17. ASTM Standard C136-06. Standard test method for sieve analysis of fine and coarse aggregate. ASTM International, West Conshohocken (2006). doi:10.1520/C0136-06
18. ASTM Standard C29/C29M-09. Standard test method for bulk density (“unit weight”) and voids in aggregate. ASTM International, West Conshohocken (2009). doi:10.1520/C0029_C0029M-09
19. ASTM Standard C1761/C1761M-13b. Standard specification for lightweight aggregate for internal curing of concrete. ASTM International, West Conshohocken (2013). doi:10.1520/C1761_C1761M-13b
20. ASTM Standard C192/C192M-14. Standard practice for making and curing concrete test specimens in the laboratory. ASTM International, West Conshohocken (2014). doi:10.1520/C0192_C0192M-14
21. ASTM Standard C1688/C1688M-13. Standard test method for density and void content of freshly mixed pervious concrete. ASTM International, West Conshohocken (2013). doi:10.1520/C1688_C1688M-13
22. ASTM Standard C1754-12. Standard test method for density and void content of hardened pervious concrete. ASTM International, West Conshohocken (2012). doi:10.1520/C1754_C1754M-12
23. ASTM Standard C39/C39M-14a. Standard test method for compressive strength of cylindrical concrete specimens.

ASTM International, West Conshohocken (2014). doi:10.1520/C0039_C0039M-14A
24. ASTM Standard C496/C496M-11. Standard test method for splitting tensile strength of cylindrical concrete specimens. ASTM International, West Conshohocken (2011). doi:10.1520/C0469_C0469M-14
25. Test Method No. Iowa 406-C: method of test for determining the shearing strength of bonded concrete. Lowa Department of Transportation, Des Moines (2000)
26. Kevern JT, Wang K, Schaefer VR (2010) Effect of coarse aggregate on the freeze-thaw durability of pervious concrete. J ASTM Int 22(2):469–475
27. Shu X, Huang B, Wu H, Dong Q, Burdette AG (2011) Performance comparison of laboratory and field produced pervious concrete mixtures. Constr Build Mater 25: 3187–3192

Paper IV

"Evaluation and comparison of freeze-thaw tests and air void analysis of pervious concrete"

M.S.M. Lund, K.K. Hansen, J.T. Kevern, and V.R. Schaefer

Published in: *Proceedings of the 11th fib International PhD Symposium in Civil Engineering, 2016*

Evaluation and Comparison of Freeze-Thaw Tests and Air Void Analysis of Pervious Concrete

Mia S.M. Lund*[1], Kurt K. Hansen*[1], John T. Kevern*[2] and Vernon R. Schaefer*[3]

*[1]) *Department of Civil Engineering,*
Technical University of Denmark,
Brovej 118, DK-2800 Kgs. Lyngby, Denmark

*[2]) *School of Computing and Engineering,*
University of Missouri-Kansas City,
352 Flarsheim Hall, 5100 Rockhill Rd. Kansas City, MO 64110, USA

*[3]) *Department of Civil, Construction and Environmental Engineering,*
Iowa State University,
Town Engineering Building, Ames, IA 50011, USA

Abstract

Pearl-Chain Bridge technology is an innovative precast arch bridge solution which uses pervious concrete as fill material. To ensure longevity of the bridge superstructure it is necessary that the pervious concrete fill is designed to be freeze-thaw durable; however, no standards exist on how to evaluate the freeze-thaw resistance of fresh or hardened pervious concrete and correspondingly what constitutes acceptable freeze-thaw durability. A greater understanding of the correlation between the freeze-thaw performance and the air void structure of pervious concrete is needed. In the present study six pervious concrete mixes were exposed to freeze-thaw testing, and their air void structure was analyzed using an automated linear-traverse method. It was found that there is a miscorrelation between these two test methods in their assumption of whether or not the large interconnected voids effectively relieve the pressure when water freezes.

1 Introduction

Pearl-Chain Bridge technology is an innovative arch bridge solution allowing faster, more environmentally friendly, and cheaper road and railway bridge constructions. The Pearl-Chain arch is constructed from plane super-light decks (SL-Decks) that are collected and post-tensioned next to the road and subsequently lifted into place by a crane (Halding, Hertz and Schmidt, 2015). With the Pearl-Chain arch in place, spandrel walls are installed and finally a fill material is placed. To ensure longevity of Pearl-Chain Bridges, Portland Cement Pervious Concrete (PCPC) is considered as fill material. PCPC is characterized by a large interconnected void structure providing excellent drainage properties; thus, penetrating rainwater is efficiently removed from the Pearl-Chain Bridge superstructure by the use of PCPC fill. Thereby the moisture exposure of the Pearl-Chain arch is reduced and the freeze-thaw damages of the fill material itself are minimized if not completely eliminated.

Hard infrastructure, such as Pearl-Chain Bridges, is expected to be in use for a period of 120 years. This places severe demands on the fill material in order to test and document its durability under various conditions. In mild climate countries like Denmark where the temperature during winter times varies around the freezing point, the fill material is particular exposed to harsh freeze-thaw impact, because the bridge superstructure is cooled from several sides; hence, the application of PCPC as fill in Pearl-Chain Bridges requires PCPC to possess some amount of freeze-thaw durability. However, no standards exist on how to evaluate the freeze-thaw resistance of fresh or hardened PCPC or suggestions on what results produce adequate performance in the field. Currently the evaluation of the freeze-thaw durability of hardened PCPC is based on the same ASTM standard, ASTM C666A (ASTM C666, 2008), as conventional concrete even though it is well-known that this test method is too harsh because it does not include the draining nature of PCPC. Several examples have shown that air-entrained PCPC performs much better in the field than in the laboratory (NRMCA, 2004).
The void structure of PCPC is more complex than that of conventional concrete because it is a combination of small entrained air voids and large interconnected voids that are also sometimes referred

to as 'effective voids' because they contribute to the main water percolation. Previous studies such as those performed by Kevern, Wang, and Schaefer (2008; 2009) have successfully tried to link the freeze-thaw performance of PCPC to the air void system by analyzing the amount of entrained air in hardened PCPC in a RapidAir analysis using the linear-traverse method described in the ASTM C457 standard (ASTM C457, 2006). However, the RapidAir analysis does not include voids larger than 4 mm in diameter and more experiments are needed to fully understand the freeze-thaw mechanisms of PCPC. In this study, the freeze-thaw durability of six different PCPC mix designs is evaluated from their change in mass and relative dynamic modulus during freeze-thaw tests. The results are linked to the air void structure determined from the linear-traverse method using the RapidAir analysis including air voids less than 1 mm, less than 4 mm, and all air voids.

2 Methods

2.1 Material Properties

All mixes were prepared with ASTM C150 cement meeting both Type I and Type II classification and ASTM C618 Class F fly ash with a specific gravity of 3.15 and 2.28, respectively (ASTM C150, 2012; ASTM C618, 2012). Two different types of coarse aggregate were used: granite A and B with a maximum aggregate size of 1/2 in. (12.7 mm) and 3/8 in. (9.5 mm), respectively. Both had a specific gravity of 2.70. Granite A had 0.6% absorption, a dry rodded unit weight of 1524 kg/m^3 and a void ratio of 0.43, whereas granite B had 0.7% absorption, a dry rodded unit weight of 1405 kg/m^3 and a void ratio of 0.48. As fine aggregate, concrete sand with 100% passing the No. 4 sieve (4.75 mm), a fineness modulus of 3.1, a specific gravity of 2.64 and 1.8% absorption was used. Moreover, vinsol resin-based air entraining agent (AEA) and polycarboxylate based high-range water reducer (HRWR) with a specific gravity of 1.02 and 1.10, respectively, were used.

2.2 Mix Designs

A total of six different mixes were placed for this study. Three used granite A (Mix A) and three used granite B (Mix B). Mix A and B had a water-to-cement ratio of 0.29 and 0.31, respectively, and 20% cement replaced with fly ash, by weight. The fine aggregate to coarse aggregate ratio was 0.09, also by weight. The mixtures were designed for 18% voids and the mixes containing AEA were designed to have additionally 3% entrained air. 'Mix 1' did not contain any AEA or HRWR, 'Mix 2' contained only AEA, and 'Mix 3' contained AEA and HRWR. The AEA dosage was slightly higher than the standard dosage used for conventional concrete, that is, 0.125% of the cementitious material mass. The HRWR dosage was 0.375%. The different mixture proportions are shown in Table 1.

Table 1 Pervious concrete mix designs A and B.

Mix	Cement [kg/m^3]	Fly ash [kg/m^3]	Water [kg/m^3]	Granite [kg/m^3]	Sand [kg/m^3]	AEA [kg/m^3]	HRWR [kg/m^3]
1-A	315	64	100	1435	133	-	-
2-A	315	64	100	1385	128	0.47	-
3-A	315	64	100	1382	128	0.47	1.42
1-B	315	64	114	1401	130	-	-
2-B	315	64	114	1350	125	0.47	-
3-B	315	64	114	1347	125	0.47	1.42

2.3 Sample Mixing and Preparation

The concrete was prepared by first mixing aggregates and 5% of the cement for one minute to ensure that all aggregates were coated with cement (Kevern, Wang, and Schaefer, 2008). The AEA was diluted in the water and added to the mix. When foam was observed, the rest of the cement and fly ash was added and mixed for three minutes. The mixture was allowed to rest for two minutes before it was mixed for additionally two minutes. In mixes with HRWR, one third of the water was held back, mixed with HRWR and added when the mix appeared uniform after addition of cement and fly ash.

The samples for the freeze-thaw tests were prepared in beam molds measuring 75 × 100 × 400 mm (3 × 4 × 16 in.), and the samples for the air void analysis were prepared in d100/h200 mm (4/8 in.) cylinder molds. The mass of PCPC corresponding to the volume of the mold was determined

from the mix design and placed in the mold in three equal lifts. Each lift was rodded a maximum of 25 times for the cylinder specimens and 75 times for the beam specimens depending on the workability of the particular mix design. The layers were meshed together by vibrating each new layer for three seconds. After 24 hours the specimens were demolded and placed in a fog room with a relative humidity of 98% until 28 days.

For the RapidAir analysis, samples measuring 100 × 100 × 15 mm were cut vertically from the cylinder specimens. One side of the sample was wet-sanded with successively finer grit paper finishing with the 6 µm grit. Afterwards, the entire surface was colored black with a broad tip black marker and the sample was heated to 80°C in an oven for two hours. Subsequently, a white zinc paste mixed from petroleum jelly and zinc oxide was applied and massaged into the heated surface, thereby melting and flowing into the air voids. The sample was cooled in a refrigerator before all excess zinc paste was removed from the surface with an angled razor blade.

2.4 Testing Procedures

Determination of the void content and the unit weight of the hardened pervious concrete beam specimens were carried out by weighing the specimens below and above water in accordance with the ASTM C1754 standard (ASTM C1754, 2012). Three beam specimens were tested for each mix design except from Mix 1-A which was not exposed to freezing and thawing.

The freeze-thaw tests were carried out in accordance with the ASTM C666 standard Procedure A (ASTM C666, 2008), where the specimens are frozen and thawed in water and their core temperature varies between –18°C±2°C and 4°C±2°C. Prior to the beginning of the freeze-thaw exposure, the specimens were water saturated for 24 hours at 4°C. The mass loss and the durability factor (*DF*) calculated from relative dynamic modulus were used to evaluate the freeze-thaw durability of the specimens, and the tests were terminated when the specimens reached 15% mass loss, 300 frost cycles or a reduction in the relative dynamic modulus to 60%. The mass loss and the transverse frequency were measured for every 30 frost cycles. *DF* [%] was calculated using the formula:

$$DF = \frac{PN}{M} \tag{1}$$

where *P* [%] is the relative dynamic modulus (RDM) at *N* cycles, *N* is the number of cycles at which *P* reaches the specified minimum value for discontinuing the test—chosen as 60% of RDM—or the specified number of cycles at which the exposure is to be terminated, whichever is less, and *M* = 300 cycles is the number of cycles at which the exposure is to be terminated.

A RapidAir analysis based on the linear-traverse method described in the EN 480-11 standard (EN 480-11, 1998) was carried out using a RapidAir device. For all samples, five traverse lines per frame were chosen. The threshold value was set to 120 and 100 for Mix A and Mix B, respectively. The paste content was 22.8% and 24.2% for Mix A and Mix B, respectively. For each sample, the RapidAir test was performed four times by rotating the sample 90 degree between each test. The values presented herein are average values of these four measurements.

3 Results and Discussion

For conventional concrete, the freeze-thaw durability is typically evaluated from one of two methods: either by exposing concrete samples to freeze-thaw tests in a freezing chamber and consider the decrease in mass and transverse frequency by following, for example, the ASTM C666 standard (ASTM C666, 2008), or by determining characteristic air void properties such as the spacing factor and the specific surface area in a microscopical analysis. Such microscopical analysis is often performed using a RapidAir system (or a similar system) that automatically scans the prepared sample and measures the linear-traverses according to the procedure described in the EN 480-11 standard (EN 480-11, 1998) or in the ASTM C457 standard (ASTM C457, 2006). The results achieved directly from the RapidAir analysis include only voids up to 4 mm. Voids larger than 4 mm are simply omitted from the analysis because the EN 480-11 standard (EN 480-11, 1998) does not consider air bubbles with a diameter greater than 4 mm. This is because the formulas used to determine the air void characteristic in the linear-traverse method build on Powers' formulas that distinguish between whether or not the paste-to-air content (*p/A*) is less than or greater than 4.342 (Powers, 1949) which relates to whether a paste has a low or a rich air content. For *p/A*-ratios greater than 4.342, the results become erroneous if air voids larger than 4 mm are included in the analysis, and for conventional concrete it is reasonable to leave such coarse air bubbles out of the analysis because they are rarely

present. In the ASTM C457 standard (ASTM C457, 2006) no upper size limit is specified; however, one should be aware of this possible error when using the method. Because PCPC and conventional concrete are similar in many perspectives it is natural to apply the same methods as used for conventional concrete to determine the freeze-thaw durability of PCPC. However, the void structure of PCPC is considerably more complex than that of conventional concrete because it contains small entrained air in the cement paste (as conventional concrete) but also larger voids that often exceed 4 mm between the aggregate particles. Hence, when considering the freeze-thaw durability of PCPC three questions naturally arise:

1) What is the error by omitting the largest voids (> 4 mm) when applying the linear-traverse method described in the EN 480-11 standard (EN 480-11, 1998) on PCPC?
2) Is it reasonable to determine the spacing factor for PCPC from the same expressions as used for conventional concrete when the void structure of PCPC is so distinctively different than the void structure assumed in the EN 480-11 standard (EN 480-11, 1998) relating to conventional concrete?
3) How do freeze-thaw tests of PCPC compare to the air void characteristics determined from the linear-traverse method described in the EN 480-11 standard (EN 480-11, 1998)?

The following sections will address these questions by considering the tendencies and correlations discovered in the present study.

3.1 Freeze-Thaw Tests

Fig. 1(left) shows the remaining mass of the specimens as function of the number of freeze-thaw cycles. Because there was a certain variation in the freeze-thaw behavior within each mix design, the results are shown for all specimens.

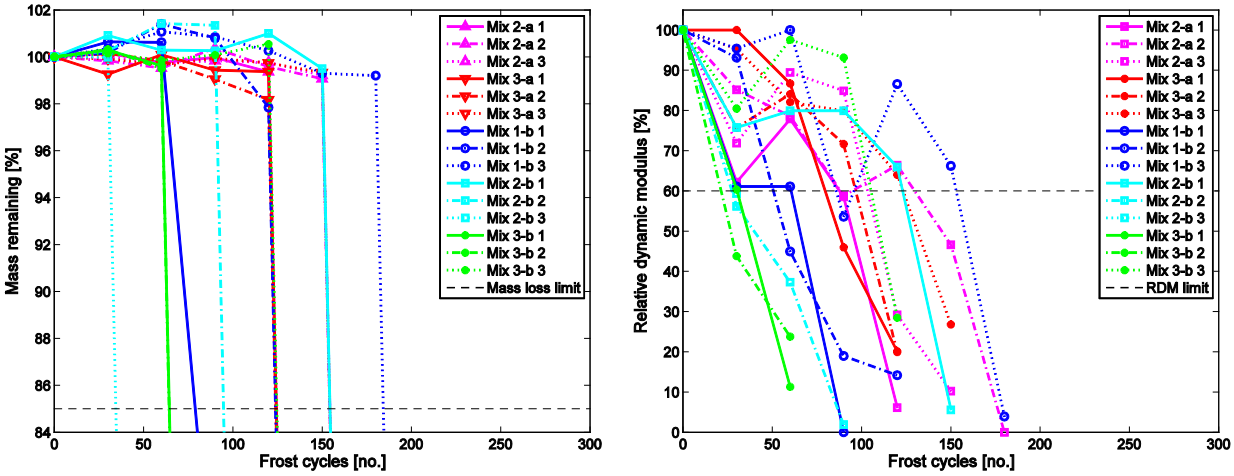

Fig. 1 Remaining mass (left) and RDM (right) for PCPC specimens as function of the number of freeze-thaw cycles.

Fig. 1(left) shows that the mass loss of most PCPC specimens was insignificant until the point of failure at which an abrupt decrease in the mass took place as the paste deteriorated to the point of loose aggregate. Although specimens were first soaked in water before initial testing, the figure also shows that some specimens gained weight during the freeze-thaw tests. This is because the cement paste absorbed water when the specimens were immersed. At the point of failure the specimens were completely deteriorated and it was not possible to measure the mass; hence, the mass loss is set to 100% in Fig. 1(left). A mass loss of 15% is typically defined as the acceptable maximum mass loss for PCPC. Table 2 summarizes the number of frost cycles at which the specimens had 15% mass loss. The table also shows the air void content of the beam specimens used in the freeze-thaw tests determined. No freeze-thaw tests were performed on Mix 1-A.

Fig. 1(right) shows the decrease in RDM as function of the number of freeze-thaw cycles, and the 60% cut-off limit. Compared to the decrease in mass loss, the decrease in RDM occurred faster and more gradually as it was also observed in Shu *et al.* (2011). Hence, most specimens failed per the selected criteria due to a reduction in RDM rather than due to the mass loss. Table 2 also shows the average *DF*s calculated from Eq. (1). The size of *DF* is very dependent on the choice of *M* and *P* which means that *DF*s can only be compared if they were calculated using the same assumptions. The

results in Kevern, Wang, and Schaefer (2010) and Shu *et al.* (2011) suggest that acceptable freeze-thaw behavior occurs for *DF*s larger than 40%; hence, the *DF*s determined for the specimens in this study are low which indicate a poor freeze-thaw resistance. Based on *DF*, Mix 3-B had the worst freeze-thaw durability even though the beams used for the test had the lowest void content which is known to improve the freeze-thaw durability of PCPC. Mix A showed slightly improved freeze-thaw durability compared to Mix B. Moreover, the freeze-thaw results were much more variable than what is typically observed and allowable for conventional concrete.

Table 2 Air void content and hardened unit weight (UW) of PCPC beam specimens used for freeze-thaw tests measured according to the ASTM C1754 standard (ASTM C1754, 2012). Moreover, the initial transverse frequency, f_0, and the durability factors, *DF*, for the different mix designs, are shown (average value (av.) and coefficient of variation (COV)), and the number of frost cycles, *n*, corresponding to a mass loss of 15%.

Mix	Voids [%]		UW [kg/m^3]	f_0 [Hz]	*DF* [%]		*n* [-]		
	Av.	COV	Av.	Av.	Av.	COV	1	2	3
2-A	19.4	0.6	2008	1627	18.6	9.6	154	184	124
3-A	18.5	1.0	1979	1673	20.0	22.0	124	124	184
1-B	18.8	2.5	1977	1680	16.3	55.1	86	124	184
2-B	19.0	1.3	1964	1685	12.0	91.0	183	95	34
3-B	13.8	5.0	1976	1696	10.5	88.3	64	64	125

3.2 Air Void Analysis using the Linear-Traverse Method

3.2.1 Air Void Content

The results achieved directly from the RapidAir analysis include only voids up to 4 mm; however, the raw data was processed to also include all void sizes. Fig. 2 visualizes the air void distribution of the mix designs by distinguishing the void content for air voids less than 1 mm, air voids less than 4 mm and all air voids. Both numerical and relative values are shown.

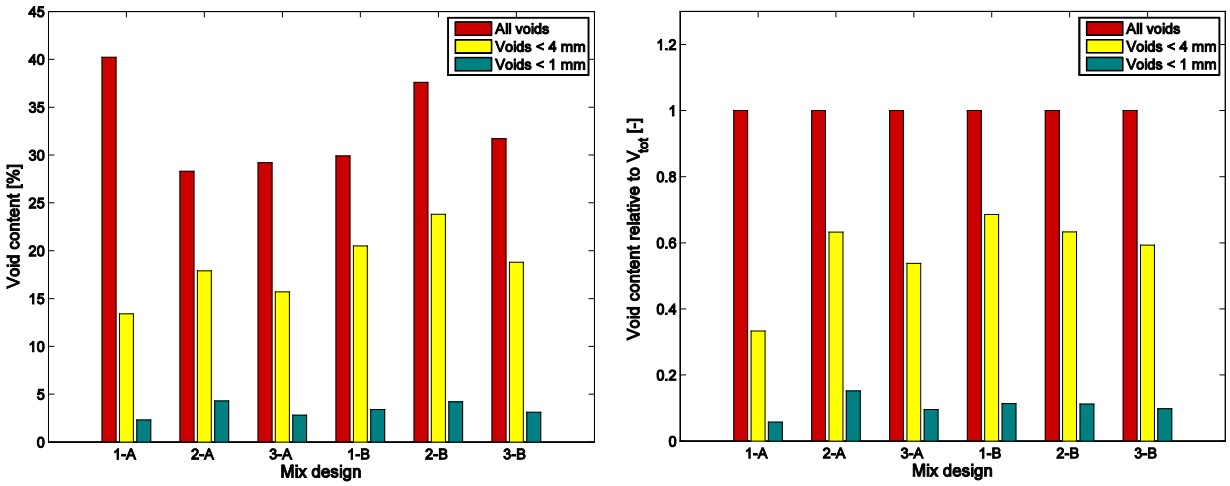

Fig. 2 Void content of specimens divided between voids less than 1 mm, 4 mm and all voids determined from the RapidAir analysis on cylinder specimens (left), and void contents relative to the void content that includes all voids for the particular mix designs (right).

Because Mix 1-A and 1-B did not contain AEA it was expected that those mixes would have less fine air than the remaining mixes. Fig. 2(right) shows that Mix 1-A had a slightly lower air content of voids less than 1 mm than Mix 2-A and 3-A; however, for Mix B the same tendency was not observed, and even for Mix A the difference was small. It is well-known that addition of AEA increases PCPC workability by which PCPC compacts better and the void size decreases. For Mix A, the voids less than 4 mm constituted a larger part of the total void content for Mix 2-A and 3-A with AEA than for Mix 1-A without AEA; however, for Mix B this was not the case. For neither Mix A nor Mix B, did the addition of AEA have the desired effect. Fig. 3 shows scanned 10 × 10 cm^2 images of specimens 2-A, 1-B and 2-B together with 1 × 1 cm^2 close-ups of the same sections.

For air entrained PCPC, a clear gray phase, that is a combination of the black solid phase and the white void phase, is typically present (Kevern, Wang, and Schaefer, 2008). Fig. 3 shows that such phase was neither present for Mix A nor Mix B. This indicates that the amount of AEA added to the mixtures was not sufficiently high enough to create a fine entrained air void system in the cement paste. The AEA dosage used has previously shown to be sufficient for PCPC (Kevern, Wang, and Schaefer, 2008; 2010). A possible explanation of the lacking entrained air content observed in this study is the high fly ash content compared to the studies in Kevern, Wang, and Schaefer (2008, 2010) that did not contain any fly ash. Fly ash is known to consume AEA and therefore a higher AEA dosage is typically used for concretes containing fly ash.

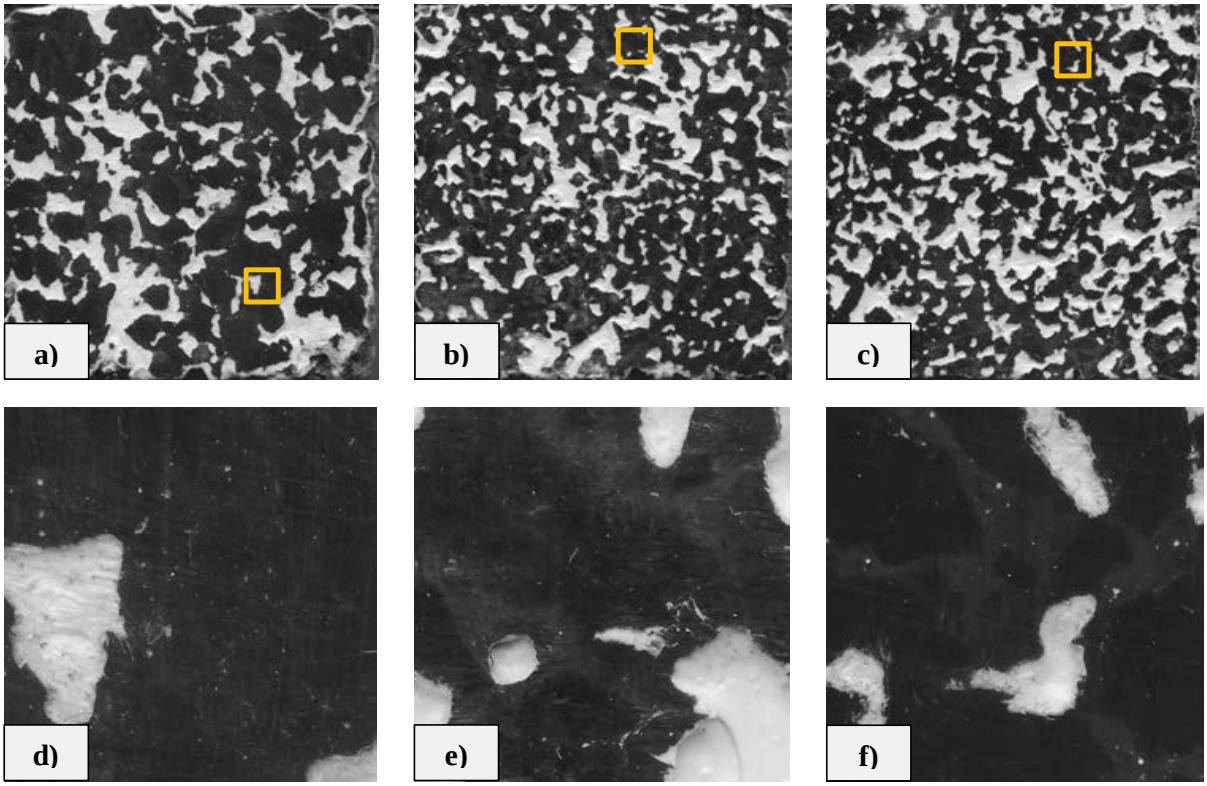

Fig. 3 Scanned PCPC images: a,b,c) 10 × 10 cm^2 section of mix 2-A, 1-B and 2-B, respectively, and d,e,f) 1 × 1 cm^2 close-up of mix 2-A, 1-B and 2-B, respectively. No entrained air phase was observed for any of the mixes.

3.2.2 Spacing factor of PCPC

The paste content and the total air void content of the PCPC mixes in this study represent typical values for PCPC, and as seen from the mix design, the *p/A*-ratio is 1.2 which is significantly less than 4.342 because of the large PCPC void content. Therefore, for PCPC the following expression is always used to determine the spacing factor, $\bar{L}$ [mm], when applying the linear-traverse method:

$$\bar{L} = \frac{T_P}{4N} = \frac{p}{SA} \quad (2)$$

where T_P is the traverse length through paste, N is the total number of air voids intersected, p is the paste content, S [mm^{-1}] is the specific surface area of the voids (the surface area of air voids divided by their volume), and A [%] is the total void content (EN 480-11, 1998; Powers, 1949). For conventional concrete, p/A is typically larger than 4.342 and a different and more complex expression is used to determine the spacing factor: $\bar{L} = \frac{3}{S}[1.4\left(1+\frac{p}{A}\right)^{1/3} - 1]$. However, for PCPC the expression used to determine the spacing factor based on Powers' formula is fairly simple. Eq. (2) builds on the assumption that for cement paste with high air content, the maximum distance to an air void can be determined by spreading the cement paste in a uniformly thick layer over each air void. The thickness of this paste layer equals the spacing factor, and Eq. (2) therefore expresses the ratio between the paste content and the total surface area (the second expression in Eq. (2)). For cement paste to be

freeze-thaw durable, it is a typical requirement that the spacing factor should be less than 0.2 mm (ASTM C457, 2006).

Table 3 shows the spacing factor determined from the linear-traverse method. The spacing factors were determined by considering air voids less than 1 mm, less than 4 mm and all air voids. Table 3 shows that the mix designs containing AEA did not have smaller spacing factors than the mix designs without AEA, which confirms the tendencies observed from Fig. 2 and Fig. 3.

Table 3 Spacing factor ($\bar{L}$) determined from the RapidAir analysis for voids less than 1 mm, less than 4 mm and for all air voids, and difference between spacing factor including voids less than 4 mm and all air voids.

Mix	$\bar{L}_{1mm}$ (< 1 mm)		$\bar{L}_{4mm}$ (< 4 mm)		$\bar{L}_{tot}$ (all voids)		$\bar{L}_{4mm} - \bar{L}_{tot}$
	Av. [mm]	COV [%]	Av. [mm]	COV [%]	Av. [mm]	COV [%]	
1-A	0.28	10.4	0.33	13.4	0.27	11.8	0.06
2-A	0.26	5.26	0.22	7.75	0.21	7.64	0.01
3-A	0.35	12.6	0.33	12.1	0.29	9.56	0.04
1-B	0.27	8.82	0.24	8.77	0.23	11.6	0.01
2-B	0.22	6.32	0.18	6.30	0.17	5.94	0.01
3-B	0.25	4.72	0.24	5.80	0.22	5.53	0.02

The spacing factors based on voids less than 4 mm and all voids were calculated from Eq. (2) which states an inverse proportionality between the spacing factor and the number of air voids. Hence, when increasing the number of air voids included in the analysis, the spacing factor decreases. Table 3 shows that the decrease was up to 0.06 mm. The large air voids have a larger total surface area (*SA*) than the small voids and Eq. (2) shows that the spacing factor decreases with increasing *SA*. Thus, the difference between spacing factors including all air voids and voids less than 4 mm depends on the content of voids larger than 4 mm. Fig. 2(right) shows that Mix 1-A had the largest content of voids larger than 4 mm; hence, this mix experienced the largest difference in the spacing factor as it is also clear from Table 3. However, for Mix 2-A, 1-B and 2-B, the content of voids larger than 4 mm was less and the difference in the spacing factor was small. Thus, if the content of air voids greater than 4 mm is low, the error by using the RapidAir analysis that includes only air voids up to 4 mm is small. Table 3 also shows that the spacing factors decrease if all voids are included rather than air voids less than 1 mm. However, in this situation a similar rationale as the abovementioned cannot be applied because the expression used to determine the spacing factor for air voids less than 1 mm is different than Eq. (2) and builds on different assumptions. However, the spacing factor determined for voids less than 1 mm can be considered to only relate to the cement paste.

3.3 Reflection and Evaluation of Freeze-Thaw Durability Test Methods for PCPC

The results in Table 3 show that even without the expected entrained air content in the cement paste, the spacing factors calculated when including all air voids were fairly close to 0.2 mm for most mixes, and for Mix 2-B less than 0.2 mm, even though Fig. 3e and Table 2 clearly show that the cement paste was not air entrained and the freeze-thaw durability was not good. Fig. 3 shows that the large air voids of PCPC are not spherical but irregular and twisted. Because the linear-traverse method directly transforms a given chord length to the volume of a spherical void, the method possibly exaggerates the total air content. This is clear by comparing the total void content of Fig. 2(left) with that in Table 1 determined from the ASTM C1754 standard (ASTM C1754, 2012).

When performing the freeze-thaw tests according to the ASTM C666 standard (ASTM C666, 2008), the large air voids are water-filled; however, in the microscopic analysis they are considered to be as effective as the small entrained air voids to relieve the pressure caused by water that freezes. This is contradictory. On one hand it is known that the large voids positively influence the freeze-thaw durability of PCPC, but on the other hand, the tools available to characterize the freeze-thaw properties of PCPC are developed for conventional concrete that has a different void structure. A possible solution to overcome this misinterpretation between the microscopic test method and the freeze-thaw test method could be to include only entrained air voids less than, for example, 1 mm in the determination of the spacing factor because these voids are not water-filled during freeze-thaw

testing. By doing so, the misinterpretation between the two methods would be minimized; however, it would not link the test methods to the PCPC freeze-thaw performance experienced in real life, and future studies should clarify how to include the large voids in a more reasonable way in laboratory testing.

4 Conclusions

The main conclusions from this study were:

1) The air entrainment (AEA) dosage of 0.125 weight-% of cement and fly ash was not sufficient to create an entrained air content in the cement paste containing fly ash even though the dosage has previously been found to provide good results for cement paste without fly ash. This is possible due to the high content of fly ash used in this study. The entrained air contents of specimens with and without AEA were similar.
2) The decrease in the relative dynamic modulus (RDM) was faster and more gradual than the decrease in the mass during the freeze-thaw tests. Most specimens failed due to reduction in RDM rather than due to reduction in mass.
3) The freeze-thaw durability results were much more variable than what is typically observed and allowable for conventional concrete. The freeze-thaw durability of all specimens tested was poor even though the spacing factor was less than 0.2 mm for one mix design and fairly close to 0.2 mm for others. When the spacing factor is determined from the linear-traverse method, the large voids are considered to effectively relieve the pressure caused by water that freezes; however, in freeze-thaw laboratory tests of PCPC they are water-filled and thereby not effective which causes a misinterpretation between the two test methods.
4) If the content of air voids greater than 4 mm is low, the error by using the linear-traverse method that includes only air voids up to 4 mm is small.

References

ASTM Standard C150/C150-M. 2012. “Standard Specification for Portland Cement”. West Conshohocken, PA: ASTM International.

ASTM Standard C457-06. 2006. “Standard Test Method for Microscopical Determination of Parameters of the Air-Void System in Hardened Concrete”. West Conshohocken, PA: ASTM International.

ASTM Standard C618-12a. 2012. “Standard Specification for Coal Fly Ash and Raw or Calcined Natural Pozzolan for Use in Concrete”. West Conshohocken, PA: ASTM International.

ASTM Standard C666/C666M-03. 2008. “Standard Test Method for Resistance of Concrete to Rapid Freezing and Thawing”. West Conshohocken, PA: ASTM International.

ASTM Standard C1754-12. 2012. “Standard Test Method for Density and Void Content of Hardened Pervious Concrete”. West Conshohocken, PA: ASTM International.

EN 480-11Standard, 1998. “Admixtures for concrete, mortar and grout – Test methods – Part 11: Determination of air void characteristics in hardened concrete”. Brussels: European Standard.

Halding, Philip S., Kristian D. Hertz and Jacob W. Schmidt. 2015. “Precast Pearl-Chain concrete arch bridges”. *Engineering Structures* 103:214–27.

Kevern, John T., Kejin Wang and Vernon R. Schaefer. 2008. “A Novel Approach to Characterize Entrained Air Content in Pervious Concrete”. *Journal of ASTM International* 5(2).

Kevern, John T., Kejin Wang and Vernon R. Schaefer. 2009. “Test Methods for Characterizing Air Void Systems in Portland Cement Pervious Concrete”. *Journal of ASTM International* 6(9).

Kevern, John T., Kejin Wang and Vernon R. Schaefer. 2010. “Effect of Coarse Aggregate on the Freeze-Thaw Durability of Pervious Concrete”. *Journal of ASTM International* 22(2):469–75.

National Ready Mixed Concrete Association (NRMCA). 2004. “Freeze-Thaw Resistance of Pervious Concrete”. Silver Spring (MD): NRMCA.

Powers, T.C. 1949. The air requirement of frost resistant concrete. *Proceedings of the Highway Research Board* 29:184–211.

Shu, Xiang, Baoshan Huang, Hao Wu, Qiao Dong and Edwin G. Burdette. 2011. “Performance comparison of laboratory and field produced pervious concrete mixtures”. *Construction and Building Materials* 25:3187–92.

Paper V

"Frost susceptibility of sub-base gravel used in Pearl-Chain Bridges: an experimental investigation"

M.S.M. Lund, K.K. Hansen, and I.B. Andersen

Published in: *International Journal of Pavement Engineering, 2016, doi: 10.1080/10298436.2016.1230429*

INTERNATIONAL JOURNAL OF PAVEMENT ENGINEERING, 2016
http://dx.doi.org/10.1080/10298436.2016.1230429

Taylor & Francis
Taylor & Francis Group

Frost susceptibility of sub-base gravel used in Pearl-Chain Bridges: an experimental investigation

M. S. M. Lund, K. K. Hansen and I. B. Andersen

Technical University of Denmark, Lyngby, Denmark

ABSTRACT

This study investigates frost susceptibility of sub-base gravel determined by the ASTM D5918-13 standard as a conservative estimate of the frost heave risk of fill in overfilled arch bridges, particularly in Pearl-Chain Bridges. Frost heave of granular materials has been of great research interest from the end of the 1920s until the present day. Most new literature relates to empirical results that are several decades old. This is also the case for Danish tender specifications according to which the frost susceptibility of a sub-base gravel is solely assessed from its fines content. However, no actual frost tests have been carried out to verify this assumption. In the present study, the frost susceptibility of four different Danish gravel materials is categorised from their heave rate. We test two Danish sub-base gravel materials, with particle size distributions of 0–8 mm and 0–31.5 mm, respectively, and also two modified sub-base gravel materials with increased and reduced fines contents. The fines content of the gravel materials is analysed by laser diffraction, and compared with two common frost susceptibility criteria, Casagrande's and Schaible's, and with Danish tender specifications. Even though the two sub-base gravel materials are expected to be frost safe, 0–31.5 mm sub-base gravel shows medium frost susceptibility, whereas 0–8 mm sub-base gravel shows negligible frost susceptibility. The gravel materials with increased and reduced fines content are categorised as having low to medium frost susceptibility and low frost susceptibility, respectively. The permeability of the gravel materials is determined, and the permeability coefficient of 0–31.5 mm sub-base gravel is five times greater than that of 0–8 mm sub-base gravel. The results suggest that the criterion used to classify the frost susceptibility of Danish sub-base gravel materials based solely on their fines content is insufficient, and that the permeability coefficient should also be considered.

ARTICLE HISTORY
Received 21 October 2015
Accepted 22 August 2016

KEYWORDS
Fill material; frost susceptibility; Pearl-Chain Bridge; permeability; sub-base gravel

1. Introduction

Typical fill materials in overfilled arch bridges are granular materials such as soil and gravel. There are several examples of modern prefabricated arch bridge systems with gravel fill, such as the TechSpan bridge system (Hutchinson *et al.* 2004), and the BEBO arch system (BEBO Arch Systems 2009), but older arch bridge constructions are also usually filled with a granular material (Sihwa 1987). Apart from the low cost, the main reason for the widespread use of this type of fill is that granular materials are expected to satisfy typical main functions of fill materials in arch bridges, such as stabilisation of the arch structure, transfer of traffic loads to the arch and overall durability of the fill material itself.

In areas where the temperature annually varies around the freezing point, a bridge is a critical part of the construction of a road because it is exposed to freezing from below, from above and from the sides. This also means that the fill material is considerably affected by freezing and thawing. Therefore, to prevent any damage of the bridge superstructure, it is important to ensure sufficient freeze–thaw durability of the fill material. Under the right circumstances some gravel materials are known to suffer from frost heaving, which among other things exerts high pressure on the spandrel walls (Sihwa 1987). Frost heaving also causes cracks in the wearing course, and thereby deterioration of the bridge. There are several examples of old arch bridges that have been strengthened by replacing old granular fill with concrete fill (Sihwa 1987).

Frost heave is caused by the formation of ice lenses in soil. When the temperature of the surrounding air, typically above the soil, falls below zero, ice crystals form and coalesce into ice lenses, thereby initiating a freezing front that descends through the soil (Anderson *et al.* 1984). The ice lenses grow because of water migration to the freezing front from a water supply below the soil. Eventually, the growth of ice lenses results in frost heaving, causing an upward displacement of the soil equal to the thickness of the ice (Taber 1929). For the ice lenses to grow, the ice has to be segregated from the soil particles. A pre-melted liquid water film around the soil particles caused by ice-particle interaction separates the ice from the soil particles, and the growth of the segregated ice increases due to these water films working as water supplying passages (Beskow 1935, Rempel 2007). Intermolecular forces across these thin water films create a fluid pressure gradient, causing the unfrozen water to be transported to the freezing zone (Rempel 2007, Rempel 2010). The theoretical understanding of the mechanisms driving frost heaving is complex, and many incorrect theories have been postulated throughout the last century. One of the most common misunderstandings is that capillary forces transport water from the water source to the freezing zone (Rempel 2010, Taber 1930). Because of ice segregation, bands of soil-free ice

CONTACT M. S. M. Lund msml@byg.dtu.dk

lenses are formed between layers consisting of a mixture of ice, particles and water (Rempel, 2007). When the air temperature changes, the temperature gradient changes and the freezing front changes position, resulting in several bands of ice lenses at different soil depths (Anderson *et al.* 1984).

Three conditions must exist for frost heaving to occur: the climate should be so cold that the freezing front can be initiated, a water supply should be available and a soil material that is susceptible to frost should lie within the freezing zone (Anderson *et al.* 1984). Since the most straightforward approach to eliminate frost heaving is to avoid using frost-susceptible soil, this has been a research field of great interest during the last century. More than 100 different criteria have been proposed to assess whether or not a specific soil material is frost susceptible (Chamberlain 1981). Two of the most simple and well known of these are Casagrande's and Schaible's frost criteria, both of which build on a consideration of the soil particle size distribution. The soils being most vulnerable to frost heaving are those being sufficiently fine-grained to allow water to be held in the material, but at the same time being sufficiently coarse-grained to provide the necessary permeability to supply liquid water to the segregated ice (Rempel 2010).

In 1931, Arthur Casagrande proposed the following rule of thumb to determine whether or not a soil type is frost susceptible:

> Under natural freezing conditions and with sufficient water supply, one should expect considerable ice segregation in non-uniform soils containing more than three per cent of grains smaller than 0.02 mm, and in very uniform soils containing more than 10 per cent smaller than 0.02 mm. (Casagrande 1931)

In Denmark, non-uniform soils are typically defined as those having a coefficient of uniformity (C_u) > 5, whereas uniform soils have a C_u < 5 (Chamberlain 1981).

In 1957, Lothar Schaible proposed his most recent classification system that divides soils into three categories based on the proportion of particles finer than 0.002 mm, 0.02 mm and 0.1 mm, respectively (Chamberlain, 1981). Figure 1 shows Schaible's frost limit curves together with Casagrande's frost criteria.

In Denmark, determination of frost susceptibility is based solely on the particle size characteristic. Danish contractors use Schaible's frost criterion to determine whether or not a gravel material is frost susceptible (NCC Denmark 2001). The prevalence of this approach is also clear from the Danish tender specification for so-called 'sub-base gravel' materials, that is, gravel materials typically used for capillary breaks. Sub-base gravel materials are considered to lie within the frost safe zone in Figure 1, and are either categorised as 'quality I' or 'quality II' depending on their particle size distribution (Sub-base of Sand and Gravel – General Work Specification (GWS), 2003). Neither quality allows particles >90 mm in diameter, and a maximum of 15% should be >63 mm in diameter. A maximum of 5% of quality I and 9% of quality II can be <63 μm in diameter, which categorises quality I and quality II sub-base gravel as UF_5 and UF_9, respectively, according to the Danish standard 13285 (DS Standard 13285 2011). The definition of these requirements is believed to have originated from, and been inspired by, Casagrande's frost criterion (Chamberlain 1981).

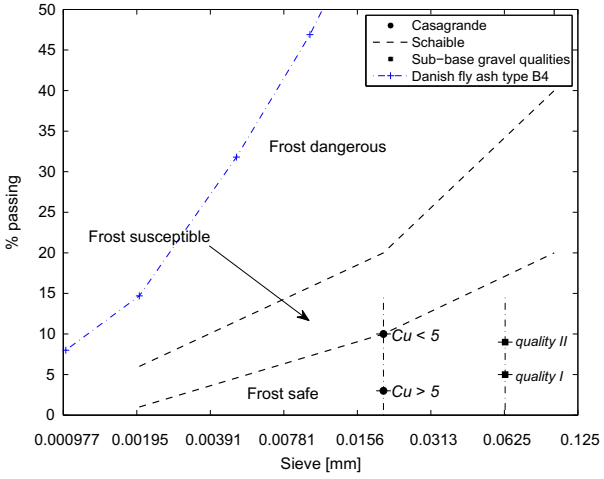

Figure 1. Frost criteria as given by Casagrande and Schaible. The mentioned frost susceptibility classes – 'frost safe', 'frost susceptible' and 'frost dangerous' – relate to Schaible's criterion. Casagrande's criterion distinguishes between soils with coefficients of uniformity < 5 and > 5. For a soil material to be frost susceptible, the proportion of soil particles at 0.02 mm needs to lie above the markings. The requirements to the maximum fines content in Danish quality I and quality II sub-base gravel materials are also shown, and the amount of soil particles at 0.063 mm needs to lie below the markings to fulfil the requirements for the specific quality. Finally, the particle size distribution of Danish fly ash type B4 is shown.

Besides the particle size distribution, other methods can be used to determine the frost susceptibility of soils, such as frost heave tests. A large number of different frost heave test variants exist around the world, making it difficult for experts to agree on a single test method. Thus, in Europe it has not been possible to reach agreement on a joint European standard test method, and therefore no such standard exists. However, in 1996 the American Society for Testing and Materials (ASTM) published a standard test method for frost heave and thaw-weakening susceptibility of soils (ASTM Standard D5918-13 2013). This standard is based on the recommendations given in the Cold Regions Research and Engineering Laboratory (CRREL) monograph 81-2 (Chamberlain, 1981), in which more than 100 different methods for determining frost susceptibility were reviewed, and four methods were proposed for further evaluation, including one frost heave test.

The original objective of the present study was to demonstrate that two Danish sub-base gravel materials suitable for use as fill in arch bridges, particularly in Pearl-Chain Bridges, were not exposed to frost heaving when tested in accordance with the ASTM D5918-13 standard (ASTM Standard D5918-13 2013). However, as the following sections will show, the results did not come out as expected, and even though sub-base gravels are in general expected to be frost safe, one of the tested sub-base gravels was found to be frost susceptible. The ASTM D5918-13 standard (ASTM Standard D5918-13 2013) is primarily developed to assess the frost susceptibility of soil materials used for pavements. Because the construction of pavements differs significantly from that of arch bridge superstructures, this choice of test procedure needs to be justified. The frost heave tests were performed in accordance with the ASTM D5918-13 standard for two main reasons: firstly, the test procedure is the only well-known procedure to determine the frost

susceptibility of soil materials; and, secondly, the test procedure can be considered a worst-case scenario which means that the frost susceptibility classification is conservative; thus, if a sub-base gravel material used for fill in Pearl-Chain Bridges is classified as 'frost safe' based on the ASTM D5918-13 standard, frost heave of the fill material will not occur. However, if a gravel material classified as 'frost susceptible' is used as fill in arch bridges, the drainage properties of the bridge superstructure become even more important than otherwise because it needs to be ensured that a constant water table is entirely prevented. The very first Pearl-Chain Bridge constructed in Denmark in 2015 consisted of a main arch and two adjacent half-arches as seen in Figure 2 (Lund *et al.* 2016). For such bridge design, a constant water table can occur over the two middle supports if the drainage of the superstructure is poor.

Furthermore, a bridge superstructure differs from pavement by being exposed to freezing from several sides; hence, the water source does not have to lie below the fill material but could also be caused by water fed from the bridge ends, for example.

In the present study, frost susceptibility is determined from frost heave tests of four gravel materials – two Danish sub-base gravels, a high fines content modified sub-base gravel, and a zero fines content modified sub-base gravel – in order to evaluate how exposed the gravel materials are to freezing and thawing. Furthermore, the results are compared with the Danish criterion for determination of frost susceptibility and to Casagrande's and Schaible's frost criteria. Finally, the permeability of the gravel materials is also determined in order to understand the freeze–thaw behaviour.

2. Background

Despite the arch being the optimal shape for road and railway bridges, it is rarely used, mainly because of the extensive use of scaffolding needed for constructing such bridges, and the subsequent closing of the underpassing road during the months-long construction period. The Pearl-Chain Bridge technology has reintroduced the arch primarily for road and railway bridges, and the road only needs to be closed for a night. This reduces traffic disturbance and carbon dioxide emissions, and minimises the cost. Furthermore, the use of material is minimised due to the optimal arch shape.

Thus, Pearl-Chain Bridge technology is an innovative arch solution for road and railway bridges. The Pearl-Chain Bridge superstructure consists of a Pearl-Chain arch, a fill material and a wearing course. Depending on the span of the bridge, a concrete top plate can be cast on top of the fill, below the wearing course. The Pearl-Chain arch is created from prefabricated Super-Light Decks (SL-Decks), which consist of lightweight concrete blocks and normal concrete (Hertz 2015, Hertz *et al.* 2014). Each SL-Deck is given a slight inclination at the ends, and has a duct cast through it longitudinally. Thereby, by collecting and post-tensioning several SL-Decks on a wire, like pearls on a string, an arch is formed from straight elements. To simplify the assembly, the Pearl-Chain arch is placed on its side; when the SL-Decks have been emplaced, self-compacting mortar joints are cast between the decks, after which the arch is post-tensioned (Lund *et al.* 2015). Next, the Pearl-Chain arch is tilted and put into place using a crane (Halding *et al.* 2015). The entire arch is constructed next to the road, and depending on the span and width of the bridge, it is possible to place the Pearl-Chain arch within a weekend. Pearl-Chain Bridges are mainly designed for spans of up to 30 metres. When the arch is placed, spandrel walls are installed, a filling material is laid out and either a post-tensioned concrete top plate is cast or the wearing course is placed directly on the fill.

3. Method

3.1. Materials

The present study investigates four different types of gravel material, which can be classified as follows: two are sub-base gravel materials, the third is sub-base gravel mixed with fly ash to increase the fines content, and the fourth is sub-base gravel with no fines <0.125 mm in diameter. The sub-base gravels from Jutland in the western part of Denmark are typically graded as 0–8 mm, whereas those from Zealand in the eastern part of Denmark are 0–63 mm. This geographical dependence is due to the expanse of the ice cap during the last ice age. The difference means that if sub-base gravel is to be used as fill in Pearl-Chain Bridges, the gradation of the fill is expected to vary substantially depending on where in Denmark the bridge is constructed. Thus, the present study investigates sub-base gravel materials from Jutland, later denoted as gravel A1, and those from Zealand, later denoted as gravel B1. The third gravel material, later denoted as gravel A2, was created by increasing the fines content of the 0–8 mm sub-base gravel to 20% by mixing it with Danish fly ash of type B4, since the particle size distribution of fly ash indicates that fly ash is frost dangerous (see Figure 1). Type B4 fly ash has a loss on ignition <4 weight-% and contains a maximum of 10% reactive lime in agreement with the requirements given in the DS 450-1 standard (DS Standard 450-1 2012). The fly ash in specimens A2 can be considered inert since the portlandite content is zero, the duration of the frost test is short and the frost test is carried out at relatively low temperatures; hence, fly ash will not positively affect the strength of the specimens. Having a fines content of 20%, Schaible's and Casagrande's frost criteria suggest that gravel A2 is susceptible to frost. The fourth gravel material, later denoted as gravel B2, was created by sieving off fines content <0.125 mm in diameter from the 0–63 mm sub-base gravel. During preparation of specimens B1 and B2, particles >31.5 mm in diameter were removed to fit the test equipment; thus, in the following sections, the particle size distribution of B1 and B2 relates to 0–31.5 mm and 0.125–31.5 mm, respectively.

3.2. Determination of particle size distribution

A standard sieving analysis does not include analysis of the fines content of particles <63 μm in diameter. In this study, therefore, the particle size distribution was carried out in two steps: a sieving analysis was used to determine the gradation curves for particle sizes >63 μm in diameter; and, since the laser diffraction method is applicable to particles as small as 0.1 μm in diameter (DS Standard 13320 2009), a laser diffraction analysis was used to determine the gradation of the particles <63 μm in diameter. The sieve analysis was carried out in accordance with the DS 933-1 standard (DS Standard 933-1 2004). The fines

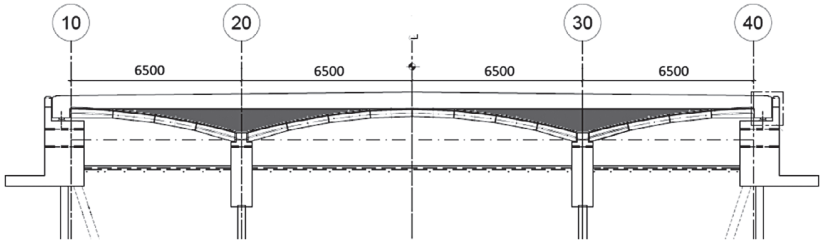

Figure 2. Longitudinal section of the very first Pearl-Chain Bridge constructed in Denmark in 2015. Dimensions are in mm. From: Lund *et al.* (2016).

content left from the sieve analysis was analysed by way of wet analysis, using the laser diffractometer. To check the reliability of the laser diffractometer, a test was also performed on pure fly ash and gave reasonable results when compared with the fly ash data sheet. Five tests were run for each gravel material, and the mean values were used to represent the materials. The results were expressed with respect to the entire particle size distribution determined from the sieve analysis of the specific gravel material.

3.3. Determination of optimal water content

The vibrating table method was used to determine the optimal water content, and the maximum dry density, for gravels A1, A2 and B1 as described in the DS 13286-5 standard (DS Standard 13286-5 2003). The applied method is similar to Method B in the ASTM D4253-16 standard (ASTM Standard D4253-16 2016). Three tests were performed for each gravel type, and the mean values were used in further tests. The optimal water content for gravel B2 was assumed to be similar to that of gravel B1.

3.4. Freeze–thaw experiments

With minor corrections, the freeze–thaw experiments were carried out in accordance with the ASTM D5918-13 standard (ASTM Standard D5918-13 2013). Each test can be divided into two steps: preparation of the specimen prior to the freeze–thaw exposure, and the freeze–thaw test itself.

3.4.1. Specimen preparation

Firstly, the gravel was wetted until its water content was one percentage point less than the optimal water content corresponding to water saturation determined from the vibrating table test. This is because Danish road regulations recommend decreasing the water content by up to three percentage points during preparation (Sub-base of Sand and Gravel – Design Guide 2003).

Afterwards, the gravel was placed in a mould consisting of six acrylic rings with an internal diameter of 140 mm, a wall thickness of 4 mm, and a height of 25 mm stacked one on top of each other. The dimension of the mould was independent of the gradation of the tested gravel material because the ASTM D5918-13 standard (ASTM Standard D5918-13 2013) does not consider the soil gradation. Each acrylic ring had a split cut through it longitudinally, and a hole with a diameter of 3.2 mm drilled at mid-height opposite to the split. The acrylic rings were stacked, with the splits placed above each other, and duct tape was used to make the acrylic rings stay in place. The six acrylic rings were placed on top of a spacer disc with a diameter of 148 mm and a height of 6.4 mm. A 3-mm thick butyl tube membrane with a diameter of 136 mm was placed inside the rings, and stretched outside the spacer disc to obtain a sealed closing at the bottom of the mould. The butyl membrane was fastened to the perimeter of the upper acrylic ring using duct tape. The acrylic mould was then placed in a steel mould with an internal diameter of 150 mm, leaving space for the acrylic mould and the spacer disc to be placed inside it. The top of the acrylic mould was in level with the top of the steel mould. A steel collar was fastened to the top of the steel mould. The mass of gravel corresponding to the inside volume of the acrylic mould was weighed, and placed in the mould in five loads of equal heights, each load compacted by 56 blows with a rammer. The rammer consisted of a steel disc with a diameter of 124 mm and a mass of 2.9 kg, fastened to a handle. Vibration was only used when compacting specimens B1 and B2 since these specimens were the most difficult to compact. After all the gravel material was in place, the collar was removed and the height of the material reaching over the top of the mould was measured. From this height, the actual volume of the material could be found, and thereby it was possible to determine the compaction degree, δ [%], using the formula:

$$\delta = \frac{\rho_{\mathrm{d}}}{\rho_{\mathrm{d,max}}} \times 100\% \tag{1}$$

where ρ_{d} [kg/m^3] is the dry density of the compacted gravel material, and $\rho_{\mathrm{d,max}}$ [kg/m^3] is the maximum dry density determined from, for example, the vibrating table method (Sub-base of Sand and Gravel – General Work Specification (GWS) 2003).

The porosity, P [%], of the material was determined using the formula:

$$P = \left(1 - \frac{\rho_d}{\rho_s}\right) \times 100\% \tag{2}$$

where ρ_d [kg/m^3] is the dry density of the compacted gravel material, $\rho_s = 2630$ kg/m^3 is the soil particle density and $\rho_s = 2300$ kg/m^3 is the fly ash particle density. For gravel mixed with fly ash, the particle density is weighted according to the percentage of fly ash.

The upper part of the specimen was removed so that its top surface aligned with the top of the mould, and the acrylic mould and spacer disc were removed from the steel mould. To copy the most vulnerable field conditions, the specimen was saturated with water prior to the freeze–thaw test. The approach used to saturate the specimen deviated from the approach described

in the ASTM D5918-13 standard (ASTM Standard D5918-13 2013), since it was performed by water absorption where the bottom of the specimen was placed in water reaching 50 mm up the sides of the specimen. The spacer disc was removed, and then a fine mesh of 73 μm and a coarser mesh of 10 mm were placed below the specimen. The coarse mesh was fastened to the sides of the specimen using a hose clamp. The fine mesh prevented any material from being washed out. The specimen was allowed to absorb water for three days, since preliminary tests had shown that the mass of the specimens with all types of gravel remained constant after three days.

3.4.2. Freeze-thaw test equipment

The equipment for the actual freeze–thaw test consisted of five main components: a base plate connected to a water supply, two temperature plate systems, a surcharge weight, temperature sensors and a refrigerator.

The base plate was placed directly beneath the water-saturated specimen that was still contained in the acrylic mould. Its purpose was to continuously supply the specimen with water through a water inlet and outlet placed on opposite sides of the base plate. The water inlet was connected to an external Mariotte water supply through a plastic tube with a diameter of 10 mm. The water supply, which consisted of a 508-mm long plastic tube with a diameter of 57 mm, worked on the principle of using a so-called 'bubble tube', a 533-mm long glass tube with an internal diameter of 3 mm. This bubble tube was passed through a vacuum-tight rubber bung inserted into the top of the plastic tube. By moving the bubble tube vertically, it was possible to adjust the water head of the entire set-up. When water flowed out of the specimen, the water head stayed at the level of the bottom of the bubble tube, as long as the end of the tube that was connected to the water outlet of the base plate remained open and was placed at the same level as the bottom of the bubble tube. During the test, the water head was set 10 mm above the bottom of the specimen. The base plate had a diameter of 150 mm and a height of 38 mm, and the top of the base plate consisted of a 10- mm high circular rim with a diameter of 138 mm, designed to hold a plastic mesh that ensured water would always be present directly below the specimen. A much finer mesh of 73 μm was placed on top of the relatively coarse 10-mm high plastic mesh. Figure 3 shows how the specimen was placed on top of the base plate in the test set-up.

Temperature plates of aluminium were placed on top of the specimen and below the base plate, as seen in Figure 3. The top and bottom temperature plates were connected to separate temperature control circulating baths controlling their temperatures. The top plate contained a 1:1 glycol–water solution, and the bottom plate contained pure water. A 10-mm plastic tube was connected from the temperature bath to the inlet of the temperature plate through a flow meter, and a 10-mm plastic tube was connected from the outlet of the temperature plate to the temperature bath. The temperature plates had a diameter of 150 mm and an internal height of 24 mm, and transverse walls ensured a water flow covering the entire surface. Before installing the top temperature plate, a small amount of silver iodide was placed on top of the specimen to initiate ice nucleation. During frost heaving, the top temperature plate would move upwards and leave a gap to the butyl membrane, exposing

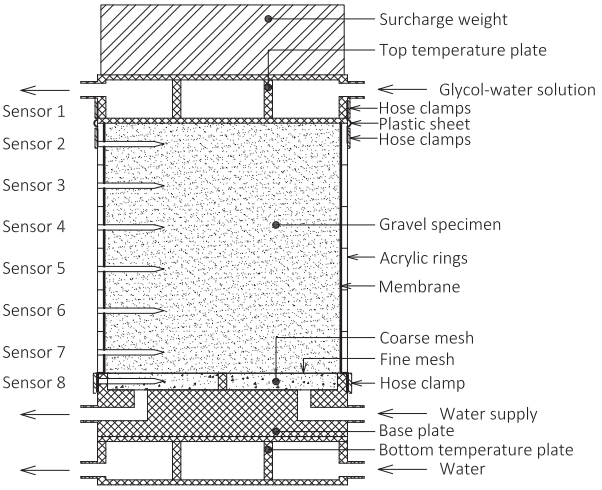

Figure 3. Principle sketch of the specimen set-up for the freeze–thaw tests. Sensors 2 to 8 are placed in dip pipes, and sensor 1 is laid between the top temperature plate and the top of the specimen. Insulation is not shown.

Table 1. Temperature variation of the two plates with time during the freeze–thaw test.

Day	t [h]	$T_{\text{top plate}}$ [°C]	$T_{\text{bot. plate}}$ [°C]	Comment
1	24	2.55	2.55	Conditioning
2	8	−3.45	2.55	Freezing period #1
	16	−12.45	0.50	
3	16	11.55	2.55	Thawing period #1
	8	2.55	2.55	Stabilisation
4	8	−3.45	2.55	Freezing period #2
	16	−12.45	0.50	
5	16	11.55	2.55	Thawing period #2
	8	2.55	3.00	Stabilisation

$T_{\text{top plate}}$ = temperature of top plate [°C], $T_{\text{bot. plate}}$ = temperature of bottom plate [°C], t = time [h].

the specimen to the surroundings. To avoid any moisture loss, a plastic sheet cut from a plastic bag was fastened to the top temperature plate and to the acrylic mould using two hose clamps, allowing enough room for the specimen to expand vertically, as seen in Figure 3. The temperature settings for the two temperature baths are given in Table 1. As this shows, the temperature of the bottom plate remained positive, and only the temperature of the top plate became negative.

The freezing point depression was determined by compacting 20-mm gravel to maximum density in a 30-mm diameter test tube, and placing a pinch of silver iodide on top of it. A temperature sensor was placed in the middle of the compacted specimen, and the test tube was conditioned in a 0 °C glycol–water bath. Subsequently, it was placed in a −3°C liquid ethylene glycol bath, and its temperature variation was logged. The freezing point depression was determined as the temperature after nucleation, and for all types of gravel it was approximately −0.45°C. The temperatures in Table 1 are based on the temperatures given in the ASTM D5918-13 standard (ASTM Standard D5918-13 2013), corrected with respect to the freezing point depression. Moreover, the minimum temperature of the bottom temperature plate was changed from the recommended 0 °C in the ASTM D5918-13 standard (ASTM Standard D5918-13 2013) to 0.5 °C, because the thermostat's temperature band

around the set point otherwise caused the temperature of the bottom plate to drop below 0 °C. This would have caused the water below the specimen to freeze and cause an erroneous heave of the specimen. This was assumed not to influence the results because of two main reasons: (1) it was measured that the temperature of the bottom plate in fact varied between 0.04 and 0.5 °C during the 16-hour freezing period. These temperature measurements were calibrated against a certified mercury thermometer. Thus, the deviation from the recommended 0 °C was considered to be minor. (2) As it will be clear from the following sections, the frost susceptibility classification relates to the 8-hour freezing period in which the temperature of the bottom plate was 2.55 °C in accordance with the ASTM D5918-13 standard.

As seen in Table 1, the specimens were exposed to two identical frost cycles after an initial 24-hour conditioning period. Each frost cycle consisted of a 24-hour freezing period where the temperature of the top plate was decreased in two steps, followed by a 16-hour thawing period and finally an 8-hour stabilisation period bringing the temperature back to the original.

The surcharge steel weight of mass 5.5 kg, with an outside diameter of 142 mm and a height of 42 mm, was placed above the top temperature plate. A deformation gauge was installed on top of the surcharge weight to measure vertical displacement with an accuracy of ±0.004 mm.

A temperature sensor was inserted in the specimen through a hole drilled through each acrylic ring. Another temperature sensor was placed at the very top of the specimen, between the upper acrylic ring and the top temperature plate and a third temperature sensor was placed below the specimen in a dip pipe inserted in the base plate. The temperature sensors inserted through the acrylic rings were also installed in dip pipes to ease the insertion, and to protect the heat-shrinkage tubing of the copper–constantan wires. Each dip pipe was 40-mm long, and had a diameter of 3.2 mm. Other temperature sensors were placed in the refrigerator and in the two temperature baths. The temperature sensors had an accuracy of ±0.1°C.

The refrigerator was set to a constant temperature of 2 °C, but the temperature was varying between −4°C and 8°C. Holes were drilled in the sides of the refrigerator to accommodate the tubes connecting the temperature baths and the temperature plates, and for the tubes supplying and draining the system of water. After connecting the entire set-up around the specimen, it was covered in 25-mm thick insulation to prevent any condensation. All plastic tubes inside and outside the refrigerator were covered as well as the specimen itself. The set-up was placed on an insulation plate of extruded thermoplastic foam. All types of insulation had a thermal conductivity of 0.04 W/(m·K). Figure 4 shows the set-up installed in the refrigerator.

A principle sketch of the entire freeze–thaw test set-up is shown in Figure 5.

In total, two different specimens were tested for each gravel material, except for gravel B2 where only one specimen was tested.

3.5. Permeability test set-up

The permeability of gravels A1, B1 and B2 was determined from a constant-head set-up, and the permeability of gravel A2 was determined from a falling-head set-up. Both set-ups are based on Darcy's law stating proportionality between flow velocity and hydraulic gradient. The constant-head set-up that is most suitable for soils with a medium to high permeability was based on the ASTM D2434-68 standard (ASTM Standard D2434-68 2006), where a constant water head, h [m], is established on top of a specimen with length L [m] and cross-sectional area A [m^2]. The water volume, Q [m^3], penetrating the specimen during time t [s] is used to calculate the permeability coefficient at 20 °C, k_{20} [m/s], using the formula:

$$k_{20} = \frac{Q\,L}{A\,h\,t}\,\frac{\eta_T}{\eta_{20}} \tag{3}$$

where η_T [Pa·s] is the water viscosity at the temperature, T [°C], at which the test is conducted and η_{20} [Pa·s] is the water viscosity at 20 °C.

The falling-head set-up is most suitable for soils with a low permeability. The time difference, t [s], between the initial and final water head difference, h_1-h_2 [m], is used to determine the permeability coefficient at 20 °C, k_{20} [m/s], using the formula:

$$k_{20} = 2.303\,\frac{a\,L}{A\,t}\log_{10}\frac{h_1}{h_2}\,\frac{\eta_T}{\eta_{20}} \tag{4}$$

where a [m^2] is the cross-sectional area of the standpipe, A [m^2] is the cross-sectional area of the specimen, L [m] is the length of the specimen, η_T [Pa·s] is the water viscosity at the temperature, T [°C], at which the test is conducted and η_{20} [Pa·s] is the water viscosity at 20 °C.

The preparation of the specimen used for the constant and falling-head tests was the same, as shown in Figure 6.

Firstly, the specimen was compacted in a 150-mm high acrylic cylinder with a diameter of 142 mm, in the same way as the specimens used in the freeze–thaw tests, except that the height of the specimen was reduced to 125 mm. The inside of the cylinder had been painted with epoxy resin, and sprinkled with 0–2 mm sand to roughen the surface and prevent water from easily escaping along the specimen sides. A 3-mm rubber membrane with an inner diameter of 150 mm was pulled over an aluminium bottom plate, and closed tightly to it using a hose clamp. A 20-mm hole had been drilled at the centre of the bottom plate,

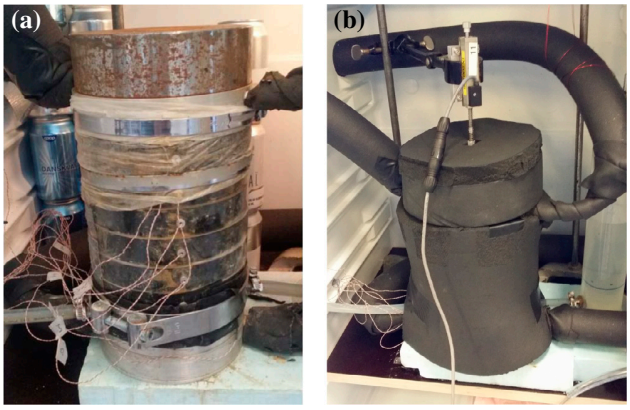

Figure 4. Freeze-thaw test set-up in the refrigerator. (a) Test set-up without insulation. (b) Test set-up covered in insulation to avoid condensation.

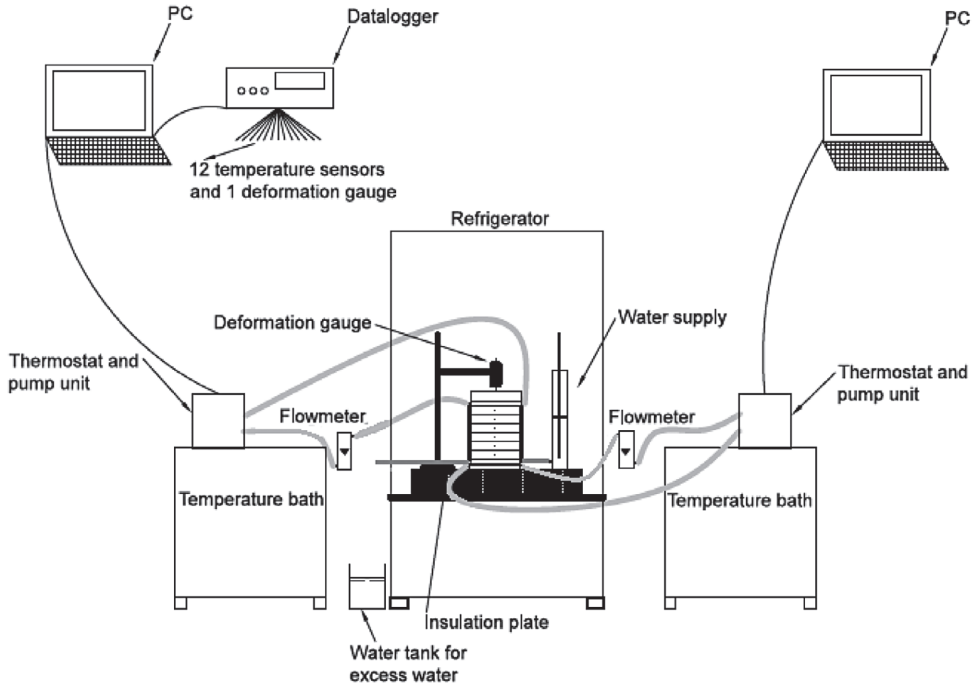

Figure 5. Principle sketch of entire freeze–thaw test set-up. Insulation is not shown.

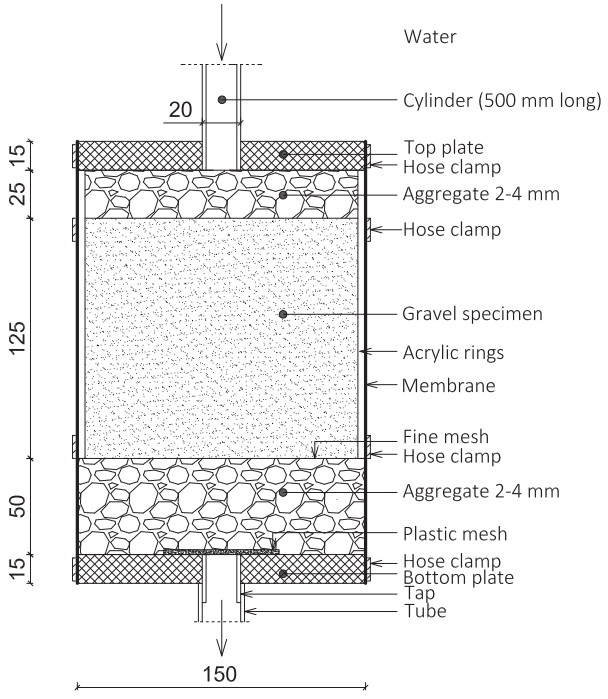

Figure 6. Constant- and falling-head permeability set-up. Dimensions are in mm.

and this connected a plastic tube to a tap for water outlet. A plastic mesh was placed above the hole to prevent any material from being washed out. A 50-mm layer of 2–4 mm aggregate was laid on top of the aluminium base inside the rubber membrane, and compacted with a rammer to provide a firm and even surface. The gravel specimen contained in the acrylic cylinder was placed on top of the aggregate inside the rubber membrane, and hose clamps were used to tighten the rubber membrane and the acrylic cylinder together. Another 25 mm layer of 2–4 mm aggregate was laid on top of the gravel specimen inside the acrylic cylinder, and compacted to provide a firm and even surface. The permeability of the 2–4 mm aggregate layer was 10.2 cm/s as determined from a constant-head set-up (Figure 6) using two water heads of 27 and 48 cm, respectively, and a specimen height of 10 cm. This permeability was considerably greater than that of the test materials and therefore did not influence the measurements. The set-up was closed by placing an aluminium top plate on top of the aggregate, pulling the rubber membrane around it, and closing it tightly with a hose clamp. A 20-mm hole had been drilled in the top plate, and a 500-mm high plastic cylinder, with an inner diameter of 16 mm and a measurement scale along its height, was fastened to this hole to control and measure the water input.

In the constant-head set-up, two water heads of 20 cm and 45 cm, respectively, were each tested for gravels A1, B1 and B2. In the falling-head set-up, the water head was varied between 60 cm down to 20 cm in steps of 5 cm for gravel A2. Three specimens were tested for each type of gravel.

4. Results

4.1. Particle size distribution and fines content

Figure 7 shows the particle size distributions for gravel particles >63 μm and <31.5 mm in diameter. Casagrande's and Schaible's frost criteria, and Danish definitions of sub-base gravel qualities I and II are also shown. Based solely on the gradation curves of gravels A1, B1 and B2, they are seen to be classified as quality I materials.

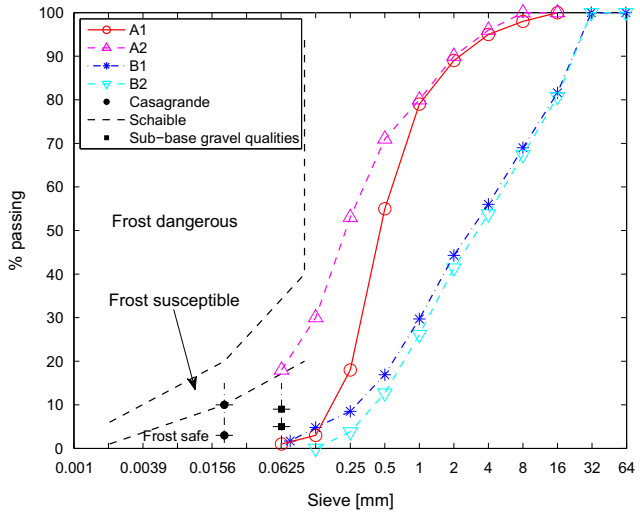

Figure 7. Gradation curves for gravels A1, A2, B1 and B2, together with Casagrande's and Schaible's frost criteria classifying whether a gravel material is frost safe, frost susceptible or frost dangerous. The gradation curves for gravels B1 and B2 are determined by removing particles >31.5 mm. The requirements for Danish quality I and quality II sub-base gravel materials are also shown. Reference is made to Figure 1 for further explanation.

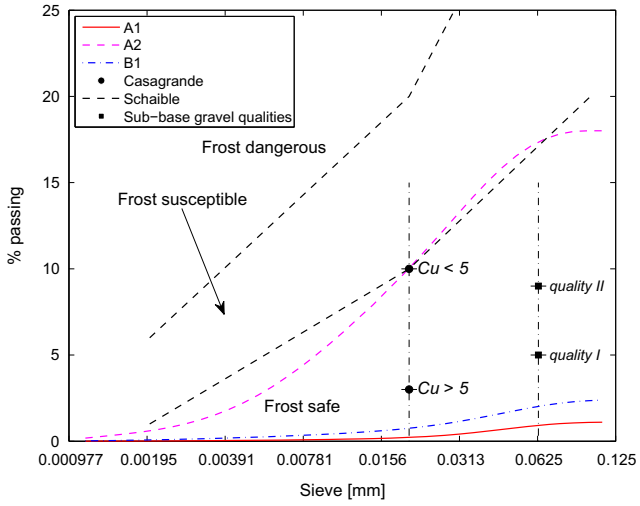

Figure 8. Fines content for gravels A1, A2 and B1 determined from laser diffraction. Gravel B2 does not have any fines content <0.125 mm in diameter. Casagrande's and Schaible's limit curves classifying whether a gravel material is frost safe, frost susceptible or frost dangerous are also shown, together with the requirements for Danish quality I and quality II sub-base gravel materials.

The coefficient of uniformity (C_u) is defined as the ratio between the particle diameters at 60% passing and at 10% passing. The C_us for gravels A1, A2, B1 and B2 were 6.0, 17.5, 16.7 and 12.5, respectively. From the sieve analysis, the fines contents were found to be 1.1, 18.2 and 2.4% for gravels A1, A2 and B1, respectively. No fines content was present for gravel B2. The results from the laser diffractometer analysis are shown in Figure 8, where it is assumed that the total percentage of fines analysed for each gravel material corresponds to the measured fines content.

Figure 8 shows that gravels A1, B1 and B2 are expected to be frost safe based on both Casagrande's and Schaible's frost criteria. This is as expected because both materials comprise sub-base gravel of quality I (Sub-base of Sand and Gravel – Design Guide 2003), which requires the material to be frost safe. However, due to its high fines content, gravel A2 is frost susceptible according to both frost criteria.

Table 2. Specimen porosity, maximum density, optimal water content, w_{opt}, water content after preparation, w_{act} and water content at termination of freeze–thaw test, w_{term}. The values describe *mean* values for the whole specimen. (*) The optimal water content for gravel B2 was assumed to be the same as for gravel B1.

Specimen	Porosity	Max. density	Water content [%]		
no.	[%]	[kg/m^3]	w_{opt}	w_{act}	w_{term}
A1-1	33.9	1911	12.8	11.9	15.4
A1-2	33.3	1911	12.8	11.9	13.0
A2-1	48.0	1417	11.1	10.1	10.0
A2-2	47.8	1417	11.1	10.1	9.9
B1-1	24.0	2171	7.9	7.1	7.2
B1-2	22.2	2171	7.9	7.1	7.1
B2-1	26.5	2171(*)	7.9(*)	7.4	7.3

4.2. Optimal water content and maximum dry density

Table 2 shows the maximum density and the optimal water content for all gravels analysed. When preparing the specimens for the freeze–thaw tests, the compaction degree was calculated using Equation (1) to be 99% for specimens A1, 100% for specimens A2, 97% for specimens B1, and 96% for specimen B2. In practice, it is very difficult to control that all specimens obtain the same degree of compaction; thus, it was intended to prepare all specimens with the highest possible degree of compaction. The results show that the variation in degrees of compaction is narrow and furthermore complies with the requirements given in Danish road regulations (Sub-base of Sand and Gravel – General Work Specification (GWS), 2003); hence, the variation represents what is expected and allowed for sub-base gravel in the field, and the variation's influence on the results is therefore not considered any further since it is expected to be minimal.

4.3. Freeze–thaw results

In the following, the results from the freeze–thaw tests will be exemplified by means of specimen B1-1. However, the analysis presented has been carried out for all types of gravel, and the corresponding results are shown for all specimens.

4.3.1. Porosity of freeze–thaw specimens

The mean porosity of the specimens is shown in Table 2. Gravel A2, which has the highest fine contents, has the highest porosity. Even though gravels A1 and B1 have approximately the same fines content, their porosity is seen to differ. Gravel B1 has the lowest porosity.

4.3.2. Moisture content of freeze–thaw specimens

Table 2 summarises the mean moisture content of the specimens during preparation, and immediately after termination of the freeze–thaw tests where each specimen was divided into six parts by removing one acrylic ring at a time, together with the gravel contained within it. The moisture content was measured for

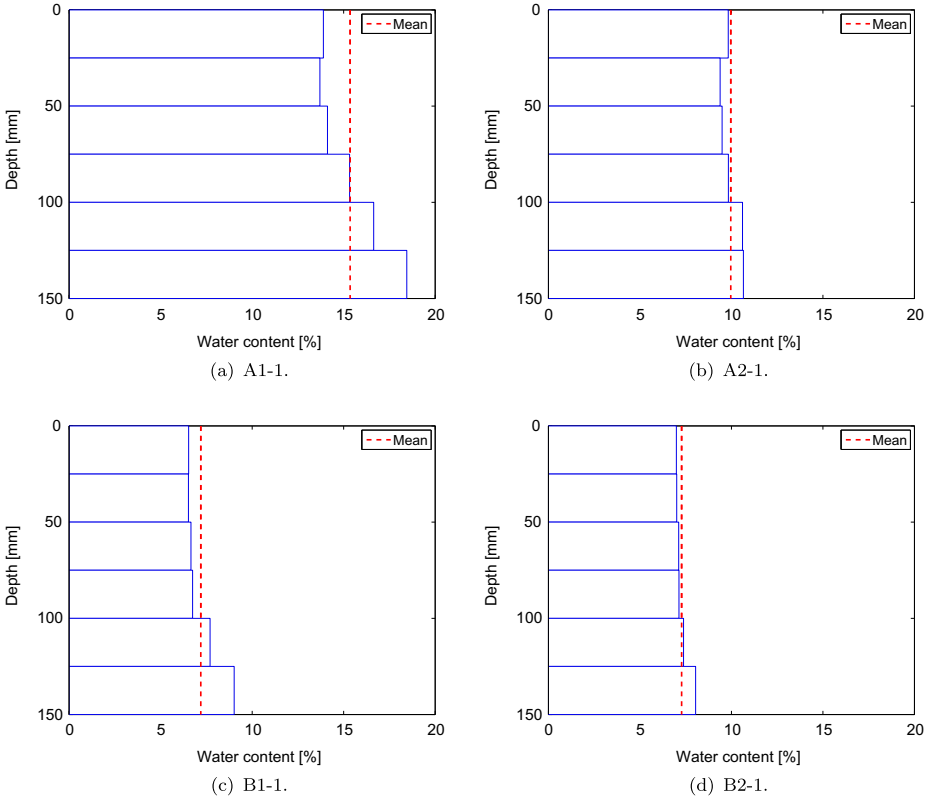

(a) A1-1. (b) A2-1. (c) B1-1. (d) B2-1.

Figure 9. Moisture profiles of specimens after termination of the frost tests. A depth of 0 cm corresponds to the top of the specimen where freezing takes place.

each of the six portions, and thereby a moisture profile was obtained as shown in Figure 9.

For specimens A1 and B1, the moisture content no longer remained homogeneous after termination of the frost tests, but increased from top to bottom, as expected since water was supplied from below. The mean moisture content of specimens A1 increased compared with the water content at the time of preparation, possibly due to water being retained in the gravel after being transported to the freezing zone. For specimens A2, B1 and B2, the mean moisture content remained at the same level as during preparation; however, as seen in Figure 9(c), the moisture content at the top of B1-1 was 6.5% and the moisture content at the bottom was 9.0%. Thus, compared with the optimal water content, the top of specimen B1-1 was no longer water-saturated, whereas the bottom was over-saturated. For specimens A2 and B2, the moisture content was homogeneous after termination of the frost tests, and the variation throughout the specimens was small.

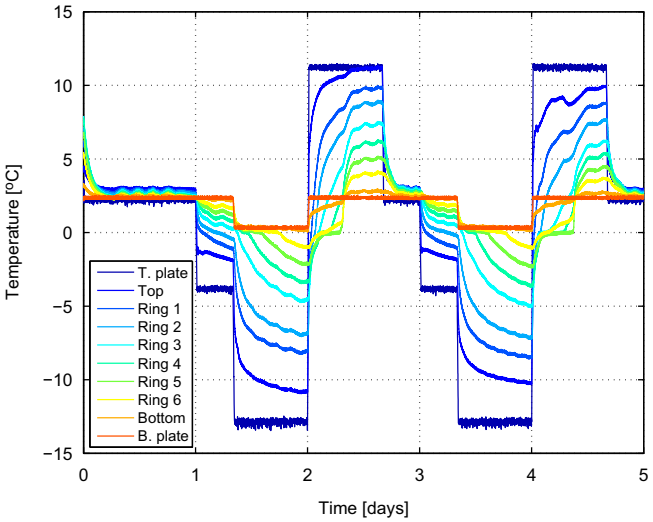

Figure 10. Temperature variations in specimen B1-1 during the freeze–thaw test. The temperature variations of the top (T) plate and the bottom (B) plate are also shown.

4.3.3. *Temperature profiles and frost penetration in freeze–thaw specimens*

The temperature variation in the specimen was measured continuously at eight points during the freeze–thaw tests, and also in the temperature baths. Figure 10 shows this variation for specimen B1-1 during the five-day long test.

The temperature variations of the top and bottom temperature plates are seen to change stepwise, in agreement with the temperature limits given in Table 1. Figure 10 also shows that all temperatures within specimen B1-1 become negative during the freezing period, which means that the entire specimen freezes. However, the temperature of the bottom plate never reaches negative temperatures during the entire test, which means that the water supply does not freeze.

Figure 11 shows the frost penetration of specimen B1-1 with time, thereby illustrating the progress of the freezing front.

Figure 11 shows that it takes a little longer than half a day for the entire specimen to freeze. After the 8-hour freezing

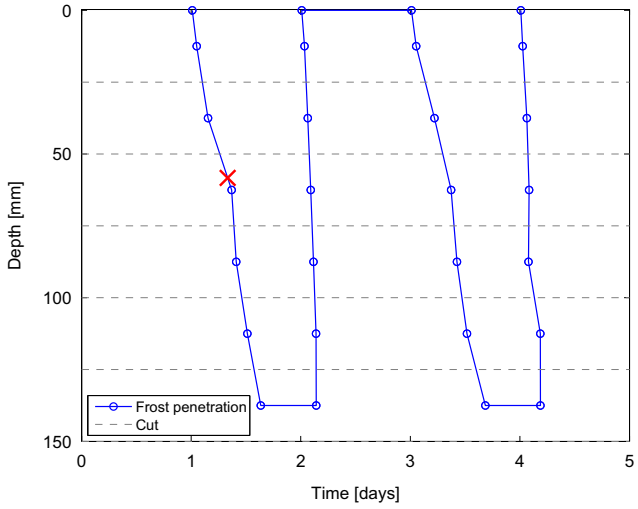

Figure 11. Frost penetration in specimen B1-1 during freezing and thawing. A depth of 0 cm corresponds to the top of the specimen where freezing takes place. The '×' marks the depth of the frost penetration (58 mm) after the first 8-hour freezing period.

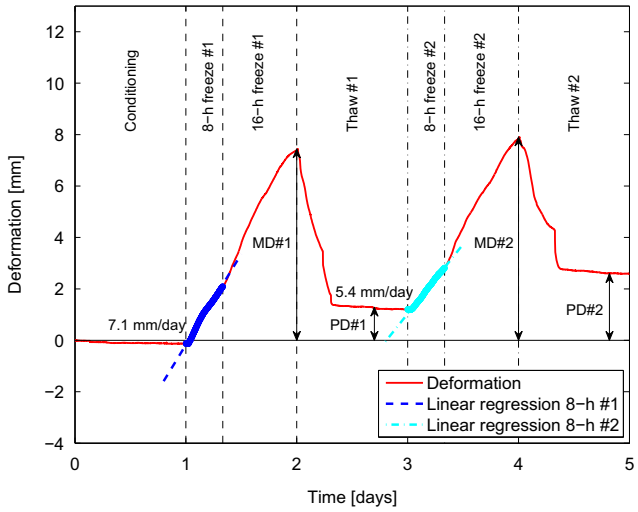

Figure 12. Vertical deformation of specimen B1-1 with time. The heave rate per day has been calculated as a linear regression of the data points during the 8-hour freezing period for frost cycles #1 and #2. The location of maximum deformations (MD) and permanent deformations (PD) are also shown.

period – on which the frost heave rate is determined and the frost susceptibility is assessed – the freezing front has reached less than halfway down the specimen. The entire specimen stays frozen for half a day, after which it is thawed. It only takes two hours for the specimen to thaw because thawing is induced from top and bottom. The specimen stays thawed for 24 hours before the second frost cycle is initiated, and the same trends are observed for the second frost cycle as for the first.

4.3.4. Heave rate, frost susceptibility and deformation of freeze–thaw specimens

Figure 12 shows the vertical deformation of specimen B1-1 with time during the five-day freeze–thaw test. Two freezing periods can be clearly discerned by the two deformation peaks.

Figure 12 shows how the specimen starts to heave during the first frost cycle until thawing is initiated, after which some of the deformation is reversed. However, a permanent deformation of approximately 1 mm occurs during the first thawing period. A similar pattern emerges for the second freeze–thaw period, with a permanent deformation of approximately 2.5 mm. According to the ASTM D5918-13 standard (ASTM Standard D5918-13, 2013), the frost susceptibility is assessed by determining the 8-hour heave rates.

During the first and second freezing period, the deformation of the specimen is a combination of (1) expansion of the pore water during phase change from liquid to solid state, and (2) formation of ice lenses due to water migration to the frozen fringe. For specimen B1-1, Figure 11 shows that after the first 8-hour freezing period, the freezing front has reached 58 mm down through the specimen measured from the top of the specimen. According to Table 2, the porosity of specimen B1-1 is 24%, which means that the deformation caused by pore water freezing and expanding 9% is approximately 1.3 mm, if assuming that the specimen is water-saturated. This deformation is less than the total deformation of 2.1 mm measured after the first 8-hour freezing period (see Figure 12); thus, frost heave does occur during the first 8-hour freezing period. This also means that the 8-hour heave rate is based on a deformation caused by a combination of frost heave and pore water that freezes and expands, and according to the ASTM D5918-13 standard the frost susceptibility classification is based on this 8-hour heave rate even though it is not solely related to the 'true' frost heave rate. The same is true for specimen B1-2, and for specimens A2. For specimens A1 and B2, the deformation after the 8-hour freezing period is primarily caused by the expansion of the pore water which, as seen from the following paragraphs, also influences the frost susceptibility classification that is less critical for specimens A1 and B2.

The 8-hour heave rates are determined from a linear regression of all data points in the 8-hour heave periods. In Figure 12, this gives heave rates of 7.1 mm/day for the first freezing period, and 5.4 mm/day for the second freezing period. In climates where many annual frost cycles take place, such as Denmark's, the second heave rate should be used to evaluate the frost susceptibility. This classifies the frost susceptibility of the material as 'medium' on a frost susceptibility scale with classifications: 'negligible', 'very low', 'low', 'medium', 'high' and 'very high'. Table 3 summarises the heave rates and the frost susceptibility classifications.

Table 3 shows that the frost susceptibility is 'negligible' for sub-base gravel A1, but 'medium' for sub-base gravel B1. Gravel A2, with increased fines content, has 'low' to 'medium' frost susceptibility and gravel B2 with decreased fines content has 'low' frost susceptibility.

The maximum and permanent deformations obtained after the first and second frost cycles are shown in Table 4. The permanent deformations are measured during the thaw periods when the specimens are known to be completely thawed.

Table 4 shows that the maximum deformation of specimen B1 is about double the amount of that of specimens A2, and more than five times greater than that of specimens A1. For specimens A1, no permanent deformation is observed. For specimens A2, a small permanent deformation is observed after the

Table 3. 8-hour heave rate during frost cycles #1 and #2, and frost susceptibility classifications for gravels A1, A2, B1 and B2.

Specimen no.	Heave rate #1 [mm/day]	Heave rate #2 [mm/day]	Frost susceptibility classification
A1-1	1.4	0.3	Negligible
A1-2	0.8	0.4	Negligible
A2-1	4.7	3.6	Low
A2-2	7.0	5.3	Medium
B1-1	7.1	5.4	Medium
B1-2	6.9	4.1	Medium
B2-1	5.4	3.5	Low

Table 4. Maximum vertical deformation (MD) during freezing and thawing in frost cycles #1 and #2, and permanent vertical deformation (PD) after frost cycles #1 and #2. All specimens were 150-mm high. (*) The maximum and permanent deformation during frost cycle #1 are not found due to PC breakdown.

	Maximum def. [mm]		Permanent def. [mm]	
Specimen no.	MD#1	MD#2	PD#1	PD#2
A1-1	0.7	0.4	0.1	−0.1
A1-2	0.8	1.0	−0.4	−0.6
A2-1	2.8	2.5	0.0	0.3
A2-2	4.2	2.6	−0.1	0.7
B1-1	6.3	5.4	1.1	2.5
B1-2	5.7	5.2	0.7	1.6
B2-1	(*)	4.0	(*)	0.8

Table 5. Permeability coefficient, k_{20}, of gravels A1, A2, B1 and B2.

k_{20} [cm/s]	A1	A2	B1	B2
Mean	7.3×10^{-4}	0.65×10^{-4}	35×10^{-4}	37×10^{-4}
Std. dev.	1.4×10^{-4}	0.0035×10^{-4}	12×10^{-4}	6.1×10^{-4}

second frost cycle. For specimens B1, a permanent deformation of up to 2.5 mm is observed. Specimen B2 experiences the second largest maximum and permanent deformations of all four types of gravel.

4.4. Permeability results

Table 5 shows the mean permeability coefficients for gravels A1, A2, B1 and B2, and the standard deviations.

Increasing the fines content of gravel A1 from 1.1% to 20% reduces the permeability coefficient by a factor of 10; hence gravel A2 has the lowest permeability coefficient. On the other hand, gravel B2 with the lowest fines content has the highest permeability coefficient.

5. Discussion

5.1. Discussion of frost susceptibility of sub-base gravels

The two gravel materials sensitive to frost heave in the present study had fines contents of 18.2 and 2.4%, respectively; counter-intuitively, the gravel material with 2.4% fines was found to be more frost susceptible than the gravel material with 18.2% fines. The gravel material with 2.4% fines was classified as Danish sub-base gravel of quality I, and such a material experiencing frost heaving was surprising and unexpected.

The results from the present study suggest that the criterion used to classify the frost susceptibility of Danish sub-base gravel materials solely from their fines content is insufficient, and that the permeability coefficient should also be considered. Moreover, the results suggest that the deformation during the freeze–thaw period is directly related to the classification of the frost susceptibility in the ASTM D5918-13 standard (ASTM Standard D5918-13 2013).

5.1.1. Influence of the fines content

According to the frost heave tests, the frost susceptibility of gravel A1 was classified as 'negligible' indicating that no problems with frost heaving were expected. This was in line with the fines content analysis, with Casagrande's and Schaible's frost criteria, and with the classification of the material as a sub-base gravel of quality I. According to the frost heave tests, the frost susceptibility of gravel A2 was classified as 'low' to 'medium', indicating that a certain frost heaving was expected to take place. The fines content of gravel A2 was considerably higher than that of gravels A1, B1 and B2, and according to Casagrande's and Schaible's frost criteria it was expected that the material would be frost susceptible. According to the frost heave tests, the frost susceptibility of gravel B1 was classified as 'medium', indicating that frost heaving was expected to take place. From the analysis of fines content, and Casagrande's and Schaible's frost criteria, it was not expected that any specific frost heaving would occur. When removing all fines <0.125 mm in diameter from gravel B1, the frost susceptibility decreased and the frost susceptibility of gravel B2 was classified as 'low'. Hence, the frost susceptibility of gravel A2 and that of gravel B1 were minimised by decreasing the fines content of the materials.

5.1.2. Influence of the permeability coefficient

The permeability coefficients shown in Table 5 represent the minimum permeability coefficients for the different gravel materials, since they are determined for specimens having the optimal water content (Lambe and Whitman, 1969). The permeability coefficients range according to the order of the particle size distributions, with gravel A2 having the smallest permeability coefficient and gravel B2 having the largest.

The permeability coefficient for gravel B1 is almost five times as big as the permeability coefficient for gravel A1, and gravel B1 has a C_u three times greater than gravel A1. It is, therefore, expected that gravel B1 should pack better than gravel A1, which is also clear from Table 2 where the porosity of gravel B1 is seen to be lower than that of gravel A1. On the other hand, the pores of gravel B1 are larger than the pores of gravel A1 because gravel B1 is coarser than gravel A1, and the tortuosity of the pore system of gravel B1 is therefore less than that of gravel A1, which means that water is more easily transported through the material for B1. As a result, the permeability coefficient of gravel B1 is greater than of gravel A1. The difference in gradation suggests that even though the fines content of the two materials is approximately the same, it is easier for water to migrate towards the freezing zone in specimens B1 than it is in specimens A1; hence, the formation of ice lenses is more

favourable for specimens B1 than for specimens A1. The same analogy can be used when comparing specimens A1 and B2.

The permeability coefficient for gravel A2 is almost 10 times less than that of gravel A1 despite the porosity of gravel A2 being the largest for the four gravel materials. However, because the fines content of gravel A2 is high, the pore system of specimens A2 is fine and the tortuosity of the pore system is thereby large, resulting in a small permeability coefficient. This small permeability coefficient is also believed to explain why the moisture profiles obtained from specimens A2 remained homogeneous after termination of frost tests.

5.1.3. Influence of deformation during the freeze–thaw cycle

A permanent deformation takes place for specimens A2, B1 and B2 (see Table 4), which are all classified as having 'low' or 'medium' frost susceptibility. The more frost susceptible the specimens are, the more vulnerable they are to permanent deformations. Specimens A1 do not experience any permanent deformation, and are classified as having 'negligible' frost susceptibility.

Gravel B1 was found to experience the largest maximum vertical deformation. The vertical deformations of specimens B1 did not reach a constant level when initiating the thaw period for any of the two frost cycles, as can be seen in Figure 12. However, specimens A1, A2 and B2 all reached a constant vertical deformation before initiating the thaw periods. When comparing specimens A1 and A2 and specimens B1 and B2, Table 4 shows that not only does the heave rate increase, but the permanent and maximum deformations also increase when the fines content of the material is increased.

Even though the deformation itself is not used as a criterion for assessing whether or not a soil material is frost susceptible according to the ASTM D5918-13 standard (ASTM Standard D5918-13 2013), the results suggest that the maximum and permanent deformations are directly related to the frost susceptibility classification.

5.2. Validity of freeze–thaw test results for Pearl-Chain Bridges

The freeze–thaw tests carried out in the present study attempt to experimentally identify potential freeze–thaw problems with sub-base gravel used as fill in Pearl-Chain Bridges. The ASTM D5918-13 standard (ASTM Standard D5918-13 2013) used in the planning of the tests is developed for the classification of frost susceptibility of soils used in pavements. It has already been justified why this standard was used (Section 1) so this section only concerns the simplicity of the applied testing procedure. The test in the present study was one-dimensional since freezing was only applied from one end. However, when used as fill in Pearl-Chain Bridges, the sub-base gravel is exposed to a three-dimensional freezing: from underneath the bridge, from above the bridge and from the sides; hence, there will be more than a single freezing front. This condition cannot be adopted in the present testing procedure because it would cause the water feed to freeze, and change the imitation of ice lens growth caused by continuous water addition from underneath a freezing line in the soil. The continuous water feed adopted in the present study can be considered a worst-case scenario. The use of the testing procedure described in the ASTM D5918-13 standard (ASTM Standard D5918-13 2013) is chosen because it provides a reasonable system that makes it possible to classify and compare the frost susceptibility of different gravel materials. Also, when modelling the frost heave of gravel fill in Pearl-Chain Bridges, the analysis would most likely be one-dimensional and not three-dimensional.

6. Conclusions

In the present study, the frost susceptibility of two Danish sub-base gravel materials with fewer than 3% particles <63 μm in diameter has been experimentally tested in a freeze–thaw test set-up based on the ASTM D5918-13 standard (ASTM Standard D5918-13 2013). Two modified sub-base gravel materials have also been tested; one 0–8 mm sub-base gravel material having the fines content increased to 20% by use of fly ash, and one 0–63 mm sub-base gravel material with all particles <0.125 mm in diameter having been removed. Particles >31.5 mm were removed from all materials to fit the test equipment. The heave rate was used to classify the frost susceptibility of the four gravel materials. Moreover, their permeability was determined. The main conclusions from the study can be summarised as follows:

(1) A water-saturated sub-base gravel material with a gradation of 0–8 mm and a fines content of 1.1% was found to have 'negligible' frost susceptibility. A water-saturated modified sub-base gravel material with a gradation of 0–8 mm and a fines content of 20% – increased from the original 1.1% by the addition of fly ash – was found to have 'low' to 'medium' frost susceptibility. A water-saturated sub-base gravel material with a gradation of 0–31.5 mm and a fines content of 2.4% was found to have 'medium' frost susceptibility. A water-saturated modified sub-base gravel material with a gradation of 0.125–31.5 mm was found to have 'low' frost susceptibility. According to Casagrande's and Schaible's frost criteria, only the gravel material with increased fines content was expected to experience frost heaving. It was not expected that any frost heaving would occur for sub-base gravel.

(2) The permeability coefficient of 0–31.5 mm sub-base gravel was five times greater than the permeability coefficient of 0–8 mm sub-base gravel due to the pore system being coarser, and the tortuosity of the pore system being less. Hence, it was easier for water to reach the freezing zone in 0–31.5 mm sub-base gravel.

(3) The permanent and maximum deformations, that occurred during the freeze–thaw cycle, were directly related to the frost susceptibility classification.

(4) The results from the present study suggest that the criterion used to classify the frost susceptibility of Danish sub-base gravel materials solely from their fines content is insufficient, and that the permeability coefficient should also be considered. This is because the fines content of both sub-base gravel materials tested in the present study was low and the main difference was their permeability; thus, the permeability is believed to cause the difference in their frost susceptibility classification even though

they were both expected to be frost safe based on the requirements in Danish road regulations.

(5) To ensure that problems with frost heaving of sub-base gravel as fill in Pearl-Chain Bridges are entirely prevented, it is necessary to perform frost heave tests on the sub-base gravel used in their fill. In the freeze–thaw test set-up used in this study, the specimens were water-saturated and constantly fed with water from below; however, this represents a conservative scenario for Pearl-Chain Bridges because water is expected to drain off the superstructure. Thus, if the sub-base gravel is not frost susceptible according to the applied test procedure it is not expected that any problems arise with frost heaving of the fill material in Pearl-Chain Bridges; however, if the sub-base gravel is frost susceptible it is particularly important to ensure that the drainage of the superstructure is good.

Acknowledgements

The authors wish to thank Innovation Fund Denmark for supporting this project.

Disclosure Statement

No potential conflict of interest was reported by the authors.

ORCID

M. S. M. Lund http://orcid.org/0000-0002-6503-7264

References

Anderson, D.M., Williams, P.J., Guymon, G.L. and Kane, D.L., 1984. Principles of soil freezing and frost heaving. *In*: R.L. Berg and E.A. Wright, eds. *Frost action and its control*. New York: American Society of Civil Engineers, 1–21. ISBN 0-87262-395-5.

ASTM Standard D2434-68. 2006. *Standard test method for permeability of granular soils (constant head)*, West Conshohocken, PA: ASTM International. doi:10.1520/D2434-68R06.

ASTM Standard D4253-16, 2016. *Standard test methods for maximum index density and unit weight of soils using a vibratory table*, West Conshohocken, PA: ASTM International. doi: 10.1520/D4253-16.

ASTM Standard D5918-13. 2013. *Standard test methods for frost heave and thaw weakening susceptibility of soils*, West Conshohocken, PA: ASTM International. doi: 10.1520/D5918-13.

BEBO Arch Systems, 2009. *Zürich: BEBO arch systems, installation guide*, BEBO system technical documentation.

Beskow, G., 1935. Soil freezing and frost heaving with special application to roads and railroads, trans. J.O. Osterberg. Evanston, IL: Technological Institute Northwestern University.

Casagrande, A., 1931. A new theory of frost heaving: discussion. Vol. 11, Washington, DC: Highway Research Board. 168–172. ISSN: 0096–1027.

Chamberlain, E.J., 1981. Frost susceptibility of soil. Review of index tests. Hanover, NH: U.S. Army Cold Regions Research and Engineering Laboratory. Monograph 81–2.

DS Standard 450-1. 2012. *Fly ash for concrete – part 1: definition, specifications and conformity criteria*. Danish Standards: København.

DS Standard 933-1. 2004. *Tests for geometrical properties of aggregates – part 1: determination of particle size distribution – Sieving method*. Danish Standards: København.

DS Standard 13285. 2011. *Unbound mixtures – specifications*. Danish Standards: København.

DS Standard 13286-5. 2003. *Unbound and hydraulically bound mixtures – part 5: test methods for laboratory reference density and water content – vibrating table*. Danish Standards: København.

DS Standard 13320. 2009. *Particle size analysis – Laser diffraction methods*. Danish Standards, Denmark: København.

Halding, P.S., Hertz, K.D., Petersen, E.V. and Kennedy, B., 2015. Assembly and lifting of pearl-chain arches. *In:* Stang, H. and Braestrup, M., eds. *Proceedings of FIB symposium*, 18–20 May 2015. Copenhagen: Danish Concrete Society, 185–186.

Hertz, K.D., Castberg, A. and Christensen, J., 2014. Super-light concrete decks for building floor slabs. *Structural concrete*, 15 (4), 522–529. doi: 10.1002/suco.201500062.

Hertz, K.D., 2015. Super-light SL-Deck elements with fixed end connections. *In:* Stang, H. and Braestrup, M., eds. *Proceedings of FIB symposium*, 18–20 May 2015. Copenhagen: Danish Concrete Society, 465–466.

Hutchinson, D., 2004. Application and design of segmental precast arches. *In*: M.K. Yegian and E. Kavazanjian, eds. *Proceedings of GeoTrans. Los Angeles, California, July 27–31 2004*. Reston, VA: American Society of Civil Engineers, 452–459. ISBN 978-0-7844-0744-8.

Lambe, T.W. and Whitman, R.V., 1969. *Soil mechanics*. New York: Wiley. ISBN 0-471-51192-7.

Lund, S.M., Arvidsson, M. and Hansen, K.K., 2015. Homogeneity and strength of mortar joints in Pearl-Chain Bridges. *In:* Stang, H. and Braestrup, M., eds. *Proceedings of FIB symposium*, 18–20 May 2015 Copenhagen: Danish Concrete Society, 187–188.

Lund, M.S.M., Hansen, K.K., Truelsen, R. and Johansen, L., 2016. Pervious concrete fill in Pearl-Chain Bridges: using small-scale results in full-scale implementation. *Construction and Building Materials*, 106, 404–414.

NCC Denmark, 2001. *Road construction – materials – wearing surfaces – pavements*. 3rd ed. Copenhagen: NCC. Danish.

Rempel, A.W., 2007. Formation of ice lenses and frost heave. *Journal of Geophysical Research*, 112 , F02S21. doi: 10.1029/2006JF000525

Rempel, A.W., 2010. Frost heave. *Journal of Glaciology*, 56 (200), 1122–1128.

Sihwa, L., 1987. Computer data base assessment of masonry bridges. Thesis (PhD). University of Edinburgh, UK.

Sub-base of Sand and Gravel – Design Guide, 2003. København: Tender specification. The Danish Road Directorate. ISBN: 87-7923-502-6. Danish.

Sub-base of Sand and Gravel – General Work Specification (GWS). 2003. København: tender specification. The Danish Road Directorate. ISBN: 87-7923-503-4. Danish.

Taber, S., 1929. Frost heaving. *The Journal of Geology*, 37 (5), 428–461.

Taber, S., 1930. The mechanics of frost heaving. *The Journal of Geology*, 38 (4), 303–317.

Appendix 1. Criteria for determination of frost susceptibility according to the ASTM D5918-13 standard

Table A1 shows the criteria given in the ASTM D5918-13 standard (ASTM Standard D5918-13, 2013) to determine the degree of frost susceptibility of soil materials from their 8-hour heave rate.

Table A1. Frost susceptibility criteria according to the ASTM D5918-13 standard (ASTM Standard D5918-13 2013).

Frost susceptibility classification	8-h heave rate [mm/day]
Negligible	<1
Very low	1–2
Low	2–4
Medium	4–8
High	8–16
Very high	>16

CHAPTER 3

Durability of mortar joints in Pearl-Chain arches

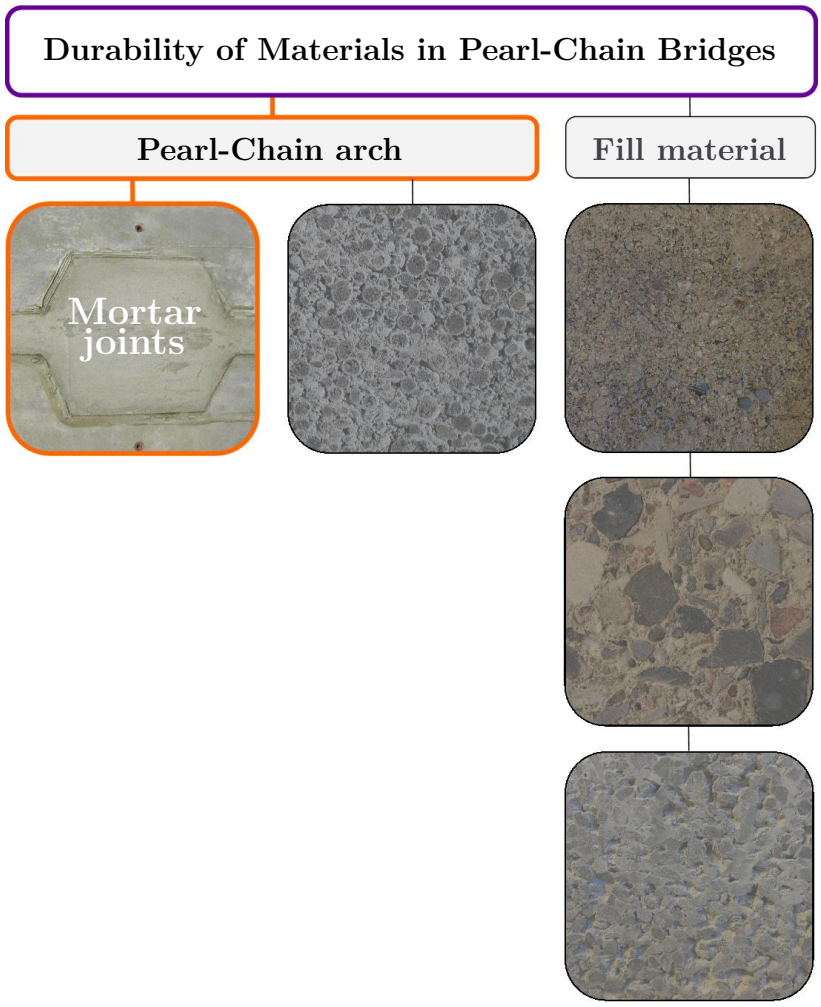

Paper VI

"Durability of vertically cast mortar joints in Pearl-Chain Bridges"

M.S.M. Lund, K.K. Hansen, and M. Arvidsson

Submitted to: *Construction and Building Materials, 2016*

Durability of vertically cast mortar joints in Pearl-Chain Bridges

M.S.M. Lund*, K.K. Hansen**, M. Arvidsson

Technical University of Denmark, Department of Civil Engineering, Brovej 118, DK-2800 Kgs. Lyngby, Denmark

Abstract

The mortar joints between the concrete elements in Pearl-Chain arches – the load carrying part of the new precast bridge concept 'Pearl-Chain Bridges' – are cast vertically with a placing depth of 2.40 m. The joint thickness of 20 mm is widened around ducts for post-tensioning wires. This study investigates the durability of the joints with respect to crack formation, bonding, freeze-thaw durability, chloride ingress, and capillary absorption. Our research established that 2.40 m-high mortar joints can be cast with a long-lasting durability, but that the expansion properties of the mortar product are of critical importance for reliable results.

Keywords: Crack formation, Durability, Mortar joint, Pearl-Chain Bridge, Vertical casting

1. Introduction

Pearl-Chain Bridge technology introduces an innovative arch solution for road and railway bridges [1]. The load-carrying part of a Pearl-Chain Bridge is the Pearl-Chain arch that is made of plane prefabricated Super-Light Decks (SL-Decks) consisting of lightweight aggregate concrete and conventional concrete [2, 3]. Each SL-Deck is 1.65 m long, 0.22 m thick, and up to 2.40 m wide, depending on the bridge design. Ducts are cast into the SL-Decks longitudinally to enable post-tensioning. Because each SL-Deck is given a slight inclination at the ends, the Pearl-Chain arch is created by collecting and post-tensioning several decks on a wire, like pearls on a string. Thus, an arch is formed from plane elements. For ease of assembly, the Pearl-Chain arch is placed on its side; when the SL-Decks are emplaced, self-compacting mortar joints are cast between the elements, after which the arch is post-tensioned. Subsequently, a crane is used to lift and tilt the Pearl-Chain arch and put it into place [4]. The number of SL-Decks collected on the wires and the number of Pearl-Chain arches placed next to each other determine the span and width of the particular Pearl-Chain Bridge. When the Pearl-Chain arches are in place, spandrel walls are installed, a filling material is placed, and the Pearl-Chain Bridge is finished by casting a post-tensioned concrete top plate on top of the fill, and also asphalt concrete if desired. Because the Pearl-Chain arch is assembled on its side, the mortar joints between the SL-Decks are cast vertically, see Figure 1.

The mortar joints between the SL-Decks in the Pearl-Chain arch transfer the forces between the SL-Decks. However, these joints can be considered a weak link as far as the durability of the Pearl-Chain arch is concerned because the post-tensioning wires in the Pearl-Chain arch must pass through the joints.

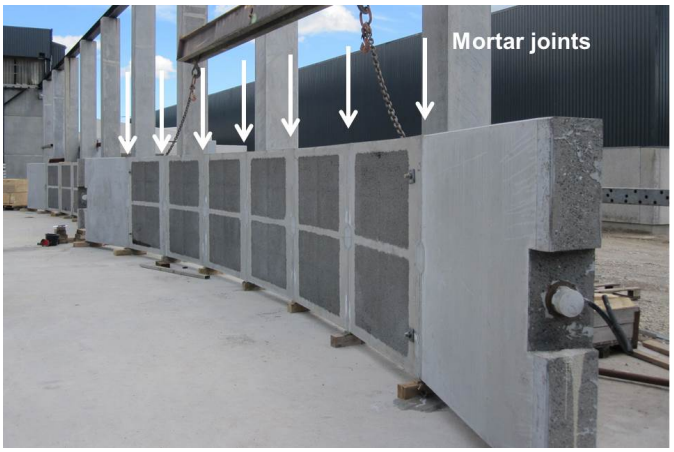

Figure 1: Pearl-Chain arch with a total span length of 13 m and a width of 1.75 m. The arch consists of six SL-Decks and two end elements, and it is collected and assembled on its side. Mortar joints are cast between all elements, and the location of the 1.75 m high mortar joints is highlighted with arrows.

Hence, if the joints are not sufficiently resistant to water and chloride ingress, the post-tensioning wires become exposed, and corrosion can initiate. Due to the optimal arch shape, the Pearl-Chain arch is under compression for almost all load combinations when it is in place, and in this case the post-tensioning wires do not contribute to the load-carrying capacity of the Pearl-Chain Bridge. However, for a few load combinations involving large and heavy vehicles, the Pearl-Chain arch is subject to tensile stresses, and the post-tensioning wires are activated. Therefore, it is very important to ensure that they are in a good condition, which falls back on the durability of the mortar joints.

Self-compacting mortar products are typically applied in constructions with joint thicknesses of less than 150 mm. However, in Pearl-Chain Bridges, a placing depth of up to 2.40 m is needed, which far exceeds the thickness of typical fields of application for self-compacting mortar products. Therefore,

*Corresponding author. Tel.: +45 45 25 17 52
**Tel.: +45 45 25 18 26
Email addresses: msml@byg.dtu.dk (M.S.M. Lund), kkh@byg.dtu.dk (K.K. Hansen)

the mechanical and moisture properties of the mortar joints in Pearl-Chain Bridges need to be tested. To the author's knowledge, no previous published work has investigated the durability of vertical cast mortar joints of such depth.

For Pearl-Chain Bridges, a commercialized high-strength, expansive, self-compacting mortar product is desired in order to provide sufficient strength, eliminate shrinkage problems and facilitate the casting procedure. In this study, two such commercialized mortar products were considered, and the influence of different pre-treatments of the concrete surface facing the joint was examined. The durability of 2.40 m-high mortar joints cast between SL-Decks was considered in terms of crack formation, bonding, capillary absorption, freeze-thaw durability, and chloride ingress. The idea behind all experiments was to test and compare pure concrete and pure mortar specimens with specimens with a concrete/mortar interface, and thereby to consider whether or not they had different properties from each other. The study was divided into four phases, with subsequent phases building on the experiences drawn from the previous phases.

2. Methods

2.1. Material properties and mix designs

Table 1 summarizes the characteristic values of the two high-strength, expansive and self-compacting mortar products examined in this study.

Table 1: Characteristic values of mortar products A and B.

	Mortar A	Mortar B
Placing depth [mm]	20–150	10–50
Pot life* [min.]	15	20
Aggregate size [mm]	0–4	0–4
Water addition [kg per 25 kg mortar]	3.40	3.10
$f_{c,1\ \mathrm{day}}$ [MPa]	> 20	> 40
$f_{c,28\ \mathrm{days}}$ [MPa]	> 80	> 90
Expansion [%]	0–2	N/A†

* At 25°C.
† No information about the size of the expansion is provided for mortar B even though it is declared as 'expansive'.
f_c = compressive strength.

Because the two mortar products are ready-mixed, the suppliers give no information about their mix designs.

The concrete used for the SL-Decks contained Portland cement, CEM II 52.5 N, and the water-to-cement ratio was 0.38. Concrete sand with a density of 2650 kg/m^3, 0.1% absorption, and a gradation of 0–2 mm was used with a single granite fraction of 4–16 mm having a density of 2770 kg/m^3 and 0.2% absorption. Moreover, a combination of a natural and synthetic air entraining agent, a superplasticizer with polyether ester as the active component, and an accelerator with nitrate as the active component were used. The air entraining agent, the superplasticizer and the accelerator dosages comprised 0.35%, 0.68% and 1.0% of the total powder mass, respectively. The concrete mix design is shown in Table 2.

Finally, an alkali-resistant latex primer based on styrene-butadiene was used for some mortar joints.

Table 2: Mix design of the concrete used in the SL-Decks.

Material	Mass [kg/m^3]
Cement, CEM II 52.5 N	455.0
Water	144.2
Air entraining agent	1.57
Superplasticizer	3.07
Accelerator	4.55
Sand 0–2 mm	698.6
Granite 4–16 mm	1047.9
Total density	2354.9

2.2. Experimental setup

2.2.1. Overall experimental setup

During the study, the experimental setup was continually improved from the experiences made along the way. The total study can be divided into four phases that all have certain similarities. In all four phases, the experimental setup consisted of two 2.40 m-high concrete elements with the dimensions shown in Figure 2a.

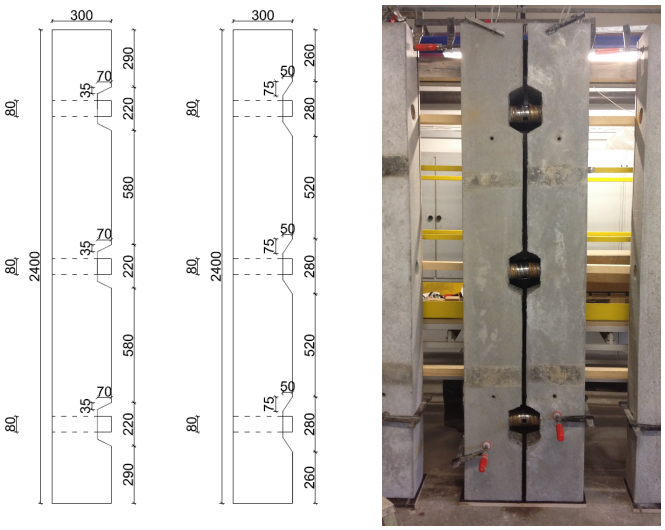

(a) Left: Geometry of 2.40 m-high concrete element used in phases 1 and 2. The dashed lines mark the location of the ducts for post-tensioning wires. Dimensions are in mm. Right: Geometry of 2.40 m-high concrete element used in phases 3 and 4. The dashed lines mark the location of the ducts for post-tensioning wires. Dimensions are in mm.

(b) Test setup. Two concrete elements were placed with a gap of width 20 mm where the mortar was cast. The thickness of each concrete element was 220 mm. When casting the mortar, a coated plywood formwork was installed in front of and behind the concrete elements covering the gap between them.

Figure 2: Geometry and test setup of mortar joints.

Each concrete element was identical to the end of a SL-Deck used in the Pearl-Chain arch, though shortened. The concrete elements were cast at a concrete mixing plant more than 28 days before the time of testing. Three sheet metal ducts, in which post-tensioning wires are to be placed, were cast into the SL-Decks at different positions. A recess around each duct (see Figure 2b) makes it possible to manually connect the ducts of neighboring SL-Decks by the use of aluminum tape. The

concrete elements were 220 mm thick, and the distance between two adjacent concrete elements positioned as in Figure 2b was 20 mm; hence, the thickness of the mortar joint was also 20 mm. To improve the bonding between concrete and mortar, the concrete elements had exposed aggregates on the side facing the joint. Figures 3a and 3b show how the ducts from adjacent elements were closed with aluminum tape to seal the gap and strengthen the connection.

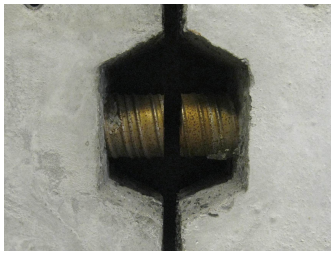

(a) Ducts from adjacent SL-Decks meeting.

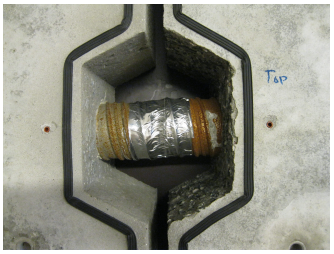

(b) Ducts from adjacent SL-Decks closed with aluminum tape.

(c) Shrinkage crack reinforcement with a mesh size of 1 cm × 2 cm installed around the ducts.

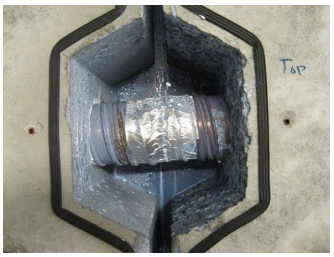

(d) Surface treatment with water and primer.

Figure 3: Recesses around ducts.

Rubber strips were fastened on the surface of the concrete elements, 20 mm from the perimeter of the joint on both sides of each element, as seen in Figures 3b and 3d. The concrete elements were placed vertically with a horizontal distance of 20 mm between them, and fastened to a 24 mm-thick coated plywood rear formwork with screws every 200 mm vertically. Together with the rubber strips this ensured a tight seal of the setup when the mortar was poured. After joining the ducts, a 24 mm-thick coated plywood front formwork was placed in front of the mortar joint, and tightly fastened to the concrete elements with screws every 200 mm vertically.

The mortar was mixed for five minutes in a 60 liter compulsory mixer. 100 kg ready-mix mortar powder was mixed with the corresponding water amount given in Table 1. After two minutes of mixing and again after four minutes, the mixer blades were cleaned for lumps of mortar powder. The mortar was poured into each joint through a funnel from above, thereby having a depth of 2.40 m. After casting the joint, the upper surface of the joint was covered with plastic foil to prevent any moisture evaporation. For phases 1 and 2, the formwork was removed after the mortar had cured at 20°C for two days, whereas for phases 3 and 4 the formwork was removed after a minimum of five days curing at 20°C, to conform with the requirements for concrete to be exposed to an aggressive environment [5].

2.2.2. *Characteristics of different phases*

In order to try to solve challenges with crack formation in the joints, four different phases were initiated during this study. Figure 4 illustrates the main initiatives taken during each phase.

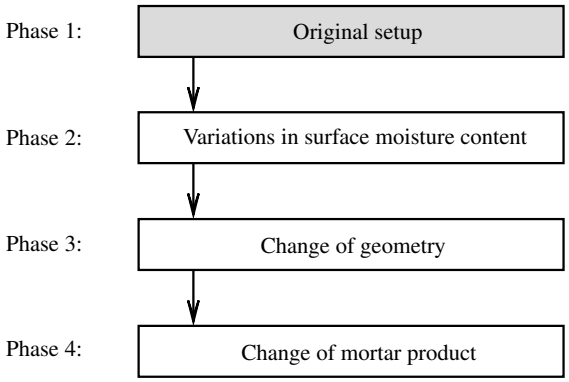

Figure 4: Overall initiatives in the different phases for improving the durability of the mortar joints in Pearl-Chain Bridges.

Phase 1. In phase 1, two mortar joints were cast with mortar A. Since most self-compacting, high-strength, expansive mortar products are only advocated to support depths of less than 150 mm, the objective of phase 1 was to investigate if it was possible to cast 2.40 m-high mortar joints with good durability properties. The preparation of the concrete elements before casting with mortar A was as follows:

- *Mortar joint 1-a*: After having installed the formwork, the whole joint was pre-wetted by filling it with water. The water pressure was kept constant for three hours, after which the front formwork was moved, and excess surface water was removed by using pressurized air until no surface water was seen.
- *Mortar joint 1-b*: No pre-wetting took place. The concrete elements were dry.

Cores were drilled from the joints after 28 days hardening at 20°C. The location of the cores are shown in Figure 5. Cores with a diameter of 100 mm were drilled for splitting tensile strength tests and rapid chloride migration tests; cores with a diameter of 150 mm were drilled for freeze-thaw tests; and cores with a diameter of 50 mm were drilled for capillary absorption tests.

Phase 2. In phase 2, four mortar joints were cast with mortar A. The preparation of the concrete elements before casting with mortar A was as follows:

- *Mortar joint 2-a*: The upper two-thirds of the joint, including the two upper recesses, were not pre-wetted. The lower third, including the lower recess, was pre-wetted three times using a vaporizer. The water was allowed to penetrate into the concrete for half an hour between each

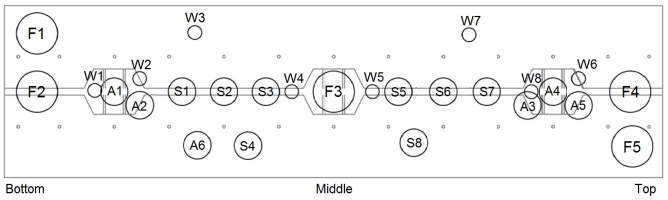

Figure 5: Locations of cores taken from mortar joint 1-a and mortar joint 1-b to examine splitting tensile strength (cores marked with 'S', d = 100 mm), rapid chloride migration (cores marked with 'A', d = 100 mm), capillary absorption (cores marked with 'W', d = 50 mm), and freeze-thaw durability (cores marked with 'F', d = 150 mm). Core A3 was only drilled from mortar joint 1-a, and core A2 was only drilled from mortar joint 1-b. 'Top' indicates the end of the joint that faced upwards during casting of the mortar.

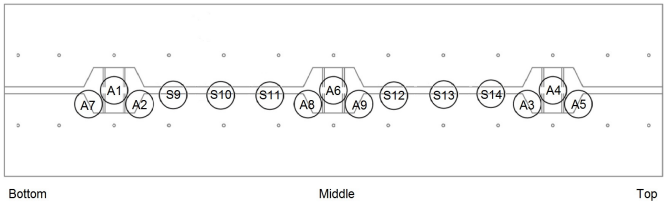

Figure 6: Locations of cores taken from mortar joint 2-a for splitting tensile strength (cores marked with 'S', d = 100 mm), and from mortar joint 2-c, 2-d, 3-a, 3-b, 3-c, 4-a and 4-b to investigate rapid chloride migration (cores marked with 'A', d = 100 mm). Not all cores that were actually tested, as will be explained in the following sections. 'Top' indicates the end of the joint that faced upwards during casting of the mortar.

spraying. After the third and final spraying, excess surface water was removed by use of pressurized air until no surface water was seen.

- *Mortar joint 2-b*: Shrinkage crack reinforcement was installed around the ducts in the two upper recesses as shown in Figure 3c. The reinforcement was shaped rectangular around the duct and fastened to the concrete with two screws on each side. Moreover, small plastic blocks were placed above each duct to keep the distance to the reinforcement constant. The mesh size of the reinforcement was 1 cm $\times$ 2 cm, which was considered sufficient for the mortar to be able to flow through. The lower third of the joint, including the lower recess, was pre-wetted in the same manner as the lower third of mortar joint 2-a.

- *Mortar joint 2-c*: The surface of the concrete elements, including all three recesses, was pre-wetted in the same way as mortar joint 1-a.

- *Mortar joint 2-d*: The surface of the concrete elements, including all three recesses, was sprayed with a primer one hour before the mortar joint was cast (see Figure 3d). During this hour, the surfaces were continuously sprayed to keep them wet. Immediately before casting the mortar joints, excess water was removed by the use of pressurized air until no further surface water was seen. One of the concrete elements did not have exposed aggregates, but rather a smooth surface facing the joint.

Cores were drilled from the mortar joints after 28 days hardening at 20°C. From mortar joint 2-a, cores with a diameter of 100 mm were drilled for splitting tensile strength tests. The locations of the cores are shown in Figure 6.

From mortar joint 2-b, cores with a diameter of 150 mm were drilled from the upper and middle recess in the pure mortar phase to investigate crack formation. From mortar joints 2-c and 2-d, cores with a diameter of 100 mm were drilled for rapid chloride migration tests and splitting tensile tests. The locations of the cores are shown in Figure 6.

Phase 3. In phase 3, the geometry of the recesses was changed, as shown in Figure 2a, so that the recesses were narrowed but steepened to make it easier for air to escape, and to minimize the vertical component of shrinkage stresses along the concrete/mortar interface. Three mortar joints were cast with mortar A. The preparation of the concrete elements before casting with mortar A was as follows:

- *Mortar joint 3-a*: The surface of the concrete elements, including all three recesses, was pre-wetted in the same manner as mortar joint 2-d, the only difference being that pure water rather than a primer was used.

- *Mortar joint 3-b*: The concrete elements were wrapped in plastic foil directly after casting them to prevent any moisture evaporation. Moreover, the surface of the concrete elements, including all three recesses, was pre-wetted with a primer in the same manner as mortar joint 2-d.

- *Mortar joint 3-c*: The surface of the concrete elements, including all three recesses, was pre-wetted with a primer in the same manner as mortar joint 2-d.

- *Mortar joint 3-d*: The surface of the concrete elements, including all three recesses, was pre-wetted in the same manner as mortar joint 2-d, but the joint was cast between elements positioned horizontally. Moreover, the temperature variation of the mortar was measured in two of the recesses during casting and hardening.

Cores were drilled from the mortar joints after seven days hardening at 20°C to investigate crack formation. The location of the cores for mortar joints 3-a, 3-b and 3-c is shown in Figure 6. No cores were drilled from mortar joint 3-d.

Phase 4. In phase 4, the geometry of the recesses used in phase 3 was maintained. Two mortar joints were cast with mortar B. The preparation of the concrete elements before casting with mortar B was as follows:

- *Mortar joint 4-a*: Identical to mortar joint 3-b, but cast with mortar B. The temperature variation of the mortar was measured in the upper and middle recesses during casting and hardening.

- *Mortar joint 4-b*: The surface of the concrete elements, including all three recesses, was pre-wetted in the same manner as mortar joint 2-d.

Cores were drilled from mortar joints 4-a and 4-b after 28 days hardening at 20°C to investigate crack formation and splitting tensile strength. The locations of the cores drilled from mortar joints 4-a and 4-b are shown in Figure 6, together with the cores for the splitting tensile strength tests.

2.3. Expansion test setup

The expansion of the mortars was determined from dilatometer tests, whereby the unrestrained deformation of the mortar is measured during hardening. Both manual and automatic dilatometer tests were carried out. To obtain a complete overview of the entire expansion course of the mortars, it was necessary to start the measurements as soon as possible after the water had been added. For the automatic dilatometer tests, after the water is added, it takes from 15 to 20 minutes before the first measurement can be taken because the preparation of the samples is time-consuming. Since it was not known whether the most rapid expansion of the mortars would take place during this initial period, it was also necessary to perform the manual dilatometer test. The preparation of the samples for the manual dilatometer test only takes approximately five minutes, and thereby it is possible to determine the expansion of the mortars at the very beginning of the expansion course. However, since the automatic dilatometer test is carried out in a controlled environment at a constant temperature and under completely sealed conditions, it is considered to be more accurate than the manual dilatometer test.

In both tests, 2 kg of mortar powder and the corresponding amount of water (see Table 1) was mixed in a Hobart mixer at maximum speed for one minute, after which the mortar was filled in a corrugated plastic tube with an outer diameter of 29 mm. Figure 7 shows the test setup for the automatic dilatometer test carried out, as described by Jensen and Hansen [9].

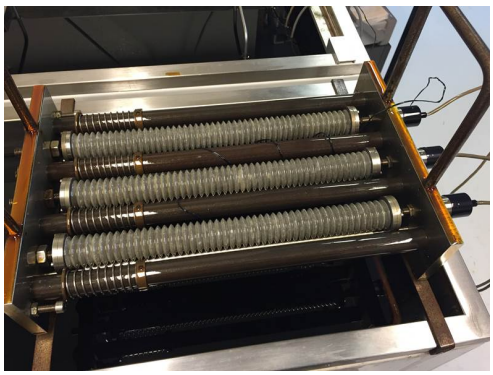

Figure 7: Test setup for the automatic dilatometer test for expansion measurements of mortars during the first 28 days after mixing. A displacement transducer measured the deformation in one end of each of the specimens. During testing, the specimens were immersed in a thermo-bath filled with polyalkylene glycol at a constant temperature of 20°C.

Displacement transducers measured the deformation of each sample with an accuracy of 0.3 μm. The samples were immersed in a thermo-bath filled with polyalkylene glycol maintained at a constant temperature of 20°C. In total, four specimens of mortar A and three specimens of mortar B were tested in the automatic dilatometer for 28 days, and the time between the measurements was five minutes. Figure 8 shows the manual dilatometer test setup. The manual tests were carried out as described in the American Society for Testing and Materials (ASTM) C1698-09 standard [10]. In total, four specimens each of mortars A and B were tested in the manual dilatometer in the one hour immediately after mixing, and the time between the measurements was 30 seconds. The measurements were carried out at a temperature of 23±0.5°C. The internal temperatures of one specimen cast with mortar A and one cast with mortar B were also measured.

Figure 8: Test setup for manual dilatometer test for expansion measurements of mortars during the first hour after mixing. The deformation was read from a digital length gauge at one end of the specimen.

2.4. Splitting tensile strength test setup

In the splitting tensile strength tests, pure mortar specimens, pure concrete specimens and specimens with two concrete/mortar interfaces were tested. Two different configurations were used to test the mortar joint specimens: either the load was applied in the middle of the mortar joint between two concrete elements (cores from phase 1), or it was applied directly at the concrete/mortar interface (cores from phases 2 and 4), as shown in Figure 9.

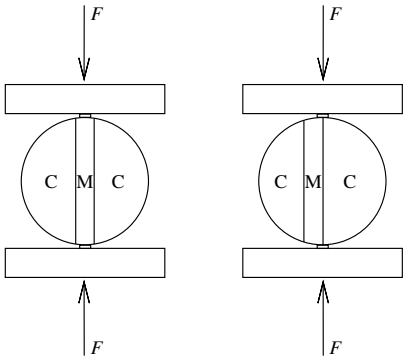

Figure 9: Splitting tensile strength test configurations for test of mortar joints. The force, F, was either applied at the center of the 20 mm-wide mortar joint or directly at the concrete/mortar interface. C = concrete, M = mortar.

The concrete specimens and mortar joints used to determine the splitting tensile strength had a diameter of 100 mm and a

height of 220 mm. However, because the ducts passed through the recesses, it was not possible to drill pure mortar specimens of the correct height for the splitting tensile strength tests from the recesses. Therefore, 200 mm-high pure mortar specimens with a diameter of 100 mm were cast from the same batch as used to cast the mortar joints. For mortars A and B, the specimens were tested at 28 days. The splitting tensile strength tests were carried out on a TONI 3000 kN test machine in accordance with the International Organization for Standardization (ISO) standard ISO 4108 [6]. Specimens from phases 1, 2 and 4 were tested.

2.5. Capillary absorption test setup

The capillary absorption was measured on specimens with a diameter of 50 mm and a height of 100 mm. Only specimens from phase 1 were tested. Pure concrete specimens, pure mortar specimens, and specimens with one or two concrete/mortar interfaces were tested. Firstly, the specimens were dried at 105°C until their masses remained constant. Next, the surface of the specimens, except for the ends, was sealed with epoxy resin to ensure one dimensional water transportation. Then, the specimens were placed on small distance blocks in a tray containing demineralized water. The water depth, which reached two millimeters up the sides of the specimens, was kept constant during the test. The mass of each specimen was measured every eight minutes during the first hour, and subsequently after 4 h, 7 h, 12 h, 24 h, 48 h and 177 h, at which time the test was terminated. After termination, the specimens were dried at 105°C until their masses remained constant. The water absorbed by capillary rise, Q [kg/m^2], was determined using the formula:

$$Q = \frac{m_t - m_0}{A} \quad (1)$$

where m_t [kg] is the mass of the specimen at time t, m_0 [kg] is the dry mass of the specimen dried at 105°C, and A [m^2] is the cross-sectional area of the specimen.

2.6. Freeze-thaw test setup

The freeze-thaw test followed the Borås method for conventional concrete described in the Danish Standard (DS/CEN/TS) DS12390-9 [7], using 28-day-old specimens of height 50 mm and diameter 150 mm. For the first 50 frost cycles, the scaling of each specimen was collected and measured after every sixth frost cycle. After the first 50, the number of frost cycles between the measurements increased. 224 frost cycles were run in total. The frost test was conducted on pure concrete specimens, pure mortar specimens and on specimens with two concrete/mortar interfaces. Only specimens from phase 1 were tested. Refer to Figure 5 to see the locations of cores drilled for the freeze-thaw tests. Three specimens were cut and tested from each mortar joint core. Two specimens were cut and tested from each pure concrete core and pure mortar core.

2.7. Chloride ingress test setup

The chloride ingress was tested on 50 mm-high cylinder specimens with diameters of 100 mm. Pure concrete specimens, pure mortar specimens, and specimens with one concrete/mortar interface were tested. The concrete specimens were 70 days old, whereas the mortar specimens were 28 days old. The chloride ingress was examined using the rapid chloride migration test described in the Nordtest method NT BUILD 492 [8], where an external electrical potential is used to force the chloride ions through the specimen. After it had been exposed to the electrical potential for a well-defined period of time, the specimen was split axially, and sprayed with a silver nitrate solution. A change in color due to the formation of silver chloride indicated the chloride penetration depth, and thereby the chloride migration coefficient could be calculated. The purpose of the chloride ingress tests was not only to determine the chloride migration coefficient, but also to easily visualize potential cracks, because any crack formation and subsequent chloride penetration was immediately visible due to the shift in color.

3. Results and discussion

3.1. Crack formation in mortar joints

Any crack formation in the mortar joints is of great concern for the durability of the joints, and is thus highly undesirable. During the first three phases of this study, a significant number of cracks appeared in the mortar in the recesses. No crack formation was observed in the 20 mm-thick mortar joint between the recesses in any of the tests. Three different types of cracks that were observed: shrinkage cracks parallel to the ducts, settlement cracks, and cracks along the edges of the recesses. A major focus of this study, and the reason why different phases were initiated, was to identify the phenomena causing the cracks, and to determine ways to eliminate the crack formation.

3.1.1. Crack formation in phase 1

In phase 1, two mortar joints were cast. The moisture content of the concrete surface facing each mortar joint was different. Immediately after removing the formwork from mortar joint 1-b (using dry concrete elements), it was clear that cracks had formed. The cracks were parallel to the ducts, and extended all the way from one surface of the 220 mm-thick mortar joint to the other, as shown in Figure 10a. The cracks were visible in the upper and middle recesses in mortar joint 1-b, and they could easily be seen from the surface and from the cores by wetting. Figure 10b shows how a moistened crack clearly appeared.

Cracks stretching over the ducts from one surface of the joint to the other are extremely critical because they serve as a direct and easy route for chlorides to reach the ducts, and subsequently the post-tensioning wires. This is of critical importance due to the risk of corrosion of the wires, which in the worst case scenario could cause the bridge to collapse. To investigate the cause of the crack formation, a number of thin sections from the cracked area was prepared and analyzed. The cracks were found to be due to shrinkage because they were created in the early hydration of the cement. This conclusion was based on the following three arguments:

- The cracks went through the cement paste, but avoided the aggregates (see Figure 11).

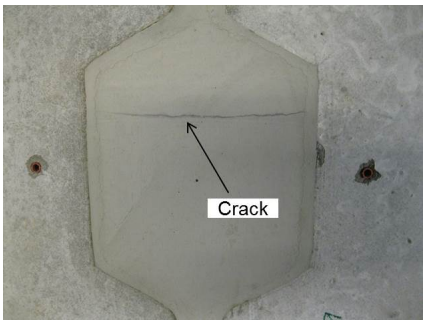

(a) Example of shrinkage crack parallel to the duct seen from the surface of the mortar joint.

(b) Shrinkage crack extending through 220 mm-thick mortar joint.

Figure 10: Shrinkage crack formation in recesses.

- The cracks were not continuous, but stopped and started again at different locations (see Figure 11). This only occurs when the cracks are created during the early hydration of the cement.
- The carbonation depth at the surface of the joint was the same as that along the crack (see Figure 12). This means that the mortar along the crack was exposed to carbon dioxide for the same amount of time as the mortar along the surface of the joint, and that the crack was therefore formed during the early hydration of the cement.

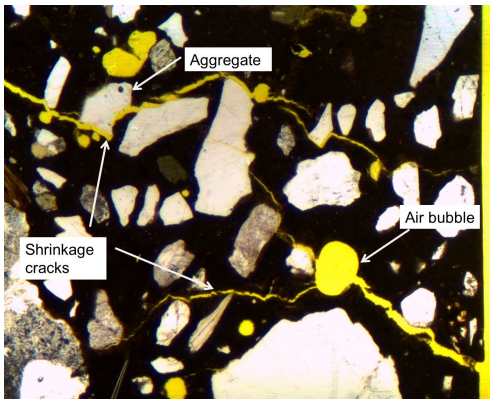

Figure 11: Thin section image of shrinkage crack formation in mortar joint 1-b using plane polarized light. The crack avoids the aggregates and extends only through the cement paste, which indicates that it was created during the early cement hydration, and was caused by shrinkage. The image is enlarged 16 times.

At first, the visual assessment did not indicate any problems with shrinkage crack formation parallel to the ducts in mortar joint 1-a (using pre-wetted concrete elements). However, cracks that were not visible to the eye later became clear from the rapid chloride migration tests, and thus shrinkage cracks also appeared in the upper recess in mortar joint 1-a. Figure 13a shows the shrinkage crack formation revealed from the rapid chloride migration test for the mortar in the upper recess in mortar joint 1-b. The result for the upper recess in mortar joint 1-a was identical. The rapid chloride migration test did not show

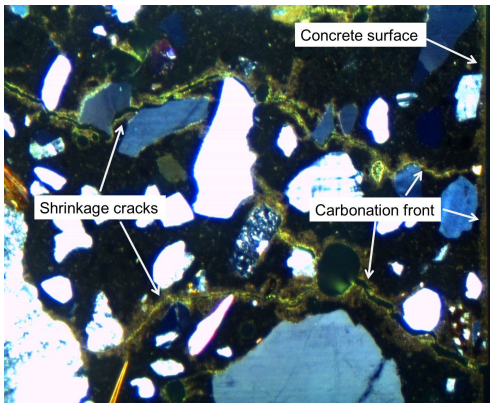

Figure 12: Thin section images of shrinkage cracks in mortar joint 1-b using crossed polarized light. The carbonation depth is the same along the concrete surface and along the cracks, which indicates that it was created during the early cement hydration. The image is enlarged 16 times.

any shrinkage cracks in the lower recess of either mortar joint 1-a or joint 1-b.

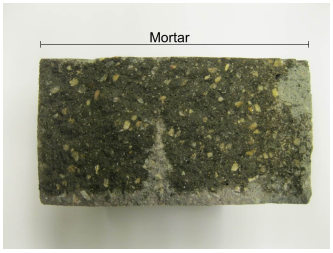

(a) Chloride ingress in mortar drilled from the upper recess in mortar joint 1-b. A shrinkage crack is clearly visible where the color changes to light gray at the center of the specimen.

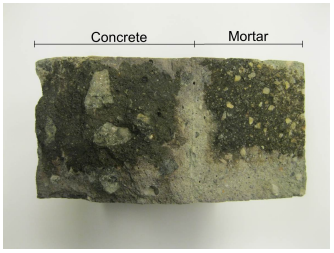

(b) Chloride ingress in concrete/mortar interface of a core drilled from the upper inclined edge of the upper recess in mortar joint 2-d. A crack formation along the interface is clearly present, as seen from the light gray color change.

Figure 13: Crack formation in mortar joints revealed by a color change in rapid chloride migration tests. When chloride ions are present, the color changes from dark gray to light gray.

Table 3 gives a complete overview of the presence of shrinkage cracks.

Another type of crack formation became clear from the mortar cores drilled from the middle recess of mortar joint 1-a. This crack formation differed from the shrinkage cracks because it was not visible on the surface, and because it was coarser and had a more limited extent. A thin section analysis showed that the crack was caused by settlement. This was concluded because the crack was non-uniform, and because the same crack structure was found on opposite sides of a crack, which indicated that it was pulled apart by movement (see Figure 14a).

3.1.2. Crack formation in phase 2

Phase 2 was initiated in an attempt to avoid the shrinkage cracks found in phase 1. Because drying shrinkage was a possible explanation of the crack formation, it was tested whether the concrete elements absorbed water from the fresh mortar. The results from phase 1 suggested that this could be an explanation

Table 3: Overview of the presence of shrinkage cracks in upper, middle and lower recesses of mortar joints; '+' indicates that a shrinkage crack was observed, '-' indicates that no shrinkage crack was observed, '∗' indicates that no shrinkage crack was visible to the eye, but that no final conclusion could be made because a rapid chloride migration test was not performed, and 's' indicates that a settlement crack was present.

	Mortar joint					
Recess	1-a	1-b	2-a	2-b	2-c	2-d
Upper	+	+	+	s	+	-
Middle	s	+	∗	s	+	-
Lower	-	-	∗	∗	-	-

	Mortar joint					
Recess	3-a	3-b	3-c	3-d	4-a	4-b
Upper	∗	∗	∗	+	-	-
Middle	+	+	+	+	-	-
Lower	∗	+	+	+	-	-

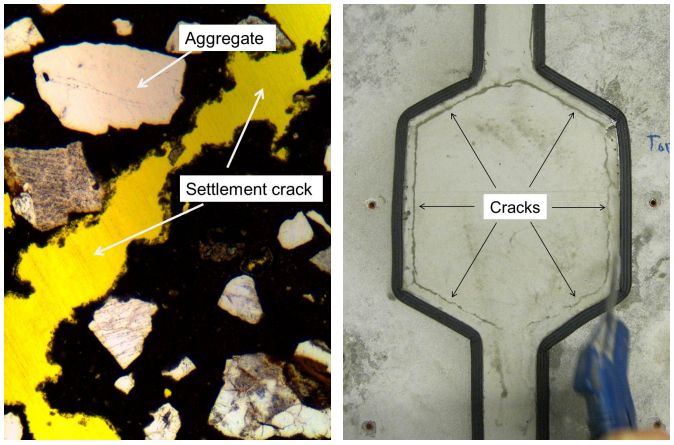

(a) Thin section image of the middle recess of mortar joint 1-a using plane polarized light. The crack is non-uniform, and is pulled apart, which indicates that it is a settlement crack. The image is enlarged 25 times.

(b) Crack formation in the concrete/mortar interface in mortar joint 2-d. The crack formation was visible on the surface of the mortar.

Figure 14: Settlement crack formation, and crack formation along the concrete/mortar interface in the recesses.

because the shrinkage crack formation in mortar joint 1-b using dry concrete elements was coarser than the shrinkage crack formation in mortar joint 1-a using pre-wetted concrete elements. Therefore, the main focus in phase 2 was to test various surface moisture contents, and various surface pre-treatments of the concrete surfaces adjacent to the joint. Moreover, it was tested whether shrinkage crack reinforcement could be a possible precaution against the observed shrinkage crack formation.

Table 3 shows the crack formation in phase 2 based on the visual assessment and the rapid chloride migration tests performed on pure mortar cores drilled from mortar joints 2-a, 2-b, 2-c and 2-d. A coarse shrinkage crack was observed on the mortar surface in the upper recess of mortar joint 2-a. No cracks were visible to the the eye for mortar in the other two recesses, and no rapid chloride migration tests were carried out. To prevent the formation of shrinkage cracks parallel to the duct, a shrinkage crack reinforcement was installed in the upper two recesses in mortar joint 2-b. However, after removing the formwork, coarse cracks were noticed. These cracks were believed to be caused by settlement because of the shrinkage crack reinforcement. Since such coarse settlement cracks are highly undesirable, the installation of shrinkage crack reinforcement was dismissed as an appropriate initiative against shrinkage crack formation. In mortar joint 2-c, no shrinkage cracks were visible to the eye, but the rapid chloride migration test showed that the mortar in the upper and middle recesses was subject to shrinkage cracking. No shrinkage cracks were seen in any of the recesses in mortar joint 2-d.

The results from phase 2 give no indication that the shrinkage cracks observed over the ducts can be prevented by increasing the moisture content of the concrete surface facing the mortar. Mortar joint 2-c, which was identical to mortar joint 1-a and pre-wetted by keeping the joint under a constant water pressure for three hours immediately prior to casting, experienced the same level of shrinkage cracking as the joints cast with dry concrete surfaces. The shrinkage cracks are a result of the tensile strength of the mortar being less than the shrinkage stresses in the mortar during the early cement hydration. The shrinkage crack phenomenon in the recesses can be understood by considering a single recess, where the inclined concrete surfaces retain the mortar at two opposite ends, that is, along the upper inclined edges and along the lower inclined edges of the recess. Because the cross-section of the mortar joint is reduced over the ducts, this is the where the greatest shrinkage stresses occur; hence, this is where the shrinkage cracks develop. However, this is only true if the mortar is in fact retained along the inclined edges. In the case of mortar joint 2-d, one of the concrete elements did not have exposed aggregates, but rather a smooth surface facing the joint. This reduces the adhesion between concrete and mortar at the interface between the two materials. It is believed that the reason why no shrinkage cracks were observed for mortar joint 2-d was because the mortar volume in the recesses was able to contract. However, a different crack formation took place in mortar joint 2-d, as seen in Figure 14b. Immediately after removing the formwork, cracks that had developed along the edges of the recesses at the concrete/mortar interface were seen. The cracks were clearly visible because they extended through the thin mortar layer that overlapped the concrete. Rapid chloride migration tests were used to determine whether the cracks were extensive, or just a surface phenomenon. Figure 13b shows the chloride ingress in specimens drilled from the upper inclined edge of the upper recess in mortar joint 2-d. The cracks passed through the joint, and extended along the interface between mortar and concrete. Specimens drilled from the lower inclined edge of the three recesses in mortar joint 2-d were also tested, and no crack formation was observed.

The same type of crack formation along the interface between concrete and mortar was also found for other mortar joints. Table 4 gives a complete overview of the presence of cracks at the concrete/mortar interface along the inclined edges in the recesses for all mortar joints. For each mortar joint, the results distinguish between the inclined edges at the top and

those at the bottom of the three recesses. The vertical edges were not considered.

Table 4: Overview of the presence of cracks along concrete/mortar interface at the inclined edges at the top and at the bottom (bot.) of the upper, middle and lower recesses of mortar joints; '+' indicates that a crack was observed, '-' indicates that no crack was observed, '∗' indicates that no crack was visible to the eye, but that no final conclusion could be made because a rapid chloride migration test was not used, and 's' indicates that a settlement crack was present.

		Mortar joint					
Recess	Edge	1-a	1-b	2-a	2-b	2-c	2-d
Upper	top	+	-	+	∗	+	+
	bot.	-	∗	+	∗	+	-
Middle	top	∗	∗	+	∗	+	+
	bot.	∗	∗	+	∗	∗	-
Lower	top	∗	-	∗	∗	+	+
	bot.	∗	∗	∗	+	∗	-

		Mortar joint					
Recess	Edge	3-a	3-b	3-c	3-d	4-a	4-b
Upper	top	∗	s	s	∗	+	-
	bot.	s	s	s	∗	-	-
Middle	top	∗	∗	∗	∗	-	-
	bot.	s	∗	∗	∗	-	-
Lower	top	∗	∗	∗	∗	-	-
	bot.	s	∗	∗	∗	-	-

3.1.3. Crack formation in phase 3

In phase 3, the geometry of the recesses was changed for two main reasons:

- There seemed to be a tendency for most of the cracks along the interface between mortar and concrete to form at the top of the recesses (see Table 4). This could be a result of entrapped air in the mortar that could not escape. Mortar A was self-compacting; hence it needed no vibration, and at the beginning of the cement hydration entrapped air would have moved upwards. However, the top inclined surfaces of the recesses might act like bottlenecks, preventing some air from escaping because the inclination of the recesses was not steep enough.

- The observed shrinkage cracks were due to vertical shrinkage stresses because the cracks were formed horizontally, that is, perpendicular to the casting direction. The vertical component of the shrinkage stresses was minimized by making the inclined edges of the recesses steeper.

Hence, the new geometry of the recesses was narrower and had steeper inclinations than the original, as shown in Figure 15. This decreased the volume of mortar, and reduced the amount of entrapped air.

The new geometry failed to eliminate problems with shrinkage cracks for any of the concrete surface pre-treatments, as seen in Table 3. Several internal settlement cracks that were not visible on the surface became clear from the cores taken

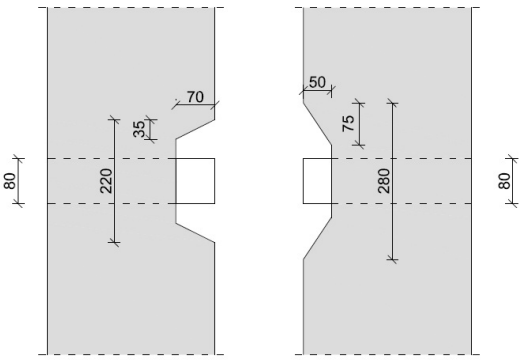

Figure 15: Comparison of recesses used in phases 1 and 2 (left) and recesses used in phases 3 and 4 (right). Dimensions are in mm.

along the inclined edges, as seen in Table 4. No rapid chloride migration tests were performed to estimate the degree of crack formation along the interface between concrete and mortar.

To investigate whether the shrinkage crack formation was due to temperature movements, the temperature changes of the mortar were recorded in two of the recesses in mortar joint 3-d during hardening. Figure 16 shows the result, where it can be seen that the maximum temperature variation for the mortar in joint 3-d was approximately 10°C. Assuming that the mortar has the same coefficient of linear thermal expansion as concrete, that is, approximately 10×10^{-6} °C^{-1} [12], this corresponds to a temperature induced shrinkage of approximately 0.1‰. Thus, the temperature-dependent deformation of a 2.40 m-high mortar joint is 0.24 mm, which is considered insignificant, and is not a possible explanation for the shrinkage cracks.

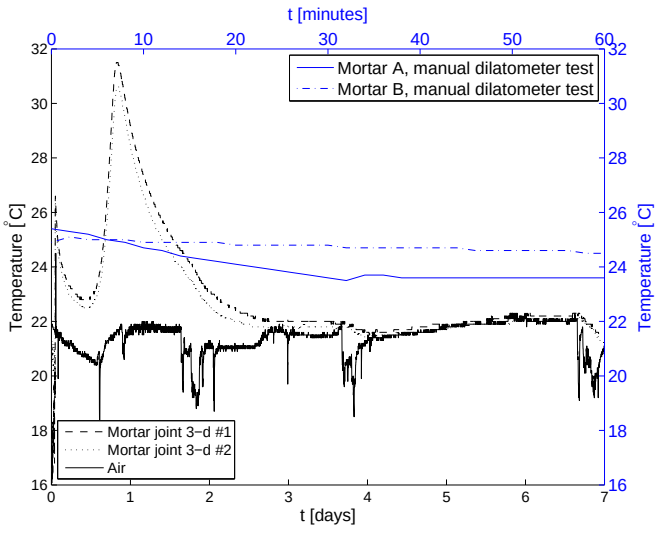

Figure 16: Air temperature and temperature variation of the mortar in the upper (#1) and middle (#2) recesses of mortar joint 3-d during the first seven days after water addition. The temperature variation of mortars A and B during the first hour after water addition measured in manual dilatometer tests is also shown. The air temperature was 23±0.5°C during the manual dilatometer tests.

Because mortar joint 3-d was also exposed to shrinkage cracks, it was concluded that the crack formation was not re-

lated to the mortar joints being cast vertically.

3.1.4. Crack formation in phase 4

The mortar product used to cast the joints in phases 1–3 was a so-called 'expansive' mortar (see Table 1). Therefore, it was not expected that the shrinkage crack formation experienced was due to problems with the mortar itself. However, since all previous attempts to eliminate the shrinkage cracks had met with little success, it was decided to measure the shrinkage properties of the mortar product in a dilatometer test. The expansion properties of mortar B (see Table 1), were also measured. Figure 17 compares the expansions of mortars A and B measured in a manual dilatometer, where the time from water addition to the first measurement was approximately five minutes.

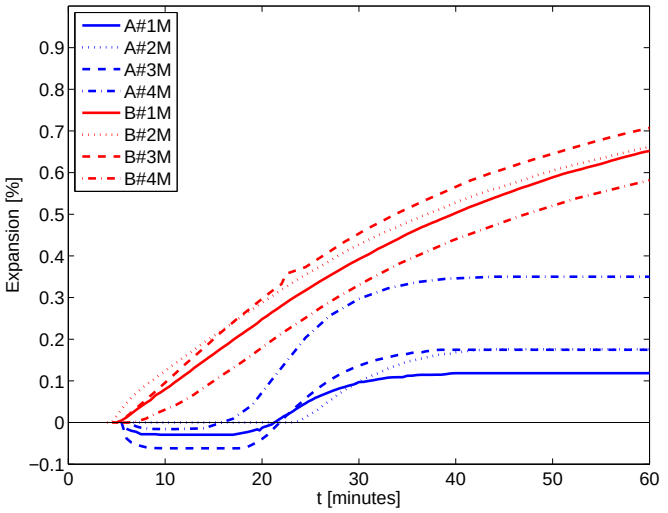

Figure 17: Expansions of mortars A and B measured in manual dilatometer tests during the first hour after mixing. Four specimens were tested for each mortar product.

Figure 17 shows a distinct difference in the expansion behavior of mortars A and B. Firstly, the expansion of mortar A did not begin until approximately 20 minutes after water addition, and until then there was a slight negative expansion. For mortar B, the expansion began immediately. Secondly, the expansion of mortar A reached a constant value approximately 20 minutes after the expansion was initiated, whereas the expansion of mortar B continued during the entire test. For mortar A, the minimum and maximum expansions after one hour were 0.12% and 0.35%, respectively. This expansion was much smaller than what was expected from a product described as 'expansive', with an expansion of up to 2%. For mortar B, the minimum and maximum expansions after one hour were 0.60% and 0.73%, respectively. Hence, the variation in expansion measured for mortar A was larger than that for mortar B. Moreover, the expansion during the first hour after water addition was more than two times greater for mortar B than it was for mortar A. Figure 16 shows that the difference in expansion was not explained by a difference in temperature, because the temperature variation during the test period was small for both mortars.

Figure 18 shows the expansion of mortars A and B measured using an automatic dilatometer, where the time between water addition and the first measurement was approximately 15 minutes. The figure does not take into consideration the result from Figure 17, which shows that mortar B had already expanded by more than 0.1% after 15 minutes, and that mortar A had a slight negative expansion after 15 minutes. The automatic dilatometer test was continued for 28 days, but Figure 18 only shows the expansion for the first seven days, because for all specimens the expansion after 28 days was the same as after seven days.

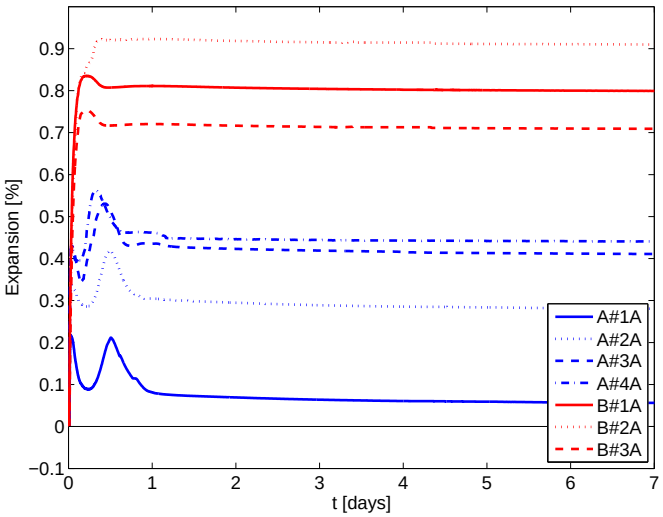

Figure 18: Expansion of mortars A and B measured in an automatic dilatometer test during the first seven days after mixing. Four specimens were tested for mortar A and three for mortar B. The temperature was 20°C.

Figure 18 shows that mortar A experienced two expansion peaks during the first day after water addition, but that it was unable to sustain the expansion. For example, mortar A#1A in Figure 18 had a final expansion of 0.07% but one hour after mixing the expansion peaked at 0.21%, and again after 12 hours. Mortar B also experienced a peak; however, the peak occurred approximately five hours after water addition, and was considerably smaller than that of mortar A. For example, mortar B#1A in Figure 18 had a final expansion of 0.80% but five hours after water addition the expansion peaked at 0.84%. Moreover, Figure 18 shows that the measured final expansion of mortar A varied between 0.07% and 0.43%, whereas the final expansion of mortar B varied between 0.70% and 0.90%. Hence, the expansion values determined from the automatic dilatometer tests were slightly larger than those determined from the manual dilatometer tests for both mortar A and mortar B. Nevertheless, the results from the automatic dilatometer tests confirmed the tendencies from the manual dilatometer test. The final expansion of mortar B was approximately two times larger than that of mortar A, and the variation in the expansion of mortar B was less than that of mortar A.

Based on the expansion test results, it was clear that a possible explanation of the shrinkage crack formation in phases 1–3 was the autogenous deformation of mortar A. Since mortar B showed much better autogenous deformation characteristics than mortar A, the mortar joints in phase 4 were cast with mor-

tar B. Table 3 shows that when using mortar B, the shrinkage crack formation parallel to the duct disappeared. This was confirmed from rapid chloride migration tests performed on pure mortar cores drilled from all recesses in mortar joints 4-a and 4-b (see Figure 19a).

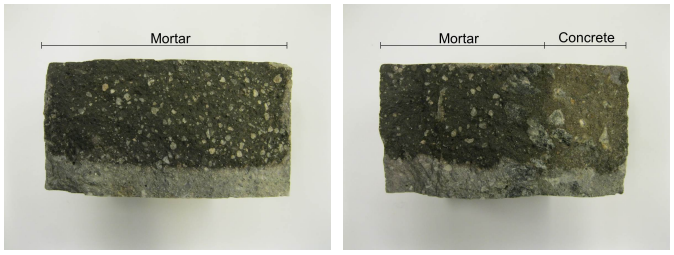

(a) Chloride ingress in pure mortar from the upper recess. No crack formation was observed.

(b) Chloride ingress in concrete/mortar interface of the upper inclined edge of the upper recess. No crack formation was observed along the interface.

Figure 19: Chloride ingress in mortar joint 4-b.

Hence, this study has shown that shrinkage cracks were only prevented by using a mortar product with a constant expansion of minimum 0.7%, and a small difference between the final expansion and the maximum (peak) expansion. It is believed that a possible explanation for the shrinkage cracks in mortar joints cast with mortar A was the two expansion peaks, the second of which occurred 12 hours after mixing. The decrease in expansion after this peak was more than 0.14 percentage points. It is expected that the setting time of mortar A was less than 12 hours, and thus mortar A had set at the time of the second expansion peak. Hence, mortar A was exposed to 0.14% shrinkage after setting, which resulted in shrinkage crack formation. For mortar B, the peak expansion had already occurred after five hours, and the subsequent shrinkage was only 0.04%.

Table 4 also shows that the crack formation along the concrete/mortar interface at the top and bottom of the inclined edges was prevented when using mortar B (see Figure 19b). The only exception was the upper inclined edge in the upper recess in mortar joint 4-a. However, the same crack formation was not found at the same location in mortar joint 4-b. To investigate if the primer could be eliminated now that the mortar product had been changed, another mortar joint was cast between a pair of concrete elements that were pre-wetted with water instead of primer. For this mortar joint, no shrinkage cracks were observed, but a crack did form along the concrete/mortar interface. The primer works by plugging and sealing the pores in the concrete surface. Thereby, the concrete surface becomes non-porous, so it cannot absorb free water from the mortar mixture. We believe that the decrease in porosity in the interface between concrete and mortar explains the reduction in chloride ingress along the interface. Because the primer reduces the porosity, it is more difficult for chloride ions to be pass through the interface. When the primer is not used, the porosity along the interface is so large that chloride ions more easily penetrate the interface rather than the mortar phase. Hence, the primer should be used when casting the mortar joints in Pearl-Chain Bridges.

3.2. Splitting tensile strength of mortar joints

The splitting tensile strength test was used to evaluate the bonding between mortar and concrete, and to investigate if the splitting tensile strength of the mortar joints with one or two concrete/mortar interfaces was significantly less than that of pure concrete or pure mortar. The splitting tensile strength of the mortar joints was determined by either applying the load directly at the interface between concrete and mortar, or by applying the load at the center of the mortar joint for specimens with two concrete/mortar interfaces. Figure 20 shows the splitting tensile strength results for cores from mortar joints 1-a, 1-b and 4-b.

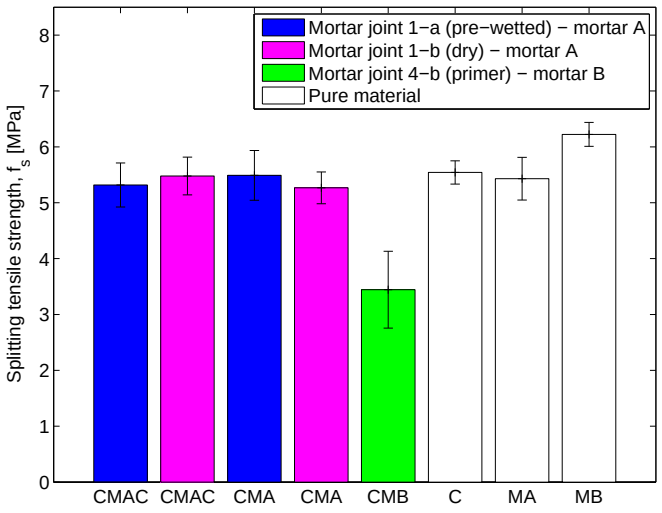

Figure 20: Average splitting tensile strength for pure mortar A (MA) and pure mortar B (MB), pure concrete (C) and concrete/mortar joints. Two different mortar joint configurations were tested: one where the load was applied directly at the concrete/mortar interface (CMA and CMB for mortars A and B, respectively) and one where the load was applied at the center of the 20 mm-wide mortar joint for specimens with two concrete/mortar interfaces (CMAC for mortar A).

For mortar A, Figure 20 shows that there is no statistical difference between the splitting tensile strength of the pure mortar specimens, the pure concrete specimens and the mortar joint specimens. Nor is there any statistical difference in the splitting tensile strength between using pre-wetted and dry elements, or between specimens with two concrete/mortar interfaces where the load was applied directly at the concrete/mortar interface or in the mortar. As far as the bonding is concerned, this indicates that the joints cast with mortar A using dry or pre-wetted concrete elements were no weaker than pure mortar A or concrete. In tests where the load was applied directly at the concrete/mortar interface, the crack propagated along the interface, as expected. However, in the tests where the load was applied in the mortar, the crack propagated through the mortar, or through the concrete/mortar interface, or through the concrete. The last-mentioned shows a particularly strong bonding between concrete and mortar.

However, for mortar B, Figure 20 shows that the splitting tensile strength of specimens with concrete/mortar interfaces decreases by 45% compared with pure mortar B, and by 38% compared with pure concrete specimens. We do not believe that the decrease in splitting tensile strength is influenced by a change from mortar A to mortar B, because the two mortar products have similar strength properties. Therefore, we believe that the decrease in splitting tensile strength is entirely due to the surface state of the concrete elements. For mortar joint 4-b, the concrete elements were pretreated with a primer, whereas the concrete elements for mortar joints 1-a and 1-b were either pre-wetted with water or left dry. The primer used in this study was an alkali-resistant latex emulsion, which means that it was impermeable for the mortar. If a primer that was not alkali-resistant had been used, the bonding between concrete and mortar might have improved because that would have allowed the mortar to react with the primer. We did not investigate this in this study, but we do consider it to be a possible solution for improving the splitting tensile strength of the joints.

3.3. Capillary absorption in mortar joints

Figure 21 shows the results from the capillary absorption tests for mortar joint 1-a. The average amount of absorbed water for four different types of specimen are shown: pure mortar specimens, pure concrete specimens, joint specimens with half concrete and half mortar (see specimens W2 and W8 in Figure 5), and joint specimens with mortar between concrete (see W4 and W5 in Figure 5). The results for mortar joint 1-b are omitted because the exact same tendency was observed for this mortar joint.

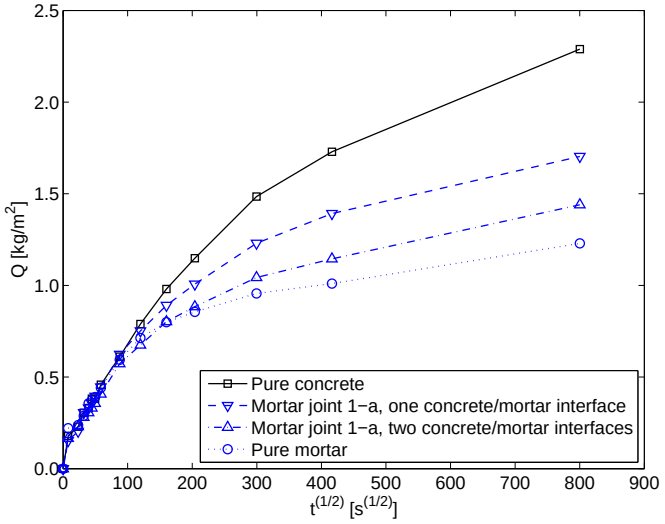

Figure 21: Average amount of absorbed water, Q, during capillary absorption tests for pure concrete (cores W3 and W7 in Figure 5), pure mortar (cores W1 and W8 in Figure 5), and two different mortar joint configurations for specimens taken from mortar joint 1-a (cores W2, W4, W5 and W6 in Figure 5). The exact same tendency was observed for mortar joint 1-b.

Figure 21 shows that the amount of absorbed water for mortar joint 1-a was dependent on the amount of concrete, and not on whether or not a specimen represented a pure material, or had one concrete/mortar interface or two. The water absorption of the four different types of specimen is ranked according to the volume of concrete. The more concrete, the higher the water absorption since the concrete is seen to have a higher absorption than the mortar. This explains why the mortar joint specimens with half concrete and half mortar had a higher absorption than the sandwich joint specimens that had a smaller volume of concrete.

Table 4 shows that there were cracks present in mortar joint 1-a along the upper inclined concrete/mortar interface in the upper recesses. The specimens with half concrete and half mortar were drilled from the upper inclined edges in the recesses because it was interesting to investigate whether entrapped air would influence the results. Figure 21 shows that this is not the case, because the water absorption of these specimens is not increased when compared with the remaining specimens. This is because the crack formation along the concrete/mortar interface is so fine that it does not allow an increase in water transportation. Thus, the results from the capillary absorption test indicate that, with a placing depth of 2.40 m, it is possible to cast mortar joints that do not have any problems with increased water absorption at the joint interface between concrete and mortar.

3.4. Freeze-thaw durability of mortar joints

Figure 22 shows the surface scaling due to freeze-thaw as a function of the number of freeze-thaw cycles for specimens taken from mortar joints 1-a and 1-b.

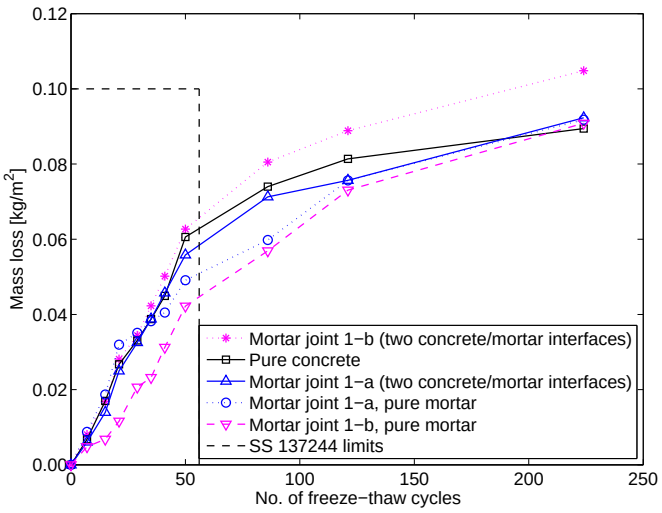

Figure 22: Average mass loss in freeze-thaw test of cores drilled from mortar joints 1-a and 1-b. The results distinguish between pure mortar (core F3 in Figure 5), pure concrete (cores F1 and F5 in Figure 5) and mortar joints with two concrete/mortar interfaces (cores F2 and F4 in Figure 5). The requirement to classify the frost durability of concrete as 'very good' according to the SS 137244 standard [11] is also shown.

The pure mortar specimens from mortar joints 1-a and 1-b all had a visible shrinkage crack extending from one side of the specimen to the other (see Table 3). However, Figure 22 shows that the extension of this crack did not influence the freeze-thaw durability of the mortar joints because no increased scaling was

observed for these pure mortar specimens. We believe the reason to be that the crack formation was so fine that water ingress into the crack was very slow, as we also concluded from the capillary absorption tests.

Figure 22 shows that no significant difference in the amount of surface scaling was observed between the different types of specimen. The pure mortar specimens had the smallest amount of surface scaling during the first 100 frost cycles, but the difference was minimal from then onwards. The surface scaling of mortar joint 1-b was slightly higher than for the other joints. According to the Swedish Standard (SS) 137244 [11], the freeze-thaw durability of concrete is classified as 'very good' if the mass loss after 56 frost cycles does not exceed 0.10 kg/m^2. Figure 22 shows that, even after 224 frost cycles, the mass loss of mortar joint 1-b was the only one that exceeded this criterion, and this did not occur until after 200 frost cycles. Overall, this indicates a very good freeze-thaw durability of the mortar joints, and that no problems with freezing and thawing of the mortar joints in Pearl-Chain Bridges should be expected.

3.5. Chloride ingress in mortar joints

The average chloride migration coefficient for the concrete and mortar from phases 1–4 is summarized in Table 5.

Table 5: Chloride migration coefficients, $D \times 10^{12}$ [m^2/s], for concrete and mortars A and B.

	Concrete	Mortar A	Mortar B
Average	5.93	1.22	7.21
Standard deviation	1.95	0.46	0.41

The results shown in Table 5 cannot be directly compared since the concrete and mortars were tested at different maturity ages. The concrete was tested after 70 days, whereas the mortar was tested after 28 days. The migration coefficients in Table 5 indicate that the mortars both have a good resistance against chloride ingress. Guiding values for the chloride migration coefficient for concrete with a maturity of 28 days are suggested in [13]. Concretes and mortars with chloride migration coefficients less than 8×10^{-12} m^2/s are defined as having a 'good' chloride resistance, and concretes and mortars with chloride migration coefficients less than $4{\times}10^{-12}$ m^2/s are defined as having a 'very good' chloride resistance. The locations from which the specimens were taken did not influence the results.

3.6. Concluding remarks

The experiments in the present study were designed to focus on the concrete/mortar interface itself. We tested for ways in which the interface influenced different durability parameters compared with the durability parameters of pure concrete and pure mortar. If the results for the specimens with one or two concrete/mortar interfaces did not deviate significantly from those for pure concrete and pure mortar, we concluded that the interface did not influence the durability. The overall focus was to test whether the presence of the interface caused any increased water and/or chloride transportation, whether it increased scaling during freeze-thaw, or whether it caused reduced splitting tensile strength due to poor bonding. In this study, we performed capillary absorption tests and freeze-thaw tests on specimens cast with mortar A, and in both tests the interface did not significantly influence the results. Furthermore, because the rapid chloride migration tests did not show any crack formation along the interface when using mortar B, we also believe that the interface would neither influence the capillary absorption results, nor the freeze-thaw results, if the mortar joints had been cast with mortar B.

4. Conclusions

In this study, the durability properties of 2.40 m-high, vertically cast mortar joints in Pearl-Chain Bridges were tested when using a commercialized high-strength, expansive and self-compacting mortar product. The joint thickness was 20 mm, but was widened around the ducts enclosing the post-tensioning wires. The main conclusions from the study can be summarized as follows:

1. It is essential for the durability of the mortar joints in Pearl-Chain Bridges that they are cast with a mortar product with good expansion properties, including that the expansion of the mortar increases and remains constant without large variations. In this study, two mortar products, A and B, were tested. Mortar A had a final expansion of 0.07–0.43%, but one hour after mixing, the expansion peaked at a value approximately 0.14 percentage points higher than the final expansion, and this occurred again 12 hours after mixing. Mortar B had a final expansion of 0.70–0.90%, and five hours after mixing, the expansion peaked at a value approximately 0.04 percentage points higher than the final expansion. Mortar B was the only one that did not cause problems with shrinkage crack formation. It is believed that the reason for this is a combination of two factors: firstly, the final expansion of mortar B was twice as large as that of mortar A; and secondly, the second expansion peak of mortar A occurred after the mortar had set, and consequently this introduced significant shrinkage stresses in the mortar.
2. It cannot be assumed that commercialized mortar products described as 'expansive' have any significant expansion, and therefore tests should be made to determine the actual expansion.
3. To avoid increased chloride ingress along the interface between concrete and mortar, an alkali-resistant latex emulsion was sprayed on the concrete surfaces, thus reducing the porosity of the interface.
4. The bonding between concrete and mortar was good when the concrete elements were either dry or pre-wetted with water before casting the mortar. In such cases, the splitting tensile strengths of pure concrete specimens, of pure mortar specimens, and of mortar joint specimens with two concrete/mortar interfaces, were all statistically equivalent. However, when the concrete surfaces were pre-treated with an alkali-resistant latex emulsion (primer), the

splitting tensile strength of the mortar joint specimens decreased by 45% compared with the pure mortar. It is believed that the splitting tensile strength of the joints could be improved by changing the primer to a product that is not alkali-resistant.

5. At the interface between concrete and mortar, the mortar joints were considered to be resistant against increased water ingress, because the capillary absorption of specimens with a concrete/mortar interface did not deviate from that of pure concrete or pure mortar. This was also the case for specimens with a fine crack formation along the interface, because the crack was too fine to make a difference.
6. The freeze-thaw durability of the mortar joints was classified as 'very good' according to the SS 137244 standard [11]. The freeze-thaw durability of the mortar joint specimens did not deviate from that of pure concrete or pure mortar. No increased scaling of the pure mortar specimens was observed even though there was a fine crack propagating through them.This was because the crack was too fine to make a difference.
7. The rapid chloride migration tests [8] proved to be an easy and efficient way to visualize possible cracks in the mortar and in the concrete/mortar interface. The chloride resistance of the mortar was considered to be good. No increased chloride ingress took place in the concrete/mortar interface.

Acknowledgments

The authors wish to thank Innovation Fund Denmark for supporting this project.

References

[1] Halding PS, Hertz KD, Schmidt JW. Precast Pearl-Chain concrete arch bridges. J Eng Struct, 2015;103:214–27.
[2] Hertz KD, Castberg A, Christensen J. Super-light concrete decks for building floor slabs. Structural Concrete Journal of the fib. 2014;3.
[3] Hertz KD. Super-light SL-Deck elements with fixed end connections. In: Proceedings of fib Symposium; 2015 May 18–20; Copenhagen. p. 465–66.
[4] Halding PS, Hertz KD, Petersen NEV, Kennedy B. Assembly and lifting of Pearl-Chain arches. In: Proceedings of fib Symposium; 2015 May 18–20; Copenhagen. p. 185–86.
[5] Aalborg Portland. Cement and Concrete. Handbook of cement, concrete and mortar. 19th ed. Aalborg, Denmark: Aalborg Portland; 2010. 162 p. Danish.
[6] ISO Standard 4108. Concrete – Determination of tensile splitting strength of test specimens. London: International Standard; 1980.
[7] DS/CEN/TS Standard 12390-9. Testing hardened concrete – Part 9: Freeze-thaw resistance – Scaling. Copenhagen: Danish Standards; 2006.
[8] NT BUILD 492. Concrete, mortar and cement-based repair materials: Chloride migration coefficient from non-steady-state migration experiments. Finland: Nordtest; 1999, ISSN 0283–7153.
[9] Jensen OM, Hansen PF. A dilatometer for measuring autogenous deformation in hardening Portland cement paste. Mater Struct. 1994;28:406–09.
[10] ASTM Standard C1698-09. Standard Test Methods for Autogenous Strain of Cement Paste and Mortar. West Conshohocken, PA: ASTM International; 2009.
[11] SS Standard 137244. Concrete testing – Hardened concrete – Scaling at freezing. Stockholm: Swedish Standards; 2005.
[12] Neville AM. Properties of concrete. 4th ed. Essex: Pearson Education Limited; 1995.
[13] Hasholt MT. Durability. Main report. Taastrup, Denmark: Danish Technological Institute, Center for green concrete; 2002. Danish.

CHAPTER 4

Durability of lightweight aggregate concrete in Pearl-Chain arches

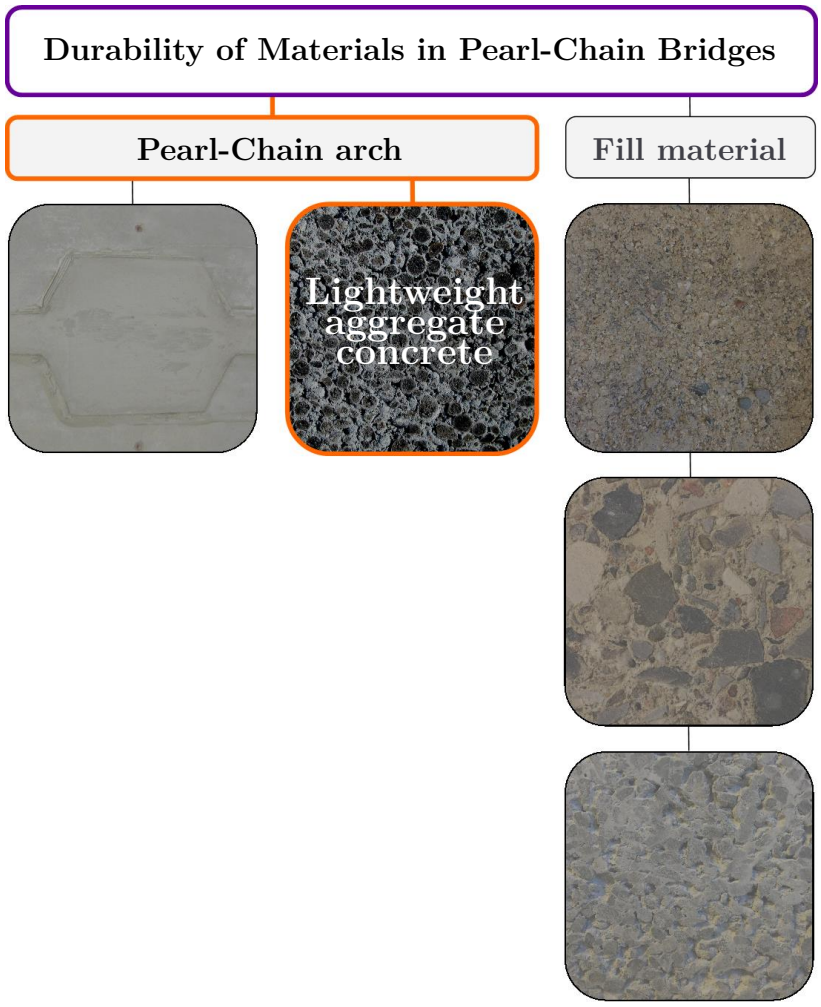

4.1 Introduction to lightweight aggregate concrete

Regular lightweight aggregate concrete (LWAC) blocks composed from a standard mix cannot be used in Pearl-Chain Bridges because they cannot resist the harsh exposure during winter months when bridges freeze and thaw and deicing salt is used. The LWAC mix design for Pearl-Chain Bridges must be designed to have strong freeze-thaw durability, which has not been considered previously for LWAC in Denmark.

Although no LWAC freeze-thaw standards exist, literature provides examples of several different freeze-thaw test methods for determination of internal frost damages of LWAC. Klieger and Hanson (1961) used $7.6 \times 7.6 \times 28.6$ cm^3 prisms that were frozen and then thawed in tap water. The temperature varied between -23°C to 13°C; two frost cycles were obtained per day, and after 300 frost cycles, the tests were terminated. Chandra *et al.* (1982) used $25 \times 25 \times 25$ cm^3 cubes that were frozen in a saturated NaCl solution at -20°C for eight hours and thawed in tap water at 20°C for 16 hours. After 50 frost cycles, the tests were terminated. Whiting and Burg (1991) followed the ASTM C666 standard (ASTM C666, 2008) in which $7.5 \times 10 \times 40$ cm^3 beams were frozen and thawed in water during six frost cycles per day at a temperature varying between -18°C to 4°C. Various numbers of freeze-thaw cycles were tested. Also, a large variety of test methods have been adopted for determination of LWAC surface scaling under the influence of salt (Klieger and Hanson, 1961; Chandra and Berntsson, 2002).

Several studies have shown that it is possible to improve the freeze-thaw durability of LWAC by increasing the entrained air content (Klieger and Hanson, 1961; Chandra and Berntsson, 2002). In their comprehensive work, Klieger and Hanson (1961) tested nine different lightweight aggregates (LWAs) and one normal density aggregate for LWAC. Both air-entrained and non-entrained LWAC were mixed for all aggregates; moreover, both air-dried and water saturated aggregates were used, and two different LWAC strengths were tested, all together providing a large experimental data set. The study's main conclusions were that (1) the use of entrained air improves the freeze-thaw durability of LWAC, (2) entrained air can be used to make LWAC as resistant to deicing salts as conventional concrete with entrained air, (3) the amount of entrained air required for adequate frost durability of LWAC is similar to that of conventional concrete, (4) the moisture content of the LWA significantly influences the freeze-thaw resistance because LWAC cast with air-dried LWA showed better freeze-thaw durability than LWAC cast with soaked LWA, and (5) the LWA properties influence the freeze-thaw durability significantly, as normal density aggregates used in conventional concrete. Therefore, three main parameters are known to determine the freeze-thaw durability of a particular LWAC mix:

1. The entrained air content
2. The LWA moisture content before mixing
3. The LWA properties (frost resistance, porosity, stiffness, strength etc.)

The strength properties of LWAC have been shown to influence the LWAC freeze-thaw durability to some degree (Chandra and Berntsson, 2002). Moreover, the LWA strength properties influence those of the LWAC, which is discussed further in Section 4.2.2.

In general, when working with LWA, the moisture content is particularly important because LWA is highly porous and can hold a large amount of water. Water absorbed by the LWA before setting is not considered part of the effective w/c-ratio of a LWAC mix (Castro *et al.*, 2011). Hence, unless the water absorption is known, the effective w/c-ratio of a particular mix design will be impossible to control. Castro *et al.* (2012) showed that a particular type of oven-dried expanded shale absorbed 71% of the 24-hour absorption value when it was initially pre-soaked with the mixing water for five minutes and subsequently mixed with cement and normal density aggregate. This result was in good agreement with the five minutes absorption value, which was determined to be 63% of the 24-hour value. The results indicate that an additional amount of water, corresponding to 71% of the 24-hour absorption value, should be added to the free water to obtain the desired w/c-ratio. If no additional water is added, the LWA absorbs free water, which decreases the effective w/c-ratio. On the other hand, if too much water is added, LWA cannot absorb it all, and the effective w/c-ratio increases. Because the absorption characteristics of all LWAs are different, it is extremely important to determine the water absorption properties of a particular LWA before using it for LWAC.

The "surface dry" condition for LWA is defined as the condition in which LWA neither contributes water to nor absorbs water from an LWAC mix (Castro *et al.*, 2011). The surface dry condition can be determined with a number of methods. A standard test method for determination of the water absorption of LWA is described in the DS/EN 1097-6 standard, Appendix C (DS/EN 1097-6, 2013). In this test method, oven-dried LWA is immersed in water for a certain period of time, after which it is dried to a surface dry condition by gently rolling it in a cloth for a maximum of 15 seconds until no surface water can be seen. A similar procedure is suggested by the Department of Transportation for the State of New York, as cited in Chandra and Berntsson (2002). The method used to determine the water absorption of normal density aggregates, the ASTM C128 standard (ASTM C128, 2012), also is commonly used for LWA (Castro *et al.*, 2011). Another is the cobalt chloride method in which a color shift from blue to pink indicates the presence of water at the LWA surface (Castro *et al.*, 2011).

At most LWAC mixing plants, the LWA is transported on a belt and sprinkled with water on its way to the mixer; however, the LWA's exact moisture content cannot be controlled. The purpose of this process is to ensure that the LWA is sufficiently wet to prevent it from absorbing any free water from the mix; but because the procedure results in additional free water in the mixture, the mix design subsequently has to be corrected to reach the desired w/c-ratio. The correction is based on experience and an assessment of whether a given mixture is too wet. At mixing plant A, the LWA is not pre-wetted, and the water correction is performed solely by assessing the LWAC moisture content in the mixer.

In this study, the LWAC mix design used for SL-Decks for indoor usage was tested with respect to the 28-day compressive strength, density, and freeze-thaw

durability to determine its applicability for SL-Decks for Pearl-Chain Bridges. As a result, an improved LWAC mix design for Pearl-Chain Bridges is suggested. This mix design was developed under controlled laboratory conditions by measuring and controlling the LWA water absorption. This chapter describes the work carried out to (1) develop a non-subjective method for determination of the water absorption properties of LWA; (2) optimize the strength and density of LWAC compared with the current mix design for SL-Decks for indoor usage; and (3) design the LWAC to be resistant to freeze-thaw. To achieve full durability of LWAC in Pearl-Chain Bridges, the moisture-dependent shrinkage also must be considered because it can be expected to differ from that of conventional concrete in the SL-Decks and can potentially cause movements. However, this study did not address shrinkage.

4.2 Experimental method for LWAC

In this study, four different LWAC mix designs were considered: two mix designs used at mixing plant A for SL-Decks for indoor use (mix designs A), and two mix designs developed in this study for use in SL-Decks for Pearl-Chain Bridges (mix designs D).

4.2.1 LWAC material properties

Figure 4.1a shows the gradations of three types of light expanded clay aggregate (Leca) from Weber Denmark considered in this study: Leca 0–4 mm, Leca 2–4 mm, and Leca 4–10 mm. For mix designs A, Leca 0–4 mm and Leca 4–10 mm were used; however, for mix designs D, Leca 2–4 mm was used rather than Leca 0–4 mm for three reasons: First, the variation in gradation between different deliveries of Leca 0–4 mm was large; second, the fines content of Leca 0–4 mm was high (Figure 4.1a); and finally, the water absorption of Leca 0–4 mm could not be determined because of the high fines content, which would make it very difficult to control the amount of free water in the LWAC mix.

Figure 4.1b shows the water absorption of Leca 2–4 mm and Leca 4–10 mm as a function of time. Water absorption levels after 5, 15, and 60 minutes are listed in Table 4.1, together with the dry particle density of the two Leca fractions. Descriptions of the procedures used to determine the water absorption and dry particle density can be found in Section 4.2.5.1 and Section 4.2.5.2, respectively.

Table 4.1: Dry particle density, ρ_d, and water absorption, w, after 5, 15 and 60 minutes for Leca 2–4 mm and Leca 4–10 mm.

	ρ_d [kg/m^3]	w [%]		
		5 min.	15 min.	60 min.
Leca 2–4 mm*	663	18.4	20.9	24.0
Leca 4–10 mm*	526	22.6	26.6	30.5

* Based on three specimens.

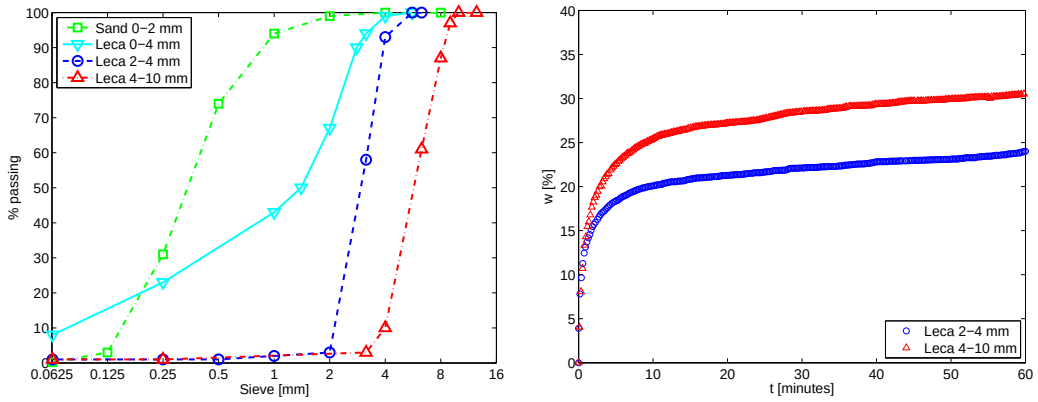

(a) Gradation curves. (b) Water absorption as function of time.

Figure 4.1: Gradation curves for Leca 0–4 mm, Leca 2–4 mm, Leca 4–10 mm, sand 0–2 mm, and water absorption as function of time for Leca 2–4 mm and Leca 4–10 mm.

As fine aggregate, 0–2 mm of quarry sand was used; Figure 4.1a shows the gradation. The sand had a density of 2,650 kg/m^3 and 0.20% absorption. Also used were Portland cement, CEM II/A-LL 52.5 N, with a particle density of 3,100 kg/m^3, and Danish fly ash type B4 with a particle density of 2,300 kg/m^3. Finally, a combination of natural and synthetic AEA was used.

4.2.2 Mix design of LWAC

In this study, the mix design of LWAC was characterized by trial and error. No standardized method exists to design LWAC mix for LWAC blocks, and in general, the process is based on experience and can vary from mixing plant to mixing plant. In this study, the point of origin was a LWAC mix design, with a dry density of 700 kg/m^3, that had previously been used at a Danish LWAC mixing plant. However, the mix design had to be modified because different materials were available and other requirements for the LWAC's strength and durability existed.

Two different mix designs were made, one with fly ash (mix D-1) and one without (mix D-2). More than 30 different mix designs were tested to find the amount of air entrainment, aggregate proportions, water content, and so on, that would provide the desired density and workability. Table 4.2 shows the final mix designs used in this study. The table also shows two LWAC mix designs that have been used at mixing plant A for SL-Decks for indoor use. The production of SL-Decks is very new, and therefore, several LWAC mix designs have been tried in an attempt to find the optimal. Because I had no influence on these two mix designs, they are listed only for comparison. The remainder of this section concerns mix D-1 and D-2.

The most important assumptions and findings made during the trial and error design of mix D-1 and D-2 were as follows:

- **Void content:** The void content was defined as the large open voids between

Table 4.2: Two LWAC mix designs, A-1 and A-2, used at mixing plant A for LWAC in SL-Decks for indoor use, and suggestion of two new mix designs, D-1 and D-2, with improved strength and durability properties.

	Mixing plant A		DTU	
	Mix A-1	Mix A-2	Mix D-1	Mix D-2
Date	Oct. 18, 2013	Feb. 21, 2014	Nov., 2015	
Cement [kg/m^3]	187.5	178.0	114.4	129.3
Fly ash [kg/m^3]	-	-	29.8	-
Free water [kg/m^3]	75.0*	80.0*	65.4	66.5
Air entrainment [kg/m^3]	-	-	1.87†	0.78†
Sand 0–2 mm [kg/m^3]	72.2	265.0	120.4	121.9
Leca 0–4 mm [kg/m^3]	-	36.2‡	-	-
Leca 2–4 mm[kg/m^3]	-	-	118.3(99.9)§	119.7(101.1)§
Leca 4–10 mm [kg/m^3]	216.7‡	176.7‡	230.1(187.6)§	233.8(190.7)§
Fresh density [kg/m^3]	609.3‖	765.8‖	680.5	672.7
Dry density** [kg/m^3]	675.4‖	853.1‖	682.8	674.7

* For mixes A-1 and A-2, the water amount included free water *and* water absorbed by the Leca particles. Hence, mixes A-1 and A-2 contained considerably less free water compared with mixes D-1 and D-2. Consequently, the fresh density of mix A-1 was considerably less than those of mixes D-1 and D-2 even though the dry density of mix A-1 was in the same size as that of mixes D-1 and D-2.

† The mass of AEA diluted in water in the ratio 1:2.

‡ For mixes A-1 and A-2, the mass of Leca included an unknown amount of absorbed water.

§ Mass of Leca that has absorbed a water amount corresponding to the five-minute water absorption value (the Leca particles were dried at 105°C for 24 hours prior to absorption). The value in brackets is the dry mass of the Leca particles.

‖ For mixes A-1 and A-2 the original mix design assumed a total void content of 43% and 37%, respectively, before compaction. It was impossible to achieve such high void contents with the aggregates used; hence, mixing plant A's mix designs were mistaken, and the densities have been corrected by assuming a void content of 30% instead.

** Assuming 23% of the water is bound by cement (Powers and Brownyard, 1948), and the volume is compacted 15%. For mixes A-1 and A-2 the dry density is based on the mass of Leca particles containing an unknown amount of water; however, because the Leca particles were stored under a roof at mixing plant A and thus not directly exposed to water, the moisture content is expected to be low.

the aggregates, that is, the voids did not include entrained air in the cement paste. In both mix design D-1 and D-2, the void content was assumed to be 30%. Leca 2–4 mm and Leca 4–10 mm were both relatively well sorted (Figure 4.1a), which made it impossible to achieve optimum package; however, because hard compaction was applied during the preparation of the specimens (Section 4.2.3), the void content was assumed to decrease to 15%.

- **Entrained air content:** For mix designs D-1 and D-2, the entrained air content was assumed to be 3.0%, and sufficient to resist freezing and thawing. For conventional concrete exposed to an aggressive or extra aggressive environment, the entrained air content of the fresh concrete should be minimum 4.5% (DS 2426, 2011). However, this requirement cannot be immediately adapted to LWAC because the entrained air is present in the cement paste and the cement paste content of LWAC varies from that of a conventional concrete.

Therefore, a more relevant consideration was the entrained air content in the cement paste itself. Based on the mix design of mixes D-1 and D-2, an entrained air content of 3.0% corresponds to an air content in the cement paste of 22%. Here, the cement paste includes the volume of cement, fly ash, water, *and* entrained air, and the term "cement paste" should be considered as such throughout this chapter. Such entrained air contents were achieved by using an AEA dosage of 1.3% and 0.6% of the powder mass for mixes D-1 and D-2, respectively. The dosage was higher for mix D-1 because it contained fly ash that is known to consume AEA. Assuming that the volume of cement paste in a typical conventional concrete constitutes 25% of the total concrete volume, an entrained air content of 4.5% in the concrete corresponds to an air content of 18% in the cement paste. Hence, an entrained air content of 22% in the cement paste of LWAC was considered sufficient to resist freezing and thawing, based on typical requirements for conventional concrete.

- **w/c-ratio:** The strength of LWAC is very much determined by the strength of the LWA, which is the weakest link, rather than the cement paste. Therefore, a low w/c-ratio is typically not used for LWAC. The amount of cement paste in the mix design should be carefully chosen. If the amount of cement paste is too high, excess paste drains off the LWA and collects at the bottom of the mold which is not desired. On the other hand, if the amount of cement paste is too low and does not coat all LWA particles, the strength of the LWAC decreases. Cement paste can be adjusted by changing the amount of cement, water, or both. In this study, the amount of cement was kept constant, and when excess cement paste was observed to drain off the aggregates, the water was reduced. Figure 4.2 illustrates how a variation in w/c-ratio was used to control the amount of cement paste. When the water was decreased, all other parameters were kept constant, except the amount of Leca 4–10 mm, which was increased to keep the total volume constant. A final w/c-ratio of 0.52 was chosen. However, for LWAC, the w/c-ratio is usually not used to characterize strength, and neither was it applied in this study.

(a) w/c = 0.60. (b) w/c = 0.55. (c) w/c = 0.52.

Figure 4.2: End surface of three LWAC cylinders with different w/c-ratios.

- **Free water:** The water amounts for mixes D-1 and D-2 shown in Table 4.2 represent the amount of free water in the mixture, that is, water that is free to

react with for cement. Because the void content of LWAC is high, the surface area exposed to the surrounding climate during the hydration process is large; therefore, if curing is not performed under completely sealed conditions, the water evaporation from LWAC during hydration is large. Typically, LWAC is designed with a high content of free water to ensure the best conditions during hydration.

- **Dry LWA:** At most LWAC mixing plants, the amount of LWA used for a given batch is not based on a mass consideration, like the aggregates for conventional concrete, but rather on a volume consideration because pre-wetted LWA with an unknown moisture content is used rather than dry LWA. The LWA is transported on a belt and sprinkled with water; however, this process makes it impossible to control the exact moisture content of the LWA. The mass of LWA is extremely dependent on the moisture content, first, because the water absorption of LWA is much higher than for typical aggregates used for conventional concrete, and second, because the particle density of LWA is considerably less than the density of water (Table 4.1). The exact moisture content of LWA is impossible to control unless the LWA is either dried or water saturated, and only in such two cases is it sensible to apply a mass consideration when mixing LWAC. Therefore, LWAC mixing plants use a volume consideration to obtain the same amount of LWA in each mix. For this study, however, the LWA was dried in an oven at 105°C for 24 hours before mixing, and a mass consideration was applied. This process allowed complete control of the moisture content in the mixes. As a result, better and more consistent strength and durability results were obtained.

- **Density:** For LWAC, the highest density constituents are cement, fly ash, and sand. Therefore, to increase the LWAC density, these constituents should be increased, which also requires the water content to be increased to keep the w/c-ratio constant (as discussed above). The addition of extra cement paste and/or mortar reduces the void content. As the ratio between the amount of cement paste and LWA increases, at a certain point, the excess cement paste will drain off the aggregates; hence, there is a limit to how much the levels of high-density constituents can be raised. Therefore, there is a natural limit to the highest possible density a given mix can obtain. Because the water absorption of Leca is high, the fresh LWAC density can be expected to deviate considerably from the dry LWAC density due to LWA water evaporation. Cement is assumed to bind 23% of the free water. In this study, the dry density of the LWAC mix design was intended to be 700 kg/m^3 (Table 1.2). Table 4.2 shows the fresh density of the non-compacted LWAC, and the dry density of the same mixes compacted 15% and having 23% of the free water bound. The densities are slightly lower than 700 kg/m^3.

4.2.3 Preparation of LWAC specimens

For mixes A-1 and A-2 the LWAC blocks used for testing were delivered directly from mixing plant A.

For mixes D-1 and D-2, all aggregates (Leca 2–4 mm, Leca 4–10 mm and sand 0–2 mm) were dried in an oven at 105°C for 24 hours and subsequently cooled to room temperature. Next, Leca 2–4 mm and Leca 4–10 mm were mixed for five minutes in a rotating drum mixer with the amount of free water indicated in Table 4.2 and additional water corresponding to the five-minute absorption value (Table 4.1). The assumption was that the Leca particles would absorb the amount of water corresponding to the five-minute absorption value and leave the free water available to react with cement and fly ash. Figure 4.1b shows that the water absorption of Leca is initially large, but decreases with time. After five minutes, Leca 2–4 mm and Leca 4–10 mm reached 77% and 74%, respectively, of their 60-minute absorption values; therefore, after five minutes, any further water absorption of the Leca particles during the LWAC mixing process could be assumed to be insignificant. The water absorption of Leca particles mixed with water for five minutes in the rotating drum mixer also was assumed to correspond to the five-minute water absorption of Leca, determined in the absorption test. Subsequently, cement, fly ash, and sand were added to the mix and mixed for 15 seconds before AEA was added and mixed for three minutes. The AEA was diluted 1:2 in water that was subtracted from the free water. Afterwards, the mass of LWAC corresponding to the volume of the final block was calculated from the fresh mix design density, and placed in the LWAC block machine shown in Figure 4.3. Because a certain compaction of the fresh LWAC would occur, an additional mass of LWAC ideally should have been added; however, after compaction, the height of the LWAC block seemed to agree well with the desired dimension of 190 mm (Figure 1.9). As discussed in the following sections, the compaction provided by the block machine was less than expected.

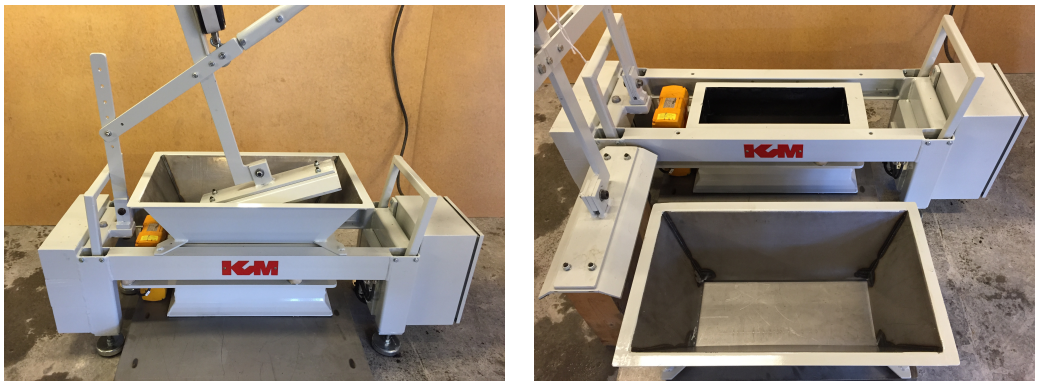

(a) LWAC block machine with collar attached. The cap is placed in position for compacting the LWAC in the mold. During compaction the cap levels out.

(b) LWAC block machine with collar detached from mold. The cap is placed in position for filling the mold with LWAC.

Figure 4.3: LWAC block machine for casting a single LWAC block having the same geometry as the LWAC blocks in the SL-Decks.

The LWAC block machine was specially fabricated for this study to produce blocks with the same geometry as those in the SL-Decks. Figure 4.3a shows the

LWAC block machine placed astride a casting table consisting of a 10-mm metal plate welded on to a steel frame. The mold and casting table were separated by a distance of 5 mm to avoid vibrations from the LWAC machine. The geometry of the mold was identical to that of the LWAC blocks in the SL-Decks (see Figure 1.9). A steel collar was attached on top of the mold to ease filling. Two horizontal vibrators were installed in one end of the mold, each with a maximum impact force of 1,760 N, and a rotational speed of 3,000 rev./min. at 50 Hz. The amplitude was not measured, but was expected to be 2.5 mm similar to that at the LWAC block machine for SL-Decks where the same vibrators are used. A "cap" was mounted on a 2.0 m-long handle that could be lifted and rotated 90 degrees (Figure 4.3). The force applied during compaction was measured from a scale attached to the handle. During compaction, vibration was turned on, and when the desired mass of LWAC was placed in the mold, the cap was rotated and pressed down. Steel blocks installed as ballast at one end of the mold prevented the mold from lifting when pressure was applied. Between 250–300 kg of pressure was applied for approximately one minute, after which the vibration was stopped and the LWAC block machine was lifted and removed. Figure 4.4a shows a LWAC block immediately after removal of the mold.

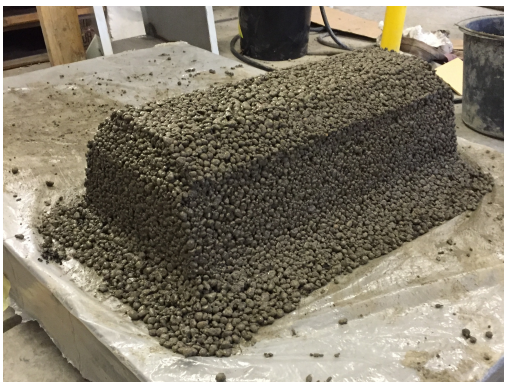

(a) LWAC block immediately after casting. Immediately after removal of the mold, the block was covered in three layers of plastic.

(b) Test setup for strain measurements of LWAC. Two rigid rings were each tightly fastened to the specimen with three screws, and two extensometers were placed between the rings on opposite sides.

Figure 4.4: Fresh LWAC immediately after casting, and hardened LWAC in test setup for determination of Young's modulus.

The LWAC was tightly covered with three layers of plastic to prevent any moisture evaporation. After 24 hours, the block was removed to a 40°C water bath.

4.2.4 Determination of LWAC air void content

4.2.4.1 Determination of entrained air content in fresh LWAC

The entrained air content in the fresh LWAC was measured with a so-called "roll-a-meter". The void content of the LWAs themselves is large, and therefore, a press-ur-meter cannot be used to measure the air content in fresh LWAC, as with

conventional concrete, because the void content of the LWA would be mistakenly included in the reading. The roll-a-meter works on the principle that entrained air is released – and measured – when rolling the air meter apparatus filled with fresh LWAC and an isopropyl alcohol solution, a procedure described in the ASTM C173 standard (ASTM C173, 2014). In this study, stable readings were obtained with 500 ml isopropyl alcohol (70 volume-%). Furthermore, a grid was installed at the bottleneck to prevent the LWA from ascending and disturbing the readings. A comparison of the entrained air content in a conventional concrete mixture measured in a press-ur-meter test and a roll-a-meter test verified that the grid did not disturb the readings. The air void content was measured for all LWAC mixes made – even though the mix design was the same – in order to determine the entrained air content of all LWAC blocks cast.

4.2.4.2 Determination of void content of hardened LWAC

Determination of the void content of hardened LWAC was complicated by the fact that LWAC density is less than water density, which precludes using Archimedes' Law to measure the mass of the LWAC specimen under water. Instead, the void content was assessed by wrapping plastic around the sides and one end surface of LWAC cylinder cores (drilled from the LWAC blocks), which measured 140 mm high and 100 mm in diameter. A container was filled with a liter of water, and that water was slowly poured onto the top of the cylinder core not covered by plastic. When the water reached the top, the remaining water in the container was weighed, and the difference between that amount and the initial liter represented the volume of the voids in the specimen.

4.2.5 Test setup for LWAC

4.2.5.1 Water absorption test setup for LWA

A standard test method for determination of the water absorption of LWA is described in the DS/EN 1097-6 standard, Appendix C (DS/EN 1097-6, 2013). This test method prescribes that dried LWA be immersed in water for a certain period of time, and then be gently rolled in a cloth for a maximum of 15 seconds until all surface water is gone (surface dry state). However, this test method is a subjective assessment, extremely dependent on the person performing the measurement. It is more difficult to control the amount of free water when mixing LWAC than with conventional concrete because LWA generally is more absorbant than aggregates used in conventional concrete. Also, LWA is seldom water saturated during mixing because it takes several hours or days to reach this state. Therefore, to control the free water in a LWAC mix, the absorption properties of the LWA must be well-known. During this study, another method – independent of the person performing the test – was developed to determine LWA absorption.

In this method, a representative sample of 100 g of either Leca 2–4 mm or Leca 4–10 mm, dried at 105°C for 24 hours and cooled and sieved at the 2 mm-sieve, were weighed and placed in a fabric net with a mesh size of 1 mm. The net was closed with non absorbant copper wire and attached to a steel plunger. The Leca particles

lay "loose" in the net to ensure that air was not caught between the particles. A tripod was placed on a scale, and an arm that was attached to the tripod held the steel plunger in a vertical position. The scale was connected to a PC that logged the mass every 10 seconds. A container that was big enough to contain the net with the Leca was filled with water and placed below the steel plunger holding the net, as shown in Figure 4.5.

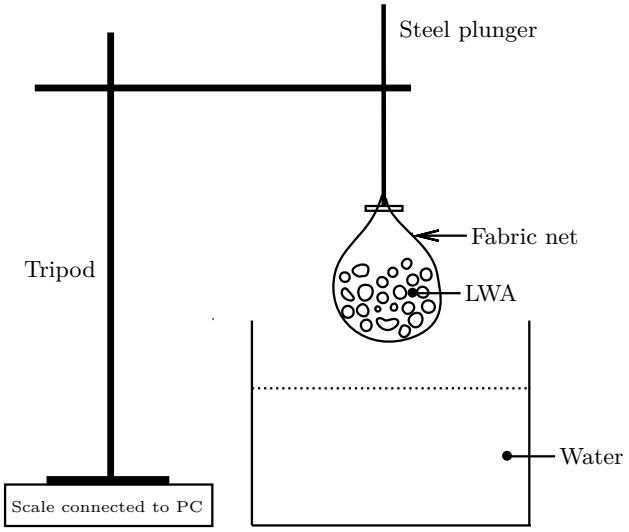

Figure 4.5: Water absorption test setup for LWA. A representative sample of 100 g of dried Leca particles were placed in a fabric net attached to a steel plunger and connected to a tripod. The tripod was placed on a scale connected to a PC that recorded the mass every 10 seconds. The Leca particles were immersed in water, and the water absorption of the Leca corresponded to the change in mass read from the scale.

Immediately after the PC logged the mass of the container with water, the net with Leca particles was immersed in the water. For the first five minutes, the net was gently massaged by hand between each measurement to remove air caught between the Leca particles. The test was finished after 60 minutes. In total, three tests were performed on both Leca 2–4 mm and Leca 4–10 mm. The mass read from the scale was the resultant force of (1) the gravity of the tripod, the arm, the steel plunger, and the net; (2) the gravity of the Leca particles and the water absorbed by the Leca particles; and (3) the buoyancy of the Leca, the net, and the part of the steel plunger below water. With time, the gravity of the Leca particles increased as they absorbed water; hence, the scale reading increased accordingly. Since all other forces were constant, the difference between the initial reading at t_0 and any subsequent reading described the mass of water absorbed by the Leca particles. However, the first measurement at t_1 was first taken approximately 10 seconds after immersion of the Leca particles. To find the initial measurement at t_0, the variation in mass during the first three measurement points was assumed to be linear, and the results found at t_1 and t_2 were extrapolated to find the mass at t_0 by assuming that $t_1 - t_0 = 10$ s. In Section 4.4.1 the uncertainty on the initial reading is discussed.

4.2.5.2 Dry particle density test setup for LWA

Leca 2–4 mm and Leca 4–10 mm were dried at 105°C for 24 hours and cooled. Next, a representative sample of 100 g of either Leca 2–4 mm or Leca 4–10 mm were weighed and poured into a container filled with impregnation ("SurfaPore-C"). A steel plunger was used to prevent the Leca particles from floating. After five minutes, the Leca particles were removed from the impregnation, allowed to drain in a sieve, and placed for 24 hours on a piece of baking paper that would not absorb the impregnation. When the impregnated Leca particles were immersed in water, the water level remained stable, indicating that the impregnation worked as expected and that the Leca particles did not absorb water after impregnation. Water was filled up to the zero line of a two-liter volumetric flask having a slender bottleneck for accurate measurement of the water level as shown in Figure 4.6.

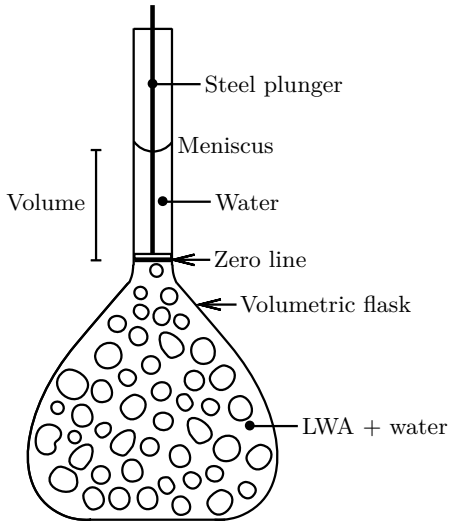

Figure 4.6: Dry particle density test setup. A representative sample of 100 g of dried impregnated Leca particles were immersed in water in a two-liter volumetric flask; the increase in water level corresponded to the volume of the Leca particles.

The zero line was drawn just above the point where the glass container discharged into the bottleneck. A measurement scale starting at the zero line was fastened to the bottleneck. 250 ml of the water were poured into a 250-ml glass container. The Leca particles were then poured into the two-liter volumetric flask, and a steel plunger with a perforated plate was placed at the bottom of the bottleneck to prevent the Leca particles from ascending into the bottleneck. The 250 ml of water were poured back into the two-liter container, and the container was rotated and tapped to allow air bubbles between the Leca particles to escape. The rise in water level between the zero line and the new water level corresponded to the total volume of the Leca particles; however, the rise in water level was corrected to account for the volume of the steel plunger under water. The ratio between the dry mass of Leca particles and their volume corresponded to the dry particle density.

4.2.5.3 Strength and stiffness test setup for LWAC

The 28-day compressive strength was tested according to the DS/EN 1354 standard (DS/EN 1354, 2005). For mixes D-1 and D-2, cores with a diameter of 100 mm were drilled from the LWAC blocks when they reached 26 days of maturity, and the end surfaces were removed such that the specimens for compressive strength testing had a height of 100 mm. After cutting the specimens they were placed in a climate chamber at a temperature of 23°C and a relative humidity of 65% for 48 hours to reach their 28-day maturity. On reference specimens that were subsequently dried out, it was found that the moisture content was 18% at the time the specimens were removed from the climate chamber and tested. For mix A-1, cubes with dimensions of $100 \times 100 \times 100$ mm^3 were cut from the LWAC blocks and placed in a climate chamber at a temperature of 23°C and a relative humidity of 65% for seven days before testing. For mix A-2, cylindrical specimens with the same geometry as specimens from mix D-1 and D-2 were used. Also mix A-1 and A-2 specimens were tested at 28-day maturity; however, their moisture content was unknown. Both the cylindrical specimens and the cubes used in this study are applicable for compression test according to the DS/EN 1354 standard (DS/EN 1354, 2005). The compressive tests were performed on a MAN 6t loading machine with a load rate that caused the specimens to fail within 60 seconds. Soft fiberboard with a thickness of 12 mm was placed between the specimen end surfaces and the loading machine to distribute the pressure evenly. Six specimens were tested for mix D-1, mix D-2, and mix A-1, and three specimens were tested for mix A-2.

The 28-day Young's modulus and 28-day splitting tensile strength were tested only for specimens from mixes D-1 and D-2. The specimens used for determination of Young's modulus were 157 mm high (maximum possible height after removing the end surfaces) with a diameter of 100 mm. The specimens used for determination of the splitting tensile strength were 140 mm high with a diameter of 100 mm. Because the height of the LWAC blocks was 190 mm (Figure 1.9), it was not possible to obtain specimens with a ratio between the height and diameter of $h/d = 2.0$. For determination of Young's modulus and splitting tensile strength, specimens were also placed in a climate chamber with a temperature of 23°C and a relative humidity of 65% for 48 hours, by which they obtained a moisture content of 18%, before they were tested.

For determination of Young's modulus, the strain was measured by installing a system with two rigid rings tightly mounted with three screws around cylindrical specimens, and placing two extensometers between the rings, as shown in Figure 4.4b. Metal plates measuring 1×1 cm^2 were glued onto the specimen at the position of the screws to make sure the grip between the screws and the specimen was sound. The specimens were loaded to 30% of the average 28-day compressive strength on an Instron 100 kN loading machine at a load rate of 5 kN/min. Young's modulus was found from the stress-strain curves as the slope of best straight line of the data points between $f_c = 0.20$–0.50 MPa. After the Young's modulus measurements, the specimens were loaded to failure in agreement with the above procedure for determination of compressive strength.

The 28-day splitting tensile strength was tested by placing the specimens

centrally in the testing machine and subsequently placing hard fiberboard plates, 3 mm-thick and 150 mm-long, on opposite sides of the specimens, directly above each other. The splitting tensile strength tests were performed on a MAN 6t loading machine with a load rate that caused the specimens to fail within 60 seconds.

4.2.5.4 Freeze-thaw test setup for LWAC

No standard exists for testing the freeze-thaw durability of LWAC. Instead, the EN 15304 standard (EN 15304, 2010) was used as inspiration for the specimen dimensions and the temperature variation because the standard concerns freeze-thaw test of aerated concrete that is also classified as a type of LWAC. According to the EN 15304 standard, the temperature limits in Table 4.3 apply to the core temperature of $100 \times 100 \times 100$ mm^3 specimens.

Table 4.3: Core temperature limits during freeze-thaw test of aerated concrete according to the EN 15304 standard (EN 15304, 2010).

Temperature	20°C to 0°C	0°C to −15°C	−15°C to 0°C	0°C to 20°C
Time [h]	2–4	> 8	4–6	> 8

For mix A-1, 36 freeze-thaw specimens measuring $100 \times 100 \times 100$ mm^3 were cut from the LWAC blocks after 28-maturity days. The cubes were dried at 55°C until weight-constant. Subsequently, 18 of the specimens were placed in a 3% NaCl solution (method "S"), and 18 were placed in demineralized water (method "W"). After three days, the specimens were removed and allowed to drain before wrapping them in two layers of plastic. Next, they were placed in a freezing cabinet with the temperature variations shown in Figure 4.7a. The core temperatures of two specimens were measured and found to be the same (Figure 4.7a also shows this variation). The core temperatures remained within the limits shown in Table 4.3, except the duration of the thawing period was only four hours instead of eight. The duration of a single freeze-thaw cycle was 28 hours, which differs from the normal 24-hour frost cycles because the LWAC specimens were tested parallel with another material; however, a maximum frost cycle duration is not given in the EN 15304 standard (EN 15304, 2010). The freeze-thaw durability of mix A-2 was not tested.

For mixes D-1 and D-2, the freeze-thaw specimens were cylinders, 100 mm-high and 100 mm in diameter, which were drilled from the LWAC blocks with 28-day maturity. The end surfaces were removed to obtain the desired cylinder height. Subsequently, the specimens were tested according to one of these three methods:

1. Method W-1: Specimens were immersed in demineralized water for three days and allowed to drain before being wrapped in two layers of plastic.
2. Method S-1: Specimens were immersed in a 3% NaCl solution for three days and allowed to drain before being wrapped in two layers of plastic.
3. Method S-2: Specimens were dried at 55°C until weight constant. Subsequently, they were immersed in a 3% NaCl solution for three days and allowed to drain before being wrapped in two layers of plastic.

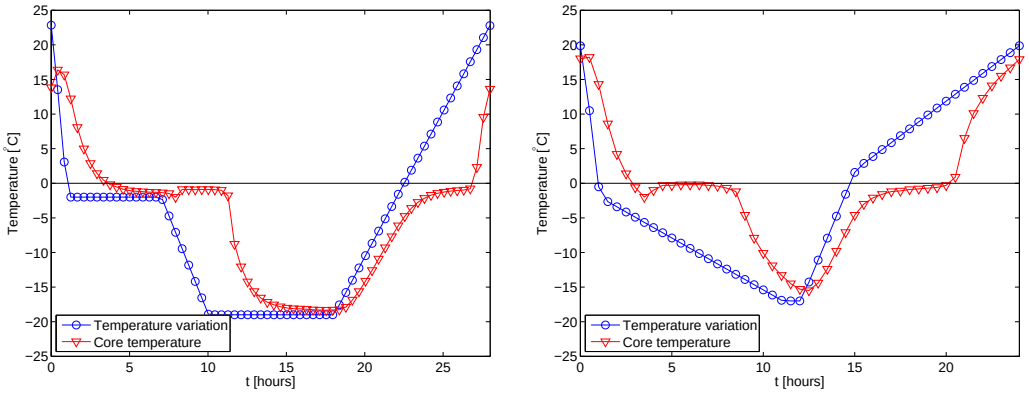

(a) Mix A-1. Duration of freeze-thaw cycle = 28 hours.

(b) Mixes D-1 and D-2. Duration of freeze-thaw cycle = 24 hours.

Figure 4.7: Temperature variation and core temperature of LWAC during a single freeze-thaw cycle.

When wrapped in plastic, the specimens were placed in a freezing cabinet with the temperature variations shown in Figure 4.7b. For each of mix D-1 and mix D-2, eight specimens were tested, following method "W-1", and four specimens were tested following methods "S-1" and "S-2". The core temperatures of two specimens were measured and found to be the same (Figure 4.7b also shows this variation for one of the specimens). The core temperature remained within the limits in Table 4.3. A comparison of Figure 4.7a and Figure 4.7b indicates, the main difference between the core temperatures of specimens A-1, D-1, and D-2 is the duration at which the specimens were kept frozen at the minimum temperature. However, the rates at which the core temperature froze and thawed were comparable, and therefore, the results from tests performed under the two different temperature variations can be considered comparable.

4.3 Results for LWAC

4.3.1 Water absorption and dry particle density results for LWA

Table 4.1 shows the water absorption after 5 minutes, 15 minutes and 60 minutes, and the dry particle density, of Leca 2–4 mm and Leca 4–10 mm, determined as described in Section 4.2.5.1 and Section 4.2.5.2. The water absorption and the dry particle density are calculated as the average value of three samples for each of the two Leca gradings.

4.3.2 Air void content results for LWAC

Table 4.4 shows the entrained air content in the concrete, the entrained air content in the cement paste, and the void content of mixes D-1 and D-2.

Table 4.4: Entrained air content in concrete, P_{co}, entrained air content in cement paste (volume of cement, fly ash, water, and entrained air), P_{cp}, and void content, V, for mixes D-1 and D-2. Average values (av.) and standard deviations (std. dev.) are shown.

Mix	P_{co}* [%]		P_{cp}* [%]		$V^{\dagger}$ [%]	
	Av.	Std. dev.	Av.	Std. dev.	Av.	Std. dev.
D-1	3.75	0.35	22.3	1.5	21.3	5.1
D-2	5.20	0.97	29.5	3.8	16.4	8.7

* Based on five specimens of each mix design.
† Based on seven specimens of each mix design.

4.3.3 Strength results for LWAC

Figure 4.8 shows the 28-day compressive strength and splitting tensile strength as a function of the dry density for mixes D-1 and D-2. The moisture content of the specimens was 18% when they were removed from the climate chamber just before testing. Therefore, the dry densities shown in Figure 4.8 were found by reducing the density of the specimens at the time of testing by 18%. For comparison, Figure 4.8a shows the compressive strengths determined from the specimens used for determination of Young's modulus, although they were 157 mm-high, which deviates from the DS/EN 1354 test standard (DS/EN 1354, 2005). Therefore, the figure distinguishes between specimens with $h/d = 1.0$ and $h/d = 1.6$. Both Figure 4.8a and Figure 4.8b show a linear regression of the measurements for mixes D-1 and D-2. However, in Figure 4.8a the linear regression of the measurements of mix D-2 with $h/d = 1.6$ is omitted because the measurements did not cover a very wide range of densities.

Table 4.5 shows the average dry density, 28-day compressive strength, 28-day Young's modulus, and 28-day splitting tensile strength for mixes D-1 and D-2. The table also shows the dry density and 28-day compressive strength for mixes A-1 and A-2. The dry densities in Table 4.5 refer to average values measured for the particular mix design after casting and drying at 105°C until weight constant.

4.3.4 Freeze-thaw results for LWAC

Figure 4.9 shows the average mass loss of specimens from mixes A-1, D-1 and D-2 as a function of the number of freeze-thaw cycles. A mass loss of maximum 15% is considered acceptable.

Table 4.6 summarizes the main freeze-thaw results for mixes A-1, D-1, and D-2, that is, the number of frost cycles at which the mass loss exceeded the acceptable limit, or the mass loss at 56 frost cycles if the acceptable limit was not exceeded.

Table 4.6 shows that for mix A-1 exposed to salt ions, the limit for the acceptable mass loss of 15% was exceeded after 12 frost cycles. For mix A-1 exposed to water, the final measured mass loss was only 2.1% after 28 frost cycles. For mix D-1 exposed to salt ions using method "S-1", the limit for the acceptable mass loss was exceeded after 27 frost cycles. For mix D-2 using method "S-1", the acceptable

Table 4.5: Dry density, ρ_d, 28-day compressive strength, f_c, 28-day Young's modulus, E, 28-day splitting tensile strength, f_s, for mixes D-1 and D-2, and dry density and 28-day compressive strength for mixes A-1 and A-2. Average values (av.) and standard deviations (std. dev.) are shown.

Mix	ρ_d* [kg/m^3]		f_c† [MPa]		E‡ [GPa]		f_s† [MPa]	
	Av.	Std. dev.	Av.	Std. dev.	Av.	Std. dev.	Av.	Std. dev.
A-1	672.1	20.5	1.83	0.09	-	-	-	-
A-2	853.1§	-	4.22	0.28	-	-	-	-
D-1	622.6	19.7	2.28	0.24	2.05	0.29	0.41	0.07
D-2	629.7	19.3	2.23	0.18	2.25	0.23	0.35	0.02

* Based on 18 specimens of mix A-1, and 15 specimens of mixes D-1 and D-2.
† Based on three specimens of mixes A-1 and A-2, and seven specimens of mixes D-1 and D-2.
‡ Based on three specimens of mixes D-1 and D-2.
§ The dry densities of specimens from mix A-2 were not measured; the given value corresponds to the dry mix design density after 15% compaction (Table 4.2).

Table 4.6: Average mass loss, m_n, after either $n = 56$ cycles ($n = 28$ for mix A-1) *or* after n cycles, at which the average mass loss is 15%, corresponding to 85% remaining mass (the acceptable limit) for specimens A-1 exposed to method "W" or "S", and specimens D-1 or D-2 exposed to either method "W-1", "S-1" or "S-2" (see Section 4.2.5.4 for explanation of the different methods).

Mix	Method	No. of frost cycles n [-]	Mass loss at n frost cycles m_n [%]
A-1	W*	28	2.1
	S*	12	15.0
D-1	W-1†	56	1.3
	S-1‡	27	15.0
	S-2‡	56	3.2
D-2	W-1†	56	1.3
	S-1‡	56	8.1
	S-2‡	56	1.2

* Based on 18 specimens.
† Based on eight specimens.
‡ Based on four specimens.

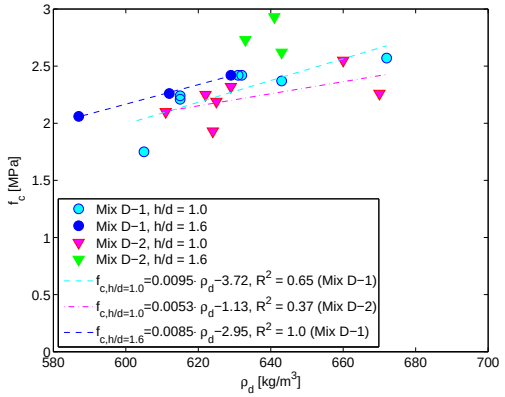

(a) 28-day compressive strength, f_c, as function of dry density. Specimens with $h/d = 1.0$ were tested according to the DS/EN 1354 standard (DS/EN 1354, 2005), whereas the height of the specimens with $h/d = 1.6$ deviates from the standard.

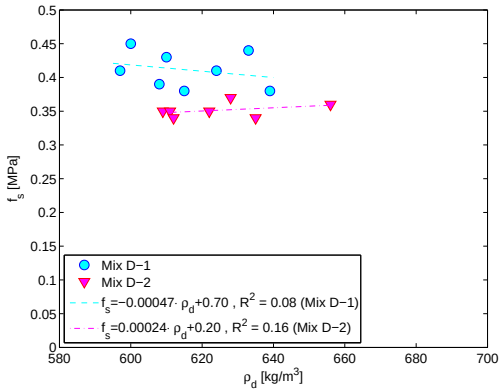

(b) 28-day splitting tensile strength, f_s, as a function of dry density for specimens with $h/d = 1.4$.

Figure 4.8: 28-day compressive strength and splitting tensile strength as a function of dry density of mixes D-1 and D-2.

mass loss limit was not exceeded within the test period, and after 56 frost cycles, the mass loss was 8.1%. Among specimens exposed to method "S-2", mix D-2 also performed better than mix D-1. The acceptable mass loss limit was not exceeded in the test, but after 56 frost cycles the mass loss of mixes D-1 and D-2 was 3.2% and 1.2%, respectively. Among specimens exposed to method "W-1", there was not observed any difference between mixes D-1 and D-2, and after 56 frost cycles the mass loss of both mixes was 1.3%.

4.4 Discussion of LWAC

4.4.1 Discussion of LWA water absorption

The water absorption determined for Leca 4–10 mm falls within the limits stipulated in the Leca 4–10 mm data sheet; however, these limits are wide. The five-minute absorption value in the data sheet, for example, varies from 19% to 33%, a range that can either be due to the variability in the applied testing procedure (DS/EN 1097-6, 2013) or to the variability of the material. The Leca 2–4 mm data sheet gave no information about the water absorption or the dry particle density. A larger data set is needed to assess whether the water absorption test procedure described in the present study is more reliable than that described in the DS/EN 1097-6 standard (DS/EN 1097-6, 2013).

When determining the water absorption according to the procedure described in Section 4.2.5.1, the initial measurement at t_0 was determined by extrapolating the first reading at t_1, and the second reading at t_2, by assuming a linear correlation between these three data points. The initial reading has a great influence on the

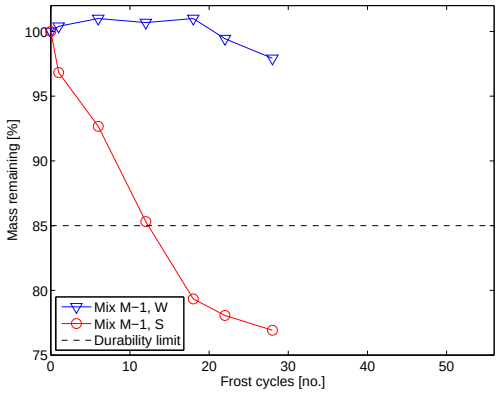

(a) Mix A-1. Number of freeze-thaw cycles = 28. "W" and "S" refer to different test methods applied as mentioned in Section 4.2.5.4.

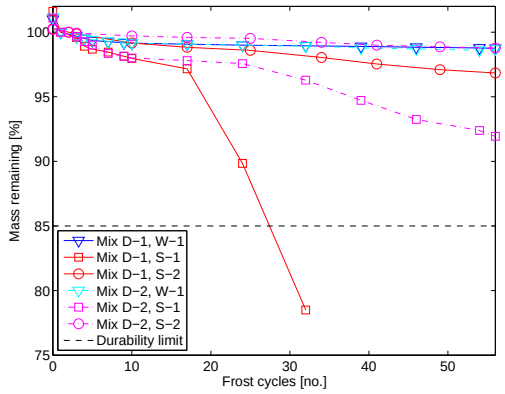

(b) Mixes D-1 and D-2. Number of freeze-thaw cycles = 56. "W-1", "S-1" and "S-2" refer to different test methods applied as mentioned in Section 4.2.5.4.

Figure 4.9: Average values of remaining mass for LWAC mixes A-1, D-1, and D-2 as function of the number of frost cycles.

water absorption value because it is subtracted from all subsequent readings; hence, this reading should be chosen carefully. It is unknown exactly how many seconds after t_0 the first reading was obtained because it took some seconds to immerse the net with the Leca particles into the water. The time between all PC readings was 10 seconds; thus, the time between t_0 and t_1 was a maximum of 10 seconds; and, because the net with Leca particles was immersed immediately after a PC reading had been made, $t_1 - t_0$ cannot be less than approximately five seconds. Table 4.7 shows the five-minute absorption results for Leca 4–10 mm, assuming that $t_1 - t_0$ was 5 seconds, 8 seconds, and 10 seconds, respectively. Three Leca 4–10 mm samples were tested, and Table 4.7 shows the results for all three samples, together with the standard deviations relating to the choice of $t_1 - t_0$, and to the three different Leca samples.

For the five-minute absorption value, Table 4.7 shows that the standard deviation of the three Leca samples was much larger than the standard deviation of the three values of $t_1 - t_0$. The same tendency was observed for the water absorption determined after 15 minutes, and after 60 minutes, and for Leca 2–4 mm. In general, it was observed that there was a large variation in the water absorption of different Leca samples. Thus, the variation caused by the material properties exceeds the variation caused by the choice of $t_1 - t_0$; hence, it is reasonable to assume $t_1 - t_0 = 10$ s in the calculations. The results shown in Table 4.1 and in Figure 4.1b use this assumption.

4.4.2 Discussion of LWA dry particle density

Leca 2–4 mm contains an unknown amount of crushed particles. The outer surface of the crushed particles consists of fine porous shell and a coarse core. The

Table 4.7: Five-minute water absorption value, w, for three Leca 4–10 mm samples, assuming the time difference between the initial reading and the first reading, $t_1 - t_0$, was either 5 seconds, 8 seconds, or 10 seconds. The standard deviation is shown for the water absorption of: (1) a given Leca sample for three values of $t_1 - t_0$, and (2) three Leca samples for a given value of $t_1 - t_0$.

w (5-min.) [%]	$t_1 - t_0$			Std. dev.† [%]
	5 s	8 s	10 s	
Leca 4–10 mm #1	14.9	15.6	16.1	0.6
Leca 4–10 mm #2	22.4	24.4	25.6	1.6
Leca 4–10 mm #3	24.5	25.5	26.2	0.9
Std. dev.* [%]	5.0	5.4	5.7	

* The standard deviation of the five-minute water absorption for three Leca samples for a given value of $t_1 - t_0$.
† The standard deviation of the five-minute water absorption for three values of $t_1 - t_0$ for a given Leca sample.

impregnation that is used to determine the dry particle density (Section 4.2.5.2) only seals the fine pores; thus, the coarse pores of crushed particles are not included as part of the Leca particle volume when determining the dry particle density. Therefore, the calculation of the Leca 2–4 mm dry particle density is subject to some uncertainty. However, this uncertainty is not considered any further, for three reasons: firstly, there is no testing method that describes how to correct for the uncertainty associated with the determination of the volume of crushed particles; secondly, a visual inspection indicates that the amount of crushed particles is not very large; and thirdly, the ratio between the volumes of Leca 2–4 mm and Leca 4–10 mm in mixes D-1 and D-2 is only 0.4 to 1.

4.4.3 Discussion of LWAC density and strength

As Figure 4.8a indicates, the compressive strength of LWAC increased with increasing dry density. This finding was most clear for mix D-1 with $h/d = 1.6$ that had $R^2 = 1.0$, but also was observed for mixes D-1 and D-2 with $h/d = 1.0$. At LWAC mixing plants, the density of LWAC blocks is used to indicate the blocks' compressive strength. Based on experience, mixing plant personnel know which density ranges correspond to certain compressive strengths; therefore, the compressive strength is typically adjusted solely from an assessment of the block density. In this study, the range of densities considered was very narrow (Figure 4.8) because a dry density of 700 kg/m^3 was aimed for[1]. A stronger linear correlation would be observed if mix designs with different densities were included. For the splitting tensile strength, the same linear dependency on the dry density was not observed (Figure 4.8b).

The desired 28-day compressive strength of 3 MPa was not reached[2], possibly because the block machine used for testing was not capable of providing sufficient

[1] Average value.
[2] Characteristic value.

compaction, and therefore, the dry density was closer to 600 kg/m^3 (Table 4.5), resulting in lower compressive strengths. As Table 4.4 shows, the measured void content was approximately 20% for both mixes D-1 and D-2. As stated previously, this void content was ambiguous due to the test method. However, the results indicated that the volume was compressed less than the 15% assumed in the mix design. If the compression was in fact only 8%, the mix design and the measured density would correspond with each other. This also corresponds with the measured void content of approximately 20%. For mix A-1, the actual density and that determined from the mix design when assuming 15% compaction (Table 4.2) were equal. This indicates that the compaction achieved using the LWAC block machine fabricated for the present study was less than the compaction achieved using the LWAC block machine at mixing plant A. Therefore, it is expected that if mixes D-1 and D-2 were cast at mixing plant A, the compaction would be larger, and in turn, the compressive strength would increase. Nevertheless, the LWAC block machine fabricated for this study made it possible to cast LWAC blocks with the same geometry as the blocks used in SL-Decks, by exerting a pressure and vibration that were much larger than what could be achieved by hand compaction.

Because the densities of mix designs D-1 and D-2 were approximately the same, the strength properties of the two mix designs can be compared. As Table 4.5 indicates, the 28-day compressive strength and the 28-day splitting tensile strength were 3% and 17% larger for mix D-1 compared with mix D-2. However, the Young's modulus for mix D-2 was 10% larger than for mix D-1. Thus, this study did not find that the addition of fly ash had any significant positive influence on the strength properties. Also, the entrained air content in the cement paste of mix D-2 was 32% larger than of mix D-1 (Table 4.4). For conventional concrete, the entrained air content in the cement paste has a great influence on the strength properties, and as a rule of thumb, the compressive strength decreases 4% for every percentage point the entrained air content is increased (Munch-Petersen, 2003a). Since fly ash is not believed to have a negative influence on the strength properties of LWAC, the results indicated that entrained air did not have the same negative influence on the strength properties of LWAC as on conventional concrete. The reason for this result may be because the strength properties of the LWA are more dominate than the strength of the cement paste, which also may be why the mix design containing fly ash did not have improved strength properties compared with that without fly ash.

A direct comparison of the 28-day compressive strength of this study's mix designs with those from mixing plant A is not possible because the densities are different. However, the 28-day compressive strength of mix A-1 was 18% less than that of mix D-1, even though the density of mix A-1 was 50 kg/m^3 larger. For mix A-1, the actual dry density of the specimens equaled the mix design in Table 4.2, with a compaction of 15%. For mix A-2, the actual dry density of the specimens tested was unknown. Based on the mix design, the dry density was 853 kg/m^3 with a compaction of 15%; therefore, the dry density of mix A-2 was approximately 230 kg/m^3 larger than the dry density of mix D-1 which was 623 kg/m^3 (Table 4.5). If mix D-1 with $h/d = 1.0$ had a dry density of 853 kg/m^3 (which would correspond to a compaction of the volume of 30%), the 28-day compressive strength would be approximately 4.4 MPa based on extrapolation of Figure 4.8a. Because the R^2

value of mix D-2 with $h/d = 1.0$ was considerably less than that of mix D-1 with $h/d = 1.0$, the same extrapolation was not performed for mix D-2. Hence, the mix designs developed in this study had improved strength properties compared with those used at mixing plant A, even though they had an entrained air content of up to 30%, unlike mixes A-1 or A-2.

4.4.4 Discussion of LWAC freeze-thaw durability

The test methods "S" for mix A-1 and "S-2" for mixes D-1 and D-2 corresponded to each other because, in these two test methods, the specimens were dried at 55°C before being immersed in a 3% NaCl solution for three days prior to freezing and thawing. Compared with mix A-1, the freeze-thaw durability of mix designs D-1 and D-2 was much improved, as Figure 4.9 and Table 4.6 clearly show. For mix design A-1, the mass loss was 15% after 12 frost cycles for specimens exposed to method "S". For mix designs D-1 and D-2 the mass loss was only 0.93% and 0.32%, respectively, after 12 frost cycles for specimens exposed to method "S-2". The main factor that influenced the difference in freeze-thaw durability between mix design A-1 and mix designs D-1 and D-2 was the air entrainment contained in mix designs D-1 and D-2. When comparing the results for the specimens exposed to water, mix design A-1 had a mass loss of 2.1% after 28 frost cycles, whereas the mass losses of mix designs D-1 and D-2 were 1.0% after 28 frost cycles (Figure 4.9).

The freeze-thaw durability of mix design D-2 was better than that of D-1, as Figure 4.9b and Table 4.6 indicate, because of the different amount of entrained air in the two mix designs. As Table 4.4 shows, mix designs D-1 and D-2 had 22.3% and 29.5% entrained air in the cement paste, respectively, and therefore, mix D-2 was expected to have improved freeze-thaw durability compared with mix D-1. This improvement was observed for specimens exposed to method "S-1" and "S-2"; however, the differences were insignificant for specimens exposed to method "W", and the freeze-thaw durability for both mixes was good. Thus, as experienced with conventional concrete, the presence of salt ions worsens the freeze-thaw behavior of LWAC considerably.

The freeze-thaw durability of specimens exposed to method "S-1" was worse than of specimens exposed to method "S-2" (Figure 4.9b) for both mix D-1 and D-2. The reason for this finding is that specimens tested according to method "S-2" were dried at 55°C prior to immersion in a 3% NaCl solution, unlike specimens tested with method "S-1". Although specimens tested with method "S-2" were immersed in a 3% NaCl solution for three days after drying, their initial mass was less than that of specimens tested with method "S-1", which indicated that they did not absorb as much water as evaporated during the drying process. According to Klieger and Hanson (1961), the LWA moisture content has a great impact on the freeze-thaw durability of LWAC: the higher the moisture content, the worse the freeze-thaw durability. Other parameters influencing the freeze-thaw durability of LWAC are the entrained air content and the LWA properties; however, for all specimens of either mixes D-1 or D-2, these parameters were the same. Therefore, the difference in LWA moisture content explains the observed difference between the specimens tested according to methods "S-1" and "S-2".

Immediately after casting, the moisture content of the LWAC is high because the Leca particles absorb a large amount of water during mixing. The moisture content can be located in: (1) the coarse pores in the cores of the Leca particles, (2) the partition walls in the cores of the Leca particles, (3) the surfaces (shells) of the Leca particles, and (4) the cement paste between the Leca particles. The pore size distributions of the various parts are different. The core has the largest pore size distribution, and the cement paste has the smallest. The pore size distribution of the surface is smaller than that of the core, but larger than that of the cement paste. This variation has not been measured, but is visible to the eye. The pore size distribution of the partition walls is believed to be approximately the same as that of the Leca shell. When dry Leca particles are in contact with water, the shell becomes water-saturated at first. Subsequently, the partition walls and core become water-saturated. However, this latter process takes a long time. Because the suction of smaller pores is larger than that of larger pores, water cannot be sucked from a small to a larger pore. Therefore, with time, suction causes the moisture in the core, in the partition walls, and in the shell of the Leca particles to be transferred to the cement paste. Furthermore, Leca particles are not hygroscopic; hence, the only moisture bonding from the surrounding air takes place in the cement paste. After casting, the Leca particles can only be water-filled if they are exposed to a water pressure, which is never the case for the LWAC in the SL-Decks in Pearl-Chain Bridges. Hence, the moisture content of LWAC peaks when the blocks are cast, and subsequently decreases.

For both specimens tested with methods "S-1" and "S-2", the cement paste contained salt water; however, the Leca shell (and core) only contained water for specimens tested with method "S-1". Therefore, the LWAC exposed to method "S-1" corresponds only to the situation that would occur if 28-day old LWAC cured in water (or at a relative humidity of approximately 100%) was immediately exposed to freezing and thawing. I do not believe that this situation is representative of the LWAC in Pearl-Chain Bridges, because the moisture content of the LWAC in Pearl-Chain Bridges is only this great for a very short period of time. On the other hand, I believe that the LWAC exposed to method "S-2" is more representative of the LWAC in Pearl-Chain Bridges, because the Leca particles are not water-saturated using this method. Using this method, the freeze-thaw results indicated that an entrained air content of 30% in the cement paste will provide good freeze-thaw durability results. Therefore, based on this study, an entrained air content of 30% is recommended for LWAC in Pearl-Chain Bridges.

4.5 Future experiments with LWAC

Although the work performed in this study reveals several tendencies in absorption procedures, mix design, and freeze-thaw behavior of LWAC, more work remains to be done before the LWAC blocks in SL-Decks for Pearl-Chain Bridges can be considered to have the correct density, 28-day compressive strength, and freeze-thaw durability. Because this study did not find that the addition of fly ash had any positive influence, it is recommended that mix D-2, which had the best freeze-thaw

properties, be cast at mixing plant A. This recommendation includes two aspects: First, a method should be developed to control the moisture content of the LWA during mixing at mixing plant A. In this study, oven-dried Leca was initially mixed for five minutes with an amount of water corresponding to the five-minute absorption value, and the desired amount of free water. If an initial mixing time of five minutes for pre-wetting LWA restricts the concrete mixer for too long, a different method for pre-wetting the Leca particles should be developed at mixing plant A. If the Leca particles are pre-wet on a belt on their way to the concrete mixer, a determination should be made regarding how much free water that is present on the Leca particle surface during this procedure. This should be considered in light of the original moisture content of the Leca particles. Second, blocks should be cast at the LWAC block machine at mixing plant A for greatest density to mix D-2. According to this study's results, mixing plant A's block machine provided up to 15% compaction compared with only 8% from DTU's block machine. According to this study, 30% entrained air in the cement paste is necessary to obtain good freeze-thaw durability. An interesting study of LWAC blocks with such entrained air content would be to prepare thin sections of the cement paste and analyze the air void distribution in terms of spacing factor and specific surface area.

4.6 Conclusions for LWAC

In this study, a LWAC mix design for Pearl-Chain Bridges was exposed to a harsh freeze-thaw impact. The mix design was compared to the LWAC mix design used for SL-Decks for indoor usage. The main findings from the study were the following:

1. The water absorption of Leca 2–4 mm and Leca 4–10 mm was determined by continuously logging the change in the mass of oven-dried Leca particles immersed in water in a net. The increased mass was equivalent to the mass of water absorbed by the Leca particles, by which the absorption properties for Leca 2–4 mm and Leca 4–10 mm were determined. This method distinguishes from other commonly applied water absorption test methods in which the Leca particles are typically dried to a "surface dry" state by gently rolling them in a cloth; however, such methods are subjective to the person performing them.

2. After five minutes, dry Leca 2–4 mm and Leca 4–10 mm had absorbed 77% and 74%, respectively, of their 60-minute absorption value; hence, the absorption was largest at the beginning, but slowed with time.

3. The amount of free water was controlled by initially mixing oven-dried Leca particles for five minutes with an amount of water corresponding to the five-minute absorption value and the desired amount of free water. Afterwards, cement, fly ash, sand, and air entrainment were added.

4. Two LWAC mix designs were considered, one with fly ash and one without. The LWAC used for Pearl-Chain Bridges should have an average dry density of 700 kg/m^3 and a characteristic 28-day compressive strength of 3 MPa. The desired 28-day compressive strength of minimum 3 MPa was not reached,

possibly because the block machine used for testing was incapable of providing sufficient compaction, and therefore, the dry density was closer to 600 kg/m^3 than 700 kg/m^3, resulting in lower compressive strengths.

5. The LWAC mix design with fly ash had an average dry density of 623 kg/m^3, an entrained air content in the cement paste (including the volume of entrained air itself) of 22%, an average 28-day compressive strength of 2.22 MPa, an average 28-day Young's modulus of 2.05 GPa, and an average 28-day splitting tensile strength of 0.41 MPa. The LWAC mix design without fly ash had an average dry density of 630 kg/m^3, an entrained air content in the cement paste (including the volume of entrained air itself) of 30%, an average 28-day compressive strength of 2.16 MPa, an average 28-day Young's modulus of 2.25 GPa, and an average 28-day splitting tensile strength of 0.35 MPa. Thus, this study did not find that the addition of fly ash had any significant influence on the strength properties.

6. The entrained air was not observed to influence the strength properties of LWAC, as for conventional concrete, because the strength of LWAC is determined to a high degree by the strength of the LWA, rather than the strength of the cement paste.

7. The compressive strength of LWAC increased with density.

8. Entrained air significantly improved the freeze-thaw durability of LWAC. A mass loss of a maximum 15% was chosen as the acceptable limit. Specimens without air entrainment (from the LWAC mix design for SL-Decks for indoor usage) had a mass loss of 15% after 12 frost cycles when they were dried to weight constant at 55°C and immersed in a 3% NaCl solution before testing. For a similar exposure, the air entrained LWAC mix designs developed for Pearl-Chain Bridges had a mass loss of 3.2% and 1.2% after 56 frost cycles with an entrained air content in the cement paste of 22% and 30%, respectively; hence, they did not exceed the acceptable limit.

9. An entrained air content in the cement paste (including the volume of the entrained air itself) of 30% provided better freeze-thaw durability than an entrained air content of 20%. An entrained air content of 30% in the cement paste is recommended for LWAC in Pearl-Chain Bridges.

10. LWAC specimens exposed to salt ions before freezing and thawing had a significantly reduced freeze-thaw durability compared with specimens exposed to demineralized water. For example, the mix design with 30% entrained air in the cement paste had a mass loss of 8.1% and 1.2% after 56 frost cycles, when immersed in a 3% NaCl solution and demineralized water respectively, for three days prior to testing.

11. The freeze-thaw durability of LWAC was dependent on the moisture content of the LWA at the time the freeze-thaw tests were conducted: the higher the LWA moisture content, the worse the freeze-thaw durability.

CHAPTER 5

Conclusions

5.1 Novelty and major contributions

This PhD study investigated the durability of the materials used for so-called "Pearl-Chain Bridges" in order to ensure that this type of bridges meets today's high standards of durability. To demonstrate the overall durability of Pearl-Chain Bridges, the work carried out as part of this study considered three main components of the bridges: (1) the fill material, (2) the mortar joints, and (3) the lightweight aggregate concrete. These three were chosen because these materials, and the application of them, differ from the materials in typical bridge superstructures. The main contributions and findings relating to each of these parts are summarized in the following paragraphs.

Fill material in Pearl-Chain Bridges (Papers I–V)

- The application of sub-base gravel, cement-stabilized gravel and pervious concrete as fill material in Pearl-Chain Bridges was investigated, with respect to their strength properties, permeability, and freeze-thaw durability. The most suitable fill material depends on the design of the particular bridge project, and the strength and durability results determined in this study can help to decide which fill material is most suitable for a certain project (Paper I).

- The 28-day Young's modulus of cement-stabilized gravel and pervious concrete was 100 times greater than that of sub-base gravel. Moreover, the use of either pervious concrete or cement-stabilized gravel allows the fill material to transfer shear stresses (Paper I).

- The application of a pervious concrete fill rather than a sub-base gravel or cement-stabilized gravel fill improves the drainage properties of the superstructure, which reduces water accumulation in the fill, and exposure of the concrete arch to moisture. Pervious concrete is able to drain the rain from a 100-year

rain event in Denmark, whereas sub-base gravel and cement-stabilized gravel are unable to drain the rain from a 1-year rain event in Denmark (Paper I).

- The applicability of pervious concrete as fill material in Pearl-Chain Bridges was demonstrated by using pervious concrete fill in the very first Pearl-Chain Bridge constructed in Denmark in 2015 (Paper II).
- When casting a pervious concrete fill, in order to obtain a homogenous void content through the layer, the layer thickness should not exceed approximately 30 cm before compaction. Multiple layers can be cast upon each other without influencing the void content of underlying layers (Paper II).
- The focus was particularly on the development of a suitable pervious concrete mix design, and it was found that the strength properties were improved by the addition of air entrainment, a high-range water reducer (superplasticizer), and internal curing provided by the addition of lightweight sand (expanded shale) (Paper II and Paper III).
- The freeze-thaw durability of pervious concrete was assessed using freeze-thaw tests and air void analysis performed by using the linear-traverse method. The comparability of these two procedures was questioned because there is a disagreement between the two test methods in their assumption of whether or not the large interconnected voids effectively relieve the pressure when water freezes. Moreover, the inclusion of these large voids in the linear-traverse method can be erroneous when determining the spacing factor (Paper IV).
- According to the Danish road regulations, sub-base gravel is frost safe; however, the experimental results of four different gravel materials suggested that the frost susceptibility criterion of sub-base gravel should be based, not only on the gradation curve, but also on the permeability (Paper V).

Mortar joints in Pearl-Chain arches (Paper VI)

- It cannot be assumed that commercialized mortar products described as "expansive" have any significant expansion.
- The mortar joints in the Pearl-Chain arch were found to be greatly exposed to crack formation during hardening. This was a combination of shrinkage crack formation in the pure mortar phase and crack formation along the interface between concrete and mortar. The crack formation was eliminated by using an expansive mortar product with a constant expansion, and by applying a primer on the concrete surfaces facing the joint in order to decrease the porosity along the construction joint.
- The mortar joints did not decrease the durability of the Pearl-Chain arch with regard to chloride ingress, water absorption, or freeze-thaw durability.
- By using an alkali-resistant primer, the splitting tensile strength of the mortar joints decreased by 45% compared with pure mortar specimens. It is suggested

that the splitting tensile strength is tested for joints cast with a primer that is permeable for the mortar, because this is expected to improve the adhesion between concrete and mortar.

Lightweight aggregate concrete in Pearl-Chain arches (Chapter 4)

- A lightweight aggregate water absorption test method that is independent of the person performing it was suggested. Using this method, the change in mass of oven-dried lightweight aggregate particles immersed in water was continuously logged, by which their absorption properties over time were determined.
- By the addition of air entrainment, the freeze-thaw durability of the lightweight concrete was considerably improved. It was found that an entrained air content of 30% in the cement paste (including the volume of the entrained air) provided good results even when salt ions were present if the lightweight aggregates were not water saturated.
- The strength and freeze-thaw durability results of the mix designs developed in this PhD study showed improvement when compared with the lightweight aggregate concrete used in Super-Light Decks for indoor purposes.
- The requirements for the density and strength properties of the lightweight aggregate concrete that is used in Pearl-Chain Bridges were not met in the laboratory tests using the laboratory block machine; however, it is suggested that the mix design developed in this study should be mixed and cast at mixing plant A, because the block machine available there is capable of providing a greater compaction. If so, the density and the strength properties are expected to increase.

5.2 Concluding remarks

Much of the experimental work carried out as part of this PhD study was conducted in collaboration with a number of different concrete mixing plants and contractors. This collaboration demonstrated the challenges that arise when methods and theory from university are combined with practices from industry. It is not surprising that university and industry methods often come to a clash because they belong to different agendas. At university, the search for explanation and a greater understanding is the overall focus, whereas efficiency and economy primarily govern the industry. During this PhD project several compromises had to be made in an attempt to bring university standards and industry practices together. Several situations exemplify this, such as the decision of which material to use when connecting the ducts for post-tensioning cables between adjacent Super-Light Decks, how to control the moisture content of lightweight aggregates during mixing, and how to provide optimal curing conditions. Such compromises were challenging but also educational because they forced creative solutions while complying with current standards.

A final remark should be made on the scope of this PhD study. All materials that are unique to Pearl-Chain Bridges were given priority in order to document the overall durability of Pearl-Chain Bridges. Several materials were considered and tested which gave this PhD study a greater breadth than a "typical" PhD study; however, this also limited its depth. In particular, the PhD study explored the use of pervious concrete and the durability of the mortar joints in great detail; but, as a consequence, other subjects such as the frost susceptibility of sub-base gravel and the design of a frost safe lightweight aggregate concrete never reached the same depth.

References

Aalborg Portland. Cement and Concrete. 19th ed. Aalborg, Denmark: Aalborg Portland; 2010. 162 p. Danish.

Anderson DM, Williams PJ, Guymon GL, Kane DL. Principles of soil freezing and frost heaving. In: Berg RL, and Wright EA, editors. Frost action and its control. New York: American Society of Civil Engineers; 1984. p. 1–21.

BEBO Arch Systems. BEBO system technical documentation: Installation guide. Zürich: BEBO Arch Systems; 2009.

Bernini J. Overfilled precast concrete arch bridge structures. Zürich: BEBO of America, Inc; 2000.

Beskow G. Soil freezing and frost heaving with special application to roads and railroads. Osterberg JO, translator. Evanston, IL: Technological Institute Northwestern University; 1935.

Bourke J, Taylor S, Robinson D, Long A. Analysis of a flexible concrete arch. In: Chen B, Wei J, editors. ARCH'10: Proceedings of 6th International Conference on Arch Bridges; 2012 Oct 11–13; Fuzhou, China. p. 133–39.

Busch E. Lightweight aggregates. In: The concrete handbook. Copenhagen: Dansk Betonforening; 2013a. p. 3.7.1–6. Danish.

Busch E. Lightweight aggregate concrete blocks. In: The concrete handbook. Copenhagen: Dansk Betonforening; 2013b. p. 12.4.1–10. Danish.

Casagrande A. A new theory of frost heaving: Discussion. Washington, DC: Highway Research Board; 1931;11:168–72, ISSN: 0096-1027.

Castro J, Keiser L, Golias M, Weiss J. Absorption and desorption properties of fine lightweight aggregate for application to internally cured concrete mixtures. Cement Concrete Comp. 2011;33:1001–08.

Castro J, Varga IDL, Weiss J. Using isothermal calorimetry to assess the water absorbed by fine LWA during mixing. J Mater Civil Eng. 2012;24(8):996–1005.

Chamberlain EJ. Frost susceptibility of soil. Review of index tests. Hanover, NH: U.S. Army Cold Regions Research and Engineering Laboratory; 1981. Monograph 81-2.

Chandra S, Aavik J, Berntsson L. Influence of polymer microparticles on freeze-thaw resistance of structural lightweight aggregate concrete. Int J Cem Compos Lightweight Concr. 1982;4(2):111–15.

Chandra S, Berntsson L. Lightweight aggregate concrete. Science, technology and applications. Norwich, NY: William Andrew; 2002.

Crouch LK, Pitt J, Hewitt R. Aggregate effects on pervious portland cement concrete static modulus of elasticity. J Mater Civil Eng ASCE. 2007;19(7):561–68. doi: 10.1061/(ASCE)0899-1561(2007)19:7(561).

Danish Road Directorate. Concrete Bridge—General note—GN-P. Tender specification. Copenhagen: The Directorate; 2014. Danish.

Danish Road Directorate. Concrete Bridge—SWP-P. Copenhagen: The Directorate; 2012. Danish.

Danish Road Directorate. Design of bitumen based waterproofing and bridge surfacing. Handbook. Planning and construction. Copenhagen: The Directorate; 2010.

Danish Road Directorate. Design of pavements and reinforcement layers. Handbook. Construction and planning. Copenhagen: The Directorate; 2013. Available from: `http://english-vejregler.lovportaler.dk/showdoc.aspx?q=Design+of+pavements+and+reinforcement+layers&docId=vde-2015-0060-full`.

Danish Road Directorate. Hydraulic bound layers—General work specification (GWS). Tender specification. Copenhagen: The Directorate; 2009, ISBN: 978-87-7060-129-0. Danish.

Danish Road Directorate. Sub-base of sand and gravel—Design guide. Tender specification. Copenhagen: The Directorate; 2003, ISBN: 87-7923-502-6. Danish.

Danish Road Directorate. Sub-base of sand and gravel—General Work Specification (GWS). Tender specification. Copenhagen: The Directorate; 2003, ISBN: 87-7923-503-4. Danish.

Halding PS, Hertz KD, Petersen NEV, Kennedy B. Assembly and lifting of Pearl-Chain arches. In: Proceedings of fib Symposium; 2015 May 18–20; Copenhagen, Denmark. p. 185–86.

Halding PS, Hertz KD, Schmidt JW. Precast Pearl-Chain concrete arch bridges. J Eng Struct, 2015;103:214–27.

Haselbach LM, Freeman RM. Vertical porosity distributions in pervious concrete pavement. ACI Mater J. 2006;103(6):452–58.

Hasholt MT. Durability. Main report. Taastrup, Denmark: Danish Technological Institute, Center for green concrete; 2002. Danish.

Henderson V, Tighe S. Evaluation of pervious concrete pavement performance in cold weather climates. Int J Pavement Eng. 2012;13(3):197–208. doi: 10.1080/10298436.2011.572970.

Hertz KD. A new patented building technology based on ancient Roman knowledge. In: Proceedings of Workshop in Handling Exceptions in Structural Engineering: Structural Systems, Accidental Scenarios, Design Complexity; 2010 Jul 8–9; Rome.

Hertz KD. Super-light SL-Deck elements with fixed end connections. In: Proceedings of fib Symposium; 2015 May 18–20; Copenhagen, Denmark. p. 465–66.

Hertz KD, Castberg A, Christensen J. Super-light concrete decks for building floor slabs. Structural Concrete Journal of the fib, 2014;3.

Hutchinson D. Application and design of segmental precast arches. In: Yegian MK, Kavazanjian E, editors. Proceedings of Geo-Trans; 2004 Jul 27–31; Los Angeles. p. 452–59.

IDA Wastewater Commission. Regional variation of extreme rain in Denmark – a new analysis, 1979–2005. Pamphlet No. 28. Copenhagen: The Commission; 2006. ISBN: 87-7923-502-6. Danish.

Jensen OM, Hansen PF. A dilatometer for measuring autogenous deformation in hardening Portland cement paste. Mater Struct. 1994;28:406–09.

Kevern JT. Self-consolidating pervious concrete: A discussion of material properties and behaviors. In: Proceedings of the Fifth North American Conference on the Design and Use of Self-Consolidating Concrete; 2012 May 12–15; Chicago.

Kevern JT. Reducing the curing requirements of pervious concrete using prewetted lightweight aggregate for internal curing [Internet]. Kansas City, MO: University of Missouri-Kansas City; 2013. Available from: `http://www.escsi.org/uploadedFiles/Technical_Docs/Internal_Cur-ing/Pervious%20Report%20-%20Kevern.pdf`.

Kevern JT, Biddle D, Cao Q. Effect of macro-synthetic fibers on pervious concrete properties. J Mater Civil Eng. 2015;27(9):119–34. doi: 10.1061/(ASCE)MT.1943-5533.0001213.

Kevern JT, Schaefer VR, Wang K, Suleiman ST. Pervious concrete mixture proportions for improved freeze-thaw durability. J ASTM Int. 2008;5(2):JAI101320.

Kevern JT, Wang K, Schaefer VR. A novel approach to characterize entrained air content in pervious concrete. J ASTM Int. 2008;5(2).

Kevern JT, Wang K, Schaefer VR. Test methods for characterizing air void systems in Portland cement pervious concrete. J ASTM Int. 2009;6(9):119–34. doi:10.1520/JAI102451.

Kevern JT, Wang K, Schaefer VR. Effect of coarse aggregate on the freeze-thaw durability of pervious concrete. J ASTM Int. 2010;22(2):469–75.

Klieger P, Hanson JA. Freezing and thawing tests of lightweight aggregate concrete. J Am Concrete I. 1961;779–96.

Lauridsen J, Ulstrup OB, Hansen HJ, Mølgaard A. Bridges in Denmark – an overview. Dansk Vejtidsskrift, 2002;3:40–2. Danish.

Lambe TW, Whitman RV. Soil mechanics. New York: John Wiley & Sons; 1969.

Lund MSM, Hansen KK. Shrinkage properties of cement stabilized gravel. In: The Nordic Concrete Federation, editors. Proceedings of XXII Nordic Concrete Research Symposium; 2014 Aug 13–15; Reykjavik. Oslo: Norsk Betongforening; 2014. p. 303–06.

Lund MSM, Hansen KK, Hertz KD. Experimental study of properties of pervious concrete used for bridge superstructure. In: Proceedings of 12th International Symposium on Concrete Roads; 2014 Sep 23–26; Prague.

Lund MSM, Hansen KK, Hertz KD. Frost resistance and permeability of cement stabilized gravel used as filling material for Pearl-Chain Bridges. In: Bastien J, Rouleau N, Fiset M, Thomassin M, editors. Proceedings of 10th fib International PhD Symposium in Civil Engineering; 2014 Jul 21–23; Québec, Canada. Québec: Research Center on Concrete Infrastructure (CRIB), Université Laval; 2014. p. 155–60.

Lund MSM, Arvidsson M, Hansen KK. Homogeneity and strength of mortar joints in Pearl-Chain Bridges. In: Proceedings of fib Symposium; 2015 May 18–20; Copenhagen. p. 187–88.

Lund MSM, Hansen KK, Truelsen R, Johansen L. Pervious concrete fill in Pearl-Chain Bridges: Using small-scale results in full-scale implementation. Constr Build Mater. 2016;106:404–14.

Long A, McPolin P, Kirkpatrick J, Gupta A, Courtenay D. FlexiArch: From concept to practical applications. The Structural Engineer, 2014;92(7):10–5.

Melbourne C. The testing of a mass concrete arch bridge. In: Garas FK, Armer GST, Clarke JI, editors. Building the future: Innovation in design, materials and construction. London: E & FN Spon; 1993. p. 226–33.

Munch-Petersen GN. Mix design. In: The concrete handbook. Copenhagen: Dansk Betonforening; 2013. p. 6.0-1–34. Danish.

NCC Denmark. Road Construction – materials – wearing surfaces – pavements. 3rd ed. Copenhagen: NCC; 2001. Danish.

Neville AM. Properties of concrete. 4th ed. Essex: Pearson Education Limited; 1995.

National Ready Mixed Concrete Association (NRMCA). Freeze-thaw resistance of pervious concrete. Silver Spring, MD: NRMCA; 2004.

Portland Cement Association [Internet]. Skokie, IL: The Association [cited Jan 17, 2016]. Available from: `http://www.cement.org/for-concrete-books-learning/concrete-technology/durability`.

Poulsen E et al. Concrete 4: 13 concrete diseases. Hørsholm, Denmark: Danish Building Research Institute (SBi); 1985. Danish.

Powers TC. The air requirement of frost resistant concrete. In: Proceedings of the Highway Research Board. 1949;29:184–211.

Powers TC, Brownyard TL. Studies of physical properties of hardened Portland cement paste. PCA Bulletin 22; 1948.

Rempel AW. Formation of ice lenses and frost heave. J Geophys Res. 2007;112, F02S21. doi:10.1029/2006JF000525.

Rempel AW. Frost heave. Journal of Glaciol. 2010;56(200):1122–28.

Schaefer VR, Wang K, Suleiman MT, Kevern JT. Mix design development for pervious concrete in cold weather climates. Ames, IA: National Concrete Pavement Technology Center and Iowa State University; 2006.

Schaefer VR, Kevern JT. An integrated study of pervious concrete mixture design for wearing course applications. Ames, IA: National Concrete Pavement Technology Center and Iowa State University; 2011.

Schmit HKM, Reid ERE, Beatty AA, Stratford TJ, Bisby LA. Shear strength of concrete at elevated temperature. In: Proceedings of Application of Structural Fire Engineering; 2011; Prague.

Shu X, Huang B, Wu H, Dong Q, Burdette AG. Performance comparison of laboratory and field produced pervious concrete mixtures. Constr Build Mater. 2011;25:3187–92.

Sihwa L. Computer data base assessment of masonry bridges [dissertation]. Edinburgh, UK: University of Edinburgh; 1987.

Stoltzner E, Wegan V, Henriksen C. The Road Directorate's strategy for waterproofing of concrete bridges. Dansk Vejtidsskrift. 2005;40–1. Danish.

Taber S. Frost heaving. J Geol. 1929;37(5):428–61.

Taber S. The mechanics of frost heaving. J Geol. 1930;38(4):303–17.

Tennis PD, Leming ML, Akers DJ. Pervious concrete pavements. EB302.02, Skokie, IL: Portland Cement Association, and Silver Spring, MD: National Ready Mixed Concrete Association; 2004.

Whiting D, Burg R. Freezing and thawing durability of high strength lightweight concrete. ACI Special Publication, SP-126. 1991;83–100.

Standards

ACI 522.1M-13. Specification for Pervious Concrete Pavement. ACI Standard, Reported by ACI Committee 522; 2013. ISBN-13: 978-0-87031-848-1.

ASTM Standard C29/C29M-09. Standard Test Method for Bulk Density ("Unit Weight") and Voids in Aggregate. West Conshohocken, PA: ASTM International; 2009. doi: 10.1520/C0029_C0029M-09.

ASTM Standard C39/C39M-14a. Standard Test Method for Compressive Strength of Cylindrical Concrete Specimens. West Conshohocken, PA: ASTM International; 2014. doi: 10.1520/C0039_C0039M-14A.

ASTM Standard C128/C128M-12. Standard Test Method for Density, Relative Density (Specific Gravity), and Absorption of Fine Aggregate. West Conshohocken, PA: ASTM International; 2012. doi: 10.1520_C0128-12.

ASTM Standard C136-06. Standard Test Method for Sieve Analysis of Fine and Coarse Aggregate. West Conshohocken, PA: ASTM International; 2006. doi: 10.1520/C0136-06.

ASTM Standard C150/C150M-12. Standard Specification for Portland Cement. West Conshohocken, PA: ASTM International; 2012. doi: 10.1520/C0150_C0150M-12.

ASTM Standard C173/C173M-14. Standard Test Method for Air Content of Freshly Mixed Concrete by the Volumetric Method. West Conshohocken, PA: ASTM International; 2014, DOI: 10.1520/C0173_C0173M-14.

ASTM Standard C192/C192M-14. Standard Practice for Making and Curing Concrete Test Specimens in the Laboratory. West Conshohocken, PA: ASTM International; 2014. doi: 10.1520/C0192_C0192M-14.

ASTM Standard C311/C311-13. Standard Test Methods for Sampling and Testing Fly Ash or Natural Pozzolans for Use in Portland-Cement Concrete. West Conshohocken, PA: ASTM International; 2014. doi: 10.1520/C0311-13.

ASTM Standard C457-06. Standard Test Method for Microscopical Determination of Parameters of the Air-Void System in Hardened Concrete. West Conshohocken, PA: ASTM International; 2011. doi: 10.1520/C0469_C0469M-14.

ASTM Standard C496/C496M-11. Standard Test Method for Splitting Tensile Strength of Cylindrical Concrete Specimens. West Conshohocken, PA: ASTM International; 2011. doi: 10.1520/C0469_C0469M-14.

ASTM Standard C618-12a. Standard Specification for Coal Fly Ash and Raw or Calcined Natural Pozzolan for Use in Concrete. West Conshohocken, PA: ASTM International; 2012. doi: 10.1520/C0618-12a.

ASTM Standard C666/C666M-03. Standard Test Method for Resistance of Concrete to Rapid Freezing and Thawing. West Conshohocken, PA: ASTM International; 2008. doi: 10.1520/C0666_C0666M-03R08.

ASTM Standard C1688/C1688M-13. Standard Test Method for Density and Void Content of Freshly Mixed Pervious Concrete. West Conshohocken, PA: ASTM International; 2013. doi: 10.1520/C1688_C1688M-13.

ASTM Standard C1698-09. Standard Test Methods for Autogenous Strain of Cement Paste and Mortar. West Conshohocken, PA: ASTM International; 2009.

ASTM Standard C1754-12. Standard Test Method for Density and Void Content of Hardened Pervious Concrete. West Conshohocken, PA: ASTM International; 2012. doi: 10.1520/C1754_C1754M-12.

ASTM Standard C1761/C1761M-13b. Standard Specification for Lightweight Aggregate for Internal Curing of Concrete. West Conshohocken, PA: ASTM International; 2013, DOI: 10.1520/C1761_C1761M-13b.

ASTM Standard D2434-68. Standard Test Method for Permeability of Granular Soils (Constant Head). West Conshohocken, PA: ASTM International; 2006. doi: 10.1520/D2434-68R06.

ASTM Standard D4253-16. Standard Test Methods for Maximum Index Density and Unit Weight of Soils Using a Vibratory Table. West Conshohocken, PA: ASTM International; 2016. doi: 10.1520/D4253-16.

ASTM Standard D5918-13. Standard Test Methods for Frost Heave and Thaw Weakening Susceptibility of Soils. West Conshohocken, PA: ASTM International; 2013. doi: 10.1520/D5918-13.

DS Standard 450-1. Fly ash for concrete – Part 1: Definition, specifications and conformity criteria. Copenhagen: Danish Standards; 2012.

DS Standard 933-1. Tests for geometrical properties of aggregates – Part 1: Determination of particle size distribution – Sieving method. Copenhagen: Danish Standards; 2004.

DS Standard 1991-2. Eurocode 1: Actions on structures – Part 2: Traffic loads on bridges. Copenhagen: Danish Standards; 2003.

DS Standard 1991-2 DK NA. Annex A (Normative) Load models for classification and evaluation of load carrying capacity. Copenhagen: Danish Standards; 2003. Danish.

DS Standard 2426. Concrete – Materials – Rules for application of EN 206-1 in Denmark. Copenhagen: Danish Standards; 2011.

DS Standard 12390-3. Testing hardened concrete – Part 3: Compressive strength of test specimens. Copenhagen: Danish Standards; 2009.

DS Standard 12390-6. Testing hardened concrete – Part 6: Tensile splitting strength of test specimens. Copenhagen: Danish Standards; 2002.

DS Standard 13285. Unbound mixtures – Specifications. Copenhagen: Danish Standards; 2011.

DS Standard 13286-2. Unbound and hydraulically bound mixtures – Part 2: Test methods for laboratory reference density and water content – Proctor compaction. Copenhagen: Danish Standards; 2011.

DS Standard 13286-5. Unbound and hydraulically bound mixtures – Part 5: Test methods for laboratory reference density and water content – Vibrating table. Copenhagen: Danish Standards; 2003.

DS Standard 13320. Particle size analysis – Laser diffraction methods. Copenhagen: Danish Standards; 2009.

DS Standard 14227-1. Hydraulically bound mixtures – Specifications – Part 1: Cement bound granular mixtures. Copenhagen: Danish Standards; 2004.

DS/CEN/TS Standard 12390-9. Testing hardened concrete – Part 9: Freeze-thaw resistance – Scaling. Copenhagen: Danish Standards; 2006.

DS/EN Standard 1097-6. Tests for mechanical and physical properties of aggregates – Part 6: Determination of particle density and water absorption. Copenhagen: Danish Standards; 2013.

DS/EN Standard 1354. Determination of compressive strength of lightweight aggregate concrete with open structure. Copenhagen: Danish Standards; 2006.

DS/EN Standard 1992-1-1. Design of concrete structures – Part 1.1: General rules and rules for buildings. Copenhagen: Danish Standards; 2008.

DS/EN Standard 1992-1-1 DK NA. National annex for Eurocode 2: Design of concrete structures – Part 1.1: General rules and rules for buildings. Copenhagen: Danish Standards; 2013. Danish.

EN Standard 480-11. Admixtures for concrete, mortar and grout – Test methods – Part 11: Determination of air void characteristics in hardened concrete. Brussels: European Standards; 1998.

EN Standard 13286-41. Unbound and hydraulically bound mixtures – Part 41: Test method for the determination of the compressive strength of hydraulically bound mixtures. Brussels: European Standards; 2003.

EN Standard 13286-42. Unbound and hydraulically bound mixtures – Part 42: Test method for the determination of the indirect tensile strength of hydraulically bound mixtures. Brussels: European Standards; 2003.

EN Standard 13286-43. Unbound and hydraulically bound mixtures – Part 43: Test method of the modulus of elasticity of hydraulically bound mixtures. Brussels: European Standards; 2003.

EN Standard 13286-50. Unbound and hydraulically bound mixtures – Part 50: Method for the manufacture of test specimens of hydraulically bound mixtures using Proctor equipment or vibrating table compaction. Brussels: European Standards; 2011.

EN Standard 15304. Determination of the freeze-thaw resistance of autoclaved aerated concrete. Brussels: European Standard; 2010.

ISO Standard 4108. Concrete – Determination of tensile splitting strength of test specimens. London: International Standard; 1980.

ISO Standard 6784. Concrete – Determination of static modulus of elasticity in compression. London: International Standard; 1984.

NT BUILD 492. Concrete, mortar and cement-based repair materials: Chloride migration coefficient from non-steady-state migration experiments. Finland: Nordtest; 1999, ISSN 0283–7153.

prEN Standard 13286-54. Unbound and hydraulically bound mixtures – Part 54: Test method for determination of frost susceptibility – Resistance to freezing and thawing of hydraulically bound mixtures. Brussels: European Standard; 2011.

SS Standard 137244. Concrete testing – Hardened concrete – Scaling at freezing. Stockholm: Swedish Standards; 2005.

Test Method No. Iowa 406-C: Method of test for determining the shearing strength of bonded concrete. Des Moines, IA: Iowa Department of Transportation; 2000.

Pearl-Chain Bridge technology is a new prefabricated arch solution for road and railway bridges. Bridges are designed for a service life of a minimum of 100 years; hence, the materials used in Pearl-Chain Bridges need to be durable and live up to high standards. This thesis is a collection of papers that investigate and document the durability of (1) three different types of fill for Pearl-Chain Bridges: sub-base gravel, cement-stabilized gravel and pervious concrete, (2) the mortar joints in the Pearl-Chain arch, and (3) the lightweight aggregate concrete in the Super-Light Decks in the Pearl-Chain arch.

DTU Civil Engineering
Technical University of Denmark

Brovej, Bygning 118
2800 Kongens Lyngby

www.byg.dtu.dk

ISBN 9788778774323
ISSN 1601-2917